

TECHNISCHE UNIVERSITÄT MÜNCHEN

Anorganisch-Chemisches Institut

**Bifunctional Transition Metal Amido Complexes:
Cooperative H₂ Activation and Catalytic Dehydrogenation**

Anja Friedrich

Vollständiger Abdruck der von der Fakultät für Chemie der Technischen
Universität München zur Erlangung des akademischen Grades eines

Doktors der Naturwissenschaften

genehmigten Dissertation.

Vorsitzender: Univ.-Prof. Dr. Fritz E. Kühn

Prüfer der Dissertation:

1. Univ.-Prof. Dr. Sven Schneider
Friedrich-Alexander-Universität Erlangen-Nürnberg
2. Univ.-Prof. Dr. Lukas Hintermann
Technische Universität München
3. Univ.-Prof. Dr. Rhett Kempe
Universität Bayreuth

Die Dissertation wurde am 03.11.2010 bei der Technischen Universität
München eingereicht und durch die Fakultät für Chemie am 24.11.2010
angenommen.

*To Christian.
Thanks for making me part of your life.*

This thesis originated in the time between March 2008 and October 2010 at the Anorganisch-Chemisches Institut of Technische Universität München.

I am deeply indebted to my mentor

Professor Dr. Sven Schneider

Thank you for this fascinating topic, your absolute trust in my skills, for the interest which you had in my work and for all these invaluable scientific discussions, which were crucial for the success of this thesis.

I also want to express my gratitude to

Professor Dr. Dr. h. c. mult. Wolfgang A. Herrmann

Thank you very much for the possibility to work in your chair, for the excellent infrastructure which I was allowed to use and for all the support which I was granted.

This thesis was supported by a scholarship of the *Elitenetzwerk Bayern*, the international doctorate program *NanoCat* and the *TUM graduate school*.

Furthermore, my very special thanks go to:

Prof. Dr. Jörg Eppinger and his group members at the TU München Dr. Thomas Reiner, Dr. Alice Schlichtiger, Dr. Stefan Faul and Dominik Jantke for several stimulating scientific and nonscientific discussions and especially Alexander Nicandro Marziale for being my best friend since the early steps of our chemistry studies.

I specifically want to thank my colleagues in the Schneider group Björn Askevold, Dr. Jorge Torres Nieto, Jenni Meiners and Markus Scheibel for a wonderful time in the lab.

Dr. Markus Drees (DFT calculations and co-supervisor in the framework of the TUM graduate school) and Dr. Eberhardt Herdtweck (X-ray diffraction) for their tireless efforts and many instructive discussions.

Special thanks go to the members of the microanalytical lab Mrs. Ulrike Ammari and Mr. Thomas Tafelmaier for their continuous efforts in enabling the measurement of highly air sensitive samples.

I would further like to acknowledge the administrative staff, particularly Mrs. Irmgard Grötsch, for her dedication.

Further acknowledgements are made to the external collaborators of the Schneider group, Dr. Jörn Schmedt auf der Günne (Ludwig Maximilians Universität München) and Prof. Dr. Ian Manners and Dr. Anne Staubitz (University of Bristol).

Many thanks also to Prof. Dr. Fritz Kreißl, Mr. Tobias Kubo, Mr. Peter Richter and Prof. Dr. Peter Härter for an inspiring time in the laboratories of the Wissenschaftszentrum Weihenstephan during the inorganic practical courses each year.

I would also like to thank the many other researchers from the Department Chemie. Most of you have become friends over the years.

Felix Gnerlich, Tobias Harschneck, Martin Köppen, Stefan Prill and Anna Skrollan-Geiermann - how can I thank you for the exciting and amazing time we spent together during our undergraduate studies. Thank you for staying friends over the years.

Abbreviations

Å	angstrom
ATR	attenuated total reflection, infrared spectroscopic method
ACN	acetonitrile
BDE	bond dissociation energy
br	broad
Calcd.	calculated
DCM	dichloromethane
DFT	density functional theory
DMSO	dimethylsulfoxide
d	doublet
dd	doublet of doublet
δ	chemical shift (ppm)
Eq.	equation
equiv.	equivalent
FT-IR	fourier transform infrared spectroscopy
G	Gibbs energy (J mol^{-1})
GPC	gel permeation chromatography
H	molar enthalpy (J mol^{-1})
Hz	hertz
HETCOR	heteronuclear correlation, NMR spectroscopic method
HMQC	heteronuclear multiple quantum coherence, NMR spectroscopic method
h	hour(s)
η^n	hapticity, number of ligand atoms coordinated to a central atom
^iPr	isopropyl
J	coupling constant (Hz)
K	equilibrium constant
k	rate constant
KIE	kinetic isotope effect
L	ligand
M	molar (mol L^{-1})
Me	methyl
MHz	megahertz

MQ-MAS	multiple-quantum magic-angle spinning spectroscopy
m	multiplet (NMR), medium (IR)
min	minute(s)
mL	milliliter(s)
μ	micro
μ_n	specifying a bridging ligand
NMR	nuclear magnetic resonance
ν	wave number (cm^{-1})
Ph	phenyl
ppm	parts per million
q	quartet
R	alkyl or aryl
r	reaction constant
r.d.s	rate determining step
rt	room temperature
S	entropy ($\text{J mol}^{-1} \text{K}^{-1}$)
s	second(s); singlet (NMR); strong (IR)
SOQE	second-order quadrupolar effect
sp	septet
THF	tetrahydrofurane
TOF	turnover frequency
TON	turnover numer
t	triplet
^t Bu	tertiary butyl
vt	virtual triplet
X	halide

Table of Contents

A Introduction	11
1 Electron Rich Transition Metals with Amido Ligands	12
1.1 Metal-Ligand Bonding	12
1.2 Reactivity	13
2 Late Transition Metal Amido Complexes for Catalysis	16
2.1 Cooperative Catalysis	17
3 Catalytic Dehydrocoupling of Amine-Boranes	19
4 Motivation and Goals	22
B Results and Discussion	25
1 Published Research Articles	26
1.1 Iridium Olefin Complexes bearing Dialkylamino/amido PNP Pincer Complexes: Synthesis, Reactivity, and Solution Dynamics	26
1.1.1 Abstract	27
1.1.2 Introduction	27
1.1.3 Results	30
1.1.4 Discussion	43
1.1.5 Conclusion	47
1.1.6 Experimental details and syntheses	47
1.1.7 2D NMR spectra	53
1.1.8 Kinetic experiments	58
1.1.9 Crystallographic details	59
1.2 Ruthenium Complexes with Cooperative PNP Ligands: Bifunctional Catalysis for the Dehydrogenation of Ammonia-Borane	61
1.2.1 Introduction	62
1.2.2 Results and discussion	63
1.2.3 Conclusion	67
1.2.4 Experimental details and syntheses	68
1.2.5 NMR spectra	73
1.2.6 Catalytic protocols	75
1.2.7 Characterization of H ₃ B-NH ₃ dehydrocoupling products	76
1.2.8 Computational results	78
1.3 Ruthenium catalyzed Dimethylamineborane Dehydrogenation: Stepwise Metal Centered Dehydrocyclization	80
1.3.1 Introduction	81
1.3.2 Results and discussion	82
1.3.3 Conclusion	87
1.3.4 Experimental details and syntheses	88
1.3.5 NMR Spectra	91

A Introduction

1.3.6 Catalytic protocols	93
1.3.7 Computational results	95
1.4 Highly Stereoselective Proton/Hydride-Exchange: Assistance of Hydrogen-Bonding for the Heterolytic Splitting of H ₂	98
1.4.1 Introduction	99
1.4.2 Results and discussion	100
1.4.3 Conclusion	104
1.4.4 Experimental details and syntheses	104
1.4.5 ¹ H 2D EXSY NMR measurements	106
1.4.6 Computational results	110
1.5 Ruthenium Complexes with Cooperative PNP-Pincer Amine, Amido, Imine, and Enamido Ligands: Facile Ligand Backbone Functionalization Processes	111
1.5.1 Abstract	112
1.5.2 Introduction	113
1.5.3 Results and discussion	117
1.5.4 Concluding remarks	138
1.5.5 Experimental details and syntheses	139
1.5.6 NMR spectra	144
1.5.7 Crystallographic details	148
1.5.8 Computational results	163
2 Unpublished Results	165
2.1 The Mechanism of Borane-Amine Dehydrocoupling with Bifunctional Ruthenium Catalysts	165
2.1.1 Introduction	166
2.1.2 Results	171
2.1.3 Discussion	183
2.1.4 Conclusions	187
2.1.5 Experimental details and syntheses	187
2.1.6 Kinetic experiments	189
2.1.7 Computational results	190
3 Published Review Article	192
3.1 Acceptorless Dehydrogenation of Alcohols: Perspectives for Synthesis and Hydrogen-Storage	192
C Summary	198
D Zusammenfassung	214
E List of Publications	231
1 Journal Publications	232
2 Presentations	234
F Curriculum Vitae	235

A Introduction

1 Electron Rich Transition Metals with Amido Ligands

1.1 Metal-Ligand Bonding

Complexes of electron poor early transition metals in high oxidation states are well stabilized by covalently bound π -donating ligands, such as alkoxy, oxo, amido, imido, or nitrido ligands.^[1] As hard Lewis bases, the charged ligand systems meet the electronic demand of the high-valent, Lewis acidic metal center. In contrast, electron rich late transition metal complexes in low oxidation states with these ligands were comparatively rare.^[2] Several metal-ligand bonding models have been advanced trying to rationalize an apparent lack of thermodynamic stability of these compounds as compared with analogous early transition metal complexes. The bonding of covalently bound π -donating ligands, such as amides or alkoxides, with electron rich metal centers was considered weak for a long time, owing to the hard ligand and soft metal center mismatch.^[3] In a qualitative sense, this approach has been useful; however, the hard/soft theory has many exceptions.^[4] More recently, a molecular-orbital approach has been proposed in which the π -binding ability has a strong influence on the binding to the metal. It explains the relative weakness of late M-N covalent bonds based on high d-electron count of late transition metals in low oxidation states.^[5] Since the ligands of interest exhibit nonbonding filled orbitals, the scarcity of such complexes was attributed to an unfavorable filled-filled- π -interaction (Figure A-1). Therefore, electron rich, late transition metal amides become destabilized by π -repulsion of the metal d-orbitals with the free electron pair of the nitrogen. As the high electron density on the ligand can not be effectively delocalized, this bonding scheme explains the distinctively basic character of the amido ligand.^[6] The concept of $p\pi/d\pi$ -repulsion has gained widespread acceptance, in large part

¹ (a) R. Kempe, *Angew. Chem.* **2000**, *112*, 478; *Angew. Chem. Int. Ed.* **2000**, *39*, 468. (b) M. Lappert, P. Power, A. Protchenko, A. Seeber in *Metal Amide Chemistry*, Wiley, Chichester, **2009**.

² (a) H. E. Brzynda, W. Tam, *Chem. Rev.* **1988**, *88*, 1163. (b) M. D. Fryzuk, C. D. Montgomery, *Coord. Chem. Rev.* **1989**, *95*, 1. (c) M. D. Roundhill, *Chem. Rev.* **1992**, *92*, 1. (d) R. G. Bergman, *Polyhedron* **1995**, *14*, 3227. (e) J. R. Fulton, A. W. Holland, D. J. Fox, R. G. Bergman, *Acc. Chem. Res.* **2002**, *35*, 44. (f) T. B. Gunnoe, *Eur. J. Inorg. Chem.* **2007**, 1185.

³ R. G. Pearson, *J. Am. Chem. Soc.* **1963**, *85*, 3533.

⁴ R. S. Drago, *Applications of Electrostatic-Covalent Models in Chemistry*, Surfside, Gainesville, FL. **1994**.

⁵ (a) J. M. Mayer, *Comments Inorg. Chem.* **1988**, *8*, 125. (b) K. G. Caulton, *New J. Chem.* **1994**, *18*, 25.

⁶ D. Rais, R. G. Bergman, *Chem. Eur. J.* **2004**, *10*, 3970.

because of its close relation to several studies on the stabilizing interaction between filled ligand lone pairs and empty metal orbitals in low-coordinate complexes and intermediates.^[5b]

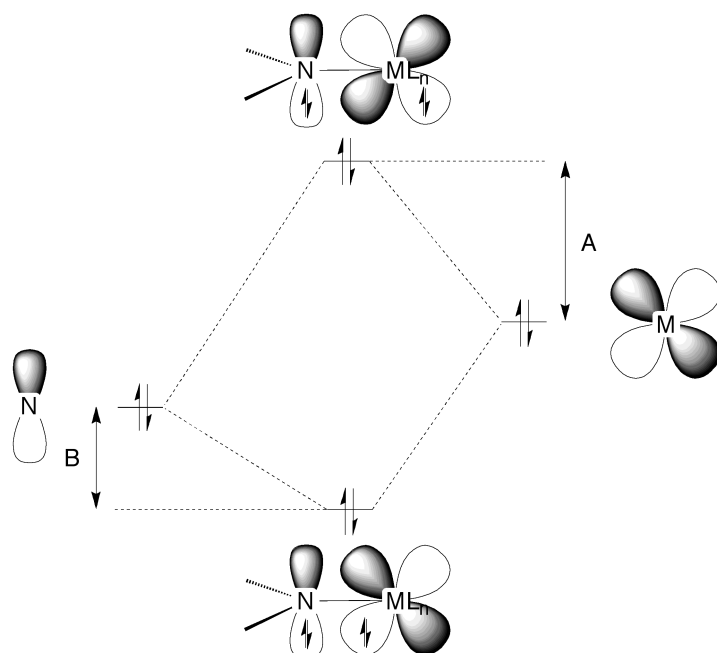


Figure A-1. 2-c-4-e filled-filled π -interaction of a dialkylamido ligand (N $p\pi$ -orbital) with an electron rich metal center (M $d\pi$ -orbital). A-B = net destabilization.

On the other hand, an almost linear relationship of d^6 and d^8 metal M–R bond dissociation energies (BDE) with the respective relative H–R BDE's (M = Ru^{II}, Pt^{II}; R = alkyl, aryl, hydride, alkoxide and amide) suggesting kinetic rather than thermodynamic reasons for the relative scarcity of alcoholate or amide complexes of the platinum metals.^[7] An alternative model, which does not consider π -bonding components, explains the reactivity of late transition metal amido complexes with the polarity of the M–N σ -bond.^[8] It therefore adheres more closely to classical conceptions of electronegativity and polarity. Additionally, it has the advantage that it can be used quantitatively.

1.2 Reactivity

Overall, the reactivity of electron rich d -block metal amido complexes can be attributed to the high electron density on the ligand, resulting from high σ -bond polarity and lack of

⁷ H. E. Bryndza, L. K. Fong, R. A. Paciello, W. Tam, J. E. Bercaw, *J. Am. Chem. Soc.* **1987**, *109*, 1444.

⁸ P. L. Holland, R. A. Andersen, R. G. Bergman, *Comments Inorg. Chem.* **1999**, *21*, 115-129.

nitrogen lone-pair delocalization. Hence, the amido ligand exhibits high basicity and nucleophilicity,^[2,9] similar to main group metal amido complexes, exemplified by C–N coupling with C-electrophiles such as MeOTf.^[9a] Weakly acidic molecules, such as terminal alkynes or benzylic hydrocarbons have been shown to add heterolytically across covalent late metal M–N bonds.^[6,9b,10] N–H/D exchange of ruthenium(II) anilido complexes with C₆D₆ suggests kinetically feasible 1,2-addition of aromatic C–H bonds and intramolecular alkane addition was demonstrated in cyclometallation reactions.^[11,12] However, the addition of H₂ has probably been studied best. In their seminal work on late transition metal amido complexes, Fryzuk and co-workers examined a series of group 9 and 10 (*d*⁶ and *d*⁸) complexes, utilizing the disilylamido PNP pincer ligand N(SiMe₂CH₂PR₂)₂ (Figure A-2, left).^[13] The authors demonstrated for H₂ to react with *d*⁸ and *d*⁶ amido complexes giving hydrido amine complexes as a result of heterolytic H₂ splitting.^[14] This reactivity is of great relevance for *bifunctional* hydrogenation catalyzed by ruthenium amine complexes (chapter A2.1).

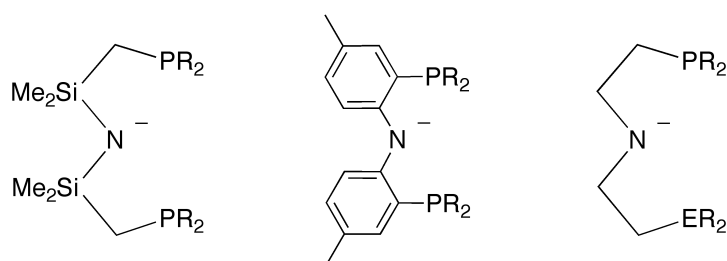


Figure A-2. Amido chelate ligands.

⁹ (a) S. Park, A. L. Rheingold, D. M. Roundhill, *Organometallics* **1991**, *10*, 615. (b) J. R. Fulton, M. W. Bouwkamp, R. G. Bergman, *J. Am. Chem. Soc.* **2000**, *122*, 8799. (c) T. Büttner, F. Breher, H. Grützmacher, *Chem. Commun.* **2004**, 2820. (d) P. Maire, F. Breher, H. Schönberg, H. Grützmacher, *Organometallics* **2005**, *24*, 3207. (e) T. Büttner, J. Geier, G. Frison, J. Harmer, C. Calle, A. Schweiger, H. Schönberg, H. Grützmacher, *Science* **2005**, *307*, 235.

¹⁰ A. N. Walstrom, L. A. Watson, M. Pink, K. G. Caulton, *Organometallics* **2004**, *23*, 4814.

¹¹ Y. Feng, M. Lail, N. A. Foley, T. B. Gunnoe, K. A. Barakat, T. R. Cundari, J. L. Petersen, *J. Am. Chem. Soc.* **2006**, *128*, 7982.

¹² D. Connor, K. N. Jayaprakash, T. R. Cundari, T. B. Gunnoe, *Organometallics* **2004**, *23*, 2724.

¹³ (a) M. D. Fryzuk, P. A. McNeil, *J. Am. Chem. Soc.* **1981**, *103*, 3592. (b) M. D. Fryzuk, P. A. McNeil, *Organometallics* **1983**, *2*, 355. (c) M. D. Fryzuk, P. A. McNeil, S. J. Rettig, *Organometallics* **1986**, *5*, 2469.

¹⁴ (a) M. D. Fryzuk, P. A. McNeil, S. J. Rettig, *Organometallics* **1983**, *2*, 682. (b) M. D. Fryzuk, P. A. McNeil, *Organometallics* **1985**, *4*, 1145. (c) M. D. Fryzuk, P. A. McNeil, S. J. Rettig, *J. Am. Chem. Soc.* **1987**, *109*, 2803.

Fryzuk's choice of disilylamido ligands for the synthesis of stable late metal amido complexes points towards another common reactivity of this class of compounds. Electron rich amido complexes exhibit a strong thermodynamic driving force for extrusion of imines. Hence, terminal late transition metal alkylamido complexes with β -hydrogen atoms typically suffer from low thermodynamic stability, owing to decomposition towards metal hydride complexes.^[15] Accordingly, amido ligands without β -hydrogen, such as the diarylamido pincer ligands established by Ozerov's group (Figure A-2, middle), were frequently utilized in recent years.^[16] While β -hydride elimination is well examined for alkyl complexes,^[17] only few mechanistic studies have been published for the corresponding amido counterparts.^[15b,18] A rare example of stabilizing late transition metal complexes with highly π -basic dialkylamido ligands is presented recently with Ir(III) amides [Ir(H)₂(PNP)] (PNP = N(CH₂CH₂P^{*i*}Pr₂)₂) and [Ir(H)₂(PNN)] (PNN = ^{*i*}Pr₂PCH₂CH₂NCH₂CH₂NEt₂)^[19] (Figure A-2, right). These complexes are active catalysts for the transfer hydrogenation of ketones with 2-propanol. A postulated Noyori-type mechanism (chapter A2.1) was confirmed in a theoretical examination.^[19c] However, no iridium(I) complexes were reported.

¹⁵ (a) S. E. Diamond, F. Mares, *J. Organomet. Chem.* **1977**, *142*, C55. (b) J. F. Hartwig, *J. Am. Chem. Soc.* **1996**, *118*, 7010. (c) J. F. Hartwig, S. Richards, D. Barañano, F. Paul, *J. Am. Chem. Soc.* **1996**, *118*, 3626. (d) S. Wagaw, R. A. Rennels, S. L. Buchwald, *J. Am. Chem. Soc.* **1997**, *119*, 8451.

¹⁶ (a) O. V. Ozerov, C. Guo, V. A. Papkov, B. M. Foxman, *J. Am. Chem. Soc.* **2004**, *126*, 4792. (b) L. Fan, L. Yang, C. Guo, B. M. Foxman, O. V. Ozerov, *Organometallics* **2004**, *23*, 4778. (c) W. Weng, C. Guo, C. Muora, L. Yang, B. M. Foxman, O. V. Ozerov, *Organometallics* **2005**, *24*, 3487. (d) L. Fan, O. V. Ozerov, *Chem. Commun.* **2005**, 4450. (e) L. Fan, S. Parkin, O. V. Ozerov, *J. Am. Chem. Soc.* **2005**, *127*, 16772.

¹⁷ (a) J. P. Collman, L. S. Hegedus, J. R. Norton, R. G. Finke, In *Principles and Applications of Organotransition Metal Chemistry*, University Science Books, Sausalito, CA, **1987**. (b) R. H. Crabtree, In *The Organometallic Chemistry of the Transition Metals*, 3rd ed., Wiley-Interscience, New York, NY, **2001**. (c) S. Niu, M. B. Hall, *Chem. Rev.* **2000**, *100*, 353.

¹⁸ (a) J. M. Mayer, C. J. Curtis, J. E. Bercaw, *J. Am. Chem. Soc.* **1983**, *105*, 2651. (b) Tsai, Y.-C.; Johnson, M. J. A.; Mindiola, D. J.; Cummins, C. C. *J. Am. Chem. Soc.* **1999**, *121*, 10426. (c) J. Zhao, H. Hesslink, J. F. Hartwig, *J. Am. Chem. Soc.* **2001**, *123*, 7220. (e) P. Zhao, J. F. Hartwig, *J. Am. Chem. Soc.* **2005**, *127*, 12066. (f) I. Matas, J. Campora, P. Palma, E. Alvarez, *Organometallics* **2009**, *28*, 6515.

¹⁹ (a) Z. E. Clarke, P. T. Maragh, T. P. Dasgupta, D. G. Gusev, A. J. Lough, K. Abdur-Rashid, *Organometallics* **2006**, *25*, 4113. (b) Choualeb, A.; Lough, A. J.; Gusev, D. G. *Organometallics* **2007**, *26*, 5224. (c) S. Bi, Q. Xie, X. Zhao, Y. Zhao, X. Kong, *J. Organomet. Chem.* **2008**, *693*, 633.

Besides the high basicity and nucleophilicity, the high electron density on the amido ligands suggests that radical cations resulting from one electron oxidation could be strongly ligand centered. Alcock, Parkins and co-workers demonstrated, that oxidation of platinum(II) anilido complexes with AgPF_6 results in oxidative C–C coupling of the anilido ligand.^[20] Furthermore, the few spectroscopically characterized or even isolable persistent late transition metal amido radical complexes confirm the presence of considerable spin density on the ligand.^[9e,21,22] However, overall the redox chemistry of electron rich amido complexes remains scarcely examined.

These examples and many other observations illustrate the distinctly different reactivity of electron rich transition metal complexes with covalently bound π -donor ligands as compared with high valent metal complexes. Their utility or proposed participation in stoichiometric activation of unreactive bonds or catalytic reactions have stimulated both fundamental studies of M–E bonding and applied research to afford novel methods for metal mediated catalytic functionalization of organic molecules.

2 Late Transition Metal Amido Complexes for Catalysis

Metal amido complexes of late transition metals are of high relevance for several catalytic C–N bond forming reactions. For example, homogeneous olefin hydroamination potentially represents an interesting alternative in using precious metal catalysts, due to the generally higher functional group tolerance compared with the successfully applied group 4 and lanthanoid based catalysts.^[23] Two mechanism are conceivable for this reaction: (1) electrophilic activation of an olefin by metal coordination and subsequent outerspere

²⁰ (a) N. W. Alcock, R. D. O'Sullivan, A. W. Parkins, *J. Chem. Soc., Chem. Commun.* **1980**, 1216. (b) R. D. O'Sullivan, A. W. Parkins, N. W. Alcock, *J. Chem. Soc., Dalton Trans.* **1986**, 571.

²¹ (a) F. N. Penkert, T. Weyhermüller, E. Bill, P. Hildebrandt, S. Lecomte, K. Wieghardt, *J. Am. Chem. Soc.* **2000**, *122*, 9663. (b) D. Adhikari, S. Mossin, F. Basuli, J. C. Huffmann, R. K. Szilagy, K.; Meyer, D. J. Mindiola, *J. Am. Chem. Soc.* **2008**, *130*, 3676.

²² (a) C. Tejel, M. A. Ciriano, M. Pilar del Rio, D. G. H. Hetterscheid, N. Tsihli i Spithas, J. M. N. Smits, B. de Bruin, *Chem. Eur. J.* **2008**, *14*, 10932. (b) C. Tejel, M. P. del Rio, M. A. Ciriano, E. J. Reijerse, F. Hartl, S. Zalis, D. G. H. Hetterscheid, N. Tsihli I Spithas, B. de Bruin, *Chem. Eur. J.* **2009**, *15*, 11878.

²³ (a) T. E. Müller, M. Beller, *Chem. Rev.* **1998**, *98*, 675. (b) P. W. Roesky, T. E. Müller, *Angew. Chem.* **2003**, *115*, 2812; *Angew. Chem. Int. Ed.* **2003**, *42*, 2708. (c) J. F. Hartwig, *Pure Appl. Chem.* **2004**, *76*, 507. (d) K. C. Hultsch, *Adv. Synth. Catal.* **2005**, *347*, 367.

nucleophilic attack of the amine; (2) amine oxidative addition, followed by the insertion of the olefin into the M–N (or M–H) bond, and final amine reductive elimination.^[23a] The first route has been shown to be operative for electrophilic platinum and palladium catalyzed olefin hydroamination. This route generally results in Markovnikov addition, similar to acid catalyzed hydroamination.^[23c,24] On the contrary, for an insertion / reductive elimination mechanism, anti-Markovnikov addition can be expected. The potentially different selectivity rendering this route particularly interesting. In fact, both amine oxidative addition and olefin insertion into late metal M–N bonds have been demonstrated in stoichiometric reactions.^[25,26] However, β -H migration from aminoalkyl intermediates is frequently observed (chapter A1.2) prior to amine reductive amination. This results in considerable amounts of imine side products (oxidative amination).^[27] Hence, only few protocols have been published with highly limited substrate scope.^[28]

2.1 Cooperative Catalysis

Late transition metal amido species are not only important intermediates in metal catalyzed C–N forming reactions. The pronounced nitrogen centered reactivity, such as the high basicity and nucleophilicity, renders these complexes ideal candidates to observe metal-ligand *cooperativity*. Therefore, late metal amido complexes have been successfully used in *bifunctional* (or *cooperative*) catalysis, where functional groups in the first coordination sphere of the metal center participate in reversible chemical reactions. This *cooperativity*

²⁴ (a) C. Hahn, *Chem Eur. J.* **2004**, *10*, 5888. (b) A. M. Johns, M. Utsunomiya, C. D. Incarvito, J. F. Hartwig, *J. Am. Chem. Soc.* **2006**, *128*, 1828. (c) B. M. Cochran, F. E. Michael, *J. Am. Chem. Soc.* **2008**, *130*, 2786.

²⁵ (a) A. L. Casalnuovo, J. C. Calabrese, D. Milstein, *Inorg. Chem.* **1987**, *26*, 971. (b) M. Schulz, D. Milstein, *J. Chem. Soc., Chem. Commun.* **1993**, 318. (c) J. Zhao, A. S. Goldman, J. F. Hartwig, *Science*, **2005**, *307*, 1080. (d) A. C. Sykes, P. White, M. Brookhart, *Organometallics* **2006**, *25*, 1664.

²⁶ (a) P. Zhao, C. Krug, J. F. Hartwig, *J. Am. Chem. Soc.* **2005**, *127*, 12066. (b) J. D. Neukom, N. S. Perch, J. P. Wolfe, *J. Am. Chem. Soc.* **2010**, *132*, 6276. (c) P. S. Hanley, D. Markovic, J. F. Hartwig, *J. Am. Chem. Soc.* **2010**, *132*, 6302.

²⁷ M. Beller, M. Eichberger, H. Trauthwein, *Angew. Chem.* **1997**, *109*, 2306; *Angew. Chem. Int. Ed. Engl.* **1997**, *36*, 2225.

²⁸ (a) A. L. Casalnuovo, J. C. Calabrese, D. Milstein, *J. Am. Chem. Soc.* **1988**, *110*, 6738. (b) R. Dorta, P. Egli, F. Züricher, A. Togni, *J. Am. Chem. Soc.* **1997**, *119*, 10857. (c) D. Vasen, A. Salzer, F. Gerhards, H.-J. Gais, R. Stürmer, N. H. Bieler, A. Togni, *Organometallics* **2000**, *19*, 539. (d) J. Zhou, J. F. Hartwig, *J. Am. Chem. Soc.* **2008**, *130*, 12220.

accelerates absolute and relative rates of bond activation reactions aimed at improving activity and selectivity.^[29] The term *bifunctional* is used in the sense of the the IUPAC definition for *bifunctional* catalysis: “Catalysis by a bifunctional chemical species involving a mechanism in which both functional groups are implicated in the rate-controlling step, so that the corresponding catalytic coefficient is larger than that expected for catalysis by chemical species containing only one of these functional groups.” In the present context the term *cooperating* can be used synonymously.^[29b]

As a prominent example, Noyori introduced ruthenium amino pre-catalysts for the hydrogenation and transfer hydrogenation of carbonyl groups with extraordinarily high activities.^[30] For these reactions, bifunctional mechanisms have been proposed.^[31] Catalyst formation is typically achieved in situ by reaction to a hydride complex. Reduction of the substrate proceeds via a concerted, bifunctional proton and hydride transfer from the N–H and Ru–H moieties, respectively (Figure A-3). The highly organized transition state can be expected to considerably contribute to the high *ee*'s obtained in asymmetric hydrogenation with chiral catalyst derivatives. Subsequent proton transfer to the amido moiety is accomplished via an intermediate, non-classical dihydrogen complex. Side-on binding to the metal acidifies the hydrogen ligand,^[32] and heterolytic H₂-activation, which represents the rate determining step of the catalytic cycle, typically exhibits higher rates than H₂ oxidative addition.^[31a] The role of hydrogen bridges with Brønstedt-acids for H₂-splitting is still controversially discussed (chapter B1.4).^[33] More recently, bifunctional ruthenium amido catalysts were also successfully applied in the reverse reaction: the acceptorless dehydrogenation of diols to lactones.^[34]

²⁹ (a) G. J. Rowlands, *Tetrahedron* **2001**, *57*, 1865. (b) H. Grützmacher, *Angew. Chem.* **2008**, *120*, 1838; *Angew. Chem. Int. Ed.* **2008**, *47*, 1814. (c) D. B. Grotjahn, *Dalton Trans.* **2008**, 6497. (d) Y. J. Park, J.-W. Park, C.-H. Jun, *Acc. Chem. Res.* **2008**, *41*, 222. (e) J. I. van der Vlugt, J. N. H. Reek, *Angew. Chem.* **2009**, *121*, 8990; *Angew. Chem. Int. Ed.* **2009**, *48*, 8832.

³⁰ R. Noyori, T. Ohkuma, *Angew. Chem.* **2001**, *113*, 40; *Angew. Chem. Int. Ed.* **2001**, *40*, 40.

³¹ (a) S. E. Clapham, A. Hadzovic, R. H. Morris, *Coord. Chem. Rev.* **2004**, *248*, 2201. (b) K. Muñiz, *Angew. Chem.* **2005**, *117*, 6780; *Angew. Chem. Int. Ed.* **2005**, *44*, 6622. (c) J. S. M. Samec, J.-E. Bäckvall, P. G. Andersson, P. Brandt, *Chem. Soc. Rev.* **2006**, *35*, 237.

³² G. J. Kubas, *Chem. Rev.* **2007**, *107*, 4152.

³³ M. Zimmer-De Iuliis, R. H. Morris, *J. Am. Chem. Soc.* **2009**, *131*, 11263.

³⁴ J. Zhao, J. F. Hartwig, *Organometallics* **2005**, *24*, 2441.

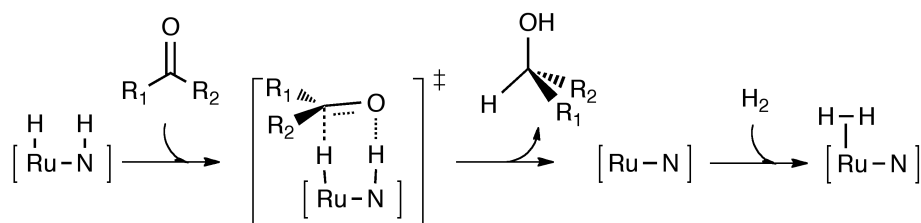


Figure A-3. Detail of the proposed mechanism of the ionic hydrogenation with Noyori-type catalysts: concerted, *bifunctional* proton/hydride transfer to the substrate and catalyst regeneration via a non-classical dihydrogen complex.

These ionic hydrogenations, which make use of the high basicity of late transition metal amido complexes, have been extensively examined over the past 15 years. In contrast, the expected redox non-innocence of the electron rich amido ligands remains scarcely investigated with respect to *cooperative* behavior. Grützmacher and co-workers recently presented the use of an iridium amido complex for the highly efficient catalytic oxidation of alcohols with benzoquinone. The authors proposed a mechanism with an aminyl radical complex as the crucial intermediate, undergoing C–H hydrogen abstraction from an alkoxide ligand.^[35] However, this account represents a rare example.

3 Catalytic Dehydrocoupling of Amine-Boranes

The majority of reports concerning the dehydrocoupling of group 13/15 adducts has centered mainly on amine-borane adducts, not least because the simplest example, ammonia-borane ($\text{H}_3\text{N}-\text{BH}_3$, AB) has been discussed extensively as a hydrogen storage material with a high gravimetric hydrogen content of 19.6%.^[36] Chemical hydrogen storage, in which (catalytic) chemical reactions release gaseous H_2 from hydrogen atoms covalently bound in the molecule, provides a promising approach. Current technology (pressurized H_2) has safety and efficiency shortcomings, requiring further research into hydrogen storage methodologies if a hydrogen economy is to become a reality.

The first catalytic dehydrocoupling of amine-boranes was briefly mentioned in the patent literature in 1989 by Laine and Blum who claimed the dehydrogenation of several amine-

³⁵ M. Königsmann, N. Donati, D. Stein, H. Schönberg, J. Harmer, A. Sreekanth, H. Grützmacher *Angew. Chem.* **2007**, *119*, 3637; *Angew. Chem. Int. Ed.* **2007**, *119*, 3567.

³⁶ A. Staubitz, A. P. M. Robertson, I. Manners, *Chem. Rev.* **2010**, *110*, 4079.

boranes using $\text{Ru}_3(\text{CO})_{12}$ at 60 °C.^[37] However, very little experimental or analytical data was presented. The first detailed report of catalytic AB dehydrocoupling focused on Rh(I) or Rh(III) based catalysts.^[38b] Shortly after this, the reaction was further explored^[38a] with a range of amine-boranes and different heterogeneous catalysts. One of the most efficient catalysts discovered was $\{\text{Rh}(1,5\text{-cod})(\mu\text{-Cl})\}_2$ in typical loadings of 0.5 - 5 mol%. Secondary amine-borane adducts were dehydrocoupled to give cyclic dimers $[\text{R}'\text{R}''\text{N-BH}_2]_2$ in good yields or, in the case of bulky substituents on nitrogen, the corresponding aminoborane monomer. Nowadays, the secondary amine-borane $\text{Me}_2\text{HN-BH}_3$ is often used as a test substrate because of its commercial availability and its easy purification by sublimation. Most importantly, in contrast to AB, the product of the dehydrocoupling reaction is soluble in a large range of solvents, which simplifies analysis of the reaction products and facilitated mechanistic studies. Primary amine-borane adducts on the other hand were reported to give cyclotriborazanes^[39] initially, which converted into borazines upon prolonged heating, tantamount to the loss of another equivalent of dihydrogen. Since then, a significant amount of work has been devoted to the search for alternative catalysts for the dehydrocoupling of amine-boranes.

In 2006, a very efficient nickel based catalyst, in terms of equivalents of hydrogen released, was presented.^[40] In combination with various *N*-heterocyclic carbene ligands (NHCs), a $\text{Ni}(\text{cod})_2$ solution in C6D6/diglyme was able to release up to 2.8 equivalents of hydrogen in approximately 4 h at 60 °C with a catalyst loading of 10 mol %. The major products showed peaks from 40 to 18 ppm in the ^{11}B NMR spectrum and were suggested to be crosslinked borazine-type species.

A very important breakthrough in terms of catalytic effectiveness for the removal of one equivalent of dihydrogen from primary amine-boranes was reported by Goldberg, Heinekey, and co-workers in 2006.^[41] They demonstrated that Brookhart's iridium pincer complex,

³⁷ Y. D. Blum, R. M. Laine, U.S. Pat. 4801439, **1989**.

³⁸ (a) C. A. Jaska, K. Temple, A. J. Lough, I. Manners, *J. Am. Chem. Soc.* **2003**, *125*, 9424; (b) C. A. Jaska, K. Temple, A. J. Lough, I. Manners, *Chem. Commun.* **2001**, 962.

³⁹ C. K. Narula, J. F. Janik, E. N. Duesler, R. T. Paine, R. Schaeffer, *Inorg. Chem.* **1986**, *25*, 3346.

⁴⁰ R. J. Keaton, J. M. Blacquiere, R. T. Baker, *J. Am. Chem. Soc.* **2007**, *129*, 1844.

⁴¹ M. C. Denney, V. Pons, T. J. Hebden, D. M. Heinekey, K. I. Goldberg, *J. Am. Chem. Soc.* **2006**, *128*, 12048.

(POCOP)Ir(H)₂ (POCOP = [η^3 -1,3-(OP^tBu)₂C₆H₃])^[42] an effective homogeneous catalyst for alkane dehydrogenation, was able to dehydrogenate AB in a dilute THF solution with a catalyst loading of 0.5 mol % within 14 min. Because of the poor solubility and the sole dependence on solid state analytical techniques (IR, WAXS, and ¹¹B MAS NMR spectroscopy), the identity of the product was difficult to determine but was proposed to be cyclopentaborazane [NH₂-BH₂]₅.^[43] The fact that only primary amine-boranes react may be the result of the sterically crowded catalytic center, which precludes the reaction of secondary amine-boranes. Interestingly, the catalyst was not stable over time, but converted into a resting state (POCOP)-IrH₂(BH₃),^[44] which could be reactivated by the addition of H₂.

Although formally isoelectronic to ethane, the polarity and electronic structure of AB might suggest a reactivity more closely resembling that of polar functional groups, such as alcohols. According to this analogy, a *bifunctional* catalyst, as used for carbonyl hydrogenation to alcohols,^[45] could be more suitable for amine-borane dehydrogenation. Therefore, at the same time and independently of this work, Fagnou and co-workers introduced the use of late transition metal catalysts with *cooperative* amino ligands for the dehydrogenation of AB with great success^[46] (see chapter B1.2). However, the catalyst screening by Fagnou was restricted to the *in situ* catalyst generation and a great excess of base (30 equiv. KO^tBu) is needed for catalyst activation. This situation hinders detailed mechanistic and kinetic studies as the exact concentration of the catalyst is unknown and varies during the time of formation. Nevertheless, density functional theory (DFT) calculations proposed an inverted Noyori-type mechanism with a Ru-hydride that is suggested as the *in situ* formed catalytically active species (Figure A-4). The active species could be protonated at the amido group of the ligand by a protic hydrogen of AB. The transfer of a substrate hydride to the ruthenium center leads to dehydrogenated AB and a *trans*-Ru-dihydride. The latter could then be protonated by the ligand to give a dihydrogen complex, which would then be able to evolve dihydrogen.

⁴² I. Göttker-Schnetmann, P. White, M. Brookhart, *J. Am. Chem. Soc.* **2004**, *126*, 1804.

⁴³ K. W. Bøddeker, S. G. Shore, R. K. Bunting, *J. Am. Chem. Soc.* **1966**, *88*, 4396.

⁴⁴ T. J. Hebden, M. C. Denney, V. Pons, P. M. B. Piccoli, T. F. Koetzle, A. J. Schultz, W. Kaminsky, K. I. Goldberg, D. M. Heinekey, *J. Am. Chem. Soc.* **2008**, *130*, 10812.

⁴⁵ (a) S. E. Clapham, A. Hadzovic, R. H. Morris, *Coord. Chem. Rev.* **2004**, *248*, 2201. (b) T. Li, R. Churlaud, A. J. Lough, K. Abdur-Rashid, R. H. Morris, *Organometallics* **2004**, *23*, 6239. (c) K. Abdur-Rashid, S. E. Clapham, A. Hadzovic, J. N. Harvey, A. J. Lough, R. H. Morris, *J. Am. Chem. Soc.* **2002**, *124*, 15104.

⁴⁶ N. Blaquiere, S. Diallo-Garcia, S. I. Gorelsky, D. A. Black, K. Fagnou, *J. Am. Chem. Soc.* **2008**, *130*, 14034.

However, the DFT calculations showed a very high barrier of 22 kcal mol⁻¹ for the formation of the dihydrogen complex which is needed to release the active catalytic species.

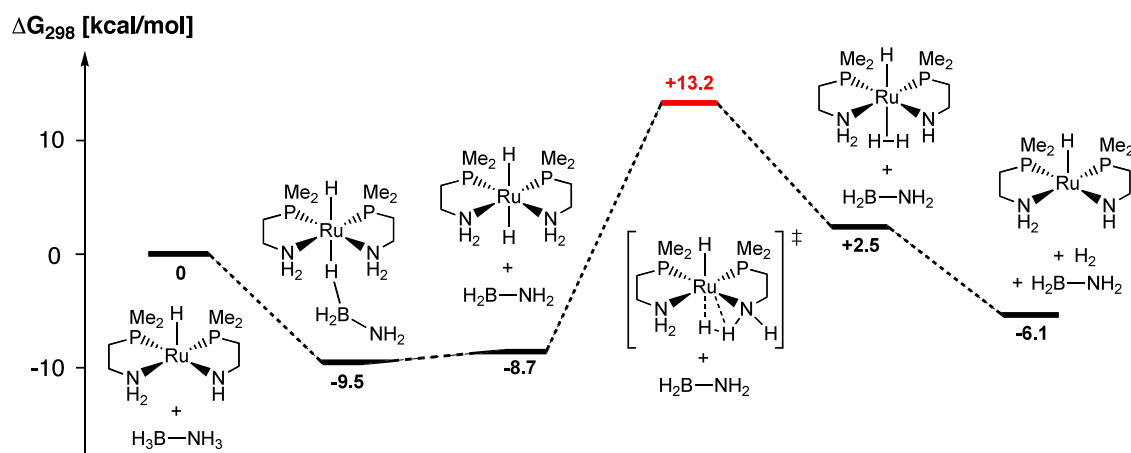


Figure A-4. Proposed mechanism for the dehydrogenation of AB with *bifunctional* ruthenium catalysts. Reported values (B3LYP/6-31G*) are in kcal mol⁻¹.

4 Motivation and Goals

The initial aim of this thesis was to apply a *bifunctional* approach in catalyst design by utilizing electron rich transition metal amido complexes. New catalytic reactions should be mechanistically examined, particularly with respect to the potential *cooperativity* of the metal-ligand framework. Out of a potential set of ligands,^[47] the ethylene bridged monoanionic pincer-type ligand $\text{N}(\text{CH}_2\text{CH}_2\text{P}^i\text{Pr}_2)_2$ ($\text{PNP}^{i\text{Pr}}$) was chosen owing to (a) the strong bonding of electron rich metal centers with phosphine ligands, (b) the high basicity and nucleophilicity of the dialkylamido-nitrogen atom, (c) the moderate barrier to β -hydride elimination, possibly enabling ligand functionalization and (d) the highly useful NMR properties of the ³¹P nucleus ($I = 1/2$) as a spectroscopic probe^[48]. Although the synthesis of amino ligand $\text{HN}(\text{CH}_2\text{CH}_2\text{P}^i\text{Pr}_2)_2$ ($\text{HPNP}^{i\text{Pr}}$) is well established,^[49] only few studies using late, electron rich

⁴⁷ (a) M. E. Wilson, R. G. Nuzzo, G. E. Whitesides, *J. Am. Chem. Soc.* **1978**, *100*, 2269. (b) S. Demeshko, G. Leibelng, W. Maringgele, F. Meyer, C. Mennerich, H.-H. Klauss, H. Pritzkow, *Inorg. Chem.* **2005**, *4*, 519. (c) R. E. Douthwaite, J. Houghton, B. M. Kariuki, *J. Chem. Soc. Chem. Commun.* **2004**, 698.

⁴⁸ P. S. Pregosin, R. W. Kunz, in *³¹P and ¹³C NMR of Transition Metal Phosphine Complexes*, Springer, **1979**.

⁴⁹ A. A. Danopoulos, A. R. Wills, P. G. Edwards, *Polyhedron* **1990**, *9*, 2413.

transition metals are reported.^[19,50] In a preliminary work, the chelate effect of this ligand was demonstrated by the establishment of a highly electron rich M(PNP) platform, which stabilizes an iridium(I) center bound to the basic amido function.^[51] Furthermore, the thorough examination of electron rich four-coordinate d^8 palladium dialkylamido complexes, including N–H pK_a values or one-electron oxidation, yielded important information about M–N bonding and reactivity as potential cooperative catalysts.^[52] An expansion to d^6 ruthenium (PNP^{*i*Pr}) complexes offered surprisingly versatile functionalization and synthetic access to amine, amido and enamido complexes.^[53] These complexes can participate in the reversible, heterolytic H₂ activation with the nitrogen atom and the ligand backbone. Moreover, highly efficient dehydrogenation of alcohols and borane-amines demonstrated the high potential of Ru(PNP) complexes as catalysts for acceptorless dehydrogenation (see chapter B1.2). Starting from this point, the M(PNP) fragment was to be examined with respect to a mechanistic concept of *bifunctional* bond activation and *cooperative* catalysis. Therefore, this thesis focused on (1) the scaling of electronic properties and reactivities of the dialkylamido complexes compared to well examined PNP ligand frameworks, such as Fryzuk's disilylamido or Ozerov's diphenylamido ligands, (2) an effective tuning of the electronic ligand properties by chemical modification of the ethylene backbone to control stability and reactivity and (3) the question, if the potential of β -hydride elimination reactivity of the M(PNP) fragments can be controlled to study this reaction pathway mechanistically and be utilized for *cooperative* catalysis?

⁵⁰ (a) K. Abdur-Rashid, WO2004/096735, **2004**. (b) D. Amoroso, T. W. Graham, R. Guo, C. W. Tsang, K. Abdur-Rashid, *Aldrichim. Acta* **2008**, *41*, 15. (c) X. Chen, W. Jia, R. Guo, T. W. Graham, M. A. Gullons, K. Abdur-Rashid, *Dalton Trans.* **2009**, 1407.

⁵¹ A. Friedrich, *Synthesis and Characterization of Iridium Complexes with chelating Amine and Amido Phosphine Ligands*, Diploma Thesis, TU München, **2007**.

⁵² A. N. Marziale, E. Herdtweck, J. Eppinger, S. Schneider *Inorg. Chem.* **2009**, *48*, 3699.

⁵³ M. Käß, *Ruthenium Pincer Complexes for acceptorless Alcohol Dehydrogenation and Dehydrocoupling of Ammonia Borane*, Diploma Thesis, TU München, **2008**.

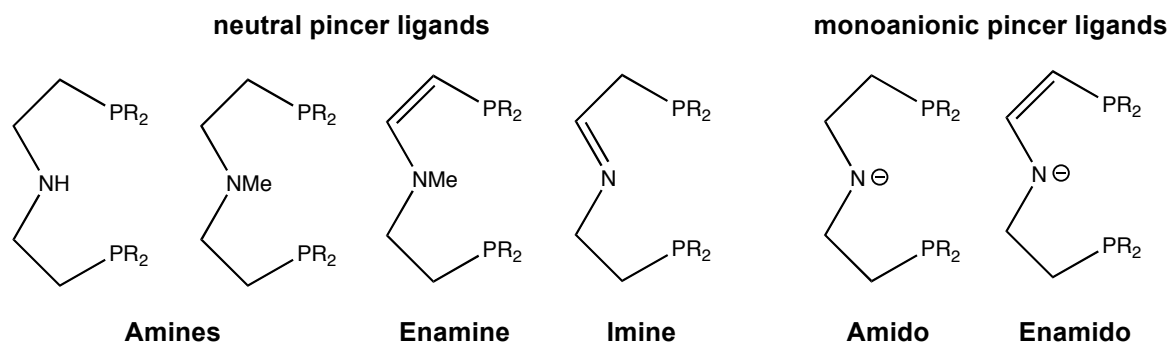


Figure A-5. PNP pincer ligands presented in this thesis ($R = i\text{Pr}$).

In the present thesis, the coordination chemistry of d^6 ($M = \text{Ru}^{\text{II}}$) and d^8 ($M = \text{Ir}^{\text{I}}$) $M(\text{PNP})$ fragments with amine, enamine, imine, amido and enamido ligands derived from the parent ethylene bridged PNP chelate framework is presented (Figure A-5). Particular emphasis will be put on the description of late transition metal amido bonding and the fundamental reactivity of the $M\text{-NR}_2$ functional group. The thermodynamic aspects of the $M\text{-N}$ bonding will be contextualized in terms of the reactivity with respect to the activation of H_2 , C-H , B-H and N-H bonds. Furthermore, the *cooperative* acceptorless dehydrogenation of borane-amine adducts as catalytic application is described and discussed mechanistically.

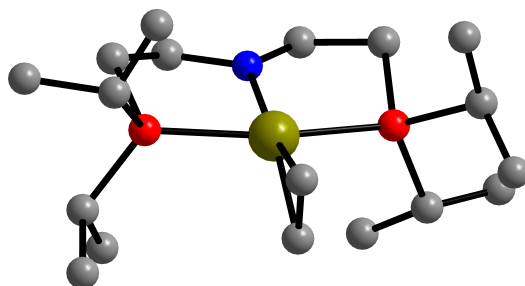
B Results and Discussion

1 Published Research Articles

1.1 Iridium Olefin Complexes bearing Dialkylamino/amido PNP Pincer Complexes: Synthesis, Reactivity, and Solution Dynamics

This chapter originated the following publication:

Anja Friedrich, Rajshekhar Ghosh, Roman Kolb, Eberhardt Herdtweck, Sven Schneider
Organometallics **2009**, 28, 208.



1.1.1 Abstract

The reaction of $[\text{IrCl}(\text{COE})_2]_2$ (**1**, COE = cyclooctene) with pincer ligand $\text{HN}(\text{CH}_2\text{CH}_2\text{P}^i\text{Pr}_2)_2$ ((PNP)^H) and AgPF_6 gives iridium(I) amino olefin complex $[\text{Ir}(\text{COE})(\text{PNP})^H]\text{PF}_6$ (**3**^{COE}-PF₆). Without anion exchange, the stability of **3**^{COE}-Cl is highly solvent dependent. In benzene or THF a mixture of amido complex $[\text{Ir}(\text{COE})(\text{PNP})]$ (**4**^{COE}), $[\text{IrHCl}_2(\text{PNP})^H]$ (**5**), and $[\text{IrHCl}(\text{C}_8\text{H}_{13})(\text{PNP})^H]$ (**6**) with a vinylic cyclooctenyl ligand is obtained. A pathway is proposed that includes concurrent trapping of intramolecular C-H vs. intermolecular N-H activation products. **3**^L-PF₆ (L = C₂H₄, C₃H₆, CO) are prepared by olefin substitution. Deprotonation with KO^tBu gives the corresponding amido complexes $[\text{IrL}(\text{PNP})]$ (**4**^L; L = COE, C₂H₄, CO). Reversible COE C-H activation is proposed to account for the fluxional behavior of **3**^{COE}-PF₆ in solution as compared with the structural rigidity of **4**^{COE} which points towards strong N→Ir π-donation in the amido complexes.

1.1.2 Introduction

In the past years, late transition metal complexes bearing pincer ligands have been utilized in numerous stoichiometric and catalytic reactions, such as Heck coupling,^[1] alkane dehydrogenation,^[2] N-H activation,^[3] or olefin hydroamination.^[4,5] With group 9 metals, particularly diphosphino pincers have proven to be effective ligands supporting intermolecular C-H activation reactions.^[2,6] Recently, Krogh-Jespersen *et al.* examined

¹ (a) Ohff, M.; Ohff, A.; van der Boom, M. E.; Milstein, D. *J. Am. Chem. Soc.* **1997**, *119*, 11687.

² Goldman, A. S.; Renkema, K. B.; Czerw, M.; Krogh-Jespersen, K. In *Activation and Functionalization of C-H Bonds*; Goldberg, K. I., Goldman, A. S., Eds.; ACS Symposium Series 885; American Chemical Society: Washington, DC, 2004; pp 198.

³ (a) Kanzelberger, M.; Zhang, X.; Emge, T. J.; Goldman, A. S.; Zhao, J.; Incarvito, C.; Hartwig, J. F. *J. Am. Chem. Soc.* **2003**, *125*, 13644. (b) Zhao, J.; Goldman, A. S.; Hartwig, J. F. *Science* **2005**, *307*, 1080. (c) Sykes, A. C.; White, P.; Brookhart, M. *Organometallics* **2006**, *25*, 1664. (d) Fafard, C. D.; Adhikari, D.; Foxman, B. M.; Mindiola, D. J.; Ozerov, O. V. *J. Am. Chem. Soc.* **2007**, *129*, 10318.

⁴ (a) Michael, F. E.; Cochran, B. M. *J. Am. Chem. Soc.* **2006**, *128*, 4246. (b) Cochran, B. M.; Michael, F. E. *J. Am. Chem. Soc.* **2008**, *130*, 2786.

⁵ van der Boom, M. E.; Milstein, D. *Chem. Rev.* **2003**, *103*, 1759.

⁶ For recent examples see: (a) Fan, L.; Parkin, S.; Ozerov, O. V. *J. Am. Chem. Soc.* **2005**, *127*, 16772. (b) Feller, M.; Karton, A.; Leitun, G.; Martin, J. M. L.; Milstein, D. *J. Am. Chem. Soc.* **2006**, *128*, 12400. (c) Ben-Ari, E.; Leitun, G.; Shimon, L. J. W.; Milstein, D. *J. Am. Chem. Soc.* **2006**, *128*, 15390. (d) Kloek, S. M.; Heinekey, M.;

theoretically and experimentally the thermodynamics of RH (R = H, aryl, alkyl) oxidative addition to (*p*-R'-PCP)IrL (*p*-R'-PCP = *p*-R'-C₆H₂-1,3-(CH₂PR''₂)₂; L = no ligand, CO, H₂), rationalizing the results in terms of C_{PCP}-Ir MO interactions.^[7] Variation of the *para* aryl substituent R' showed that RH addition to the parent (*p*-R'-PCP)Ir fragment is favored by increasing C_{PCP}→Ir π-donation due to a destabilizing filled-filled C_{PCP}-Ir repulsion. However, the influence of strongly π-donating auxiliary ligands, such as amides, on C-H bond activation reactions is not well examined. Ozerov and coworkers have recently studied halobenzene C-H and C-X oxidative addition to the diarylamido pincer fragment (PNP)'Ir ((PNP)' = N(C₆H₃-4-Me-2-P'Pr₂)₂; Figure 1 B).^[6a] Milstein and coworkers have demonstrated, that the backbone methylene groups of pyridine based pincer complex [(PNP)*Ir(COE)]⁺ ((PNP)* = C₅H₃N(CH₂P'Bu₂)₂; COE = cyclooctene) can be reversibly deprotonated. The resulting isolable amido complex adds benzene across the ligand backbone under mild conditions.^[6c]

This example illustrates the utilization of a *cooperating ligand*, which undergo reversible chemical transformations during the crucial bond activation steps.^[8] In catalysis, this concept has been applied successfully to transfer hydrogenation of polar double bonds E=CRR' (E = O, NR''), where the heterolytic activation of H₂ by Ru amido complexes was coined *bifunctional catalysis*.^[9] Grützmacher and coworkers recently used Iridium amido complexes for highly efficient transfer hydrogenation with benzochinone as hydrogen acceptor.^[10] The proposed catalytic cycle comprises stepwise N-H deprotonation, one electron oxidation, and H-transfer from the alcohol substrate and was therefore compared with the galactose oxidase catalyzed dehydrogenation of primary alcohols. Furthermore, they were able to isolate the

Goldberg, K. I. *Organometallics* **2006**, 25, 3007. (e) Whited, M. T.; Grubbs, M. T. *J. Am. Chem. Soc.* **2008**, 130, 5874.

⁷ Krogh-Jespersen, K; Czerw, M.; Zhu, K.; Singh, B.; Kanzelberger, M.; Darji, N.; Achord, P. D.; Renkema, K. B.; Goldman, A. S. *J. Am. Chem. Soc.* **2002**, 124, 10797.

⁸ Grützmacher, H. *Angew. Chem.* **2008**, 120,1838; *Angew. Chem. Int. Ed.* **2008**, 47, 1814.

⁹ (a) Noyori, R.; Ohkuma, T. *Angew. Chem. Int. Ed.* **2001**, 40, 40. (b) Clapham, S. E.; Hadzovic, A.; Morris, R. H. *Coord. Chem. Rev.* **2004**, 248, 2201. (c) Muniz, K *Angew. Chem. Int. Ed.* **2005**, 44, 6622.

¹⁰ Königsmann, M.; Donati, N.; Stein, D.; Schönberg, H.; Harmer, J.; Sreekanth, A.; Grützmacher, H. *Angew. Chem.* **2007**, 119, 3637; *Angew. Chem. Int. Ed.* **2007**, 46, 3567.

oxidation product of a rhodium(I) amide, which was described as a metal stabilized persistent aminoyl radical cation.^[11]

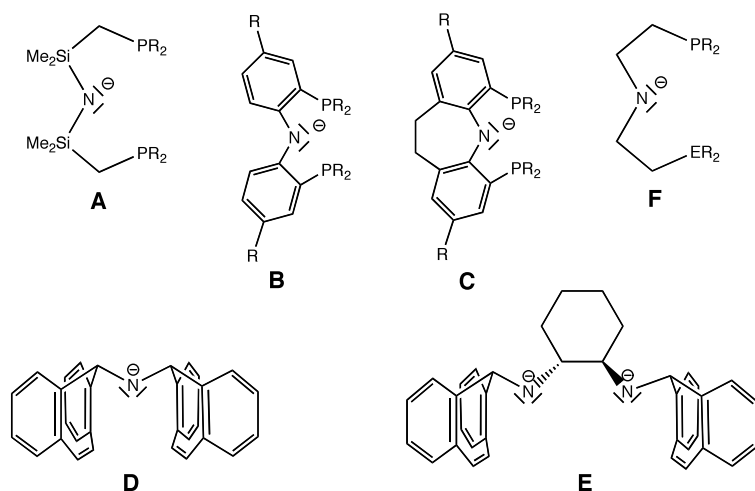


Figure 1. Amido chelate ligands used with group 9 metals.

Given this recent interest in late metal amido complexes for heterolytic and homolytic bond activation, the chemistry of group 9 amides is not well developed. Based on the pioneering work of Fryzuk,^[12] Caulton described the synthesis of disilylamido complexes (Figure 1, A),^[13] and Ozerov and coworkers utilized diarylamido pincers (Figure 1, B and C).^[6a,14]

¹¹ Büttner, T.; Geier, J.; Frison, G.; Harmer, J.; Calle, C.; Schweiger, A.; Schönberg, H.; Grützmacher, H. *Science* **2005**, *307*, 235.

¹² (a) Fryzuk, M. D.; MacNeil, P. a. *Organometallics* **1983**, *2*, 355. (b) Fryzuk, M. D.; MacNeil, P. A. *Organometallics* **1983**, *2*, 682. (c) Fryzuk, M. D.; MacNeil, P. A.; Rettig, S. J. *Organometallics* **1985**, *4*, 1145. (d) Fryzuk, M. D.; MacNeil, P. A.; Rettig, S. J. *J. Am. Chem. Soc.* **1985**, *107*, 6708. (e) Fryzuk, M. D.; MacNeil, P. A.; Rettig, S. J. *Organometallics* **1986**, *5*, 2469. (f) Fryzuk, M. D.; MacNeil, P. A.; McManus, N. T. *Organometallics* **1987**, *6*, 882. (g) Fryzuk, M. D.; MacNeil, P. A.; Rettig, S. J. *J. Am. Chem. Soc.* **1987**, *109*, 2803. (h) Fryzuk, M. D.; Bhangu, K. *J. Am. Chem. Soc.* **1988**, *110*, 961. (i) Fryzuk, M. D.; Huang, L.; McManus, N. T.; Paglia, P.; Rettig, S. J.; White, G. S. *Organometallics* **1992**, *11*, 1979. (j) Fryzuk, M. D.; Gao, X.; Joshi, K.; MacNeil, P. A.; Massey, R. L. *J. Am. Chem. Soc.* **1993**, *115*, 10581. (k) Fryzuk, M. D.; Gao, X.; Rettig, S. J. *J. Am. Chem. Soc.* **1995**, *117*, 3106.

¹³ (a) Ingleson, M.; Fan, H.; Pink, M.; Tomaszewski, J.; Caulton, K. G. *J. Am. Chem. Soc.* **2006**, *128*, 1804. (b) Ingleson, M. J.; Fullmer, B. C.; Buschhorn, D. T.; Fan, H.; Pink, Maren; Huffman, J. C.; Caulton, K. G. *Inorg. Chem.* **2008**, *47*, 407. (c) Verat, A. Y.; Pink, M.; Fan, H.; Tomaszewski, J.; Caulton, K. G. *Organometallics* **2008**, *27*, 166.

However, complexes with more π -basic dialkylamido ligands are particularly scarce, presumably due to the intrinsic tendency to undergo β -H elimination.^[15] Some rare examples are the rhodium and iridium complexes with biscycloheptatrienylamido and biscycloheptatrienyldiamido based chelate ligands developed by the Grützmacher group (Figure 1, **D** and **E**).^[11,16] Recently, Abdur-Rashid, Gusev, and co-workers used bis(2-phosphinoethyl)amido and 2-phosphinoethyl-2-aminoethylamido ligands to stabilize the iridium(III) amides [Ir(H)₂(PNP)] (PNP = N(CH₂CH₂P^{*i*}Pr₂)₂) and [Ir(H)₂(PNN)] (PNN = ^{*i*}Pr₂PCH₂CH₂NCH₂CH₂NEt₂) (**F**).^[17] Both complexes are highly active catalysts for the transfer hydrogenation of ketones with 2-propanol and the postulated Noyori-Morris-type mechanism was recently confirmed in a theoretical examination.^[18] However, no PNP iridium(I) complexes were reported.

In this manuscript we describe the synthesis and reaction pathways toward a new class of iridium(I) amino and amido complexes bearing the pincer ligands HN(CH₂CH₂P^{*i*}Pr₂)₂ ((PNP)^H) and N(CH₂CH₂P^{*i*}Pr₂)₂ (PNP). Ligand N-H activation, vinylic olefin C-H activation, solution dynamics, and amino/amido bonding to the metal, which distinguish this ligand type from related diphosphine pincers will be discussed.

1.1.3 Results

Reaction of [IrCl(COE)₂]₂ (**1**) with (PNP)^H: Solvent influence

Clarke et al. reported that the reaction of [IrCl(COE)₂]₂ (**1**, COE = cyclooctene) with (PNP)^H in 2-propanol at 80 °C results in the formation of [Ir(H)₂Cl(PNP)^H] (**2**) (Scheme

¹⁴ (a) Ozerov, O. V.; Guo, C.; Papkov, V. A.; Foxman, B. M. *J. Am. Chem. Soc.* **2004**, *126*, 4792-4793. (b) Weng, W.; Guo, C.; Moura, C.; Yang, L.; Fowman, B. M.; Ozerov, O. V. *Organometallics* **2005**, *24*, 3487-3499. (c) Gatard, S.; Çelenligil-Çetin, R.; Foxman, B. M.; Ozerov, O. V. *J. Am. Chem. Soc.* **2006**, *128*, 2808-2809.

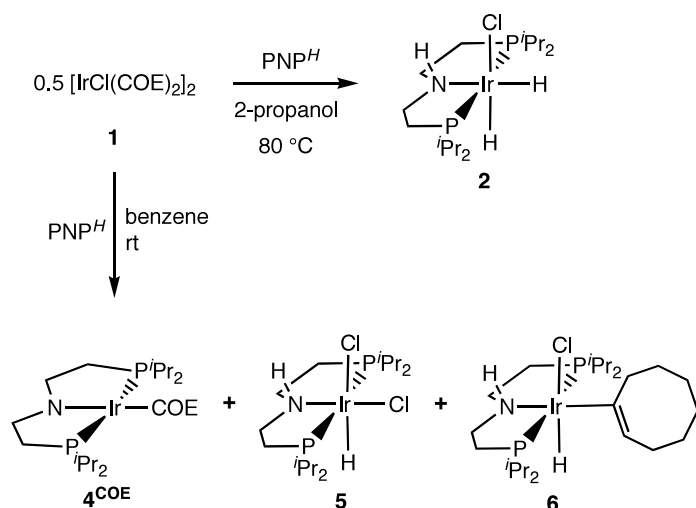
¹⁵ Bryndza, H. E.; Tam, W. *Chem. Rev.* **1988**, *88*, 1163-1188.

¹⁶ (a) Maire, P.; Büttner, T.; Breher, F.; Le Floch, P.; Grützmacher, H. *Angew. Chem.* **2005**, *117*, 6477-6481. (b) Maire, P.; Breher, F.; Grützmacher, H. *Angew. Chem.* **2005**, *117*, 6483-6487. (c) Maire, P.; Breher, F.; Schönberg, H.; Grützmacher, H. *Organometallics* **2005**, *24*, 3207-3218. (d) Maire, P.; Königsmann, M.; Sreekanth, A.; Harmer, J.; Schweiger, A.; Grützmacher, H. *J. Am. Chem. Soc.* **2006**, *128*, 6578-6580.

¹⁷ (a) Clarke, Z. E.; Maragh, P. T.; Dasgupta, T. P.; Gusev, D. G.; Lough, A. J.; Abdur-Rashid, K. *Organometallics* **2006**, *25*, 4113-4117. (b) Choualeb, A.; Lough, A. J.; Gusev, D. G. *Organometallics* **2007**, *26*, 5224-5229.

¹⁸ Bi, S.; Xie, Q.; Zhao, X.; Zhao, Y.; Kong, X. *J. Organomet. Chem.* **2008**, *693*, 633-638.

1).^[17a] However, monitoring the reaction of **1** with (PNP)^H in 2-propanol at room temperature by ³¹P NMR spectroscopy we observed quantitative formation of iridium(I) amino olefin complex [Ir(COE)(PNP)^H]Cl (**3^{COE}-Cl**) by comparison with **3^{COE}-PF₆** which was synthesized and fully characterized by anion exchange (*vide infra*). To avoid hydride transfer from the solvent the reaction was carried out in benzene, resulting in a 1:1 mixture of iridium(I) amido complex [Ir(COE)(PNP)] (**4^{COE}**) and iridium(III) hydride [IrHCl₂(PNP)^H] (**5**) (Scheme 1). Furthermore, C-H activation product [IrHCl(C₈H₁₃)(PNP)^H] (**6**) with a vinylic cyclooctenyl ligand was observed as a minor product in around 15 % yield. **5** is easily isolated by extraction of **4^{COE}** and **6** with pentane. While **4^{COE}** was synthesized and fully characterized on another route (*vide infra*), **6** could not be isolated and was characterized from this mixture by multinuclear NMR.



Scheme 1. Reaction of [IrCl(COE)₂]₂ (**1**) with HNCH₂CH₂PⁱPr₂ (PNP)^H in 2-propanol^[17a] and benzene, respectively.

Reaction of [IrCl(COE)₂]₂ (**1**) with (PNP)^H: Mechanistic studies

Monitoring the reaction of **1** with (PNP)^H in C₆D₆ by ³¹P and ¹H NMR reveals that multiple intermediates are formed over the course of 2 days at room temperature (Figure 2). Like in 2-propanol, **3^{COE}-Cl** represents the first major intermediate. The large downfield ¹H chemical shift of the broad signal assigned to the N-H proton in **3^{COE}-Cl** (9.57 ppm / C₆D₆) relative to **3^{COE}-PF₆** (4.72 ppm / C₆D₆) indicates hydrogen bonding, presumably to the chloride counter anion. [IrHCl(COE)(PNP)^H]Cl (**7-Cl**) is observed as an intermediate in an early stage of the reaction sequence decaying quickly. Two further intermediates, **8** and **9**, that could not be

B Results and Discussion

prepared independently are observed by NMR.^[19] However, the ^1H NMR spectrum of **8** strongly resembles complex **6**, indicating a vinylic cyclooctenyl ligand. On the other hand, between 3.5 and 8 ppm **9** only features a signal assignable to an N-H proton. The ^1H NMR signals for the hydride ligands of **8** (-23.39 ppm) and **9** (-23.66 ppm) are very close to each other and slightly downfield from **5** (-24.73 ppm) and **6** (-24.40 ppm). Therefore, we tentatively assign **8** and **9** to structures that are isomers of the final products **6** and **5**, respectively, with the hydride ligands in **8** and **9** in *trans* position to the $(\text{PNP})^H$ amine donor and not *trans* to the chloride ligand as in **5** and **6**.

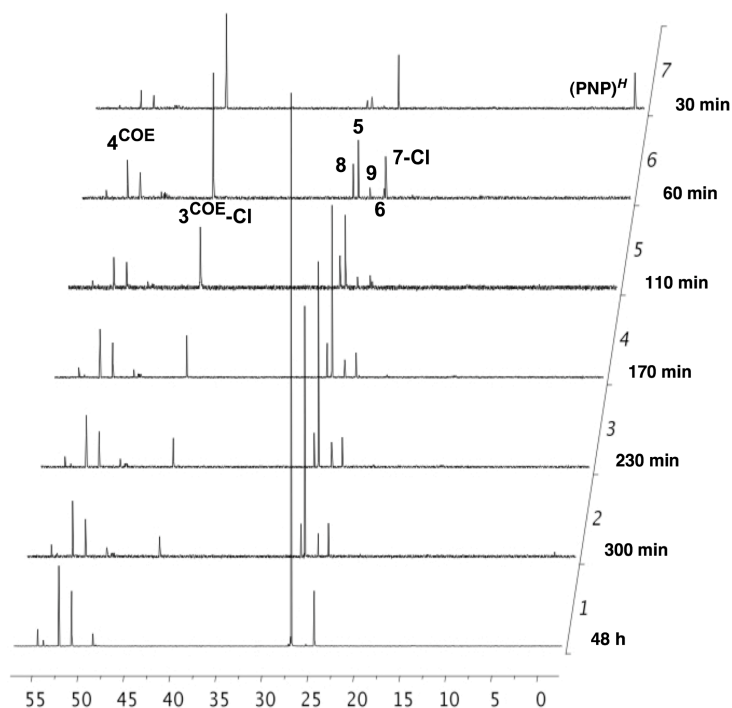
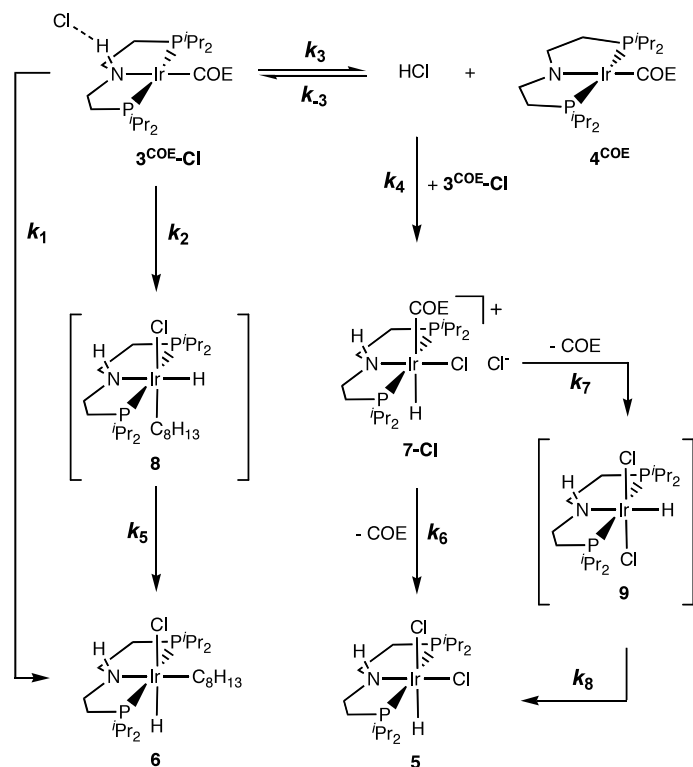


Figure 2. ^{31}P NMR spectra of the reaction of **1** with $(\text{PNP})^H$ in C_6D_6 .

These results suggest that in the reaction of **1** with $(\text{PNP})^H$ **3^{COE}-Cl** is initially formed. However, in non-protic solvents, such as benzene or THF, **3^{COE}-Cl** is not stable, slowly reacting towards **4^{COE}**, **5**, and **6**. Accordingly, **3^{COE}-PF₆** reacts with chloride sources such as

¹⁹ Selected NMR data of **8** (C_6D_6 , rt, [ppm]): ^1H NMR (399.78 MHz) δ -23.39 (t, $^2J_{\text{HP}} = 14.4$ Hz, 1H, Ir-H), 2.94 (t, $^3J_{\text{HH}} = 5.5$ Hz, 2H, IrCCH₂), 3.83 (br, 1H, NH), 6.27 (t, $^3J_{\text{HH}} = 8.6$ Hz, 1H, =CH). ^{31}P $\{^1\text{H}\}$ NMR (161.8 MHz): δ 25.8 (s, P^iPr_2). Selected NMR data of **9** (C_6D_6 , rt, [ppm]): ^1H NMR (399.78 MHz) δ = -23.66 (t, $^2J_{\text{HP}} = 13.6$ Hz, 1H, Ir-H), 6.36 (br, 1H, NH). ^{31}P $\{^1\text{H}\}$ NMR (161.8 MHz): δ 27.7 (s, P^iPr_2).

[PPh₄]Cl or [NⁿBu₃(CH₂Ph)]Cl in C₆H₆ or THF to give an equimolar amount of **4**^{COE} and **5** in combination with cyclooctenyl complex **6**, the latter in a slightly higher yield (approximately 20 %). Based on the intermediates found for this reaction a pathway is proposed (Scheme 2).



Scheme 2. Proposed pathway for the formation of **4**^{COE}, **5**, and **6** from **3**^{COE}-Cl. Iridium species in square brackets are not fully characterized.

To check for the viability of the model in scheme 2, the kinetics of the reaction of **3**^{COE}-PF₆ with chloride were studied by ³¹P NMR spectroscopy. Kinetic experiments were conducted at 295 and 300 K in THF due to a lack of a suitable water free chloride source that was soluble enough in benzene at the initial concentration [**3**^{COE}-PF₆]₀ = 57.7 mM and even in THF the equimolar amount of [NⁿBu₃(CH₂Ph)]Cl was not fully soluble.^[20] However, plots of ln [**3**^{COE}-PF₆] vs. time (Figure 3) were linear over three half-lives with *k*_{obs} at 3.2 × 10⁻³ min⁻¹ (298 K) and 4.5 × 10⁻³ min⁻¹ (300 K) indicating that preequilibria such as dissolution of [NⁿBu₃(CH₂Ph)]Cl or formation of a **3**^{COE}-Cl precomplex are fast vs. the decay of **3**^{COE}-Cl. Addition of COE did not affect *k*_{obs}. The concentrations of **3**^{COE}-Cl, **4**^{COE}, **5**, **6**, **7**-Cl, **8**, and **9**

²⁰ The solubility of [NBu₃CH₂Ph]Cl in *d*₈-THF at 295 K was derived by NMR spectroscopy (10 mM).

B Results and Discussion

were fitted to the model outlined in scheme 2 featuring a reasonable correlation of the simulation with experimental results (Figure 3 and chapter B1.1.8).

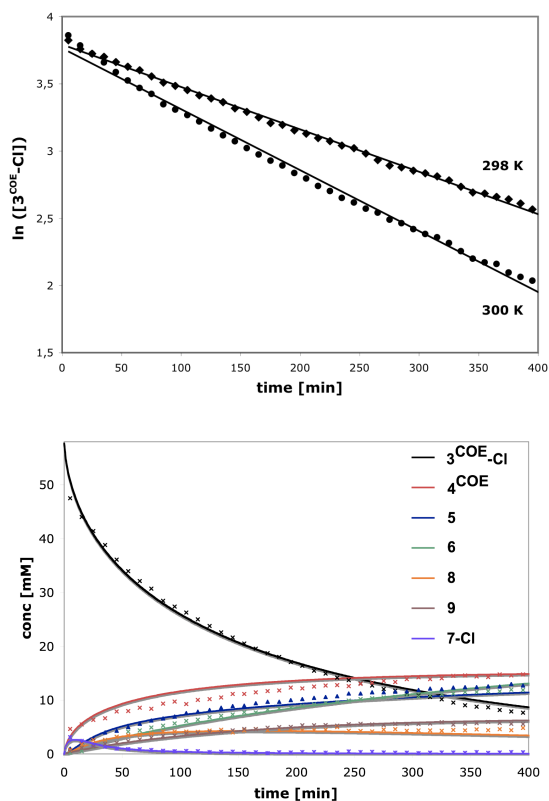
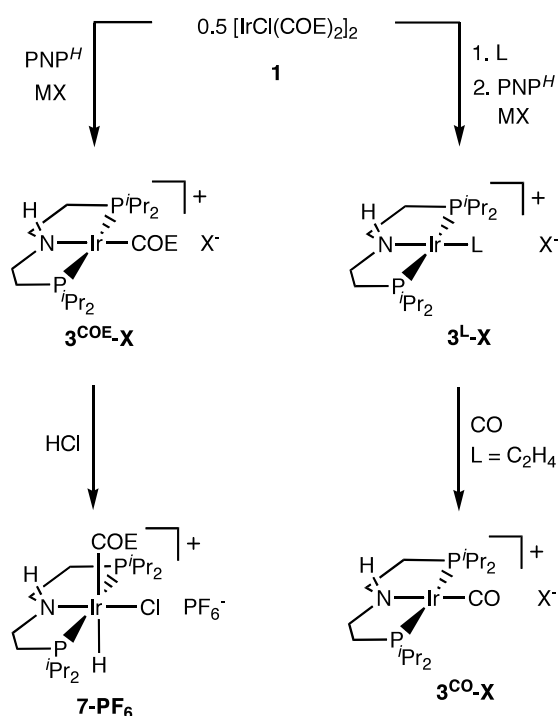


Figure 3. *Top:* Decay of $3^{\text{COE-Cl}}$ in THF at 298 K and 300 K. *Bottom:* Concentration vs. time plot of the reaction of $3^{\text{COE-PF}_6}$ with $[\text{NBu}_3(\text{CH}_2\text{Ph})]\text{Cl}$ in THF at 300 K with experimental (crosses) and fitted (lines) concentrations based on the proposed pathway in scheme 2.

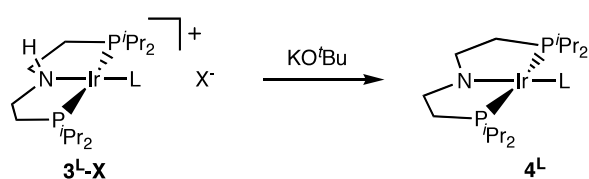
Syntheses of stable iridium PNP complexes

The reaction of **1** with $(\text{PNP})^{\text{H}}$ in the presence of AgPF_6 or NaBPh_4 gives $[\text{Ir}(\text{COE})(\text{PNP})^{\text{H}}]\text{X}$ ($3^{\text{COE-X}}$; $\text{X} = \text{PF}_6, \text{BPh}_4$), which are stable in organic solvents (Scheme 3). Likewise, olefin complexes $[\text{Ir}(\text{L})(\text{PNP})^{\text{H}}]\text{X}$ ($\text{L} = \text{C}_2\text{H}_4$ ($3^{\text{C}_2\text{H}_4-\text{X}}$), C_3H_6 ($3^{\text{C}_3\text{H}_6-\text{X}}$); $\text{X} = \text{PF}_6, \text{BPh}_4$) can be prepared upon *in situ* olefin exchange in high yield. Facile substitution of ethylene versus CO gives carbonyl complex $[\text{Ir}(\text{CO})(\text{PNP})^{\text{H}}]\text{X}$ ($3^{\text{CO-X}}$; $\text{X} = \text{PF}_6, \text{BPh}_4$). Oxidative addition of HCl to $3^{\text{COE-PF}_6}$ affords iridium(III) complex $[\text{IrHCl}(\text{COE})(\text{PNP})^{\text{H}}]\text{PF}_6$ (**7-PF₆**) in moderate yield.



Scheme 3. Syntheses of iridium PNP amino complexes (MX = AgPF₆, NaBPh₄; L = C₂H₄, C₃H₆).

Clean *N*-deprotonation of **3^{L-X}** (L = COE, C₂H₄, CO) is obtained by the reaction with KO^tBu in THF giving rise to [IrL(PNP)] (**4^L**; L = COE, C₂H₄, CO) (Scheme 4). Highly air sensitive amido complexes **4^L** are very soluble in nonpolar organic solvents such as benzene and pentane.



Scheme 4. Synthesis of iridium PNP amido complexes (X = PF₆, BPh₄; L = COE, C₂H₄, CO).

Spectroscopic Characterization

The iridium(I) amino complexes **3^{L-PF₆}** (L = COE, C₂H₄, C₃H₆, CO) exhibit N-H stretching frequencies in the IR spectra between 3223 and 3210 cm⁻¹, which are much closer to that of the free ligand (3285 cm⁻¹) compared with the octahedral iridium(III) complexes [IrH₃(PNP)^H] (3140 cm⁻¹),^[17a] **2** (3171 cm⁻¹),^[17a] and **5** (3130 cm⁻¹). While N-H⋯H-Ir hydrogen

B Results and Discussion

bonding was proposed for $[\text{IrH}_3(\text{PNP})^H]$,^[17a] N-H...Cl-Ir hydrogen bonding could account for the low N-H stretching vibration in **2** and **5**. The CO stretching vibration of $\mathbf{3}^{\text{CO}}\text{-PF}_6$ was observed at 1976 cm^{-1} . Deprotonation of the pincer ligand results in a strong bathochromic shift of this band ($\mathbf{4}^{\text{CO}}$: 1908 cm^{-1}) indicating a large increase of electron density at the metal center.

The six coordinate iridium(III) amino complexes **5**, **6**, and **7-PF₆** feature similar solution NMR spectra for the $(\text{PNP})^H$ chelate as **2**.^[17] The singlet in the ^{31}P NMR spectrum, four ^1H NMR peaks in the methyl region (doublets of virtual triplets), and two ^1H NMR signals assignable to methyne groups, indicate a meridional arrangement of the $(\text{PNP})^H$ pincer ligand with two sets of chemically inequivalent *iso*-propyl substituents each bearing diastereotopic methyl groups, respectively. Accordingly, four signals can be assigned to the ethylene backbone protons which appear as complex multiplets owing to the ABCDXX' spin system. The hydride chemical shifts of **5** (-24.73 ppm) and **6** (-24.40 ppm) suggest a *trans* arrangement to a chloride ligand and that of **7-PF₆** (-17.83 ppm) indicates a location *trans* to the olefin, as a result of HCl *cis* oxidative addition to $\mathbf{3}^{\text{COE}}\text{-PF}_6$.^[21] The NMR signals for the cyclooctenyl ligand of **6** are in agreement with vinylic C-H activation featuring the vinylic proton at 6.06 ppm and the olefinic carbon atoms at 124.0 ppm and 134.7 ppm , respectively.

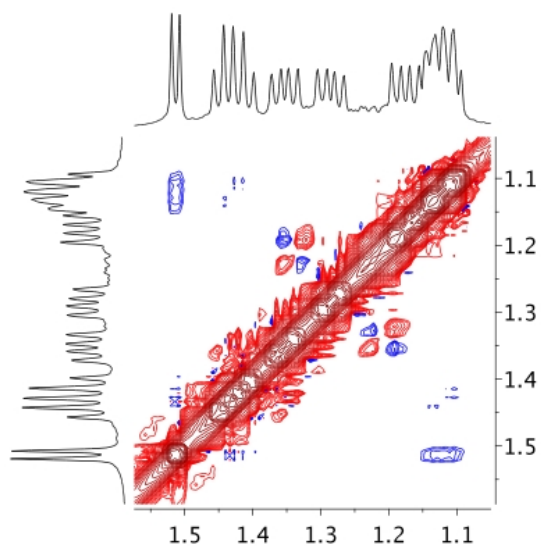


Figure 4. Methyl region of the ^1H -ROESY NMR spectrum of $\mathbf{3}^{\text{C}_3\text{H}_6}\text{-PF}_6$.

²¹ (a) Blake, D. M.; Kubota, M. *Inorg. Chem.* **1970**, *9*, 989. (b) Johnson, C. E.; Eisenberg, R. *J. Am. Chem. Soc.* **1985**, *107*, 6531.

Solution NMR spectra of iridium(I) amino complexes $\mathbf{3}^{\text{C}^{2\text{H}4}}\text{-PF}_6$, $\mathbf{3}^{\text{COE}}\text{-PF}_6$, and $\mathbf{3}^{\text{CO}}\text{-PF}_6$ resemble those of iridium(III) complexes $\mathbf{5}$, $\mathbf{6}$, and $\mathbf{7}\text{-PF}_6$ with respect to the number and coupling pattern of the (PNP)^H ligand signals, suggesting C_s symmetry on the NMR time scale. In contrast to this, propylene complex $\mathbf{3}^{\text{C}^{3\text{H}6}}\text{-PF}_6$ features two sharp doublets in the ³¹P NMR spectrum with a typical *trans* ²J_{PP} coupling constant (307 Hz). Furthermore, ¹H and ¹³C signals for the (PNP)^H ligand are in agreement with the absence of the virtual plane suggesting olefin rotation to be hindered on the NMR time scale for $\mathbf{3}^{\text{C}^{3\text{H}6}}\text{-PF}_6$. This interpretation is further backed by a ¹H-ROESY spectrum, where the doublet signal for the propylene methyl group (1.51 ppm) exhibits cross peaks only with two of the eight chemically inequivalent pincer methyl groups (Figure 4).

The mirror symmetry found for $\mathbf{3}^{\text{COE}}\text{-PF}_6$ at room temperature indicates fluxional behavior at room temperature on the NMR time scale. Addition of 0.5 equiv. COE to a solution of $\mathbf{3}^{\text{COE}}\text{-PF}_6$ in *d*₈-THF at room temperature does not result in broadening of the free (5.63 ppm) or bound (3.54 ppm) olefin ¹H NMR signals, respectively. Furthermore, a ¹H-EXSY NMR spectrum at room temperature does not indicate slow olefin exchange (chapter B1.1.7).^[22] As in $\mathbf{3}^{\text{C}^{2\text{H}4}}\text{-PF}_6$, four sharp peaks for the $\mathbf{3}^{\text{COE}}\text{-PF}_6$ backbone ethylene bridges suggest high barriers for inversion of the pyramidal amine nitrogen atom. The effect of amine inversion can be demonstrated by fast N-H proton exchange: Addition of 1 equiv. of *p*-methylphenol to the corresponding amido complex $\mathbf{4}^{\text{COE}}$ (*vide infra*) results in C_{2v} symmetry on the NMR time scale owing to fast O-H / N-H proton exchange. Cooling to -60 °C slows down the equilibrium and the signals for $\mathbf{3}^{\text{COE}}\text{-OC}_7\text{H}_7$ and $\mathbf{4}^{\text{COE}}$ are observed. While nitrogen inversion was not observed for $\mathbf{3}^{\text{COE}}\text{-PF}_6$, the ¹⁵N chemical shift (δ = -318.8 ppm, ¹H-¹⁵N HSQC) in *d*⁸-THF shows a small coordination shift relative to the free ligand (δ = -331.2 ppm, ¹H-¹⁵N HMBC),^[23] indicating weak nitrogen coordination to the metal.^[24] Furthermore, the $\mathbf{3}^{\text{COE}}\text{-PF}_6$ ¹J_{H-N} coupling constant (-72 Hz) suggests the absence of strong M···H-N interactions.^[25,26]

²² Perrin, C. L.; Dwyer, T. J. *Chem. Rev.* **1990**, *90*, 935.

²³ No signal was found in the ¹H-¹⁵N HSQC NMR spectrum of (PNP)^H, presumably due to rapid N-H exchange on the NMR time scale.

²⁴ Mason, J. *Chem. Rev.* **1981**, *81*, 205.

²⁵ The ¹J_{HN} coupling constant of HNMe₂ was reported to be -67 Hz: Alei Jr., M.; Florin, A. E.; Litchman, W. M.; O'Brien, J. F. *J. Phys. Chem.* **1971**, *75*, 932.

B Results and Discussion

To further elucidate the fluxional behavior of $3^{\text{COE}}\text{-PF}_6$, the amino olefin complexes were studied by VT NMR. Cooling of a $3^{\text{C}^2\text{H}^4}\text{-PF}_6$ solution in d_6 -acetone to $-90\text{ }^\circ\text{C}$ does not result in broadening of the ^{31}P and ^1H NMR peaks. However, propylene complex $3^{\text{C}^3\text{H}^6}\text{-PF}_6$ exhibits successive broadening of the two ^{31}P NMR doublets with coalescence of the downfield signal at around $-80\text{ }^\circ\text{C}$ (chapter B1.1.7). Low temperature ^{31}P NMR of $3^{\text{COE}}\text{-PF}_6$ in d_6 -acetone reveals that the sharp room temperature signal splits at around $-65\text{ }^\circ\text{C}$ into two broad peaks as would be expected for freezing olefin rotation. However, cooling below $-90\text{ }^\circ\text{C}$ in d_8 -THF results in further splitting of the ^{31}P NMR signals resulting in a complex pattern of broad peaks at $-100\text{ }^\circ\text{C}$, similar to $3^{\text{C}^3\text{H}^6}\text{-PF}_6$ (Figure 5). Between $+25$ and $-100\text{ }^\circ\text{C}$, no peaks assignable to hydrides were found by ^1H NMR spectroscopy, but all ^1H NMR peaks exhibit very strong broadening with half widths at $-100\text{ }^\circ\text{C}$ of around 40 Hz. Furthermore, the sharp ^{31}P and ^{19}F NMR signals of the $3^{\text{COE}}\text{-PF}_6$ counter anion remain unchanged down to $-100\text{ }^\circ\text{C}$.

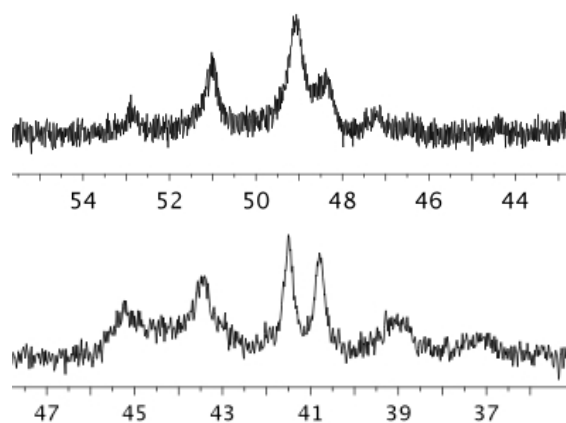


Figure 5. Top: ^{31}P NMR spectrum of $3^{\text{C}^3\text{H}^6}\text{-PF}_6$ in d_6 -acetone at 183 K. Bottom: ^{31}P NMR spectrum of $3^{\text{COE}}\text{-PF}_6$ in d_8 -THF at 173 K.

NMR spectra of ethylene amido complexes 4^{C^2H^4} and 4^{CO} are in agreement with C_{2v} symmetry, implying planarization of the dialkylamido backbone on the NMR timescale. On the other hand, NMR spectra of 4^{COE} indicate the loss of the mirror plane defined by N, Ir, and the olefinic carbon atoms, resulting in two sharp ^{31}P NMR doublets with a $^2J_{\text{PP}}$ *trans*

²⁶ (a) Pregosin, P. S.; Rügger, H.; Wombacher, F.; van Koten, G.; Grove, D. M.; Wehman-Ooyevaar, I. C. M. *Magn. Res. Chem.* **1992**, *30*, 548. (b) Lee Jr., J. C.; Müller, B.; Pregosin, P.; Yap, G. P. A.; Rheingold, A. L.; Crabtree, R. H. *Inorg. Chem.* **1995**, *34*, 6295. (c) Yao, W.; Eisenstein, O.; Crabtree, R. H. *Inorg. Chim. Acta* **1997**, *254*, 105.

coupling constant of 373 Hz. No peak broadening of these signals was observed upon heating to 100°C in d_8 -toluene.

X-ray crystal structure determinations

$3^{C^{2H_4}}-PF_6$, $3^{CO}-PF_6$, $4^{C^{2H_4}}$, 4^{CO} , and **5** were characterized by single crystal X-ray diffraction. Repeated crystallization attempts for $3^{COE}-PF_6$ and $3^{COE}-BPh_4$ resulted in heavily disordered crystals. However, the constitution and conformation of the (PNP)^H backbone in the $3^{COE}-BPh_4$ cation were confirmed to be isostructural with $3^{C^{2H_4}}-PF_6$ and $3^{CO}-PF_6$ (chapter B1.1.9).

The molecular structure of complex **5** (Figure 6, Table 1) in the solid state strongly resembles that of dihydrido chloro compound **2** which was reported by Clarke *et al.*^[17a] As a major difference, the Ir-N1 bond is considerably shorter in **5** ($\Delta D_{Ir-N} = 0.1 \text{ \AA}$), owing to the weaker *trans*-influence of chloride compared with a hydride ligand. The metal centre in **5** is located in a slightly distorted octahedral coordination geometry with a (PNP)^H chelate bite angle of 165.81(5)°. Further distortion arises from bending of C12 towards amine proton H1 (Cl2-Ir1-N1: 85.6(1)°) indicative of H1...Cl2 hydrogen bonding (H1...Cl2: 2.70 Å), which is in agreement with IR spectroscopic results.

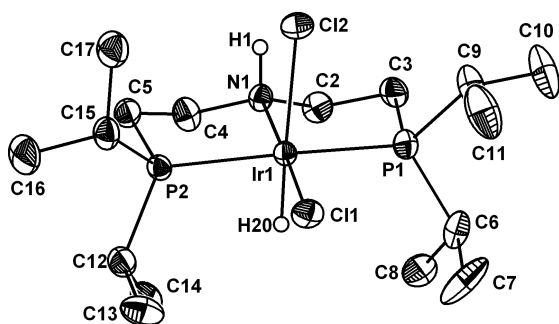


Figure 6. DIAMOND plot of **5** in the crystal (one of the two independent molecules) with thermal ellipsoids drawn at the 50% probability level. Hydrogen atoms other than H1 and H20 are omitted for clarity.

B Results and Discussion

Table 1. Selected bond lengths and angles of **2**^[17a] and **5** (one of two independent molecules in the unit cell) in the crystal.

	5		2 ^[17a]
Bond Lengths (Å)			
Ir1-H20	1.41(7)	Ir1-H1 _{Ir} [‡]	1.36(5)
Ir1-Cl1	2.386(1)	Ir1-H2 _{Ir} [‡]	1.63(5)
Ir1-Cl2	2.524(2)	Ir1-Cl1	2.506(1)
Ir1-N1	2.091(4)	Ir1-N1	2.187(3)
Ir1-P1	2.296(2)	Ir1-P1	2.276(1)
Ir1-P2	2.293(2)	Ir1-P2	2.276(1)
H1⋯Cl2	2.70(X)	H1 _N ⋯Cl1 [‡]	2.58(7)
Bond angles (°)			
Cl2-Ir1-N1	85.6(1)	Cl1-Ir-N1	86.8(1)
Cl1-Ir1-Cl2	92.71(5)	Cl1-Ir-H2 _{Ir} [‡]	91(2)
N1-Ir1-Cl1	176.9(1)	N1-Ir1-H2 _{Ir} [‡]	178(2)
P1-Ir1-P2	165.81(5)	P2-Ir1-P2	167.19(4)

[‡] H1_{Ir}: hydride *trans* to Cl1; H2_{Ir}: hydride *trans* to N1; H1_N: N-H

For iridium(I) amino complexes **3**^L-PF₆ (L = C₂H₄, CO) the structural assignments in solution are in agreement with the molecular structure in the solid state (Figure 7, Table 2). The cations feature distorted square-planar coordinated iridium centers with (PNP)^H bite angles of 166.63(4)° (**3**^{C₂H₄}-PF₆) and 166.75(6)° (**3**^{CO}-PF₆), respectively. The Ir1-H1 distances (**3**^{C₂H₄}-PF₆: 2.47(6) Å; **3**^{CO}-PF₆: 2.54 Å) and Ir1-N-H1 angles (**3**^{C₂H₄}-PF₆: 104(4)°; **3**^{CO}-PF₆: 106°) are not indicative of an intramolecular M⋯H-N interaction. The large Ir1-N1 distances (**3**^{C₂H₄}-PF₆: 2.131(4) Å; **3**^{CO}-PF₆: 2.121(6) Å) are in agreement with strong ethylene and CO *trans*-influences and weak coordinative N→M bonding. The olefinic C=C bond length in **3**^{C₂H₄}-PF₆ (C20-C21: 1.355(9) Å) is very close to the equilibrium C=C distance experimentally found for free ethylene (1.334 Å).^[27]

²⁷ Duncan, J. L. *Mol. Phys.* **1974**, *28*, 1177.

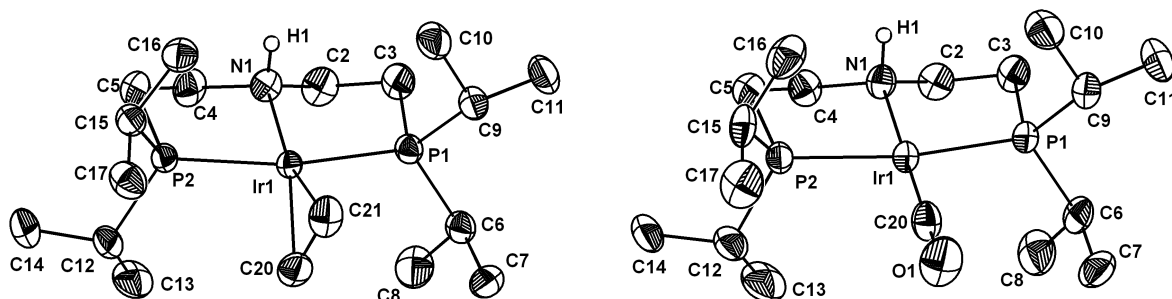


Figure 7. DIAMOND plot of the $3^{\text{C}_2\text{H}_4}\text{-PF}_6$ (left) and $3^{\text{CO}}\text{-PF}_6$ (right) cations in the crystal, respectively, with thermal ellipsoids drawn at the 50% probability level. Calculated hydrogen atoms are omitted for clarity.

The molecular structures of amido complexes 4^{C_2H_4} and 4^{CO} in the solid state (Figure 8, Table 2) confirm planarization of the amido nitrogen atom (sum of the bond angles around N1: 357° (4^{C_2H_4}), 356° (4^{CO})). Furthermore, covalent amido bonding results in significantly shorter Ir1-N1 bonds (4^{C_2H_4} : 1.99(2) Å; 4^{CO} : 2.035(4) Å) as compared with the corresponding amino complexes. Most other bond lengths and angles around the metal centers in 4^{C_2H_4} and 4^{CO} are close to those found in the respective amino complexes, indicating structural flexibility of the ethylene bridged pincer ligand. The C=C distance in 4^{C_2H_4} is considerably longer compared with $3^{\text{C}_2\text{H}_4}\text{-PF}_6$ ($\Delta D_{\text{C}=\text{C}} = 0.07$ Å) pointing towards strong M→olefin back bonding in the amido complex. Accordingly, the angle ϕ of the plane defined by the metal and the ethylene carbon atoms (Ir1, C20 and C21) with the square planar coordination polyhedron (Ir1, P1, and N1) is closer to ideal 90° ($3^{\text{C}_2\text{H}_4}\text{-PF}_6$: $72.3(4)^\circ$; 4^{C_2H_4} : $82.7(14)^\circ$). Unfortunately, the quality of the 4^{C_2H_4} crystal structure does not permit localization of the olefinic protons on the electron density map to compare pyramidalization of C20/C21 as a diagnostic tool for their hybridization.

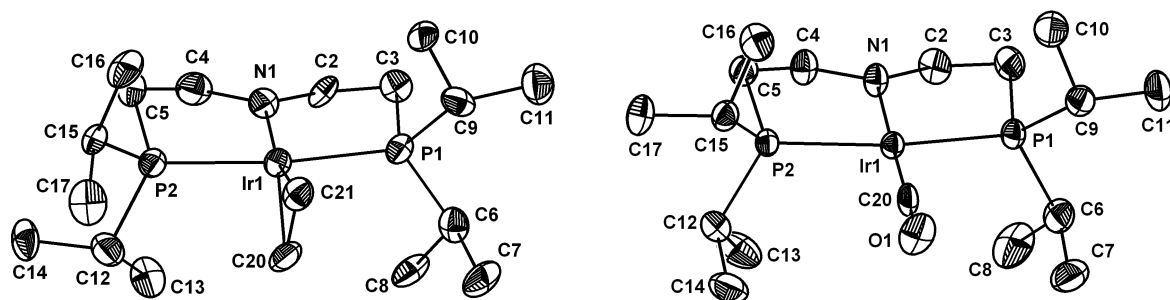


Figure 8. DIAMOND plot of $4^{C_2H_4}$ (left) and 4^{CO} (right) in the crystal, respectively, with thermal ellipsoids drawn at the 50% probability level. Hydrogen atoms are omitted for clarity.

Table 2. Selected bond lengths and angles of $3^{C_2H_4}-PF_6$, $3^{CO}-PF_6$, $4^{C_2H_4}$, and 4^{CO} in the crystal.

	$3^{C_2H_4}-PF_6$	$3^{CO}-PF_6$	$4^{C_2H_4}$	4^{CO}
Bond Lengths (Å)				
Ir1-N1	2.131(4)	2.121(6)	1.99(2)	2.035(4)
Ir1-P1	2.304(1)	2.297(2)	2.277(5)	2.284(1)
Ir1-P2	2.303(1)	2.300(2)	2.264(5)	2.281(1)
Ir1-C20	2.145(6)	1.804(7)	2.10(2)	1.839(7)
Ir1-C21	2.144(6)	-	2.17(2)	-
C20-C21	1.355(9)	-	1.42(3)	-
Bond angles (°)				
P1-Ir1-P2	166.63(4)	166.75(6)	165.49(18)	165.89(5)
N1-Ir1-C20	159.5(2)	179.8(3)	158.8(8)	177.0(2)
N1-Ir1-C21	163.7(2)	-	162.4(7)	-
Ir1-C20-O1	-	178.6(7)	-	179.3(4)
Ir1-N1-C2	113.4(3)	113.7(4)	122.4(12)	121.0(3)
Ir1-N1-C4	114.6(3)	114.7(4)	124.8(13)	122.8(4)
C2-N1-C4	111.3(4)	109.9(6)	109.5(15)	112.4(4)

1.1.4 Discussion

Reactivity and fluxional behavior of $3^{\text{COE}}\text{-PF}_6$

Scheme 2 shows our proposed model for the formation of 4^{COE} , **5**, and **6** from 3^{COE}-Cl in non-protic solvents. The reaction scheme can be broken down in two principle pathways: (1) C-H activation of the COE ligand and trapping by nucleophilic attack of the chloride at the iridium center; (2) chloride base assisted N-H activation and intermolecular HCl oxidative addition. This model explains the observed solvent dependence, as efficient solvation of the chloride ion via hydrogen bonding with protic solvents both increases the barrier to nucleophilic attack and reduces its basicity.^[28] It should be pointed out that we have no indication for intramolecular N-H activation, contrasting with other PEP (E = N, C) pincer ligands, such as $\text{HN}(\text{C}_6\text{H}_4\text{PR}_2)_2$, $\text{CH}_2(\text{C}_2\text{H}_4\text{PR}_2)_2$, or $\text{C}_6\text{H}_4(m\text{-CH}_2\text{PR}_2)_2$, where E-H oxidative addition is typically observed.^[14a,29,30]

Given the complexity of the proposed model, it is interesting that a first order rate was observed for 3^{COE}-Cl . The rate law for 3^{COE}-Cl , according to the proposed pathway, is given by:

$$r(3^{\text{COE}}\text{-Cl}) = -k_1[3^{\text{COE}}\text{-Cl}] - k_2[3^{\text{COE}}\text{-Cl}] - k_3[3^{\text{COE}}\text{-Cl}] + k_{-3}[\text{HCl}][4^{\text{COE}}] - k_4[\text{HCl}][3^{\text{COE}}\text{-Cl}] \quad (\text{eq 1})$$

This rate becomes pseudo first order assuming steady-state conditions for c_{HCl} , which is reasonable as both oxidative addition of HCl to iridium(I) (k_4) and protonation of amido complex 4^{COE} (k_{-3}) should be fast with respect to N-H deprotonation (k_3) as was found in the simulation, as well. Accordingly, calculated c_{HCl} is very small remaining below 7×10^{-4} M throughout the course of the reaction. Hence, k_{obs} for the decay of 3^{COE}-Cl ($4.5 \times 10^{-3} \text{ min}^{-1}$ at

²⁸ (a) Regan, C. K.; Craig, S. L.; Brauman, J. I. *Science* **2002**, 296, 2245. (b) Vayner, G.; Houk, K. N.; Jorgensen, W. L.; Brauman, J. I. *J. Am. Chem. Soc.* **2004**, 126, 9054. (c) Bordwell, F. G. *Acc. Chem. Res.* **1988**, 21, 456.

²⁹ Crocker, C.; Empsall, H. D.; Errington, R. J.; Hyde, E. M.; McDonald, W. S.; Markham, R.; Norton, M. C.; Shaw, B. L.; Weeks, B. *J. Chem. Soc. Dalton Trans.* **1982**, 1217.

³⁰ (a) Gupta, M.; Hagen, C.; Flesher, R. J.; Kaska, W. C.; Jensen, C. M. *Chem. Commun.* **1996**, 2083. (b) Goldman, A. S.; Ghosh, R. In *Handbook of C-H Transformations – Applications in Organic Synthesis*; Dyker, G., Ed.; Wiley-VCH: New York, 2005; pp 616.

300 K) marks an upper limit for the rates of the formation of C-H activation products **6** and **8**, with calculated values for k_1 and k_2 of $1.4 \times 10^{-3} \text{ min}^{-1}$ and $1.0 \times 10^{-3} \text{ min}^{-1}$, respectively. It is unlikely for C-H activation and trapping of the vinyl hydride by Cl^- to proceed concerted, and intermediates such as a five-coordinate hydrido vinyl species are most reasonable. However, the absence of COE exchange for $\mathbf{3}^{\text{COE}}\text{-PF}_6$ suggests that Three-coordinate $[\text{Ir}(\text{PNP})^{\text{H}}]^+$ is not involved.

Iridium vinyl hydrides have been reported for several stoichiometric and catalytic alkene functionalization reactions, such as alkane dehydrogenation,^[31] olefin dimerization,^[32] or catalytic vinylic H/D exchange.^[33] As usually the olefin η^2 -olefin complexes are the thermodynamically favored isomers they cannot be direct intermediates for thermal vinylic C-H activation in these cases and separate transition states must account for π -complexation and C-H oxidative addition during the interaction of the metal with an incoming olefin.^[34] However, stable vinyl hydrides were obtained with sterically encumbered auxiliary ligands and alkenes or by trapping of five-coordinate vinyl hydrides with a sixth ligand.^[2,31,35] For cyclooctene iridium complexes resulting from both vinylic^[35c,36] and allylic^[37] C-H activation

³¹ Kanzelberger, M.; Singh, B.; Czerw, M.; Krogh-Jespersen, K.; Goldman, A. S. *J. Am. Chem. Soc.* **2000**, *122*, 11017.

³² Alvarado, Y.; Boutry, O.; Gutierrez, E.; Monge, A.; Nicasio, M. C.; Poveda, M. L.; Perez, P. J.; Ruiz, C.; Bianchini, C.; Carmona, E. *Chem. Eur. J.* **1997**, *3*, 860.

³³ Torres, F.; Sola, E.; Martin, M.; Lopez, J. A.; Lahoz, F. J.; Oro, L. A. *J. Am. Chem. Soc.* **1999**, *121*, 10632.

³⁴ (a) Stoutland, P. O.; Bergman, R. G. *J. Am. Chem. Soc.* **1985**, *107*, 4581. (b) Stoutland, P. O.; Bergman, R. G. *J. Am. Chem. Soc.* **1988**, *110*, 5732. (c) Bell, T. W.; addleton, D. M.; McCamley, A.; Partridge, M. G.; Perutz, R. N.; Willner, H. *J. Am. Chem. Soc.* **1990**, *112*, 9212. (d) Bianchini, C.; Barbaro, P.; Meli, A.; Peruzzini, M.; Vacca, A.; Vizza, F. *Organometallics* **1993**, *12*, 2505. (e) Bell, T. W. Brough, S.-A.; Partridge, M. G.; Perutz, R. N.; Rooney, A. D. *Organometallics* **1993**, *12*, 2933. (f) Smith, K. M.; Poli, R.; Harvey, J. N. *Chem. Eur. J.* **2001**, *7*, 1679.

³⁵ examples: (a) Werner, H.; Dirnberger, T.; Schulz, M. *Angew. Chem.* **1988**, *100*, 993. (b) Ghosh, C. K.; Hoyano, J. K.; Krentz, R.; Graham, W. A. G. *J. Am. Chem. Soc.* **1989**, *111*, 5480. (c) Hermann, D.; Gandelman, M.; Rozenberg, H.; Shimon, L. J. W.; Milstein, D. *Organometallics* **2002**, *21*, 812.

³⁶ (a) Fernandez, M. J.; Rodriguez, M. J.; Oro, L. A.; Lahoz, F. J. *J. Chem. Soc., Dalton Trans.* **1989**, 2073-2076. (b) Iimura, M.; Evans, D. R.; Flood, T. C. *Organometallics* **2003**, *22*, 5370.

³⁷ (a) Tanke, R. S.; Crabtree, R. H. *Inorg. Chem.* **1989**, *28*, 3444. (b) Peters, J. C.; Feldman, J. D.; Tilley, T. D. *J. Am. Chem. Soc.* **1999**, *121*, 9871. (c) Budzelaar, P. H. M.; Moonen, N. N. P.; de gelder, R.; Smits, J. M. M. *Eur.*

are known. In a related system to ours, Milstein reported that the reaction of **1** with the pyridine based pincer ligand (PNP)^{*} gave hydrido vinyl complex [IrHCl(C₈H₁₃)(PNP)^{*}].^[35c]

We hoped for the fluxional behavior of **3**^{COE}-PF₆ to provide further information. NMR spectroscopic characterization suggests rigid olefin binding for **3**^{C³H⁶}-PF₆. Furthermore, the molecular structure of **3**^{C²H⁴}-PF₆ in the crystal features the olefin embedded in the cavity formed by the ⁱPr substituents with several close contacts to the pincer ligand. Therefore, for sterically more stressed **3**^{COE}-PF₆ rapid olefin rotation seems unlikely as origin for the fluxional behavior.^[38] Olefin exchange, anion coordination, and amine inversion could further be excluded. Unfortunately, low temperature NMR of **3**^{COE}-PF₆ remains inconclusive. However, a similarly complex pattern in the ³¹P NMR and very broad ¹H NMR peaks were found for the (PNP)^H ligand signals of **3**^{C³H⁶}-PF₆, which is not fluxional at room temperature with respect to the olefin moiety. Based on the observed reactivity of **3**^{COE}-Cl, we suggest that the fluxionality of **3**^{COE}-PF₆ can be explained with rapid, reversible vinylic C-H activation of the COE ligand. The lack of observable hydride signals in the ¹H NMR at any temperatures indicates that the equilibrium would be shifted to the olefin complex. However, further dynamic processes, e.g., isopropyl rotation or hemi-lability of the nitrogen donor, as indicated by ¹⁵N NMR, seem to be freezing in the same temperature range, so that quantitative kinetic data could not be extracted.

Comparison of amino and amido complexes

In contrast to **3**^{COE}-PF₆, amido complex **4**^{COE} features rigid olefin binding up to 100 °C on the NMR time scale. Since sterics should be comparable in these complexes, electronic factors must play a major role. The CO stretching vibrations of **3**^{COE}-PF₆ and **4**^{CO} are at the far ends of a range of iridium(I) diphosphine carbonyl complexes (Table 3), suggesting a substantial increase in electron density at the metal center upon deprotonation of the (PNP)^H nitrogen. Further indication is provided by the large increase in olefinic C=C bond distance upon N-deprotonation of the ethylene amino complex (**3**^{C²H⁴}-PF₆ / **4**^{C²H⁴}: ΔD_{C=C} = 0.07 Å).

J. Inorg. Chem. **2000**, 753. (d) Ortmann, D. A.; Gevert, O.; Laubender, M.; Werner, H. *Organometallics* **2001**, 20, 1776. (e) Turculet, L.; Feldman, J. D.; Tilley, T. D. *Organometallics* **2004**, 23, 2488.

³⁸ Activation parameters for hypothetical olefin rotation for **3**^{COE}-PF₆ were estimated by lineshape analysis of the ³¹P NMR signals to be in the range of ΔG₃₀₀[‡] ≈ 37 kJ·mol⁻¹.

B Results and Discussion

Almost identical olefinic ^{13}C up-field shifts ($\mathbf{3}^{\text{C}^{2\text{H}4}}\text{-PF}_6$ / $\mathbf{4}^{\text{C}^{2\text{H}4}}$: $\Delta\delta_{13\text{C}} = 22.1$ ppm; $\mathbf{3}^{\text{COE}}\text{-PF}_6$ / $\mathbf{4}^{\text{COE}}$: $\Delta\delta_{13\text{C}} = 20.8$ ppm) suggest comparable effects on COE binding.^[39]

Table 3. CO stretching vibrations of *trans*-diphosphine carbonyl iridium(I) complexes.

complex	ν_{CO} [cm^{-1}]	ref.
$[\text{Ir}(\text{CO})\{\text{HN}(\text{CH}_2\text{CH}_2\text{P}^i\text{Pr}_2)_2\}]\text{PF}_6$	1976	this work
$[\text{Ir}(\text{CO})\{\text{C}_5\text{H}_3\text{N}(\text{CH}_2\text{P}^i\text{Bu}_2)_2\}]\text{PF}_6$	1962	40
$[\text{Ir}(\text{CO})\{\text{C}_6\text{H}_3(\text{OP}^i\text{Bu}_2)_2\}]$	1949	41
$[\text{Ir}(\text{CO})\text{Cl}(\text{P}^i\text{Pr}_3)_2]$	1935	42
$[\text{Ir}(\text{CO})\{\text{N}(\text{SiMe}_2\text{CH}_2\text{P}^i\text{Pr}_2)_2\}]$	1930	12e
$[\text{Ir}(\text{CO})\{\text{N}(\text{C}_6\text{MeH}_3\text{P}^i\text{Pr}_2)_2\}]$	1930	43
$[\text{Ir}(\text{CO})\{\text{C}_6\text{H}_3(\text{CH}_2\text{P}^i\text{Pr}_2)_2\}]$	1920	44
$[\text{Ir}(\text{CO})\{\text{N}(\text{CH}_2\text{CH}_2\text{P}^i\text{Pr}_2)_2\}]$	1908	this work

Therefore, we attribute the structural rigidity of $\mathbf{4}^{\text{COE}}$, as compared with $\mathbf{3}^{\text{COE}}\text{-PF}_6$, to strong Ir→COE back bonding. The electron density at the metal will be strongly enhanced by repulsive π -interaction of the amido lone pair with a filled metal *d*-orbital, which is involved in Ir→L_{trans} (L = olefin, CO) back bonding. Although the higher electron density in the amido complexes would seem iridium(III) to be more accessible, the increase in Ir-olefin binding strength prevents the olefin complexes from rearrangement. The conjugate acid/base pair $\mathbf{3}^{\text{COE}}\text{-PF}_6$ and $\mathbf{4}^{\text{COE}}$ therefore represents an unprecedented example of metal complexes with

³⁹ Although rationalization of metal-olefin bonding on the basis of pure ^{13}C olefin coordination shifts has been discussed controversially, within closely related systems it is justified to use $\Delta\delta_{13\text{C}}$ values as a qualitative indicator for relative M→olefin back bonding: (a) Thoennes, D. J.; Wilkins, C. L.; Trahanovsky, W. S. *J. Magn. Res.* **1974**, *13*, 18. (b) Evans, J.; Norton, J. R. *Inorg. Chem.* **1974**, *13*, 3042. (c) Clark, P. W.; Hanisch, P.; Jones, A. J. *Inorg. Chem.* **1979**, *18*, 2067.

⁴⁰ Kloeck, S. M.; Heinekey, M.; Goldberg, K. I. *Organometallics* **2006**, *25*, 3007.

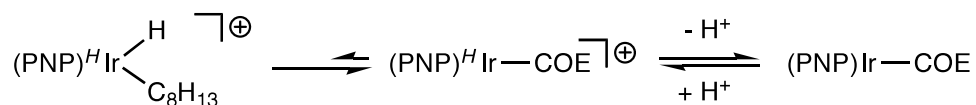
⁴¹ Göttker-Schnetmann, I.; White, P. S.; Brookhart, M. *Organometallics* **2004**, *23*, 1766.

⁴² Faraone, F.; Piraino, P.; Pietropaolo, R. *J. Chem. Soc., Dalton Trans.* **1973**, 1625.

⁴³ Whithead, M. T.; Grubbs, R. H. *J. Am. Chem. Soc.* **2008**, *130*, 5874.

⁴⁴ Rybtchinski, B.; Ben-David, Y.; Milstein, D. *Organometallics* **1997**, *16*, 3786.

switchable vinylic C-H activation by controlling olefin binding upon de-/protonation of the pincer ligand (Scheme 5).



Scheme 5. Proposed switchable C-H activation for $\mathbf{3}^{\text{COE}}\text{-PF}_6$ and $\mathbf{4}^{\text{COE}}$.

1.1.5 Conclusion

In conclusion, we described the synthesis of a new class of iridium(I) amino and amido complexes bearing the PNP pincer ligand $\text{N}(\text{CH}_2\text{CH}_2\text{P}^i\text{Pr}_2)_2$. The instability of $\mathbf{3}^{\text{COE}}\text{-Cl}$ in nonprotic solvents is attributed to both anion-assisted N-H deprotonation and trapping of vinylic C-H activation products. No indications for $\text{M}\cdots\text{H}\cdots\text{N}$ interactions or intramolecular N-H oxidative addition were found. Our results suggest that $\mathbf{3}^{\text{COE}}\text{-PF}_6$ is a rare example of an olefin complex that exhibits a fast equilibrium with a vinyl hydride isomer at room temperature on the NMR time scale, accounting at least in part for the observed fluxionality. Unfortunately, other dynamic processes on the pincer ligand seem to be coupled, preventing the extraction of quantitative data. On the other hand, the structural rigidity of the corresponding amido complex $\mathbf{4}^{\text{COE}}$ is attributed to strong olefin binding which is reinforced by the N-Ir-olefin 3c-4e π -interaction, illustrating the electron rich character of the Ir(PNP) fragment. Using the olefin ligand as a probe for Ir-N bonding, this interpretation renders $\mathbf{3}^{\text{COE}}\text{-PF}_6 / \mathbf{4}^{\text{COE}}$ an interesting system that features switchable C-H activation upon de-/protonation of the pincer ligand.

1.1.6 Experimental details and syntheses

Materials and Synthetic Methods. All experiments were carried out under an atmosphere of argon using Schlenk and glove-box techniques. The solvents were dried over Na/benzophenone/tetraglyme (benzene) or Na/benzophenone (THF) distilled under argon and deoxygenated prior to use. Deuterated solvents were dried by distillation from Na/K alloy (C_6D_6 and $d_8\text{-THF}$), stirring over 4Å molecular sieves and distillation from B_2O_3 ($d_6\text{-acetone}$) or distillation from CaH_2 (CD_2Cl_2), respectively, and deoxygenated by three freeze-pump-thaw cycles. KO^tBu and cyclooctene were purchased from VWR and sublimed (KO^tBu) / distilled (cyclooctene) prior to use. Ethene 2.7 (Messer Griesheim), propylene 2.8 (Gerling,

B Results and Discussion

Holz + Co.) and iridiumtrichloride hydrate (ABCR) were used as purchased. $\text{HN}(\text{CH}_2\text{CH}_2\text{P}^i\text{Pr}_2)_2$ ^[45] and $[\text{IrCl}(\text{COE})_2]_2$ (**1**)^[46] were prepared as reported in the literature.

Analytical Methods. Elemental analyses were obtained from the Microanalytical Laboratory of Technische Universität München. The IR spectra were recorded on a Jasco FT/IR-460 PLUS spectrometer as nujol mulls between KBr plates. NMR spectra were recorded on Jeol Lambda 400, Bruker DPX 400, Bruker DMX 500, and Bruker DMX 600 spectrometers at room temperature and were calibrated to the residual proton resonance and the natural abundance ¹³C resonance of the solvent (C_6D_6 , $\delta_{\text{H}} = 7.16$ and $\delta_{\text{C}} = 128.1$ ppm; d_6 -acetone, $\delta_{\text{H}} = 2.05$ and $\delta_{\text{C}} = 29.8 + 206.3$ ppm; d_8 -THF, $\delta_{\text{H}} = 1.73 + 3.58$ ppm and $\delta_{\text{C}} = 25.4 + 67.6$ ppm). ³¹P NMR chemical shifts are reported relative to external phosphoric acid (δ 0.0 ppm). ¹⁵N NMR shifts are given relative to MeNO₂ by referencing with external ¹⁵N-urea in d_6 -dmsO (δ -302.1 ppm). Signal multiplicities are abbreviated as: s (singlet), d (doublet), t (triplet), vt (virtual triplet), sp (septet), m (multiplet), br (broad).

*Synthesis of $[\text{Ir}(\text{COE})(\text{PNP})^{\text{H}}][\text{PF}_6]$ (**3**^{COE}-**PF**₆).* $\text{HN}(\text{CH}_2\text{CH}_2\text{P}^i\text{Pr}_2)_2$ (0.142 g; 0.466 mmol) is added to a solution of **1** (0.200 g; 0.223 mmol) and AgPF₆ (0.118 g; 0.466 mmol) in THF (5 mL) and stirred for 30 min. After filtration the orange product is precipitated with pentanes, washed twice with pentanes and dried *in vacuo*. Yield: 0.229 g (0.377 mmol; 84 %). Anal. Calcd. for C₂₄H₅₁F₆IrNP₃ (752.80): C, 38.29; H, 6.83; N, 1.86. Found: 38.28; H, 7.11; N, 1.91. IR (cm⁻¹) $\nu = 3215$ (N-H). NMR (d_6 -acetone, r.t., [ppm]) ¹H NMR (399.8 MHz): δ 1.20 (dvt, ³J_{HH} = 6.7 Hz, J_{PH} = 6.7 Hz, 6H, CH₃), 1.28 (dvt, ³J_{HH} = 6.7 Hz, J_{PH} = 6.7 Hz, 6H, CH₃), 1.34 (dvt, ³J_{HH} = 8.6 Hz, J_{PH} = 7.3 Hz, 6H, CH₃), 1.35 (2H, CH₂^{COE}), 1.40 (dvt, ³J_{HH} = 7.3 Hz, J_{PH} = 8.6 Hz, 6H, CH₃), 1.49 (m, 4H, CH₂^{COE}), 1.64 (m, 4H, CH₂^{COE}), 1.88 (m, 2H, PCH₂), 2.25-2.32 (m, 4H, PCH₂ + CH₂^{COE}) 2.41 (spvt, ³J_{HH} = 7.0 Hz, J_{PH} = 2.8 Hz, 2H, CH(CH₃)₂), 2.54 (spvt, ³J_{HH} = 7.0 Hz, J_{PH} = 2.8 Hz, 2H, CH(CH₃)₂), 2.70 (m, 2H, NCH₂), 3.33 (m, 2H, NCH₂), 3.62 (br, 2H, CH^{COE}), 5.35 (br, 1H, NH). ¹³C {¹H} NMR (100.6 MHz): δ 16.9 (s, CH₃), 18.5 (s, CH₃), 18.9 (s, CH₃), 24.3 (vt, J_{CP} = 13.8 Hz, CH(CH₃)₂), 24.5 (vt, J_{CP} = 14.5 Hz, PCH₂), 25.7 (vt, J_{CP} = 13.0 Hz, CH(CH₃)₂), 26.3 (s, CH₂^{COE}), 31.6 (s, CH₂^{COE}), 33.8 (s, CH₂^{COE}), 52.3 (s, CH^{COE}), 55.8 (d, ²J_{CP} = 2Hz, NCH₂). ³¹P {¹H} NMR (161.8 MHz): δ 43.1 (s, PⁱPr₂), -143.6 (sp, ¹J_{PF} = 707 Hz, PF₆). Assignments were confirmed by a

⁴⁵ Danopoulos, A. A.; Wills, A. R.; Edwards, P. G. *Polyhedron* **1990**, *9*, 2413.

⁴⁶ Onderlinden, A. L.; van der Ent, A. *Inorg. Chim. Acta* **1972**, *6*, 420.

^1H - ^1H COSY spectrum. $[\text{Ir}(\text{COE})(\text{PNP})^{\text{H}}][\text{BPh}_4]$ ($\mathbf{3}^{\text{COE}}\text{-BPh}_4$) can be prepared analogously by using NaBPh_4 instead of AgPF_6 (yield 90 %). The cation exhibits identical ^1H , ^{13}C and ^{31}P NMR spectra as in $\mathbf{3}^{\text{COE}}\text{-PF}_6$.

Synthesis of $[\text{Ir}(\text{C}_2\text{H}_4)(\text{PNP})^{\text{H}}][\text{PF}_6]$ ($\mathbf{3}^{\text{C}^2\text{H}^4}\text{-PF}_6$). Ethylene is bubbled through a suspension of **1** (0.402 g, 0.449 mmol) in acetone (10 mL) at -30°C until a clear colorless solution occurs. Consecutively a solution of AgPF_6 (0.215 g, 0.850 mmol) in acetone (5 mL) and a solution of $\text{HN}(\text{CH}_2\text{CH}_2\text{P}^i\text{Pr}_2)_2$ (0.260 g, 0.851 mmol) in acetone (5 mL) is added at -30°C . The resulted red suspension is warmed to rt and filtered. Precipitation with pentane gives a red oil, which is redissolved in THF, filtered and precipitated with diethylether and pentane. $\mathbf{3}^{\text{C}^2\text{H}^4}\text{-PF}_6$ is obtained as a red crystalline product upon filtration, washing with diethylether and drying *in vacuo*. Yield: 0.403 g (0.601 mmol; 67 %). Anal. Calcd. for $\text{C}_{18}\text{H}_{41}\text{F}_6\text{IrNP}_3$ (670.65): C, 32.24; H, 6.16; N, 2.09. Found: C, 32.56; H, 5.81; N, 2.07. IR (cm^{-1}) $\nu = 3210$ (N-H). NMR (d_6 -acetone, r.t., [ppm]) ^1H NMR (399.78 MHz): δ 1.19 (dvt, $^3J_{\text{HH}} = 7.2$ Hz, $J_{\text{HP}} = 7.2$ Hz, 6H, CH_3), 1.25 (m, 18H, CH_3), 1.95 (m, 2H, PCH_2), 2.35 (m, 2H, PCH_2), 2.45 (m, 2H, $\text{CH}(\text{CH}_3)_2$), 2.58 (m, 2H, $\text{CH}(\text{CH}_3)_2$), 2.75 (m, 2H, NCH_2), 2.88 (t, $^3J_{\text{HH}} = 4.0$ Hz, 4H, C_2H_4), 3.45 (m, 2H, NCH_2), 5.70 (br, 1H, NH). ^{13}C - $\{^1\text{H}\}$ NMR (100.6 MHz): δ 17.8 (s, CH_3), 17.9 (s, CH_3), 18.7 (s, CH_3), 18.9 (s, CH_3), 23.9 (vt, $J_{\text{CP}} = 14.6$ Hz, $\text{CH}(\text{CH}_3)_2$), 25.0 (vt, $J_{\text{CP}} = 13.0$ Hz, PCH_2), 25.3 (vt, $J_{\text{CP}} = 13.1$ Hz, $\text{CH}(\text{CH}_3)_2$), 31.9 (s, C_2H_4), 57.1 (s, NCH_2). ^{31}P - $\{^1\text{H}\}$ NMR (161.8 MHz): δ 49.0 (s, P^iPr_2), -143.6 (sp, $^1J_{\text{PF}} = 707$ Hz, PF_6). $[\text{Ir}(\text{C}_2\text{H}_4)(\text{PNP})^{\text{H}}][\text{BPh}_4]$ ($\mathbf{3}^{\text{C}^2\text{H}^4}\text{-BPh}_4$) can be prepared analogously by using NaBPh_4 instead of AgPF_6 (yield 81 %). The cation exhibits identical ^1H , ^{13}C and ^{31}P NMR spectra as in $\mathbf{3}^{\text{C}^2\text{H}^4}\text{-PF}_6$.

Synthesis of $[\text{Ir}(\text{C}_3\text{H}_6)(\text{PNP})^{\text{H}}][\text{PF}_6]$ ($\mathbf{3}^{\text{C}^3\text{H}^6}\text{-PF}_6$). **1** (0.200 g, 0.223 mmol) is suspended in THF (10 mL) at -80°C and propylene bubbled through the solution for 20 min. After addition of $\text{HN}(\text{CH}_2\text{CH}_2\text{P}^i\text{Pr}_2)_2$ (0.136 g, 0.445 mmol) and AgPF_6 (0.113 g, 0.446 mmol) the solution is stirred for 1 h at -80°C . Upon addition of pentane the crude product is precipitated, filtered off, and redissolved in THF. After filtration the product was precipitated as orange microcrystals with pentane, filtered off, and dried *in vacuo*. Yield: 0.169 g (0.249 mmol; 55 %). Anal. Calcd. for $\text{C}_{19}\text{H}_{43}\text{F}_6\text{IrNP}_3$ (684.68): C, 33.33; H, 6.33; N, 2.05. Found: C, 32.83; H, 6.15; N, 2.02. IR (cm^{-1}) $\nu = 3220$ (N-H). NMR (d_8 -THF, r.t., [ppm]) ^1H NMR (399.78 MHz): δ 1.09 - 1.14 (m, 9H, $3 \times \text{PCHCH}_3$), 1.17 (dd, $^3J_{\text{HH}} = 5.6$ Hz, $^3J_{\text{HP}} = 10.6$ Hz, 3H, PCHCH_3), 1.28 (dd, $^3J_{\text{HH}} = 5.6$ Hz, $^3J_{\text{HP}} = 10.0$ Hz, 3H, PCHCH_3), 1.35 (dd, $^3J_{\text{HH}} = 5.3$ Hz, $^3J_{\text{HP}} = 9.7$ Hz, 3H, PCHCH_3), 1.42 (dd, $^3J_{\text{HH}} = 6.5$ Hz, $^3J_{\text{HP}} = 12.3$ Hz, 3H, PCHCH_3), 1.44 (dd, $^3J_{\text{HH}} = 5.6$ Hz, $^3J_{\text{HP}} = 11.2$ Hz, 3H, PCHCH_3), 1.51 (d, $^3J_{\text{HH}} = 4.7$ Hz, 3H, $\text{H}_2\text{C}=\text{CHCH}_3$), 1.93 - 2.10

B Results and Discussion

(m, 3H, 3 × PCH₂), 2.22 (m, 2H, 1 × PCH₂ + PCHMe₂), 2.38 (dsp, ³J_{HP} = 5.0 Hz, ³J_{HH} = 5.3 Hz, 1H, PCHMe₂), 2.47 - 2.62 (m, 4H, 1 × H₂C=CHMe + 2 × NCH₂ + PCHMe₂), 2.71 (dsp, ³J_{HP} = 5.6 Hz, ³J_{HH} = 5.3 Hz, 1H, PCHMe₂), 2.95 (dt, ³J_{HH} = 7.9 Hz, ³J_{HP} = 5.3 Hz, 1H, H₂C=CHMe), 3.34 (dm, ³J_{HP} = 29.0 Hz, 1H, 1 × NCH₂), 3.49 (dm, ³J_{HP} = 27.8 Hz, 1H, 1 × NCH₂), 3.72 (m, 1H, H₂C=CHMe), 5.09 (br, 1H, NH). ¹³C-¹H NMR (100.6 MHz): δ 16.7 (s, PCHCH₃), 16.8 (s, PCHCH₃), 17.0 (s, PCHCH₃), 17.2 (s, 2 × PCHCH₃), 17.4 (s, PCHCH₃), 18.6 (d, ²J_{PC} = 3.1 Hz, PCHCH₃), 19.0 (d, ²J_{PC} = 2.3 Hz, PCHCH₃), 22.5 (s, H₂C=CHCH₃), 23.7 (d, ¹J_{CP} = 20.7 Hz, PCH₂), 25.2 (dd, ¹J_{CP} = 21.4 Hz, ³J_{CP} = 5.7 Hz, CH(CH₃)₂), 26.3 (dd, ¹J_{CP} = 21.4 Hz, ³J_{CP} = 4.6 Hz, CH(CH₃)₂), 32.7 (s, H₂C=CHCH₃), 42.3 (s, H₂C=CHCH₃), 56.1 (t, ²J_{PC} = 3.8 Hz, NCH₂), 57.0 (t, ²J_{PC} = 3.1 Hz, NCH₂). One PCH₂ and two CH(CH₃)₂ ¹³C signals are superimposed with one of the solvent signals. ³¹P-¹H NMR (161.8 MHz): δ 50.6 (d, ²J_{PP} = 307 Hz, PⁱPr₂), 47.5 (d, ²J_{PP} = 307 Hz, PⁱPr₂), -143.7 (sp, ¹J_{PF} = 711 Hz, PF₆).

Synthesis of [Ir(CO)(PNP)^H][PF₆] (3^{CO}-PF₆). CO is bubbled through a solution of 3^{C²H⁴}-PF₆ (0.136 g, 0.203 mmol) in THF (10 mL) at rt until a yellow, clear solution is obtained. After filtration 3^{CO}-PF₆ precipitates upon addition of diethylether and pentane as a yellow crystalline product, which is filtered off, washed with pentane and dried *in vacuo*. Yield: 0.130 g (0.194 mmol; 95 %). Anal. Calcd. for C₁₇H₃₇F₆IrNOP₃ (670.61): C, 30.45; H, 5.56; N, 2.09. Found: C, 31.20; H, 5.47; N, 2.05. IR (cm⁻¹) ν = 3223 (N-H), 1976 (s, CO). NMR (C₆D₆, r.t., [ppm]) ¹H NMR (399.78 MHz): δ 0.81 (dvt, ³J_{HH} = 7.2 Hz, J_{HP} = 7.2 Hz, 6H, CH₃), 0.87 (dvt, ³J_{HH} = 7.2 Hz, J_{HP} = 7.2 Hz, 12H, CH₃), 0.91 (dvt, ³J_{HH} = 7.2 Hz, J_{HP} = 7.2 Hz, 12H, CH₃), 1.06 (dvt, ³J_{HH} = 7.6 Hz, J_{HP} = 7.2 Hz, 6H, CH₃), 1.78 (m, 6H, PCH₂ + NCH₂), 2.09 (m, 4H, CH(CH₃)₂), 3.46 (m, 2H, NCH₂), 4.79 (br, 1H, NH). ¹³C-¹H NMR (100.6 MHz): δ 18.0 (s, CH₃), 18.2 (s, CH₃), 18.9 (s, CH₃), 19.0 (s, CH₃), 24.2 (vt, J_{CP} = 12.2 Hz, CH(CH₃)₂), 25.9 (vt, J_{CP} = 16.1 Hz, PCH₂), 26.6 (vt, J_{CP} = 15.2 Hz, CH(CH₃)₂), 55.6 (s, NCH₂), 180.8 (t, ²J_{CP} = 8.0 Hz, CO). ³¹P-¹H NMR (161.8 MHz): δ 69.8 (s, PⁱPr₂), -142.53 (sp, ¹J_{PF} = 712 Hz, PF₆).

Synthesis of [Ir(COE)(PNP)] (4^{COE}). KO^tBu (0.015 g, 0.133 mmol) is added to a solution of 3^{COE}-[PF₆] (0.100 g, 0.133 mmol) in THF (5 mL) stirred for 2h at rt. The solvent is evaporated *in vacuo* and the residue extracted with pentane, filtered and evaporated *in vacuo* to give an orange-yellow solid. Yield: 0.058 g (0.95 mmol; 72 %). Anal. Calcd. for C₂₄H₅₀IrNP₂ (606.83): C, 47.50; H, 8.31; N, 2.31. Found: 47.03; H, 8.42; N, 2.28. NMR (C₆D₆, r.t., [ppm]) ¹H NMR (399.78 MHz): δ 1.03 (m, 12H, 4 × CH₃), 1.19 (dd, ³J_{HH} = 7.6

Hz, $^3J_{\text{HP}} = 12.8$ Hz, 6H, $2 \times \text{CH}_3$), 1.31 (dd, $^3J_{\text{HH}} = 7.2$ Hz, $^3J_{\text{HP}} = 12.8$ Hz, 6H, $2 \times \text{CH}_3$), 1.42 (m, 2H, $\text{CH}=\text{CHCH}_2$), 1.59 (m, 6H, $\text{PCH}_2 + \text{CH}_2^{\text{COE}}$), 1.73 (dt, $^2J_{\text{HP}} = 7.2$ Hz, $^3J_{\text{HH}} = 6.8$ Hz, 2H, PCH_2), 1.82 (m, 2H, CH_2^{COE}) 1.97 (m, 6H, $4 \times \text{CH}(\text{CH}_3)_2 + \text{CH}_2^{\text{COE}}$), 2.40 (m, 4H, $\text{CH}=\text{CHCH}_2 + \text{HC}=\text{CH}$), 3.32 (dt, $^3J_{\text{HP}} = 14.6$ Hz, $^3J_{\text{HH}} = 6.7$ Hz, 2H, NCH_2), 3.43 (dt, $^3J_{\text{HP}} = 16.5$ Hz, $^3J_{\text{HH}} = 6.1$ Hz, 2H, NCH_2). $^{13}\text{C}-\{^1\text{H}\}$ NMR (100.6 MHz): δ 17.7 (s, CH_3), 17.9 (s, CH_3), 19.2 (d, $^2J_{\text{CP}} = 2.3$ Hz, CH_3), 20.2 (d, $^2J_{\text{CP}} = 4.5$ Hz, CH_3), 23.5 (dd, $^1J_{\text{CP}} = 20.7$ Hz, $^3J_{\text{CP}} = 5.4$ Hz, $\text{CH}(\text{CH}_3)_2$), 25.8 (dd, $^1J_{\text{CP}} = 17.0$ Hz, $^3J_{\text{CP}} = 7.0$ Hz, $\text{CH}(\text{CH}_3)_2$), 26.1 (dd, $^1J_{\text{CP}} = 24.0$ Hz, $^3J_{\text{CP}} = 3.1$ Hz, PCH_2), 27.5 (s, CH_2^{COE}), 28.9 (d, $^1J_{\text{CP}} = 22.1$ Hz, PCH_2), 31.5 (s, $\text{HC}=\text{CH}$), 33.7 (s, CH_2^{COE}), 35.3 (m, $\text{CH}=\text{CHCH}_2$), 63.6 (dd, $^2J_{\text{CP}} = 3.8$ Hz, $^4J_{\text{CP}} = 2.3$ Hz, NCH_2), 64.6 (dd, $^2J_{\text{CP}} = 5.3$ Hz, $^4J_{\text{CP}} = 3.8$ Hz, NCH_2). $^{31}\text{P}-\{^1\text{H}\}$ NMR (161.8 MHz): δ 49.9 (d, $^2J_{\text{PP}} = 373$ Hz, $P^i\text{Pr}_2$), 53.6 (d, $^2J_{\text{PP}} = 373$ Hz, $P^i\text{Pr}_2$). Assignments were confirmed by $^1\text{H}-^1\text{H}$ COSY and $^1\text{H}-^{13}\text{C}$ HETCOR spectra.

Synthesis of $[\text{Ir}(\text{C}_2\text{H}_4)(\text{PNP})]$ ($4^{\text{C}2\text{H}4}$). KO^tBu (0.011 g; 0.096 mmol) in THF (5 mL) is added to a solution of $3^{\text{C}2\text{H}4}\text{-BPh}_4$ (0.081 g; 0.096 mmol) in 5 mL THF at 0°C. The yellow solution is stirred for 1h, the solvent evaporated and extracted with pentanes. Evaporation of the solvent gives $4^{\text{C}2\text{H}4}$ as a yellow, microcrystalline solid. Yield: 0.036 g (0.069 mmol; 72 %). Anal. Calcd. for $\text{C}_{18}\text{H}_{40}\text{IrNP}_2$ (524.68): C, 41.20; H, 7.68; N, 2.68. Found: C, 40.80; H, 7.16; N 2.66. NMR (C_6D_6 , r.t., [ppm]) ^1H NMR (399.78 MHz): δ 1.04 (dvt, $^3J_{\text{HH}} = 7.2$ Hz, $J_{\text{HP}} = 7.2$ Hz, 12H, CH_3), 1.16 (dvt, $^3J_{\text{HH}} = 7.2$ Hz, $J_{\text{HP}} = 7.2$ Hz, 12H, CH_3), 1.34 (m, 4H, PCH_2), 1.64 (m, 2H, $\text{CH}(\text{CH}_3)_2$), 1.91 (t, $^3J_{\text{HH}} = 4.4$ Hz, 4H, C_2H_4), 1.92 (m, 2H, $\text{CH}(\text{CH}_3)_2$), 3.40 (m, 4H, NCH_2). $^{13}\text{C}-\{^1\text{H}\}$ NMR (100.6 MHz): δ 9.8 (s, C_2H_4), 17.7 (s, CH_3), 19.0 (s, CH_3), 23.9 (vt, $J_{\text{CP}} = 13.0$ Hz, $\text{CH}(\text{CH}_3)_2$), 26.9 (vt, $J_{\text{CP}} = 12.2$ Hz, PCH_2), 65.1 (vt, $J_{\text{CP}} = 4.6$ Hz, NCH_2). $^{31}\text{P}-\{^1\text{H}\}$ NMR (161.8 MHz): δ 55.6 (s, $P^i\text{Pr}_2$).

Synthesis of $[\text{Ir}(\text{CO})(\text{PNP})]$ (4^{CO}). KO^tBu (0.009 g, 0.080 mmol) is added to a solution of $3^{\text{CO}}\text{-[PF}_6\text{]}$ (0.041 g, 0.062 mmol) in THF (5 mL) and stirred for 1h at rt. The solvent is evaporated *in vacuo* and the residue extracted with pentane, filtered and evaporated to give a yellow solid. Yield: 0.032 g (0.061 mmol; 98 %). Anal. Calcd. for $\text{C}_{17}\text{H}_{36}\text{IrNOP}_2$ (524.64): C, 38.92; H, 6.92; N, 2.67. Found: 39.43; H, 6.28; N, 2.38. IR (cm^{-1}) $\nu = 1908$ (CO). NMR (C_6D_6 , r.t., [ppm]) ^1H NMR (399.78 MHz) $\delta =$ 1.02 (dvt, $^3J_{\text{HH}} = 7.2$ Hz, $J_{\text{HP}} = 7.2$ Hz, 12H, CH_3), 1.23 (dvt, $^3J_{\text{HH}} = 8.8$ Hz, $J_{\text{HP}} = 6.8$ Hz, 12H, CH_3), 1.81 (tt, $^3J_{\text{HH}} = 6.6$ Hz, $J_{\text{HP}} = 4.4$ Hz, 4H, PCH_2), 1.97 (spvt, $^3J_{\text{HH}} = 7.0$ Hz, $J_{\text{HP}} = 3.0$ Hz, 4H, $\text{CH}(\text{CH}_3)_2$), 3.32 (tvt, $^3J_{\text{HH}} = 6.4$ Hz, $J_{\text{HP}} = 8.8$ Hz, 4H, NCH_2). $^{13}\text{C}-\{^1\text{H}\}$ NMR (100.6 MHz) $\delta =$ 18.2 (s, CH_3), 19.5 (s, CH_3), 26.2

B Results and Discussion

(vt, $J_{CP} = 15$ Hz, $CH(CH_3)_2$), 27.1 (vt, $J_{CP} = 13$ Hz, PCH_2), 63.0 (vt, $J_{CP} = 5.0$ Hz, NCH_2), 187.8 (t, $^2J_{CP} = 9.0$ Hz, CO). $^{31}P\{-^1H\}$ NMR (161.8 MHz) δ 80.7 (s, P^iPr_2).

*Synthesis of $[IrHCl_2(PNP)^H]$ (**5**).* $HN(CH_2CH_2P^iPr_2)_2$ (0.102 g; 0.339 mmol) is added to a solution of **1** (0.147 g; 0.164 mmol) in Benzene (10 mL) and stirred over night. The solvent is evaporated *i. vac.* and the residue washed with pentanes to give a white solid which is dried *in vacuo*. Yield: 0.092 g (0.162 mmol; 49 %). Anal. Calcd. for $C_{16}H_{38}Cl_2IrNP_2$ (569.55): C, 33.74; H, 6.72; N, 2.46. Found: 33.23; H, 6.59; N, 2.22. IR (cm^{-1}) $\nu = 3130$ (N-H), 2195 (Ir-H). NMR (C_6D_6 , r.t., [ppm]) 1H NMR (399.8 MHz): δ -24.73 (t, $^2J_{HP} = 12.8$ Hz, 1H, IrH), 0.97 (dvt, $^3J_{HH} = 7.6$ Hz, $J_{PH} = 6.8$ Hz, 6H, CH_3), 1.11 (dvt, $^3J_{HH} = 6.8$ Hz, $J_{PH} = 6.8$ Hz, 6H, CH_3), 1.42 (m, 12H, CH_3 , PCH_2 , NCH_2), 1.78 (dvt, 6H, $^3J_{HH} = 7.6$ Hz, $J_{PH} = 7.6$ Hz, CH_3), 1.99 (m, 2H, $CH(CH_3)_2$), 2.56 (m, 2H, $CH(CH_3)_2$), 3.27 (m, 2H, NCH_2), 5.11 (br, 1H, NH). $^{13}C\{^1H\}$ NMR (100.6 MHz): δ 17.9 (s, CH_3), 19.0 (s, CH_3), 19.4 (s, CH_3), 20.1 (s, CH_3), 24.2 (vt, $J_{CP} = 13.7$ Hz, $CH(CH_3)_2$), 25.9 (vt, $J_{CP} = 13.8$ Hz, $CH(CH_3)_2$), 29.4 (vt, $J_{CP} = 12.2$ Hz, PCH_2), 59.3 (s, NCH_2). $^{31}P\{^1H\}$ NMR (161.8 MHz): δ 27.1 (s, P^iPr_2).

*Reaction of 3^{COE}-PF_6 with $[PPh_4]Cl$: NMR characterization of **6**.* A suspension of 3^{COE}-PF_6 (0.016 g; 0.021 mmol) and $[PPh_4]Cl$ (0.008 g, 0.021 mmol) in THF (2 mL) is stirred at room temperature for 36 h, resulting in a mixture of 4^{COE} , **5** and **6** by ^{31}P NMR. After evaporation of the solvent the residue is extracted with pentanes and filtered. Upon evaporation of the extract a mixture of 4^{COE} and **6** is obtained which could not be further separated. NMR data of $[IrHCl(C_8H_{13})(PNP)^H]$ (**6**): 1H NMR (399.78 MHz, C_6D_6) $\delta = -24.40$ (t, $^2J_{HP} = 15.0$ Hz, 1H, IrH), 0.95 (dvt, $^3J_{HH} = 6.4$ Hz, $J_{PH} = 6.4$ Hz, 6H, CH_3), 1.21 (m, 12H, CH_3), 1.34 (dvt, $^3J_{HH} = 6.6$ Hz, $J_{PH} = 6.6$ Hz, 6H, CH_3), 1.53 (m, 2H, NCH_2), 1.67 (m, 4H, PCH_2 , CH_2^{COE}), 1.82 (m, 4H, CH_2^{COE}), 1.96 (m, 2H, CH_2^{COE}), 2.11 (m, 2H, $CH(CH_3)_2$), 2.40 (m, 6H, PCH_2 , NCH_2 , IrC=CHCH₂), 3.08 (t, $^3J_{HH} = 6.0$ Hz, 2H, IrCCH₂), 3.20 (m, 2H, $CH(CH_3)_2$), 4.00 (br, 1H, NH), 6.06 (t, $^3J_{HH} = 7.7$ Hz, 1H, =CH). $^{13}C\{-^1H\}$ NMR (100.6 MHz): δ 18.8 (s, CH_3), 19.1 (s, CH_3), 19.5 (s, CH_3), 20.0 (s, CH_3), 24.5 (vt, $J_{CP} = 13.4$ Hz, $CH(CH_3)_2$), 25.7 (vt, $^1J_{CP} = 12.2$ Hz, $CH(CH_3)_2$), 27.3 (s, CH_2^{COE}), 27.7 (s, CH_2^{COE}), 28.5 (s, CH_2^{COE}), 29.7 (s, CH_2^{COE}), 31.2 (s, IrC=CHCH₂), 31.6 (s, PCH_2), 41.0 (s, IrCCH₂), 54.1 (s, NCH_2), 124.0 (t, $^2J_{CP} = 9.2$ Hz, IrC), 134.7 (s, IrC=CH). $^{31}P\{-^1H\}$ NMR (161.8 MHz) δ 24.4 (s). Assignments were confirmed by $^1H\text{-}^1H$ COSY and $^1H\text{-}^{13}C$ HSQC spectra.

*Synthesis of $[IrHCl(COE)(PNP)^H][PF_6]$ (**7-PF₆**).* HCl (0.1M in Et₂O; 0.50 mL; 0.05 mmol) is added to a suspension of 3^{COE}-PF_6 (0.038 g; 0.050 mmol) in toluene (3 mL) at -20°C.

After 1h the solution is filtered at -20°C and the product precipitated by addition of pentanes to give colorless **7-PF₆**. Yield: 0.016 g (20 μmol ; 40 %). NMR (C_6D_6 , r.t., [ppm]) ^1H NMR (399.8 MHz): δ -17.83 (t, $^2J_{\text{HP}} = 10.8$ Hz, 1H, IrH), 0.69 (dvt, $^3J_{\text{HH}} = 6.7$ Hz, $J_{\text{PH}} = 6.7$ Hz, 6H, CH_3), 0.75 (dvt, $^3J_{\text{HH}} = 7.0$ Hz, $J_{\text{PH}} = 7.0$ Hz, 6H, CH_3), 0.79 (dvt, $^3J_{\text{HH}} = 7.0$ Hz, $J_{\text{PH}} = 7.3$ Hz, 6H, CH_3), 1.05 (dvt, $^3J_{\text{HH}} = 8.9$ Hz, $J_{\text{PH}} = 7.6$ Hz, 6H, CH_3), 1.12-1.34 (m, 8H, CH_2^{COE}), 1.45 (m, 2H, $\text{CH}(\text{CH}_3)_2$), 1.47 (m, 2H, NCH_2), 1.57 (m, 2H, CH_2^{COE}), 1.87 (m, 2H, PCH_2), 1.64 (m, 4H, CH_2^{COE}), 2.33 (m, 2H, CH_2^{COE}), 2.80 (m, 2H, PCH_2), 2.89-3.09 (m, 4H, $\text{CH}(\text{CH}_3)_2 + \text{NCH}_2$), 4.06 (br, 2H, CH^{COE}), 5.67 (br, 1H, NH). ^{31}P { ^1H } NMR (161.8 MHz): δ 23.3 (s, P^iPr_2), -142.5 (sp, $^1J_{\text{PF}} = 707$ Hz, PF_6). Assignments were confirmed by ^1H - ^1H COSY NMR.

1.1.7 2D NMR spectra

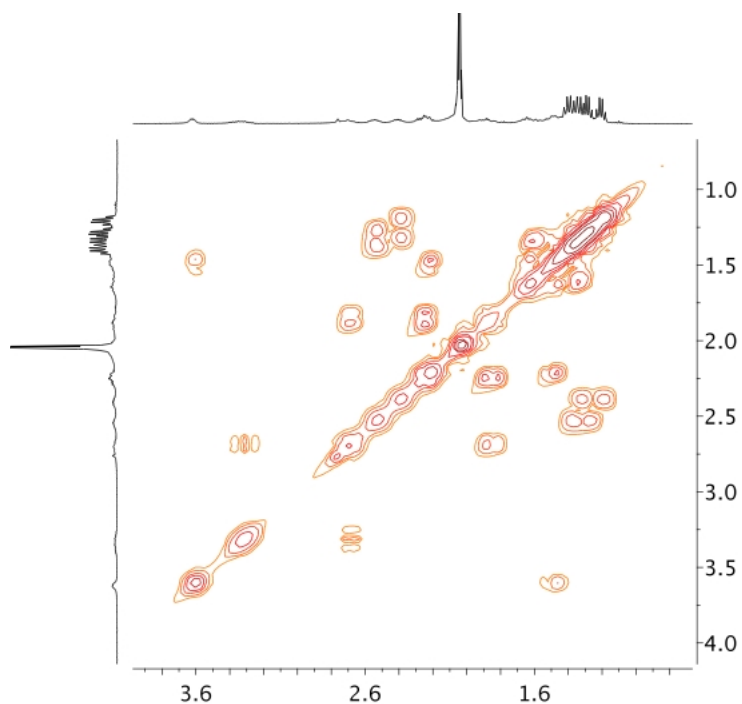


Figure 1. ^1H - ^1H COSY NMR spectrum of **3^{COE}-PF₆** in d_6 -acetone.

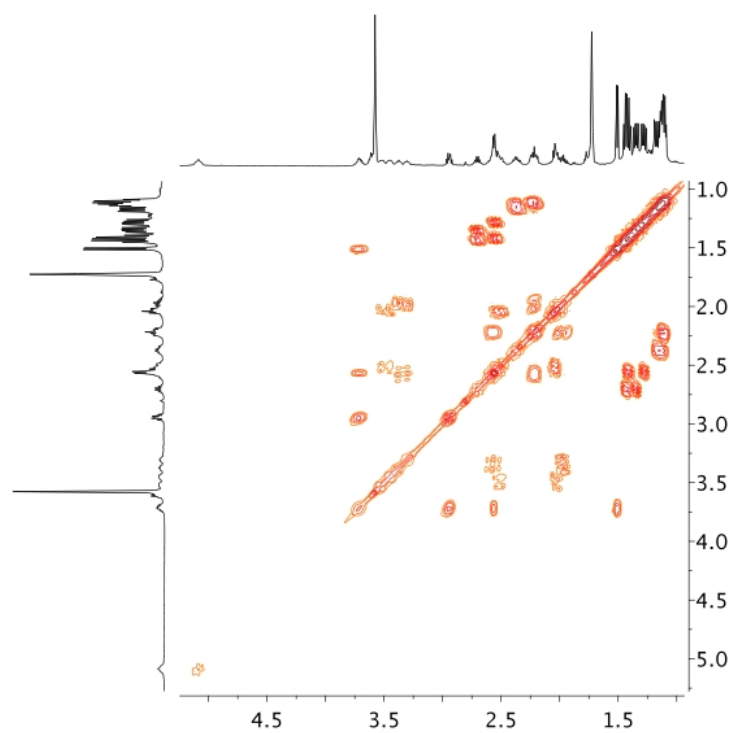


Figure 2. ^1H - ^1H COSY NMR spectrum of $3^{\text{C}^{3\text{H}6}}\text{-PF}_6$ in $d_8\text{-THF}$.

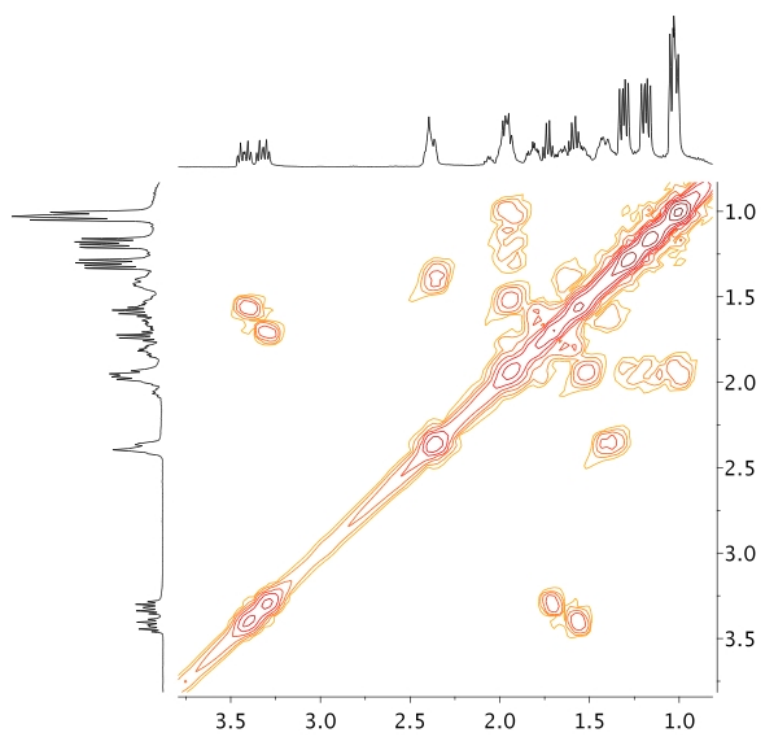


Figure 3. ^1H - ^1H COSY NMR spectrum of 4^{COE} in C_6D_6 .

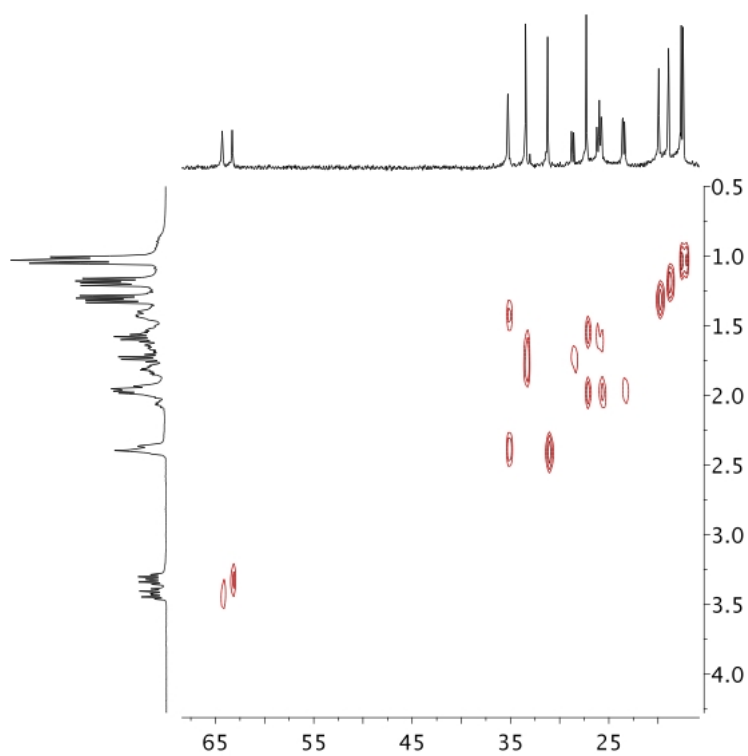


Figure 4. ^1H - ^{13}C HETCOR NMR spectrum of 4^{COE} in C_6D_6 .

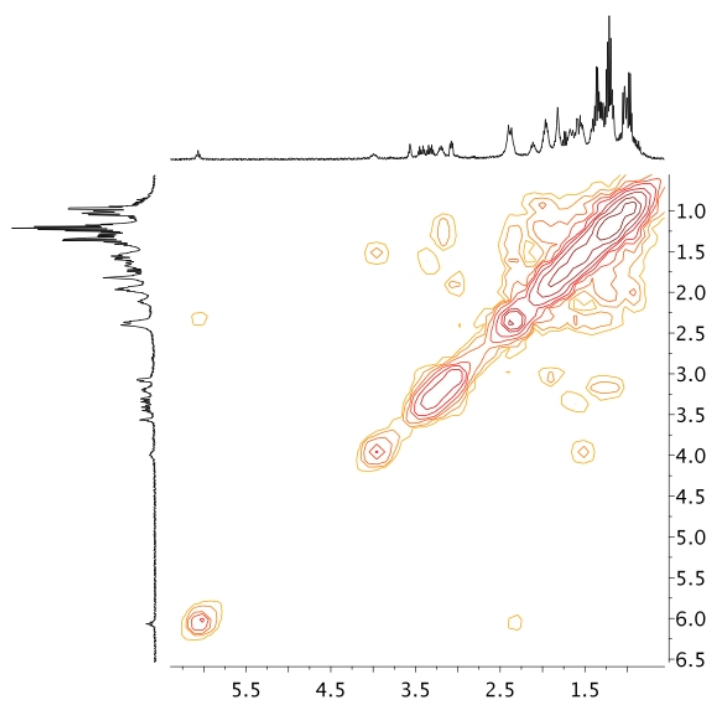


Figure 5. ^1H - ^1H COSY NMR spectrum of a mixture of 4^{COE} and **6** in C_6D_6 (hydride signal of **5** not shown; ^1H NMR peak at 3.57 ppm due to THF impurity).

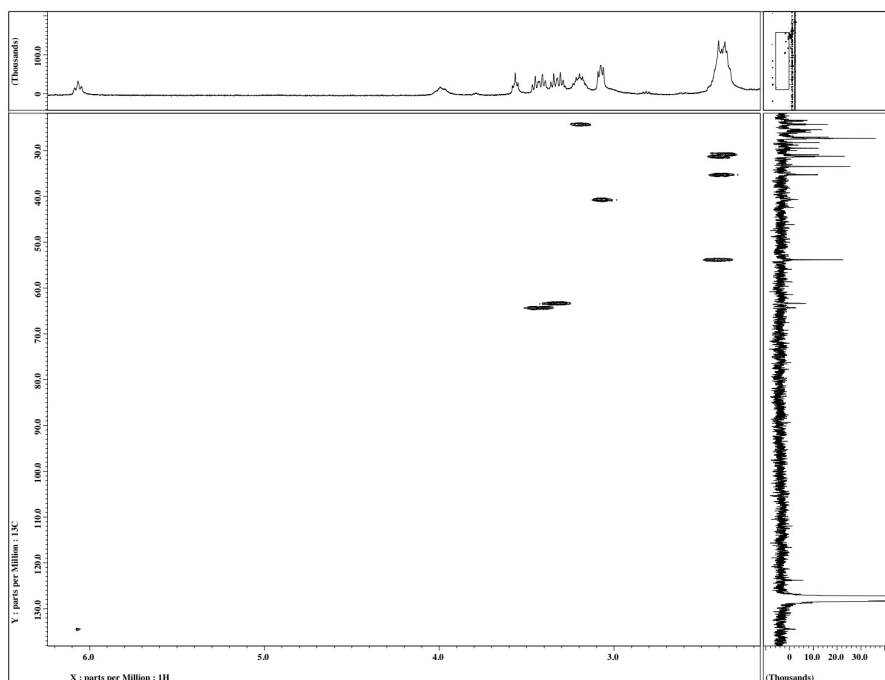


Figure 6. ^1H - ^{13}C HSQC NMR spectrum (expansion) of a mixture of 4^{COE} and **6** in C_6D_6 (^1H NMR peak at 3.57 ppm due to THF impurity).

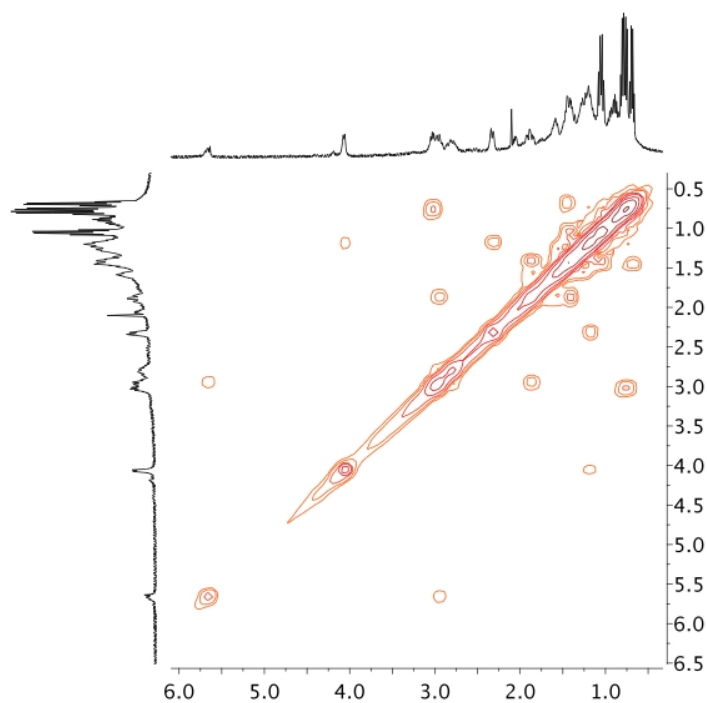


Figure 7. ^1H - ^1H COSY NMR spectrum of 7-PF_6 in C_6D_6 (hydride signal not shown).

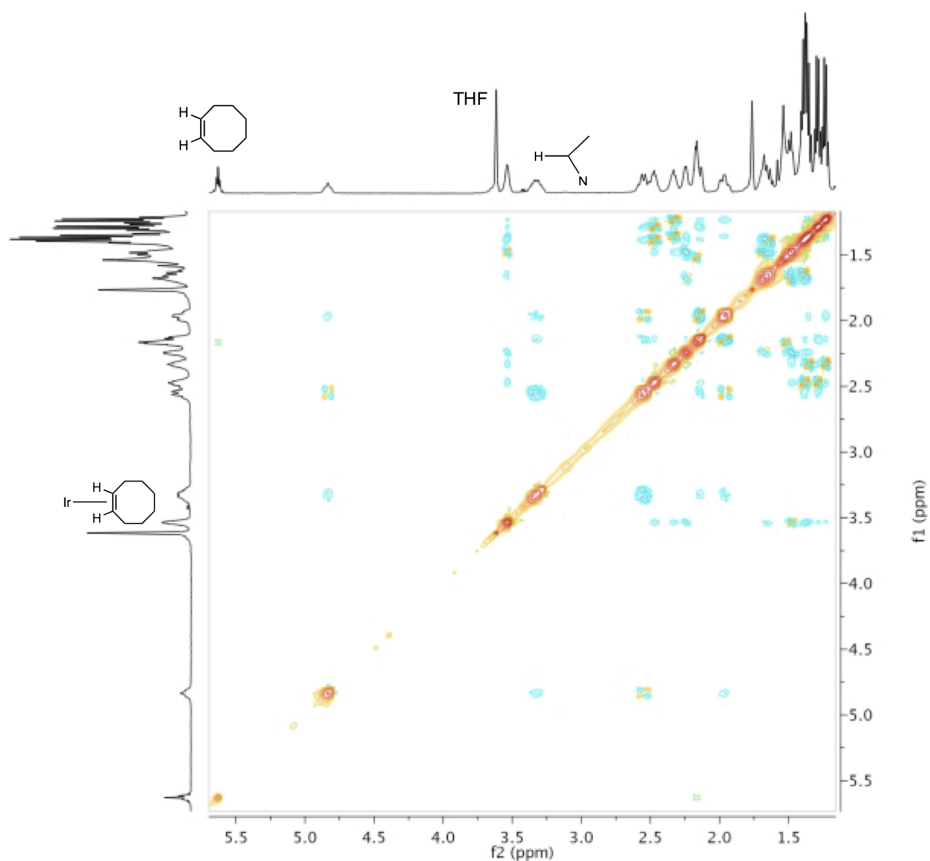


Figure 8. ¹H-EXSY NMR spectrum of **3**^{COE}-PF₆ with 0.5 equiv. COE in *d*₈-THF (25°C).

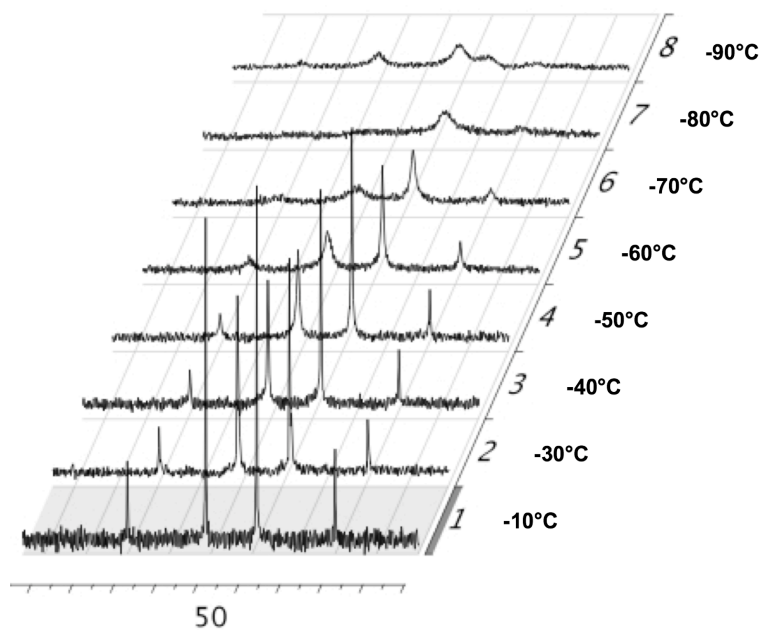


Figure 9. Variable temperature ³¹P NMR spectra of **3**^{C₃H₆}-PF₆ in *d*⁶-acetone.

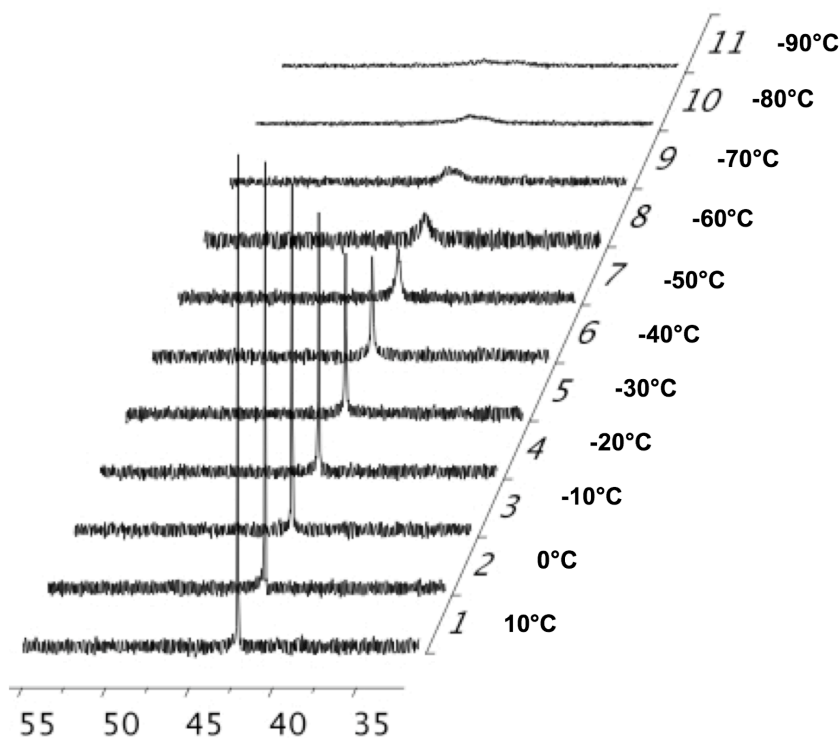


Figure 10. Variable temperature ^{31}P NMR spectra of $3^{\text{COE}}\text{-PF}_6$ in d^6 -acetone.

1.1.8 Kinetic experiments

Equimolar amounts (20.2 μmol) of $3^{\text{COE}}\text{-PF}_6$ and $[\text{N}^n\text{Bu}_3(\text{CH}_2\text{Ph})]\text{Cl}$ were dissolved in THF (0.35 mL) in a *J-Young* NMR tube equipped with a sealed capillary of phosphoric acid as internal standard. The reaction was followed recording $^{31}\text{P}\text{-}\{^1\text{H}\}$ NMR spectra every 10 min in the inverse gated mode to avoid NOE buildup. The relaxation delay was set to 15 s, which larger than $5 \cdot T_1$ of the compounds recorded, as derived by ^{31}P NMR inversion recovery experiments. Data analysis was performed using the program package COPASI.^[47]

Based on the proposed pathway for the reaction of $3^{\text{COE}}\text{-PF}_6$ with $[\text{N}^n\text{Bu}_3(\text{CH}_2\text{Ph})]\text{PF}_6$ (c.f. manuscript scheme 2) the following rate laws were used:

$$r(3^{\text{COE}}\text{-Cl}) = -k_1[3^{\text{COE}}\text{-Cl}] - k_2[3^{\text{COE}}\text{-Cl}] - k_3[3^{\text{COE}}\text{-Cl}] + k_{-3}[\text{HCl}][4^{\text{COE}}] - k_4[\text{HCl}][3^{\text{COE}}\text{-Cl}]$$

⁴⁷ Hoops, S.; Sahle, S.; Gauges, R.; Lee, C.; Pahle, J.; Simus, N.; Singhal, M.; Xu, L.; Mendes, P.; Kummer, U. *Bioinformatics* **2006**, *22*, 3067.

$$\begin{aligned}
 r(4^{\text{COE}}) &= k_3[3^{\text{COE}}\text{-Cl}] - k_{-3}[\text{HCl}][4^{\text{COE}}] \\
 r(5) &= k_6[7\text{-Cl}] + k_8[9] \\
 r(6) &= k_1[3^{\text{COE}}\text{-Cl}] + k_5[8] \\
 r(7\text{-Cl}) &= k_4[\text{HCl}][3^{\text{COE}}\text{-Cl}] - k_6[7\text{-Cl}] \\
 r(8) &= k_2[3^{\text{COE}}\text{-Cl}] - k_5[8] \\
 r(9) &= k_7[7\text{-Cl}] - k_8[9]
 \end{aligned}$$

Optimized rate constants and standard deviations from fitting to the measured concentrations for 3^{COE}-Cl , 4^{COE} , **5**, **6**, **7-Cl**, **8**, and **9** are:

rate constant	optimized value	σ	coefficient of variation %
k_1	$1.41 \times 10^{-3} \text{ min}^{-1}$	0.012×10^{-3}	0.9
k_2	$0.97 \times 10^{-3} \text{ min}^{-1}$	0.012×10^{-3}	1.2
k_3	$26 \times 10^{-3} \text{ min}^{-1}$	1.7×10^{-3}	6.3
k_{-3}	$401 \text{ mM}^{-1}\text{min}^{-1}$	709	176
k_4	8 min^{-1}	15.6	174
k_5	$0.94 \times 10^{-3} \text{ min}^{-1}$	0.073×10^{-3}	7.7
k_6	$54.7 \times 10^{-3} \text{ min}^{-1}$	1.8×10^{-3}	3.3
k_7	$37.3 \times 10^{-3} \text{ min}^{-1}$	1.3×10^{-3}	3.6
k_8	$1.76 \times 10^{-3} \text{ min}^{-1}$	0.062×10^{-3}	3.5

1.1.9 Crystallographic details

Suitable single crystals for the X-ray diffraction studies were grown by diffusion of pentane into THF solutions ($3^{\text{C}^{2\text{H}4}}\text{-PF6}$, 3^{CO}-PF6 , **5**) or slow cooling of saturated pentane solutions to $-35 \text{ }^\circ\text{C}$ ($4^{\text{C}^{2\text{H}4}}$, 4^{CO}). Crystals were stored under perfluorinated ether, transferred in a Lindemann capillary, fixed, and sealed. Preliminary examinations and data collection were carried out with area detecting systems and graphite-monochromated Mo KR radiation (λ) 0.71073 \AA . For specific crystal-structure determination details see original publication. Crystallographic data (excluding structure factors) for the structures have been deposited with the Cambridge Crystallographic Data Centre as supplementary publication no. CCDC-715654 ($3^{\text{C}^{2\text{H}4}}\text{-PF6}$), CCDC-715652 (3^{CO}-PF6), CCDC-715655 ($4^{\text{C}^{2\text{H}4}}$), CCDC-715653 (4^{CO}), and CCDC-715651 (**5**). Copies of the data can be obtained free of charge on application to CCDC, 12 Union Road, Cambridge CB2 1EZ, UK (fax: (+44)1223-336-033; e-mail: deposit@ccdc.cam.ac.uk).

B Results and Discussion

Crystal data and structure refinement for $[\text{Ir}(\text{COE})\{\text{HN}(\text{CH}_2\text{CH}_2\text{P}^i\text{Pr}_2)_2\}^+][(\text{BPh}_4)^-]\cdot\text{THF}\cdot 0.5 \text{C}_6\text{H}_6$ ($3^{\text{COE}}\text{-BPh}_4$)

Molecular Formula: $\text{C}_{55} \text{H}_{82} \text{B Ir N O P}_2$
 $[(\text{C}_{24} \text{H}_{51} \text{Ir N P}_2)^+], [(\text{C}_{24} \text{H}_{20} \text{B})^-], \text{C}_4 \text{H}_8 \text{O}, 0.5(\text{C}_6 \text{H}_6)$

Crystal Color / Shape Orange fragment

Molecular Weight: 1038.19 a.m.u.

Systematic Absences: none

Space Group: Triclinic P (I.T.-No.: 2)

Cell Constants: $a = 1331.95(11) \text{ pm}$ $\alpha = 74.459(7)^\circ$
 $b = 1408.48(12) \text{ pm}$ $\beta = 75.586(7)^\circ$
 $c = 1514.75(12) \text{ pm}$ $\gamma = 76.500(7)^\circ$
 $V = 2609.0(4) \cdot 10^6 \text{ pm}^3; Z = 2; D_{\text{calc}} = 1.322 \text{ g cm}^{-3}$

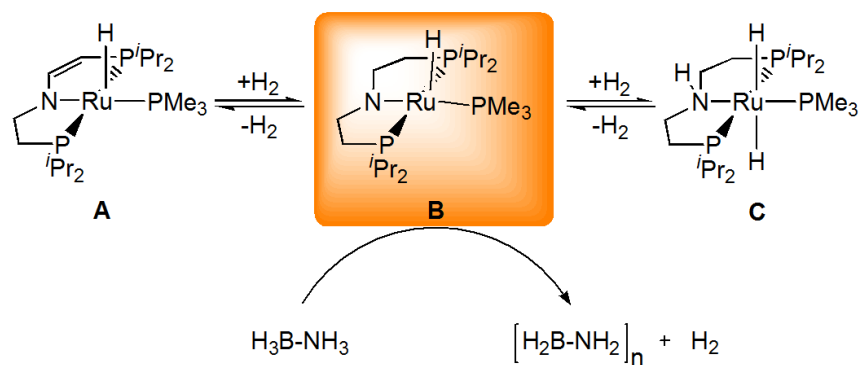
Data collection interrupted due to severe disorder in the COE- and THF-part.

1.2 Ruthenium Complexes with Cooperative PNP Ligands: Bifunctional Catalysis for the Dehydrogenation of Ammonia- Borane

This chapter originated the following publication:

M. Käß, A. Friedrich, M. Drees, S. Schneider

Angew. Chem. **2009**, *121*, 922; *Angew. Chem. Int. Ed.* **2009**, *48*, 905.



1.2.1 Introduction

The quest for alternative energy sources has sparked considerable interest in chemical hydrogen storage.^[1] A promising approach is the reversible hydrogenation and dehydrogenation of small molecules, such as alcohols or ammonia-borane (H₃B–NH₃).^[2] In particular, the latter has been proposed because of its high hydrogen to mass ratio.^[3] Although transition-metal-catalyzed homogenous hydrogenations are widespread reactions in synthetic organic chemistry and industrial processes, efficient catalysts for dehydrogenation are surprisingly rare. Only recently, few homogeneous and colloidal transition-metal catalysts were reported for the release of up to 2.8 equivalents of H₂ from ammonia-borane under mild conditions.^[4]

Bifunctional catalysts bearing cooperative amino ligands, which are involved in the catalytic cycle via reversible chemical transformations, were successfully introduced by Noyori et al. for the hydrogenation and transfer hydrogenation (TH) of polar double bonds.^[5,6] According to the principle of microscopic reversibility the dehydrogenation of polar functional groups could be possible with this catalyst class, however such bifunctional

¹ J. J. Romm, *Der Wasserstoff-Boom*, WILEY-VCH, Weinheim, **2006**.

² H. Junge, B. Loges, M. Beller, *Chem. Commun.* **2007**, 522-524.

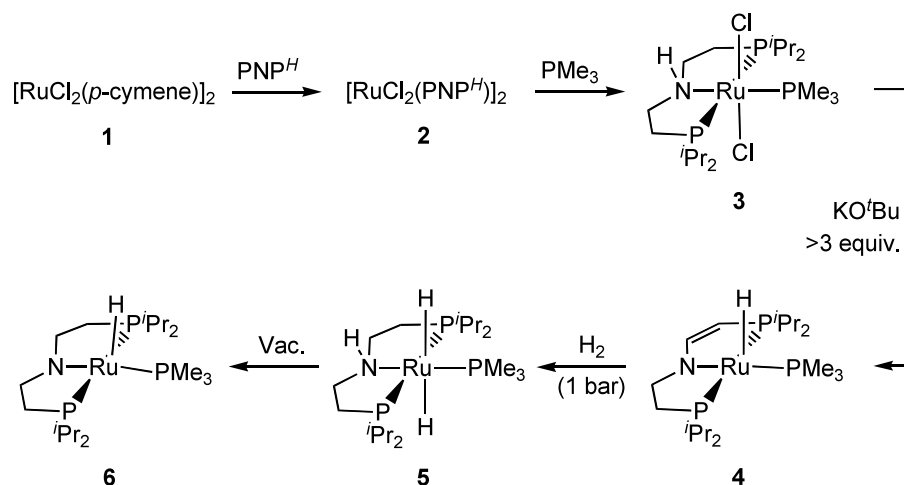
³ a) US Department of Energy Report, “Basic Research Needs for the Hydrogen Economy”, http://www.sc.doe.gov/bes/reports/files/NHE_rpt.pdf, **2004**; b) T. B. Marder, *Angew. Chem.* **2007**, *119*, 8262-8264; *Angew. Chem. Int. Ed.* **2007**, *46*, 8116-8118.

⁴ a) C. A. Jaska, K. Temple, A. J. Lough, I. Manners, *Chem. Commun.* **2001**, 962-963; b) C. A. Jaska, K. Temple, A. J. Lough, I. Manners, *J. Am. Chem. Soc.* **2003**, *125*, 9424-9434; c) T. J. Clark, C. A. Russell, I. Manners, *J. Am. Chem. Soc.* **2006**, *128*, 9582-9583; d) M. C. Denney, V. Pons, T. J. Hebden, D. M. Heinekey, K. I. Goldberg, *J. Am. Chem. Soc.* **2006**, *128*, 12048-12049; e) R. J. Keaton, J. M. Blacquiere, R. T. Baker, *J. Am. Chem. Soc.* **2007**, *129*, 1844-1845; f) F. Cheng, H. Ma, Y. Li, J. Chen, *Inorg. Chem.* **2007**, *46*, 788-794; g) J. F. Fulton, J. C. Linehan, T. Autrey, M. Balasubramanian, Y. Chen, N. K. Szymczak, *J. Am. Chem. Soc.* **2007**, *129*, 11936-11949; h) D. Pun, E. Lobkovsky, P. J. Chirik, *Chem. Commun.* **2007**, 3297-3299; i) A. Staubitz, A. Presa Soto, I. Manners, *Angew. Chem.* **2008**, *120*, 6308-6311; *Angew. Chem. Int. Ed.* **2008**, *47*, 6212-6215.

⁵ Reviews: a) Noyori, R.; Ohkuma, T. *Angew. Chem.* **2001**, *113*, 40; *Angew. Chem. Int. Ed.* **2001**, *40*, 40; b) Clapham, S. E.; Hadzovic, A.; Morris, R. H. *Coord. Chem. Rev.* **2004**, *248*, 2201; c) Muniz, K. *Angew. Chem.* **2005**, *117*, 6780; *Angew. Chem. Int. Ed.* **2005**, *44*, 6622.

⁶ Grützmacher, H. *Angew. Chem.* **2008**, *120*, 1838; *Angew. Chem. Int. Ed.* **2008**, *47*, 1814.

catalysts have not been utilized for these reactions to date.^[7] Herein we present new Ru^{II} compounds with PNP amido chelate ligands, which can undergo reversible hydrogenation/dehydrogenation reactions both at the N functionality and the ethylene backbone. The reactivity of the ruthenium complexes is utilized for the homogeneous catalytic dehydrogenation of ammonia-borane with unprecedented activities.^[7]



Scheme 1. Synthesis of amido complex **6** ($\text{PNP}^H = \text{HN}(\text{CH}_2\text{CH}_2\text{P}^i\text{Pr}_2)_2$).

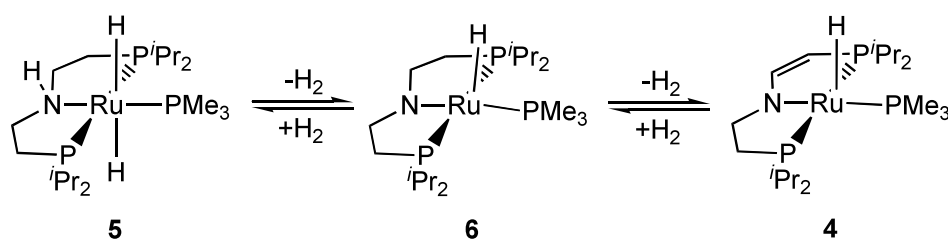
1.2.2 Results and discussion

trans- $[\text{RuCl}_2(\text{PMe}_3)(\text{PNP}^H)]$ (**3**) is prepared almost quantitatively in two steps starting from $[\text{RuCl}_2(\textit{p}\text{-cymene})]_2$ (**1**) (Scheme 1). Upon reaction with 3.3 equiv. KO^tBu , the dark green, highly air sensitive complex **4** was isolated in 95 % yield. The reaction was rapid and no intermediates were detected by ^{31}P NMR spectroscopy. When less than three equivalents of KO^tBu was used, only incomplete conversion of **3** was observed. The formation of **4** can be attributed to deprotonation of the N center of **3** and subsequent β -hydride elimination. Finally, **4** would then result from the deprotonation of an intermediate hydrido-chloro-imino complex

⁷ During the preparation of this manuscript a paper has been published which follows the same approach. The TH-catalyst $[\text{RuCl}_2(\text{R}_2\text{PCH}_2\text{CH}_2\text{NH}_2)_2]/\text{KO}^t\text{Bu}$ ($\text{R} = ^i\text{Pr}, ^t\text{Bu}$) exhibits comparable activities in the dehydrogenation of $\text{H}_3\text{B}-\text{NH}_3$ as complex **6**. Based on the analogy to TH and DFT calculations a bifunctional (Noyori-Morris) mechanism was proposed: N. Blaquiere, S. Diallo-Garcia, S. I. Gorelsky, D. A. Black, K. Fagnou, *J. Am. Chem. Soc.* **2008**, *130*, 14034.

B Results and Discussion

at the acidic α position relative to the imino group.^[8] The novel ligand type of enamido complex **4** represents an aliphatic analog of $[\text{RuH}(\text{CO})\{\text{NC}_5\text{H}_3(\text{CHP}^i\text{Pr}_2)(\text{CH}_2\text{P}^i\text{Pr}_2)\}]$ which was reported by Milstein et al. to be obtained upon deprotonation of a pyridine-based PNP pincer complex.^[9] The reversibility of the ligand backbone dehydrogenation was demonstrated by the reaction of **4** with H_2 . The resulting amino complex **5** underwent the partial elimination of H_2 during workup, and could therefore not be obtained analytically pure. However, evacuation of the solid crude-product under dynamic vacuum at room temperature gives analytically pure, dark red, and highly air sensitive amido complex **6** in yields around 85 % over five steps. Whereas **6** quantitatively adds hydrogen in solution under H_2 atmosphere, **6** slowly releases H_2 under argon at room temperature over several days, demonstrating that the heterolytic H_2 activation reactions shown in Scheme 2 are reversible. To the best of our knowledge, the reversible hydrogenation/dehydrogenation of ethylene bridges in amido chelate complexes, which are frequently used as hydrogenation catalysts, has not been directly observed.^[10]



Scheme 2. Hydrogenation/dehydrogenation equilibria between amino (**5**), amido (**6**) and enamido (**4**) complex.

The chemical shifts ($\delta = -8.00$ and $\delta = -8.52$ ppm) and $^2J(\text{H,P})$ coupling constants ($^2J(\text{H,P}) = 16.7 - 24.3$ Hz) of the two hydride signals of **5** exclude a configuration in which the hydrides are in *trans* position to the amino or a phosphine ligand.^[10] The meridional coordination of the PNP^{H} pincer results from the *trans*-dihydride configuration. For enamido complex **4**, the hydride chemical shift ($\delta = -31.68$ ppm) and $^2J(\text{H,P})$ coupling constant with

⁸ V. F. Kuznetsov, K. Abdur-Rashid, A. J. Lough, D. G. Gusev, *J. Am. Chem. Soc.* **2006**, *128*, 14388.

⁹ J. Zhang, G. Leitus, Y. Ben-David, D. Milstein, *Angew. Chem.* **2006**, *118*, 1131-1133; *Angew. Chem. Int. Ed.* **2006**, *45*, 1113.

¹⁰ R. Abbel, K. Abdur-Rashid, M. Fraatz, A. Hadzovic, A. J. Lough, R. H. Morris, *J. Am. Chem. Soc.* **2005**, *127*, 1870.

the PMe_3 ligand ($^2J(\text{H,P}) = 47$ Hz) differ significantly from amido complex **6** ($\delta = -24.18$ ppm; $^2J(\text{H,P}) = 54$ Hz), suggesting considerably different coordination geometries. Because of their high solubility we were unable to grow single crystals of either **4** and **6**, therefore DFT models of the two complexes were generated (Figure 1). Whereas the ruthenium center of enamide **4** exhibits a slightly distorted square-pyramidal coordination polyhedron, amido complex **6** can best be described as trigonal-bipyramidal having a Y-shaped distortion. The considerably smaller H–Ru– PMe_3 angle in **6** explains the NMR spectroscopic results. Such Y-shaped coordination geometries as that found in **6**, are typically found for five coordinate d^6 -complexes having a strong π -donating ligand.^[11] Therefore, the molecular structure of **4** can be an indication of weaker N→Ru π -interaction resulting from dehydrogenation of the ligand backbone, indicating the delocalization of the free electron pair of the nitrogen donor into the vinylene group.^[12]

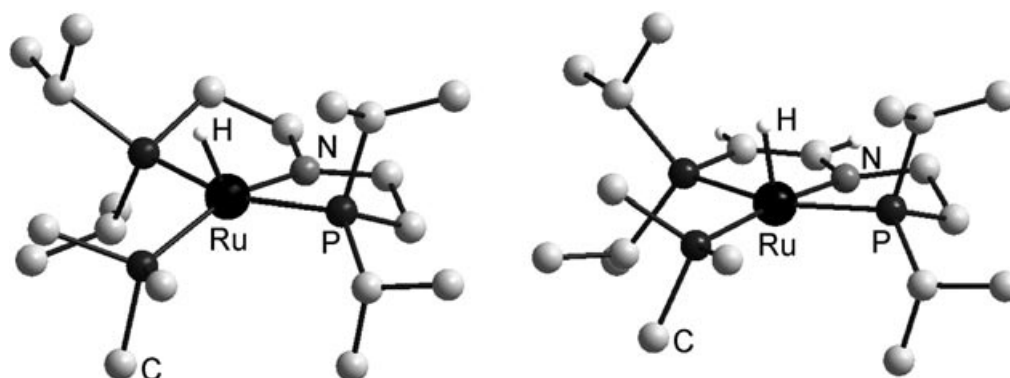


Figure 1. Minimum structures of **6** (left) and **4** (right) from DFT calculations (B3LYP/6-31+G**); H atoms except hydrides and vinylene protons are omitted). Selected bond angles of **6**: N–Ru– PMe_3 159.8° , N–Ru– H_{Hydrid} 120.9° , Me_3P –Ru– H_{Hydrid} 79.3° and **4**: N–Ru– PMe_3 172.6° , N–Ru– H_{Hydrid} 102.5° , Me_3P –Ru– H_{Hydrid} 84.6° .

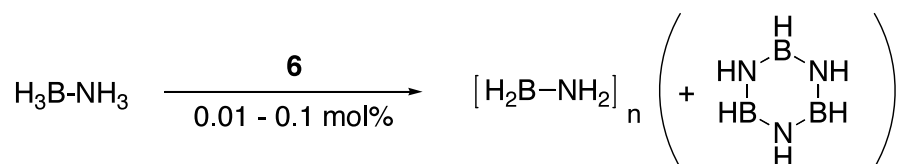
Amido complex **6** was used in the dehydrogenation of ammonia-borane (Scheme 3). Upon addition of the catalyst to a THF solution of $\text{H}_3\text{B-NH}_3$ (0.54 M) at room temperature, vigorous H_2 evolution was instantaneous and the formation of a white precipitate are observed. Even with very small catalyst loadings (0.01 mol% **6**) high catalytic activities were

¹¹ Y. Jean, *Molecular Orbitals of Transition Metal Complexes*, Oxford University Press, Oxford, **2005**.

¹² The strong contribution of the vinylene carbon p -orbitals to the Ru–N π bond (HOMO, HOMO-2), confirm this interpretation: see chapter B1.2.8.

B Results and Discussion

observed (Figure 2). Pseudo first-order rate constants of 0.013 s^{-1} (0.1 mol% **6**) and 0.0021 s^{-1} (0.01 mol% **6**) were obtained from logarithmic plots (turnover frequency = 13 - 21 s^{-1}). Whereas catalyst loadings of 0.1 mol% **6** produce slightly more than 1 equivalent of H_2 , 0.01 mol% of **6** produced 0.83 equivalents of H_2 (turnover number = 8300). The addition of Hg to the reaction affected neither the activity nor the H_2 yield. To the best of our knowledge complex **6** marks the most active known homogeneous catalyst for ammonia-borane dehydrogenation.^[7] Powder diffractogram, and MAS- ^{11}B -NMR and IR-spectra of the precipitate are in agreement with the formation of a polymer dehydrocoupling product $(\text{BH}_2\text{NH}_2)_n$.^[4i] Small amounts of borazine detected in the reaction solution by using ^{11}B NMR methods explains the H_2 yield of slightly over 1 equivalent.



Scheme 3. Catalytic dehydrogenation of ammonia-borane.

Additional information about the mechanism was obtained by running the reaction with deuterated substrates. By using 0.1 mol-% catalyst loadings large kinetic isotope effects (KIE) of 2.1 ($\text{D}_3\text{B-NH}_3$), 5.2 ($\text{H}_3\text{B-ND}_3$), and 8.1 ($\text{D}_3\text{B-ND}_3$) were found relative to $\text{H}_3\text{B-NH}_3$ dehydrogenation. In comparison, KIEs of 1.7 ($\text{D}_3\text{B-NH}_3$), 2.3 ($\text{H}_3\text{B-ND}_3$) and 3.0 ($\text{D}_3\text{B-ND}_3$) were reported for ammonia-borane dehydrogenation using a nickel carbene complex.^[4e] The KIEs are in agreement with a concerted mechanism in which N-H and B-H bond cleavages are in the rate-determining step, as was found for TH with Noyori's bifunctional ruthenium catalysts.^[13,14] At an early stage of the reaction (20 mol% **6**) only amino complex **5** was found by ^{31}P NMR methods.^[15] However, the slow H_2 elimination from

¹³ K. Abdur-Rashid, S. E. Clapham, A. Hadzovic, J. N. Harvey, A. J. Lough, R. H. Morris, *J. Am. Chem. Soc.* **2002**, *124*, 15104.

¹⁴ a) C. P. Casey, J. B. Johnson, *J. Org. Chem.* **2003**, *68*, 1998-2001; b) J. B. Johnson, J.-E. Bäckvall, *J. Org. Chem.* **2003**, *68*, 7681.

¹⁵ **5** could alternatively be formed by heterolytic addition of released H_2 to **6** and is therefore not necessarily involved in the catalytic cycle.

complex **5** indicates that spontaneous loss of H₂ to regenerate **6** cannot be of relevance for the catalytic cycle.

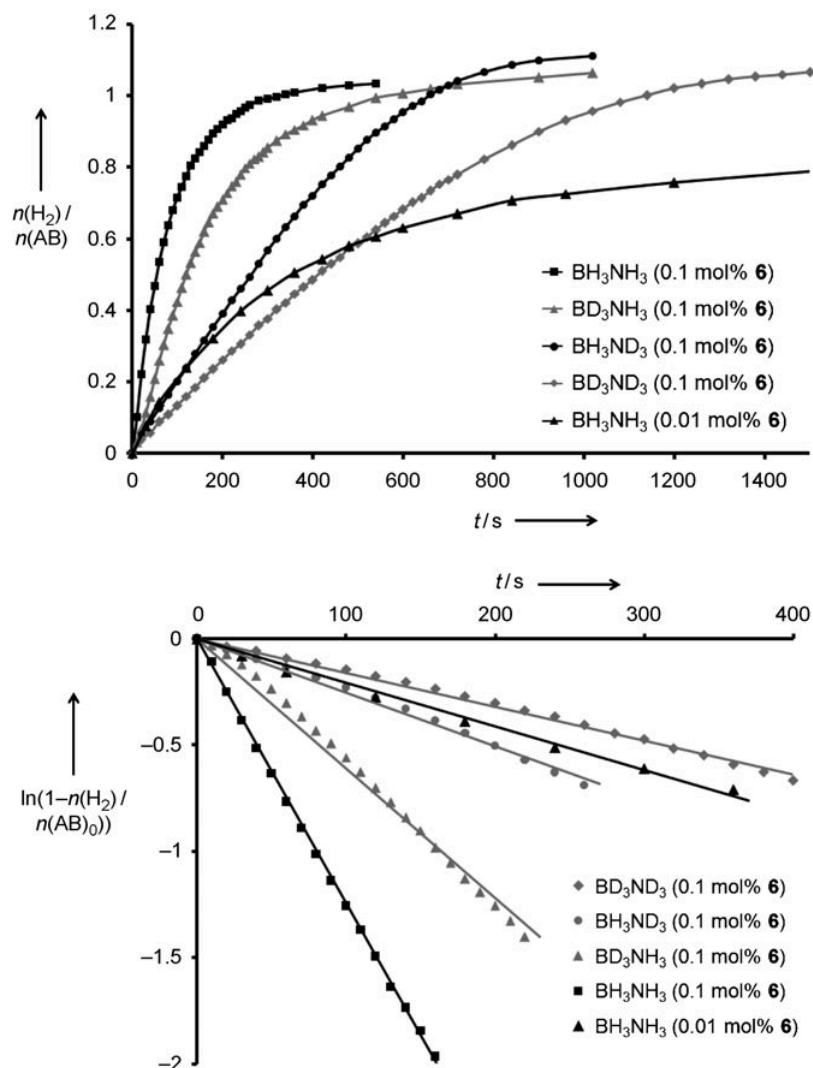


Figure 2. Time course (above) and logarithmic plot (below) for ammonia-borane (AB) dehydrogenation catalyzed by **6** in THF at room temperature. Straight lines were obtained by linear regression analysis of the data points.

1.2.3 Conclusion

In conclusion we presented ruthenium(II) complexes having PNP-pincer ligands, which can participate in the reversible, heterolytic H₂ activation with the nitrogen atom and the ligand backbone. NMR spectroscopic results and DFT calculations show that the novel cooperative enamido ligand of **4** exhibits significantly different donor properties, compared to amido analog **6**. Therefore, π donation by the amido nitrogen atom can be controlled by the

reversible chemical transformations within the pincer backbone. Amido complex **6** shows unprecedented activity and turnover numbers in the dehydrogenation of ammonia-borane under mild conditions with low catalyst loadings. The present results are in agreement with a bifunctional Noyori-Morris-type mechanism, having a concerted transfer of a hydride (B–H) and a proton (N–H) from the substrate to a catalyst species.^[5,13] Therefore, our results suggest that bifunctional catalysts could be suitable for efficient hydrogen production from other small molecules with polar E–H bonds. Initial results also show that **6** exhibits good activities in the acceptor-less dehydrogenation of alcohols.

1.2.4 Experimental details and syntheses

Materials and Methods. All experiments were carried out under an atmosphere of argon using Schlenk and glove-box techniques. Solvents were dried over Na/benzophenone/tetraglyme (benzene) or Na/benzophenone (THF), distilled under argon and deoxygenated prior to use. Deuterated solvents were dried by trap to trap distillation from Na/K alloy (C₆D₆) or CaH (CD₂Cl₂) and deoxygenated by three freeze-pump-thaw cycles. KO^tBu was purchased from VWR and sublimed prior to use. H₂ 5.0 (Messer Griesheim), [RuCl₂(*p*-cymene)]₂ (**1**) (ABCR), H₃B–NH₃ (Aldrich), PMe₃ (Aldrich, 1 M solution in THF) and NaBD₄ (ISOTEC) were used as purchased. Partially and fully deuterated ammonia boranes were prepared from deuterated starting materials as reported in the literature for H₃B–NH₃.^[16] Deuterated ammonium sulfate was prepared from NH₄SO₄ by repeated stirring in D₂O at 40°C over night. HN(CH₂CH₂P^{*i*}Pr₂)₂ was prepared as reported in the literature.^[17]

Analytical Methods. Elemental analyses were obtained from the Microanalytical Laboratory of Technische Universität München. The IR spectra were recorded on a Jasco FT/IR-460 PLUS spectrometer as nujol mulls between KBr plates or as KBr pellet. NMR spectra were recorded on a Jeol Lambda 400 spectrometer and were calibrated to the residual proton resonance and the natural abundance ¹³C resonance of the solvent (C₆D₆, δ_H = 7.16 and δ_C = 128.06 ppm; CD₂Cl₂, δ_H = 5.32 and δ_C = 53.52 ppm). ³¹P NMR chemical shifts are reported relative to external phosphoric acid (δ 0.0 ppm). ¹¹B NMR spectra in solution were referenced to external BF₃OEt₂ (0.0 ppm). For ¹¹B MAS NMR spectroscopy samples were

¹⁶ P. V. Ramachandran, P. D. Gagare, *Inorg. Chem.* **2007**, *46*, 7810.

¹⁷ A. A. Danopoulos, A. R. Wills, P. G. Edwards, *Polyhedron* **1990**, *9*, 2413.

packed under inert gas into a 4 mm ZrO₂ rotor sealed with a Kel-F cap. The spectra were recorded with a BRUKER Avance 300 spectrometer at 96.29 MHz with an MAS frequency of 15 kHz (pulse width 1.5 μs, repetition time 1 s). Chemical shifts are referenced to external B(OMe)₃ (δ 18.1 ppm). Signal multiplicities are abbreviated as: s (singlet), d (doublet), t (triplet), vt (virtual triplet), q (quartet), sp (septet), m (multiplet), br (broad).

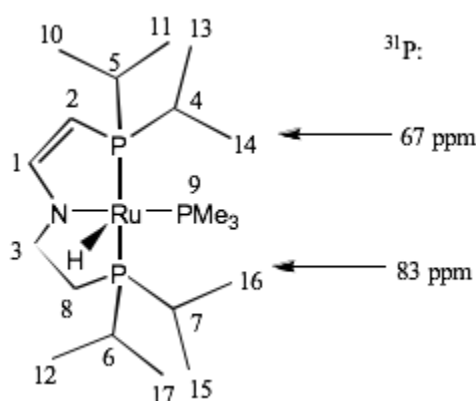
$[RuCl_2(PNP^H)]_2$ (**2**). HN(CH₂CH₂PⁱPr₂)₂ (0.499 g; 1.63 mmol) is added to a suspension of **1** (0.500 g; 0.81 mmol) in 20 mL THF. Upon heating to reflux for 24 h yellow **2** slowly precipitates from the reaction mixture. The solvent is reduced *i. vac.* to a few mL, cooled to 0°C and 30 mL pentanes are added. The product is filtered off, washed with pentane and dried *i. vac.* Yield: 0.682 g (0.71 mmol, 88%). Anal. Calcd. for C₃₂H₇₄Cl₄N₂P₄Ru₂ (954.80): C, 40.25; H, 7.81; N, 2.93. Found: C, 40.32; H, 7.64; N, 2.83. IR (Nujol, cm⁻¹) $\tilde{\nu}$ = 3156 (N-H). NMR (CD₂Cl₂, r.t., [ppm]) ¹H NMR (399.8 MHz): δ = 6.23 (s (br), 1H, NH), 3.09 (m, 2H, NCH₂), 2.80 (dsp, ²J(H,P) = 8.3 Hz, ³J(H,H) = 7.3 Hz, 2H, PCH(CH₃)₂), 2.61-2.47 (m, 2H, NCH₂), 2.09-2.04 (m, 2H, CH₂P), 1.98 (dsp, ²J(H,P) = 6.6 Hz, ³J(H,H) = 7.1 Hz, 2H, PCH(CH₃)₂), 1.47 (dvt, ³J(H,H) = 7.5 Hz, J(H,P) = 13.3 Hz, 6H, CH₃), 1.36 (dvt, ³J(H,H) = 7.0 Hz, J(H,P) = 12.0 Hz, 6H, CH₃), 1.35 (dvt, ³J(H,H) = 7.5 Hz, J(H,P) = 14.1 Hz, 6H, CH₃), 1.31-1.27 (m, partially superimposed, 2 H, CH₂P), 1.21 (dvt, ³J(H,H) = 7.2 Hz, J(H,P) = 10.2 Hz, 6H, CH₃). ¹³C {¹H} NMR (100.6 MHz): δ = 54.1-53.4 (m, superimposed by solvent signal, NCH₂), 31.3 (vt, J(C,P) = 8.5 Hz, PCH(CH₃)₂), 30.2 (vt, J(C,P) = 10.8 Hz, CH₂P), 24.3 (vt, J(C,P) = 10.0 Hz, PCH(CH₃)₂), 20.5 (s, CH₃), 20.3 (s, CH₃), 19.7 (s, CH₃), 18.7 (vt, J(C,P) = 3.5 Hz, CH₃). ³¹P {¹H} NMR (161.8 MHz): δ = 73.0 (s). The assignments were confirmed by ¹H COSY and ¹H-¹³C HETCOR NMR spectroscopy.

$[RuCl_2(PMe_3)(PNP^H)]$ (**3**). **2** (0.200 g; 0.209 mmol) is suspended in THF (5 mL) and PMe₃ (503 μL 1M solution in THF) added via syringe. After all solid is dissolved, the solution is filtered and dried *i. vac.* affording light orange, microcrystalline **3**. Yield: 0.232 g (100%). Anal. Calcd. for C₁₉H₄₆Cl₂NP₃Ru (553.48): C, 41.23; H, 8.38; N, 2.53. Found: C, 41.83; H, 8.42; N, 2.46. NMR (C₆D₆, r.t., [ppm]) ¹H NMR (399.8 MHz): δ = 3.53 (t (br), ³J(H,H) = 12.4 Hz, 1H, NH), 2.99 (vtsp, J(H,P) = 2.1 Hz, ³J(H,H) = 7.3 Hz, 2H, PCH(CH₃)₂), 2.83 (vtsp, J(H,P) = 2.5 Hz, ³J(H,H) = 7.5 Hz, 2H, PCH(CH₃)₂), 2.8-2.7 (m, 2H, NCH₂), 2.47 (m, 2H, NCH₂), 1.92 (m, 2H, CH₂P), 1.62 (d, ²J(H,P) = 8.3 Hz, 9H, P(CH₃)₃), 1.45 (tm, J = 14.2 Hz, 2H, CH₂P), 1.33 (dvt, ³J(H,H) = 7.0 Hz, J(H,P) = 13.3 Hz, 6H, CH₃), 1.29-1.17 (m, 18H, CH₃). ¹³C {¹H} NMR (100.53MHz): δ = 49.2 (s (br), NCH₂), 25.9 (vt, J(C,P) = 7.7 Hz, PCH(CH₃)₂), 24.6 (vt, J(C,P) = 8.1 Hz, CH₂P), 22.9 (d, ¹J(C,P) = 26.1 Hz, P(CH₃)₃), 22.5 (vt,

B Results and Discussion

$J(\text{C},\text{P}) = 7.7 \text{ Hz}$, $\text{PCH}(\text{CH}_3)_2$), 20.6 (s, CH_3), 20.5 (s, CH_3), 20.4 (s, CH_3), 20.3 (s, CH_3). $^{31}\text{P}\{^1\text{H}\}$ NMR (161.83 MHz): $\delta = 41.1$ (d, $^2J(\text{P},\text{P}) = 29.7 \text{ Hz}$, 2P, P^iPr_2), 8.6 (t, $^2J(\text{P},\text{P}) = 29.7 \text{ Hz}$, 1P, PMe_3). The assignments were confirmed by ^1H COSY NMR spectroscopy.

$[\text{RuH}(\text{PMe}_3)(\text{PN}=\text{P})]$ (**4**). A solution of **3** (0.232 g; 0.419 mmol) in THF (10 mL) is cooled to 0°C and KO^tBu (0.155 g; 1.383 mmol; 3.3 equiv.) in THF (3 mL) added. The color immediately changes to deep green. After 15 min at r.t. the solvent is evaporated *i. vac.* The oily residue is extracted with pentanes, filtered and evaporated to give **4** as a dark green sticky solid. Yield: 0.192 g (0.400 mmol; 95%). Anal. Calcd. for $\text{C}_{19}\text{H}_{44}\text{NP}_3\text{Ru}$ (480.56): C, 47.49; H, 9.23; N, 2.91. Found: C, 47.80; H, 9.52; N, 2.78.



NMR (C_6D_6 , r.t., [ppm]) ^1H NMR (399.8 MHz): $\delta = 7.76$ (dt, $^3J(\text{H},\text{P}) = 41.5 \text{ Hz}$, $^4J(\text{H},\text{P}) = ^3J(\text{H},\text{H}) = 4.6 \text{ Hz}$, 1H, NCH (1)), 3.86 (d, $^2J(\text{H},\text{H}) = 5.1 \text{ Hz}$, 1H, CHCHP (2)), 3.55-3.37 (m, 2H, NCH_2 (3)), 2.35 (dsp, $^3J(\text{H},\text{H}) = 6.5 \text{ Hz}$, $^2J(\text{H},\text{P}) = 5.5 \text{ Hz}$, 1H, PCH (4)), 2.08 (dsp, $^3J(\text{H},\text{H}) = 6.6 \text{ Hz}$, $^2J(\text{H},\text{P}) = 6.2 \text{ Hz}$, 1H, PCH (5)), 1.96 (dsp, $^3J(\text{H},\text{H}) = 7.0 \text{ Hz}$, $^2J(\text{H},\text{P}) = 6.2 \text{ Hz}$, 1H, PCH (6)), 1.79 (dsp, $^3J(\text{H},\text{H}) = 6.5 \text{ Hz}$, $^2J(\text{H},\text{P}) = 6.6 \text{ Hz}$, 1H, PCH (7)), 1.61 (t, $^3J(\text{H},\text{H}) = 7.3 \text{ Hz}$, 2H, $\text{CH}_2\text{CH}_2\text{P}$ (8)), 1.38 (d, $^2J(\text{H},\text{P}) = 7.0 \text{ Hz}$, 9H, $\text{P}(\text{CH}_3)_3$ (9)), 1.33-1.24 (m, 9H, CH_3 (10, 11, 12)), 1.20-1.15 (m, 6H, CH_3 (13, 14)), 1.05-0.98 (m, 6H, CH_3 (15, 16)), 0.90 (dd, $^3J(\text{H},\text{H}) = 7.0 \text{ Hz}$, $^3J(\text{H},\text{P}) = 11.0 \text{ Hz}$, 3H, CH_3 (17)), -31.68 (dt, $^2J(\text{H},\text{P}) = 46.9 \text{ Hz}$, $^2J(\text{H},\text{P}) = 18.2 \text{ Hz}$, 1H, RuH). $^{13}\text{C}\{^1\text{H}\}$ NMR (100.53 MHz): $\delta = 167.9$ (d, $^2J(\text{C},\text{P}) = 24.0 \text{ Hz}$, NCH (1)), 74.0 (dd, $^1J(\text{C},\text{P}) = 37.2 \text{ Hz}$, $^3J(\text{C},\text{P}) = 5.2 \text{ Hz}$, CHCHP (2)), 57.2 (d, $^2J(\text{C},\text{P}) = 7.4 \text{ Hz}$, NCH_2 (3)), 27.6 (d, $^1J(\text{C},\text{P}) = 17.2 \text{ Hz}$, $\text{CH}_2\text{CH}_2\text{P}$ (8)), 27.4 (d (superimposed by (9)), $\text{PCH}(\text{CH}_3)_2$), 27.2 (d, $^1J(\text{C},\text{P}) = 23.4 \text{ Hz}$, $\text{P}(\text{CH}_3)_3$ (9)), 27.0 (d (superimposed by (9)), $\text{PCH}(\text{CH}_3)_2$), 26.5 (d, $^1J(\text{C},\text{P}) = 19.7 \text{ Hz}$, $\text{PCH}(\text{CH}_3)_2$), 25.8 (d, $^1J(\text{C},\text{P}) = 24.6 \text{ Hz}$, $\text{PCH}(\text{CH}_3)_3$), 20.5 (d, $^2J(\text{C},\text{P}) = 6.2 \text{ Hz}$, CH_3 (12)), 20.0 (d, $^2J(\text{C},\text{P}) = 7.4 \text{ Hz}$, CH_3 (15)), 19.4 (d, $^2J(\text{C},\text{P}) = 5.5 \text{ Hz}$, CH_3 (16)), 19.2 (d, $^2J(\text{C},\text{P}) = 7.4 \text{ Hz}$, CH_3 (13)),

18.2 (s, CH₃ (10, 11, 14)), 17.6 (s, CH₃ (17)). ³¹P{¹H} NMR (161.83 MHz): δ = 83.4 (dd, ²J(P,P) = 244.7 Hz, ²J(P,P) = 24.8 Hz, CH₂PiPr₂), 67.1 (dd, ²J(P,P) = 244.7 Hz, ²J(P,P) = 24.8 Hz, CHPiPr₂), 5.0 (t, ²J(P,P) = 24.8 Hz). The assignments were confirmed by ¹H COSY and ¹H-¹³C HETCOR NMR spectroscopy and ¹H NMR spectra with selective phosphorous decoupling.

[Ru(H)₂(PMe₃)(PNP^H)] (**5**). A solution of **4** (0.020 g; 0.042 mmol) in C₆D₆ (0.5 mL) is degassed in a J-Young NMR tube by 3 freeze-pump-thaw cycles and set under 1 bar H₂. The color immediately changes via greenish-yellow to orange giving **5** quantitatively. Attempted isolation resulted in partial dehydrogenation and formation of **6** (see below). NMR (C₆D₆, r.t., [ppm]) ¹H NMR (399.8 MHz): δ = 2.86 (s (br), 1H, NH), 2.31-2.16 (m, 2H, NCH₂), 2.11-2.01 (m, 2H, PCH(CH₃)₂), 1.96 (sp, ³J(H,H) = 6.8 Hz, 2H, PCH(CH₃)₂), 1.59 (dvt, ³J(H,H) = 14.5 Hz, J(H,P) = 7.3 Hz, 6H, PCH(CH₃)₂), 1.6-1.5 (m, superimposed signal, 2H, NCH₂), 1.35 + 1.39-1.33 (d + m, ²J(H,P) = 7.7 Hz, 15H, P(CH₃)₃ + PCH(CH₃)₂), 1.24 (dvt, ³J(H,H) = 14.5 Hz, J(H,P) = 7.3 Hz, 6H, PCH(CH₃)₂), 1.21-1.16 (m, 6H, PCH(CH₃)₂), 1.13-1.00 (m, 4H, CH₂P), -8.00 (ddt, ²J(H,H) = 7.7 Hz, ²J(H,P) = 16.67 Hz, ²J(H,P) = 24.3 Hz, 1H, RuH), -8.52 (dq, ²J(H,H) = 7.7 Hz, ²J(H,P) = 20.5 Hz, 1H, RuH). ¹³C{¹H} NMR (100.53 MHz): δ = 54.8 (s (br), NCH₂), 31.0 (d, ¹J(C,P) = 23.4 Hz, P(CH₃)₃), 27.8 (vt, J(C,P) = 10.0 Hz, PCH(CH₃)₂), 27.3 (vt, J(C,P) = 6.5 Hz, CH₂P), 25.1 (vt, J(C,P) = 8.8 Hz, PCH(CH₃)₂), 21.5 (s, CH₃), 20.5 (s, CH₃), 20.1 (s, CH₃), 18.0 (s, CH₃). ³¹P{¹H} NMR (161.83 MHz): δ = 88.4 (d, ²J(P,P) = 34.7 Hz), 13.0 (t, ²J(P,P) = 34.7 Hz). The assignments and J(H,P) coupling constants were confirmed by ¹H COSY NMR and selectively decoupled ¹H-³¹P} NMR spectra.

[RuH(PMe₃)(PNP)] (**6**). **4** (0.192 g; 0.400 mmol) is dissolved in THF (10 mL) and cooled to -90 °C. The vessel is evacuated and set under an atmosphere of H₂. After 30 min at r.t. the orange solution is evaporated. The sticky crude product is dissolved in benzene (10 mL), the solvent sublimed off and the brick red powder evacuated over night (0.192 g; 100%). Anal. Calcd. for C₁₉H₄₆NP₃Ru (482.57): C, 47.29; H, 9.61; N, 2.90. Found: C, 47.44; H, 9.29; N, 2.78. IR (Nujol, cm⁻¹): $\tilde{\nu}$ = 1963 (s, Ru-H). NMR (C₆D₆, r.t., [ppm]) ¹H NMR (399.8 MHz): δ = 3.45 (m, 2H, NCH₂), 3.12 (m, 2H, NCH₂), 2.10 (sp, ³J(H,H) = 6.8 Hz, 2H, PCH(CH₃)₂), 1.96-1.77 (m, 4H, CH₂P), 1.60 (sp, ³J(H,H) = 7.3 Hz, 2H, PCH(CH₃)₂), 1.36 (d, ²J(H,P) = 6.4 Hz, 9H, P(CH₃)₂), 1.21 (dvt, ³J(H,H) = 7.7 Hz, J(H,P) = 7.2 Hz, 6H, PCH(CH₃)₂), 1.17-1.07 (superimposed signals, 12H, PCH(CH₃)₂), 1.04-1.97 (superimposed signals, 6H, PCH(CH₃)₂), -24.18 (dt, ²J(H,P) = 54.3 Hz, ²J(H,P) = 17.6 Hz, 1H, RuH). ¹³C{¹H} NMR

B Results and Discussion

(100.53MHz): $\delta = 63.9$ (s (br), NCH₂), 29.8 (vt, $J(\text{C,P}) = 11.5$ Hz, PCH(CH₃)₃), 29.4 (d, $^1J(\text{C,P}) = 21.5$ Hz, P(CH₃)₃), 27.3 (dvt, $J(\text{C,P}) = 7.7$ Hz, $^3J_{\text{CP}} = 3.1$ Hz, CH₂P), 26.1 (vt, $J(\text{C,P}) = 8.5$ Hz, PCH(CH₃)₃), 21.4 (vt, $J(\text{C,P}) = 3.9$ Hz, CH₃), 19.8 (s, CH₃), 19.7 (s, CH₃), 17.4 (s, CH₃). $^{31}\text{P}\{^1\text{H}\}$ NMR (161.83 MHz): $\delta = 87.8$ (d, $^2J(\text{P,P}) = 21.8$ Hz), 1.2 (t, $^2J(\text{P,P}) = 21.8$ Hz).

Reaction of [RuH(PMe₃)(PNP)] (6) with hydrogen. A solution of **6** (10.5 mg; 0.022 mmol) in C₆D₆ (0.5 mL) in a J-Young NMR tube is set under 1 bar H₂. **5** forms quantitatively (by ^1H and ^{31}P NMR spectroscopy). The solution is degassed by 3 freeze-pump-thaw cycles and set under vacuum. No change is observed within 2d at r.t. in the ^1H and ^{31}P NMR spectra.

Dehydrogenation of [RuH(PMe₃)(PNP)] (6). **6** (0.015 g; 0.031 mmol) is dissolved in C₆D₆ (0.5 mL) in a J-Young NMR tube and monitored by ^{31}P over 2 weeks (Figure S1).

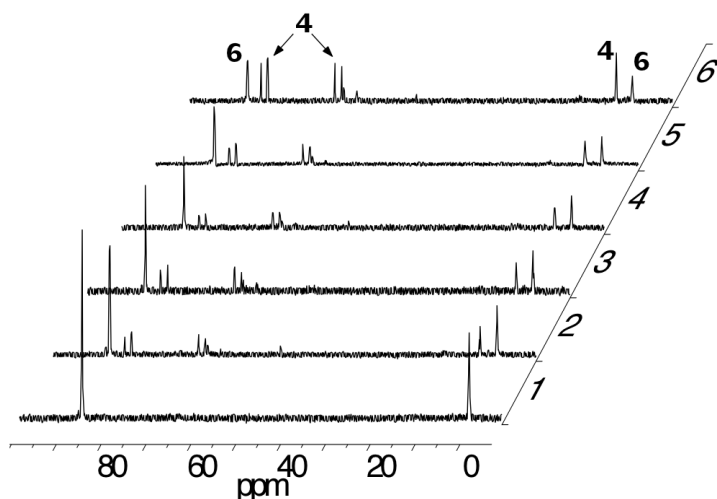


Figure S1. Slow conversion of **6** into **4** in C₆D₆ at room temperature. ^{31}P NMR spectra are recorded after 0 h (1), 53 h (2), 147 h (3), 175 h (4), 198 h (5) and 2 weeks (6).

1.2.5 NMR spectra

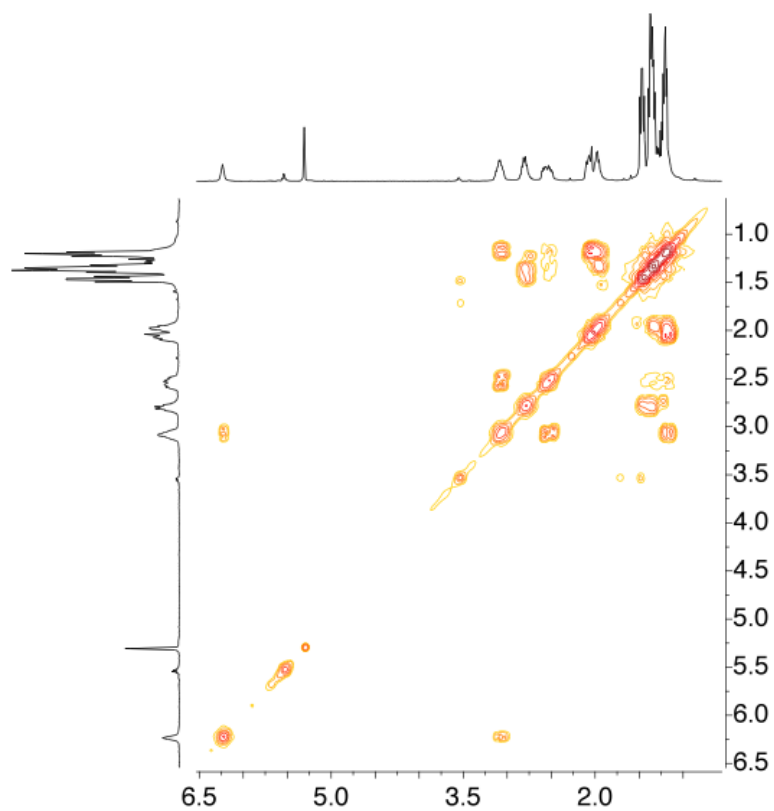


Figure S2. ^1H COSY NMR (CD_2Cl_2 , r.t.) of **2**.

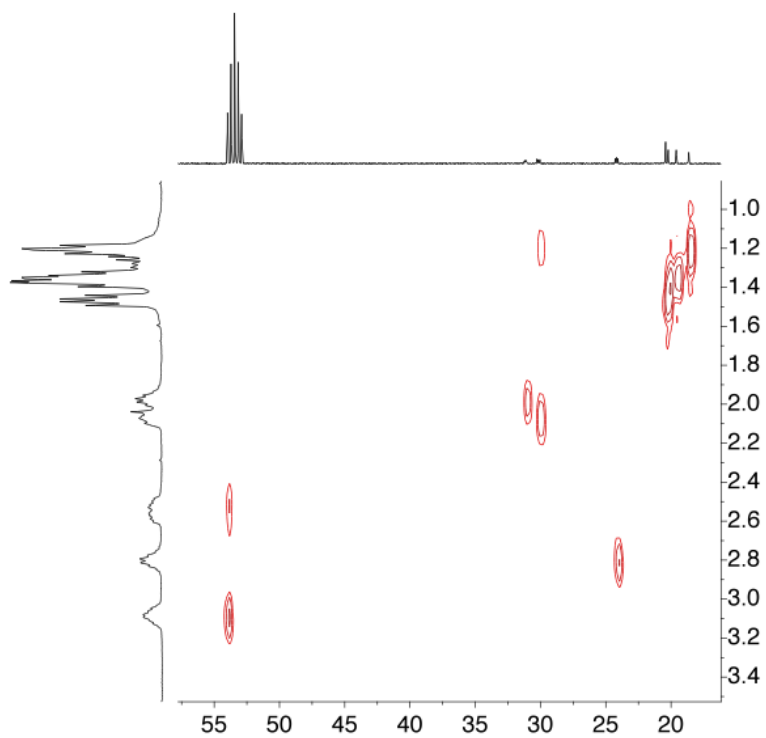


Figure S3. ^1H - ^{13}C HETCOR NMR (CD_2Cl_2 , r.t.) of **2**.

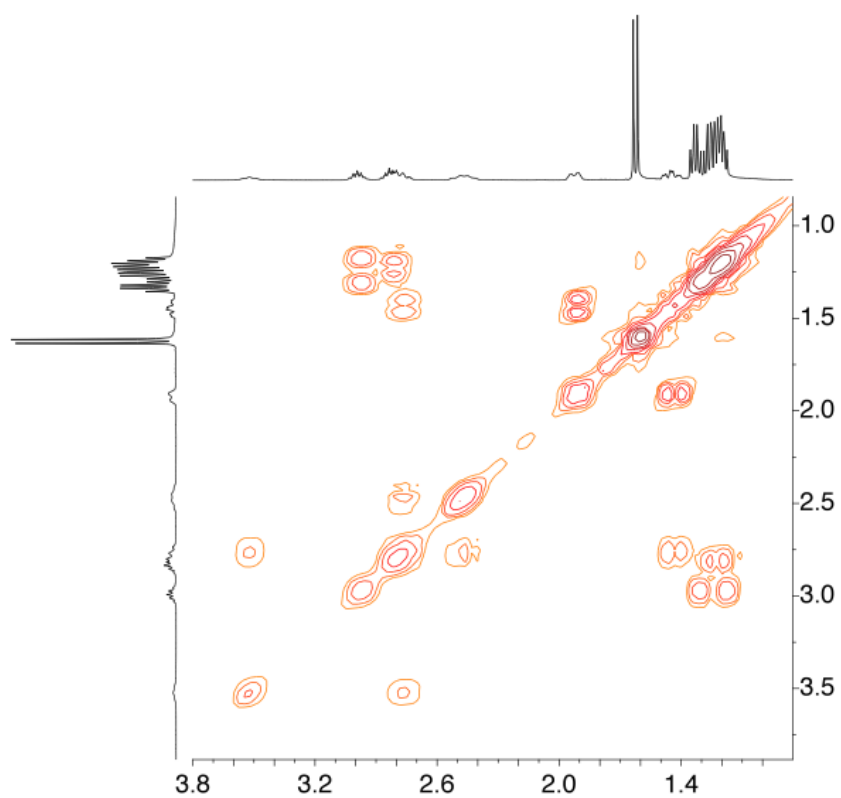


Figure S4. ¹H COSY NMR (C₆D₆, r.t.) of **3**.

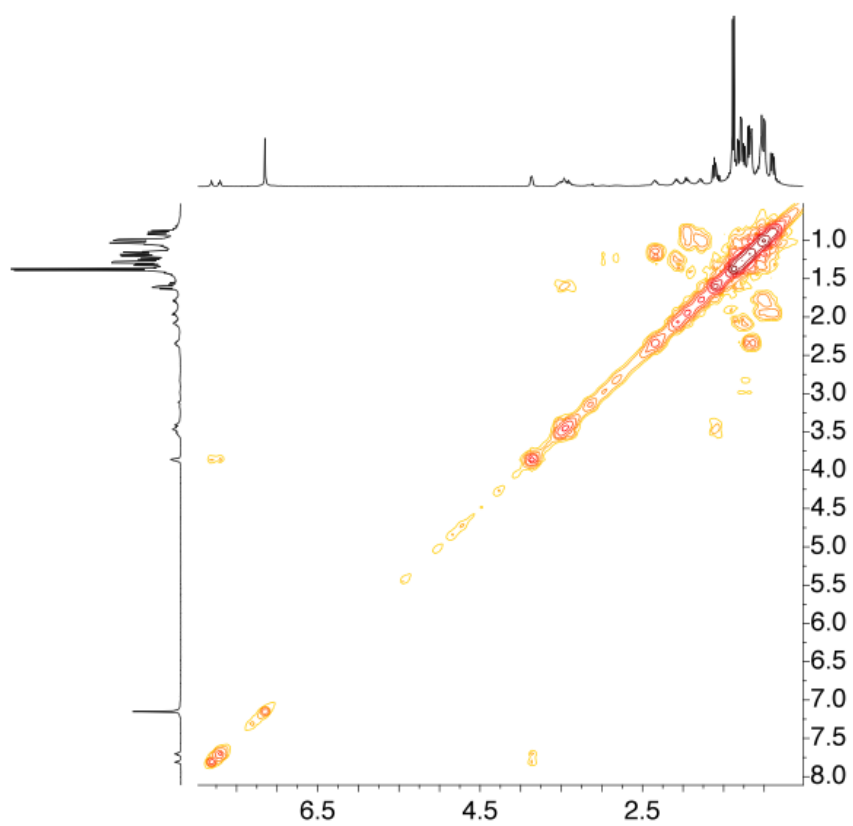


Figure S5. ¹H COSY NMR (C₆D₆, r.t.) of **4**.

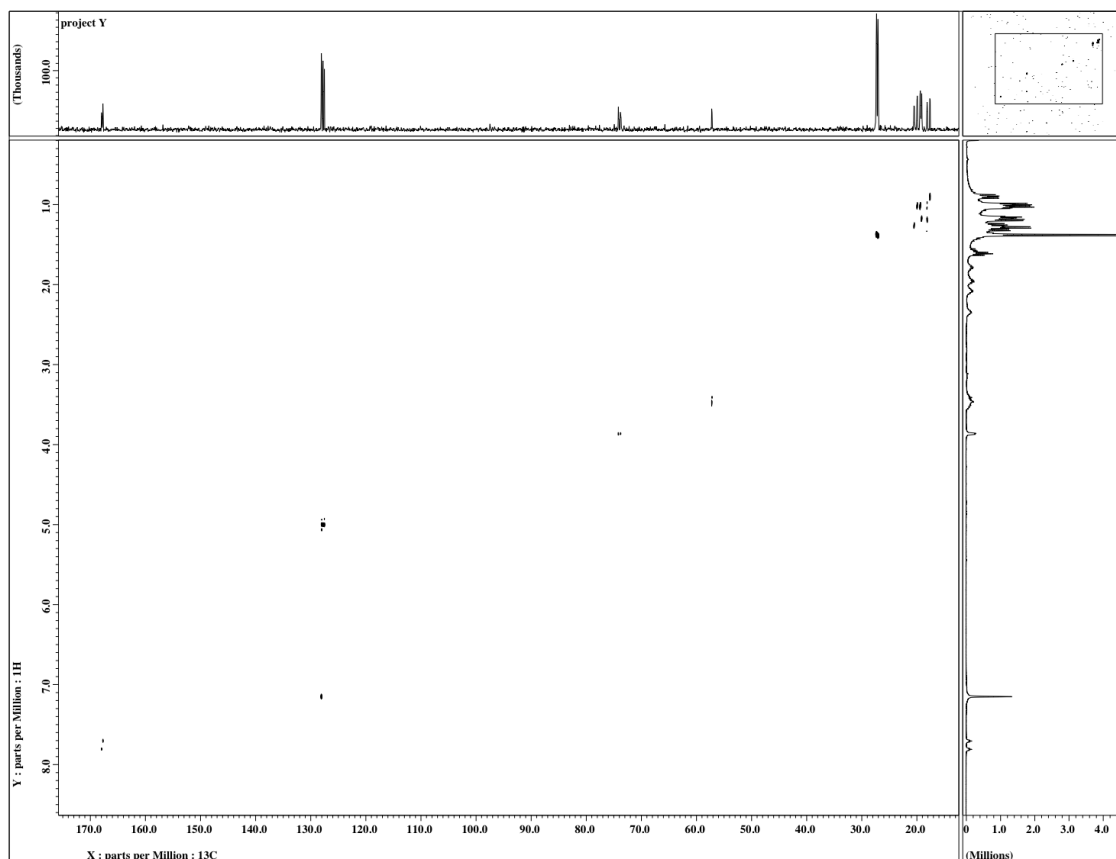


Figure S6. ^1H - ^{13}C HETCOR NMR (C_6D_6 , r.t.) of **4**.

1.2.6 Catalytic protocols

In a typical experiment, $\text{H}_3\text{B-NH}_3$ (**AB**; 100 mg; 3.24 mmol) is dissolved in 5 mL THF. The vessel is stoppered with a fresh, tight-fitting rubber septum and connected to an up-turned, water-filled graduated cylinder via a thin cannula. A solution of 1.55 mg (0.1 mol%) $\text{RuH(PNP)(PMe}_3)$ (**6**) in 1 mL THF, is quickly added via syringe. The volume of collected hydrogen gas was recorded in adequate time spans. 1st order rate constants were derived according to a rate law ($[\text{AB}] = [\text{AB}]_0 - [\text{H}_2]$):

$$d[\text{AB}]/dt = -k_{\text{obs}} [\text{AB}]$$

1st order plots for $\text{H}_3\text{B-NH}_3$ dehydrogenation with 0.1 mol-% **6** were linear over 3 substrate half lives ($k_{\text{obs}} = 0.012 \text{ s}^{-1}$, $R^2 = 0.999$). With 0.01 mol-% **6** linearity was observed over one half life ($k_{\text{obs}} = 0.0021 \text{ s}^{-1}$; $R^2 = 0.991$). At later times, rates decreased due to slow catalyst deactivation (TON = 8300). 1st order plots for dehydrogenation of deuterated substrates with 0.1 mol-% **6** are plotted over two ($\text{D}_3\text{B-NH}_3$: $k_{\text{obs}} = 0.0061 \text{ s}^{-1}$, $R^2 = 0.990$) and one half life

B Results and Discussion

($\text{H}_3\text{B-ND}_3$: $k_{\text{obs}} = 0.0025 \text{ s}^{-1}$, $R^2 = 0.993$; $\text{D}_3\text{B-ND}_3$: $k_{\text{obs}} = 0.0016 \text{ s}^{-1}$, $R^2 = 0.995$), respectively.

Mercury Poisoning – Experiment. The experiment was carried out as described above, with mercury metal (654 mg; 3.24 mmol) added to the ammonia borane solution and stirred vigorously before addition of the catalyst.

1.2.7 Characterization of $\text{H}_3\text{B-NH}_3$ dehydrocoupling products

After the catalytic experiment described above, the solid was collected by filtration, rinsed with toluene and dried *i. vac.* Anal. Calcd. for H_4BN (28.85): H, 13.98; N, 48.55. Found: H, 13.28; N, 41.90, C, 2.89 from residual solvent.

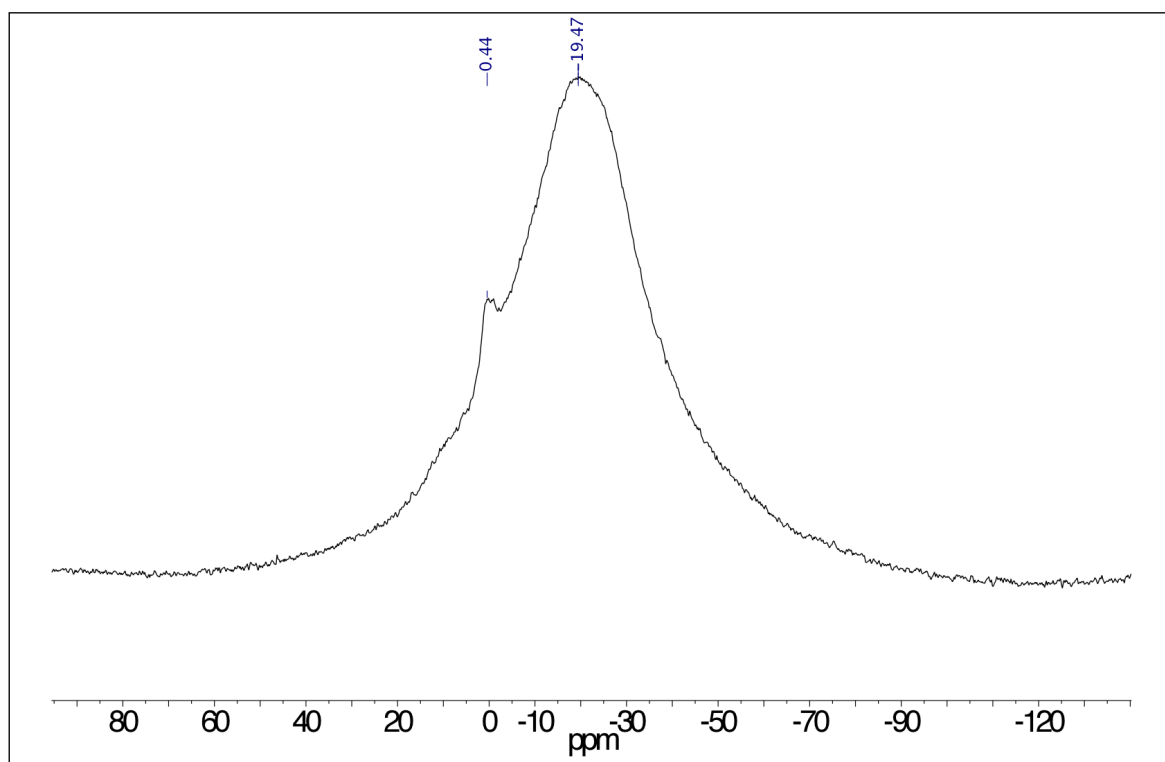


Figure S7. ^{11}B MAS NMR of the solid product from dehydrogenation of $\text{H}_3\text{B-NH}_3$ with **6** (0.1 mol-%).

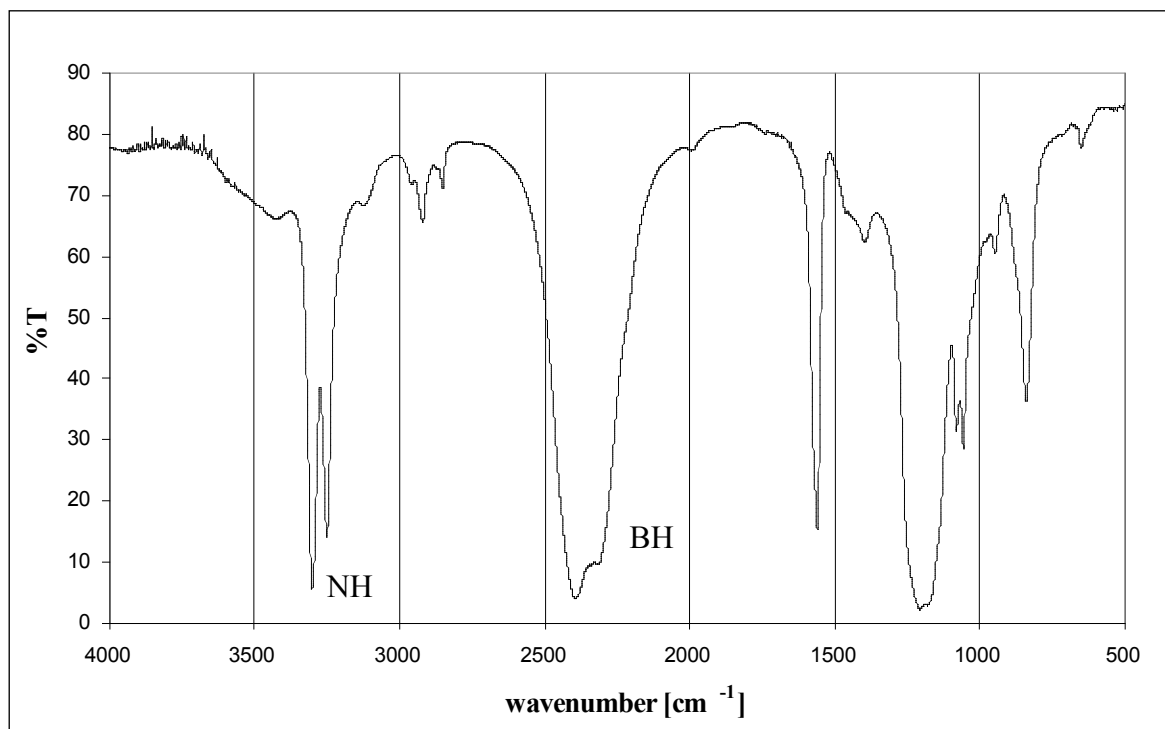


Figure S8. IR-Spectrum of the solid dehydrogenation product (KBr pellet).

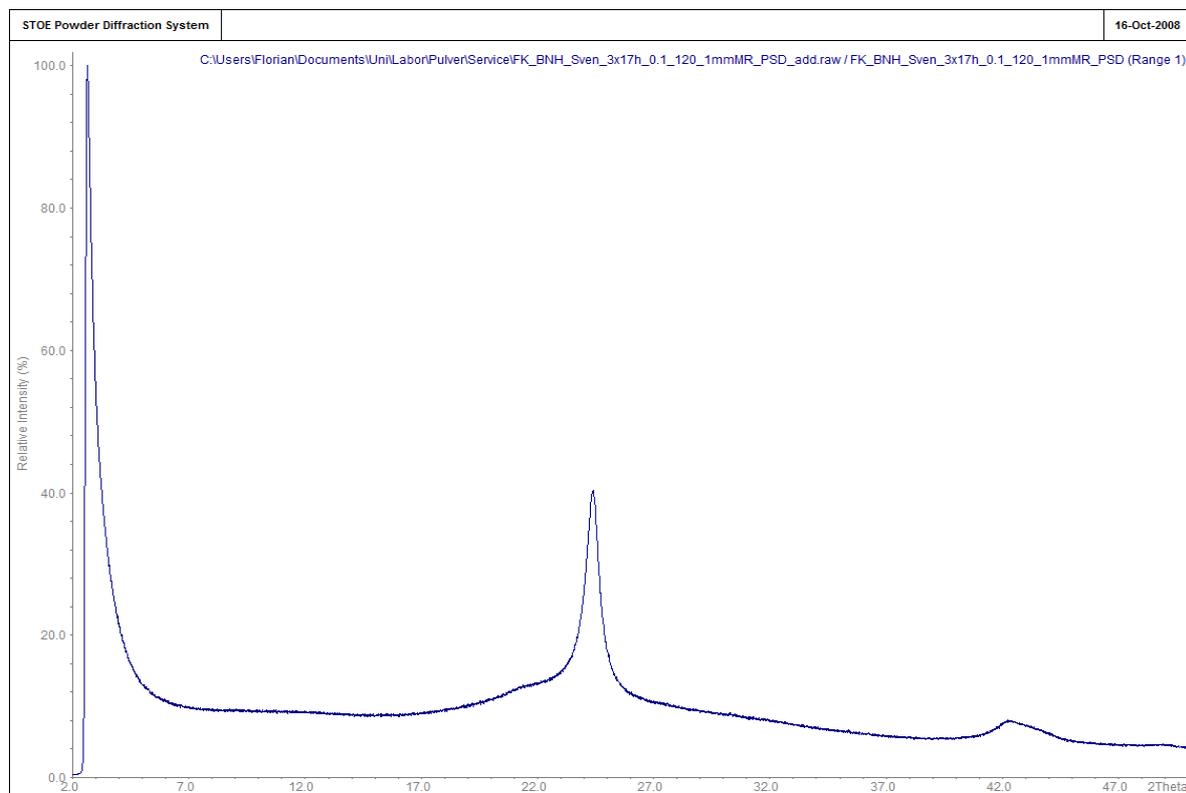


Figure S9. X-ray powder diffraction pattern of the solid dehydrogenation product.

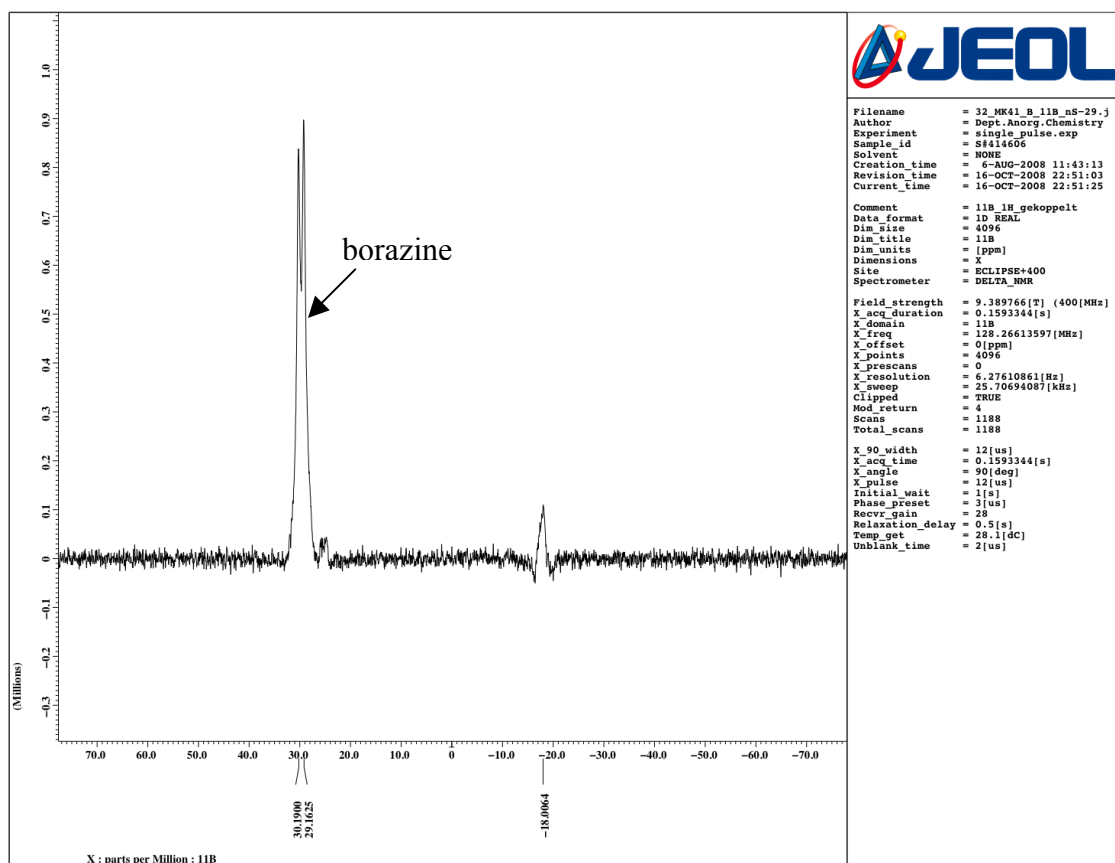


Figure S10. ^{11}B NMR (THF, r.t., 128.8 MHz) of a $\text{H}_3\text{B-NH}_3$ dehydrogenation reaction with **6** (10 mol%) carried out in a J-Young NMR tube.

1.2.8 Computational results

All calculations were performed with GAUSSIAN-03 using the density functional/Hartree-Fock hybrid model Becke3LYP and the split valence double- ζ (DZ) basis set 6-31+G**.^[18,19,20] The Ru atoms were described with a Stuttgart-RSC-ECP with a DZ

¹⁸ M. J. Frisch, G. W. Trucks, H. B. Schlegel, G. E. Scuseria, M. A. Robb, J. R. Cheeseman, J. Montgomery, J. A. , T. Vreven, K. N. Kudin, J. C. Burant, J. M. Millam, S. S. Iyengar, J. Tomasi, V. Barone, B. Mennucci, M. Cossi, G. Scalmani, N. Rega, G. A. Petersson, H. Nakatsuji, M. Hada, M. Ehara, K. Toyota, R. Fukuda, J. Hasegawa, M. Ishida, T. Nakajima, Y. Honda, O. Kitao, H. Nakai, M. Klene, X. Li, J. E. Knox, H. P. Hratchian, J. B. Cross, V. Bakken, C. Adamo, J. Jaramillo, R. Gomperts, R. E. Stratmann, O. Yazyev, A. J. Austin, R. Cammi, C. Pomelli, J. W. Ochterski, P. Y. Ayala, K. Morokuma, G. A. Voth, P. Salvador, J. J. Dannenberg, V. G. Zakrzewski, S. Dapprich, A. D. Daniels, M. C. Strain, O. Farkas, D. K. Malick, A. D. Rabuck, K. Raghavachari, J. B. Foresman, J. V. Ortiz, Q. Cui, A. G. Baboul, S. Clifford, J. Cioslowski, B. B. Stefanov, G. Liu, A. Liashenko, P. Piskorz, I. Komaromi, R. L. Martin, D. J. Fox, T. Keith, M. A. Al-Laham, C. Y. Peng, A.

description of the valence electrons.^[21] Details for the geometry optimizations and the optimized coordinates for compounds **4** and **6** see the Supporting Information under <http://dx.doi.org/10.1002/anie.200805108>. The orbital energies are taken from the Mulliken population analysis as implemented in Gaussian 03.

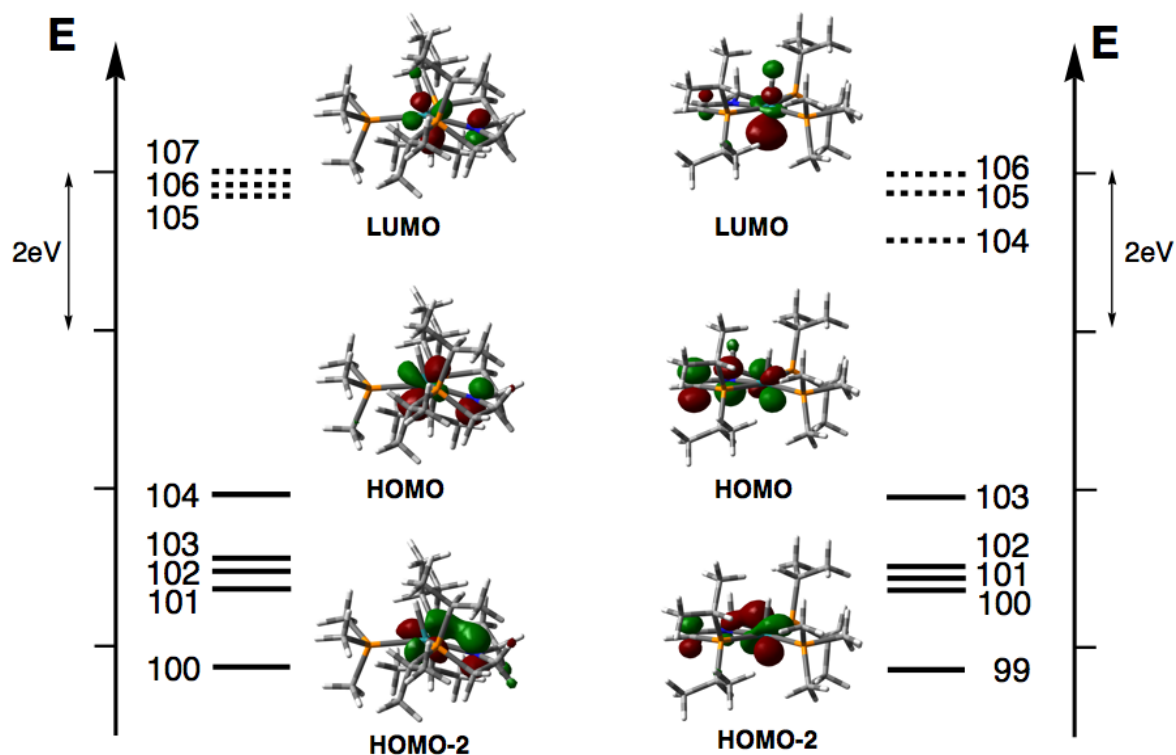


Figure S11. Relative frontier orbital energies with occupied (solid lines) and unoccupied (dashed lines) orbitals and contour plots of the LUMO, HOMO, and HOMO-2 of **6** (left) and **4** (right), respectively.

Nanayakkara, M. Challacombe, P. M. W. Gill, B. Johnson, W. Chen, M. W. Wong, C. Gonzalez, J. A. Pople, **Gaussian03, Rev. C.02**, Gaussian Inc., Wallingford, CT, 2004.

¹⁹ a) S. H. Vosko, L. Wilk, M. Nusair, *Can. J. Phys.* **1980**, *58*, 1200. b) C. Lee, W. Yang, R. G. Parr, *Phys. Rev. B.* **1988**, *37*, 785-789. c) A. D. Becke, *J. Chem. Phys.* **1993**, *98*, 5648.

²⁰ a) W. J. Hehre, R. Ditchfield, J. A. Pople, *J. Chem. Phys.* **1972**, *56*, 2257. b) M.M. Francl, W.J. Pietro, W.J. Hehre, J.S. Binkley, M.S. Gordon, D.J. DeFrees and J.A. Pople, *J. Chem. Phys.* **1982**, *77*, 3654.

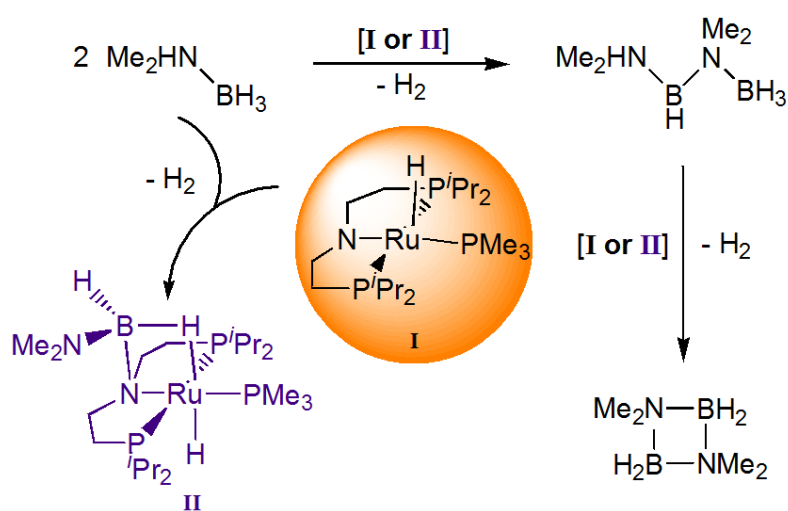
²¹ M. Dolg, H. Stoll, H. Preuss, R.M. Pitzer, *J. Phys. Chem.* **1993**, *97*, 5852.

1.3 Ruthenium catalyzed Dimethylamineborane Dehydrogenation: Stepwise Metal Centered Dehydrocyclization

This chapter originated the following publication:

A. Friedrich, M. Drees, S. Schneider

Chem. Eur. J. **2009**, *15*, 10339.



1.3.1 Introduction

Ammonia-borane (H_3NBH_3 , **A**), has recently attracted considerable interest as material for chemical hydrogen storage, owing to its high hydrogen content (19.6 weight-%).^[1] Furthermore, amine-boranes have been utilized as hydrogen source in hydrogenation reactions,^[2] and polymeric products of amine-borane dehydrocoupling provide access to novel inorganic materials.^[3] Since thermal dehydrogenation exhibits high kinetic barriers, in the last years transition metal catalysts have been developed for this reaction.^[4] Most recently, ruthenium-amido catalysts were introduced by Fagnou and co-workers and our group, which currently exhibit the highest reported activities in the dehydrocoupling of **A**.^[4l,m]

Mechanistic information for metal catalyzed amine-borane (R_2HNBH_3) dehydrogenation remains scarce. All computational studies have suggested initial proton and hydride transfer from the same substrate molecule to the catalyst,^[5] resulting in the release of aminoborane

¹ a) F. H. Stephens, V. Pons, R. T. Baker, *Dalton Trans.* **2007**, 2613; b) T. B. Marder, *Angew. Chem.*, **2007**, *119*, 8262; *Angew. Chem. Int. Ed.*, **2007**, *46*, 8116; c) C. W. Hamilton, R. T. Baker, A. Staubitz, I. Manners, *Chem. Soc. Rev.* **2009**, *38*, 279.

² a) C. A. Jaska, I. Manners, *J. Am. Chem. Soc.* **2004**, *126*, 2698; b) Y. Jiang, H. Berke, *Chem. Commun.* **2007**, 3571; c) A. Jana, C. Schulzke, H. W. Roesky, *J. Am. Chem. Soc.* ASAP.

³ a) A. Staubitz, A. Presa Soto, I. Manners, *Angew. Chem.* **2008**, *120*, 6308; *Angew. Chem. Int. Ed.* **2008**, *47*, 6212; b) V. Pons, R. T. Baker, *Angew. Chem.* **2008**, *120*, 9742; *Angew. Chem. Int. Ed.* **2008**, *47*, 9600.

⁴ a) C. A. Jaska, K. Temple, A. J. Lough, I. Manners, *Chem. Commun.* **2001**, 962; b) C. A. Jaska, K. Temple, A. J. Lough, I. Manners, *J. Am. Chem. Soc.* **2003**, *125*, 9424; c) T. J. Clark, C. A. Russell, I. Manners, *J. Am. Chem. Soc.* **2006**, *128*, 9582; d) M. C. Denney, V. Pons, T. J. Hebden, D. M. Heinekey, K. I. Goldberg, *J. Am. Chem. Soc.* **2006**, *128*, 12048; e) R. J. Keaton, J. M. Blacquiere, R. T. Baker, *J. Am. Chem. Soc.* **2007**, *129*, 1844; f) D. Pun, E. Lobkovsky, P. Chirik, *Chem. Commun.* **2007**, 3297; g) J. L. Fulton, J. C. Linehan, T. Autrey, M. Balasubramanian, Y. Chen, N. K. Szymczak, *J. Am. Chem. Soc.* **2007**, *129*, 11936; h) B. L. Dietrich, K. I. Goldberg, D. M. Heinekey, T. Autrey, J. C. Linehan, *Inorg. Chem.* **2008**, *47*, 8583; i) T. M. Douglas, A. B. Chaplin, A. S. Weller, *J. Am. Chem. Soc.* **2008**, *130*, 14432; j) V. Pons, R. T. Baker, N. K. Szymczak, D. J. Heldebrant, J. C. Linehan, M. H. Matus, D. J. Grant, D. A. Dixon, *Chem. Commun.* **2008**, 6597; k) M. E. Sloan, T. J. Clark, I. Manners, *Inorg. Chem.* **2009**, *48*, 2429. l) N. Blaquiere, S. Diallo-Garcia, S. I. Gorelsky, D. A. Black, K. Fagnou, *J. Am. Chem. Soc.* **2008**, *130*, 14034; m) M. Käb, A. Friedrich, M. Drees, S. Schneider, *Angew. Chem.* **2009**, *121*, 922; *Angew. Chem. Int. Ed.* **2009**, *48*, 905.

⁵ a) Y. Luo, K. Ohno, *Organometallics* **2007**, *26*, 3597; b) A. Paul, C. B. Musgrave, *Angew. Chem.* **2007**, *119*, 8301; *Angew. Chem. Int. Ed.* **2007**, *46*, 8153; c) X. Yang, M. B. Hall, *J. Am. Chem. Soc.* **2008**, *130*, 1798; d) P. M. Zimmermann, A. Paul, Z. Zhang, C. B. Musgrave, *Angew. Chem.* **2009**, *121*, 2235; *Angew. Chem. Int. Ed.* **2009**, *48*, 2201.

B Results and Discussion

R_2NBH_2 , which undergoes rapid oligomerization.^[6] In fact, for $[\text{TiCp}_2]$ -mediated dehydrocoupling of Me_2HNBH_3 (**B**) to aminoborane dimer $(\text{Me}_2\text{NBH}_2)_2$ (**C**) a mechanism, with stepwise, metal-centered B-N coupling via diborazane $\text{Me}_2\text{HNBH}_2\text{NMe}_2\text{BH}_3$ (**D**) was dismissed.^[5a] Likewise, for Ru-amide catalysts a mechanism was proposed with release of free aminoborane by concerted H^+/H^- transfer to the Ru-N moiety and rate-determining H_2 elimination from the resulting Ru(H)-N(H) hydrido amine species.^[4f] To our knowledge, only for an iridium catalyst has metal-centered B-N coupling been confirmed by aminoborane trapping experiments via olefin hydroboration.^[4j]

1.3.2 Results and discussion

For **A** dehydrogenation with Ru-amido pincer complex $[\text{Ru}(\text{H})(\text{PMe}_3)(\text{PNP})]$ (**1**, $\text{PNP} = \text{N}(\text{CH}_2\text{CH}_2\text{P}^i\text{Pr}_2)_2$), H/D kinetic isotope effects would be in agreement with concerted hydrogen transfer, but the small rate of H_2 loss from amino complex *trans*- $[\text{Ru}(\text{H})_2(\text{PMe}_3)(\text{PNP}^H)]$ (**2**, $\text{PNP}^H = \text{HN}(\text{CH}_2\text{CH}_2\text{P}^i\text{Pr}_2)_2$) suggest a different mechanism, at least for this step.^[4m] In this contribution we present our results on **B** dehydrocoupling with catalysts **1** and **2**, which support metal centered B-N coupling as a viable step for this system.



Addition of **1** to a THF solution of **B** (0.54 M) at room temperature results in rapid H_2 evolution [Eq. (1)]. However, volumetric monitoring reveals, that the reaction considerably slows down prior to complete conversion (Figure 1). In contrast to parent **A**, for which rapid dehydrogenation and turnover numbers (TONs) of up to 8300 were observed with catalyst **1**,^[4m] for **B** only up to 70 % H_2 are quickly released with catalyst loadings of 2 mol%. However, slow completion of the reaction is observed over 28 h by ^{11}B NMR spectroscopy (2 mol% **1**) ultimately giving quantitative conversion to **C**. Therefore, the high initial rates (turnover frequency (TOF) $\sim 3600 \text{ h}^{-1}$) contrast with a TOF of 1.5 h^{-1} after slowdown, suggesting two catalytic regimes owing to catalyst deactivation in the course of the reaction.

⁶ C. T. Kwon, H. A. McGee Jr. *Inorg. Chem.* **1970**, *9*, 2458.

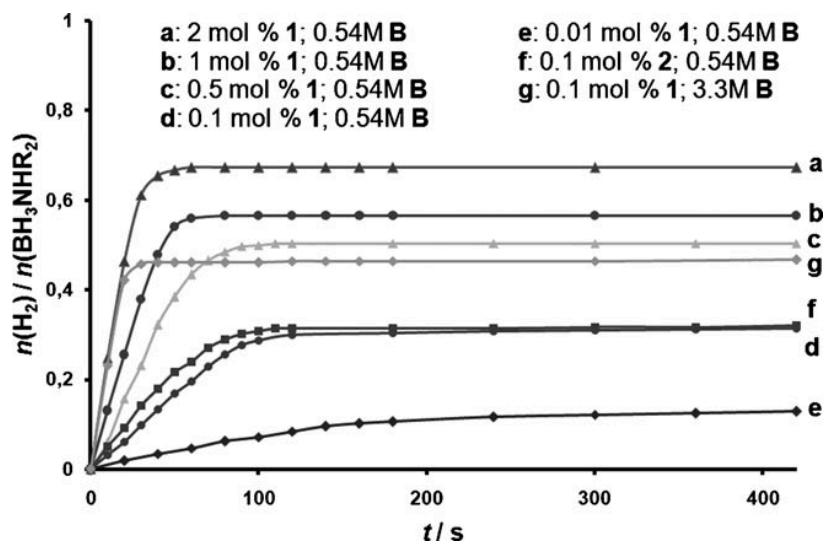


Figure 1. Volumetric monitoring of **B** dehydrocoupling with catalysts **1** and **2**.

Monitoring the reaction by ^{11}B NMR spectroscopy (Figure 2 and chapter B1.3.6) confirms almost quantitative formation of dehydrocoupling product $(\text{Me}_2\text{NBH}_2)_2$ (**C**, $\delta = 4.4$ ppm) and trace amounts of $(\text{Me}_2\text{N})_2\text{BH}$ (**E**, $\delta = 27.9$ ppm). The concentration of intermediate monomeric aminoborane Me_2NBH_2 (**F**, $\delta = 36.8$ ppm) quickly drops owing to dimerization.^[7] Furthermore, an intermediate at $\delta = 1.2$ ppm ($t, {}^1J(\text{B},\text{H}) = 109$ Hz) is observed. This signal was previously tentatively assigned to trimer $(\text{Me}_2\text{NBH}_2)_3$ in dehydrocoupling of **B** with $[\text{TiCp}_2]$, $[\text{Rh}(\text{P}i\text{Bu}_3)_2]^+$, and a Cu^{I} -carbene complex.^[4c,e,l,8] However, this peak correlates (1:1 integral ratio) with a signal at $\delta = -14.0$ ppm (q, ${}^1J(\text{B},\text{H}) = 94$ Hz) superimposed with substrate **B** ($\delta = -14.4$ ppm, q, ${}^1J(\text{B},\text{H}) = 98$ Hz). From comparison with an original sample, the signals at $\delta = 1.2$ and -14.0 ppm can be assigned to diborazane **D** and not to $(\text{Me}_2\text{NBH}_2)_3$.^[4b,9,10] Similarly, Manners and coworkers reported, that Ph_2HPBH_3

⁷ H. Nöth, H. Vahrenkamp, *Chem. Ber.* **1967**, *100*, 3353.

⁸ G. W. Campbell, L. Johnson, *J. Am. Chem. Soc.* **1959**, *81*, 3800.

⁹ a) G. A. Hahn, R. Schaeffer, *J. Am. Chem. Soc.* **1964**, *86*, 1503; b) H. Nöth, S. Thomas, *Eur. J. Inorg. Chem.* **1999**, 1373.

¹⁰ For the high field ^{11}B signal a coupling constant ${}^1J(\text{B},\text{H}) = 198$ Hz had previously been reported (ref 9b).

dehydrogenation gives $\text{Ph}_2\text{HPBH}_2\text{Ph}_2\text{PBH}_3$,^[11] and **D** was previously proposed as an intermediate in rhodium-catalyzed and thermal dehydrocoupling of **B**.^[4b,12,13]

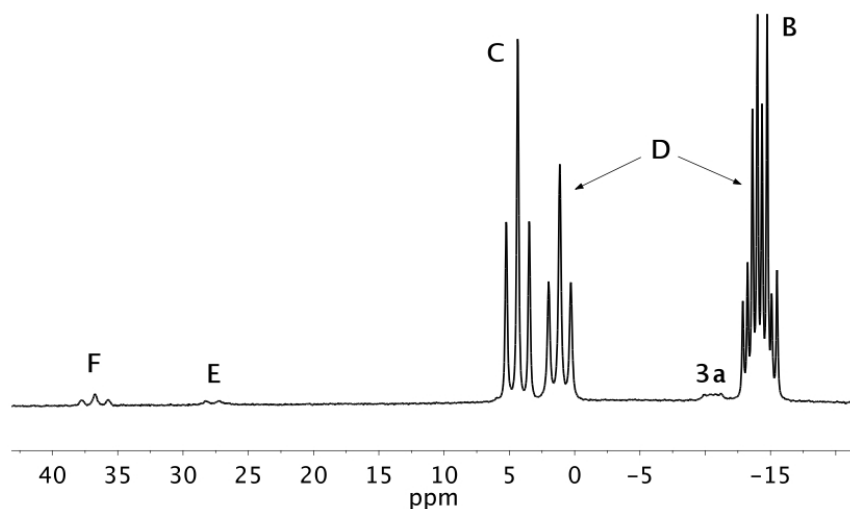


Figure 2. ^{11}B NMR spectrum of catalytic **B** (0.54 M in THF) dehydrocoupling with **1** (2 mol%) after 27 min.

Two pathways seem viable for the formation of **D**: Metal-centered dehydrogenative B–N coupling of **B** (Scheme 1, Path A), or catalytic dehydrogenation and release of **F** followed by uncatalyzed rearrangement of **B** and **F** (Path B). Thermodynamic calculations (G3MP2) showed that dehydrocoupling of **2B** to **C** is strongly exergonic ($\Delta G = -27.4 \text{ kcal mol}^{-1}$). Dehydrocoupling to **D** is thermodynamically slightly more favorable compared with dehydrogenation to aminoborane **F** ($\Delta\Delta G = -2.3 \text{ kcal mol}^{-1}$) and dimerization of **2F** to **C** is exergonic by $\Delta G = -6.6 \text{ kcal mol}^{-1}$.^[14] Therefore, rearrangement of **2B** and cyclic dimer **C** towards linear dimer **D** would be almost thermoneutral ($\Delta G = 2.0 \text{ kcal mol}^{-1}$), and **B** and **C**

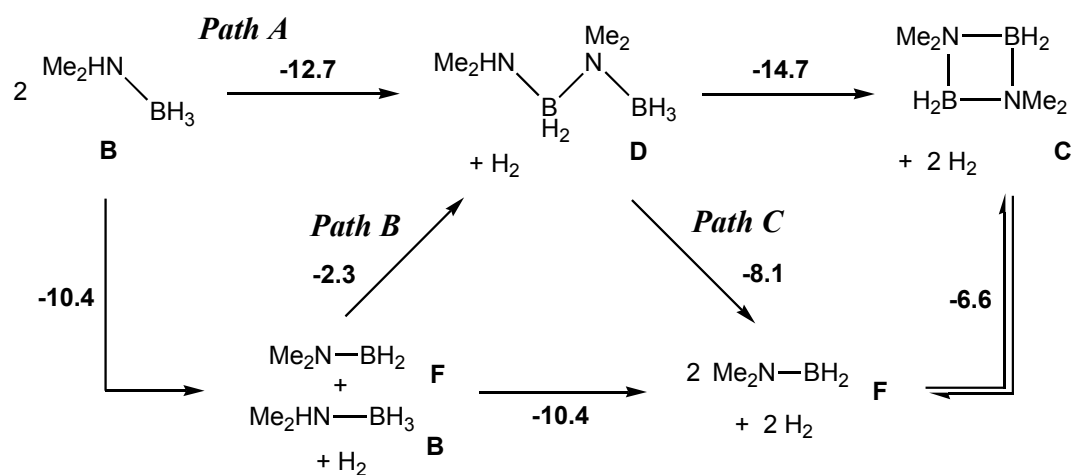
¹¹ H. Dorn, R. A. Singh, J. A. Massey, J. M. Nelson, C. A. Jaska, A. J. Lough, I. Manners, *J. Am. Chem. Soc.* **2000**, *122*, 6669.

¹² G. E. Ryschkewitsch, J. W. Wiggins, *Inorg. Chem.* **1970**, *9*, 314.

¹³ Re-evaluation of $[\text{TiCp}_2]$ -catalyzed dehydrocoupling of **B** confirmed our results: I. Manners, personal communication.

¹⁴ DFT calculations (B3LYP/6-311++G**) suggested for **F** dimerization to be endergonic by +5.2 kcal/mol (ref. 5a). We obtained similar results from DFT (B3LYP/6-31G*: $\Delta G = +5.3 \text{ kcal/mol}$). However, experiment shows that the equilibrium is on the dimer side (ref. 7).

should be in equilibrium with **D** if kinetically feasible. However, a solution of **B** and **C** in THF without catalyst **1** displayed no reaction over one week at room temperature. As the monomer-dimer equilibrium of **C** and **F** is known to be rapid,^[7] these results suggest, that the uncatalyzed Path B exhibits a high kinetic barrier,^[15] and **D** must be formed by metal-centered dehydrocoupling.



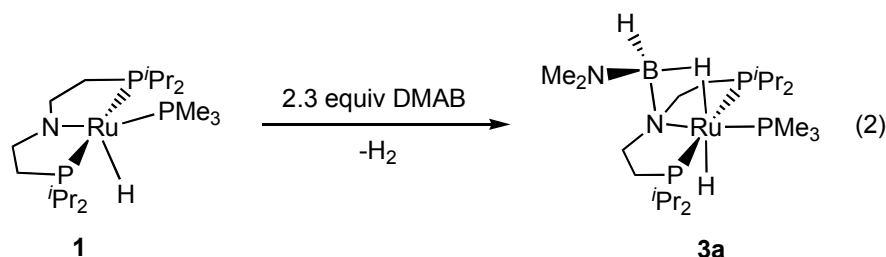
Scheme 1. Thermochemistry of **B** dehydrocoupling with free enthalpies in kcal mol⁻¹.

To account for intermediate aminoborane **F** the reaction was performed at different substrate loadings [**B**]₀. Under identical conditions, [**B**]₀ has a strong effect on the relative concentrations of intermediates **F** and **D**, with higher [**F**]/[**D**] ratios at lower substrate loadings (e.g., after 3 min, 2 mol% **1**, [**B**]₀ = 0.54 M: [**F**]/[**D**] = 0.44; [**B**]₀ = 0.1 M: [**F**]/[**D**] = 4.03). This result suggests that dehydrogenation of one **B** and release of **F** versus metal-centered dehydrocoupling of two **B** towards **D**, which should be favoured at higher **B** concentrations, are two parallel pathways. Furthermore, **F** was observed as an intermediate in catalytic dehydrogenation of diborazane **D** ([**D**]₀ = 0.54 M, 2 mol% **1**; Path C). Accordingly, for the hypothetical linear dehydrogenation product of **D**, Me₂NH₂BMe₂NBH₂, no minimum was found in calculations (MP2/6-31G* or G3MP2). Instead geometry optimizations starting from an *anti* conformation of the N–B–N–B chain resulted in B–N bond scission towards 2**F**, while

¹⁵ A barrier of $\Delta G_{298K}^\ddagger = 31.2$ kcal mol⁻¹ was calculated for uncatalyzed rearrangement of H₃NBH₃ and H₂NBH₂ towards H₃NBH₂NH₂BH₃ (ref. 16).

B Results and Discussion

the *gauche* conformation cyclized to dimer **C**. A recent computational study suggested the formation of NH_2BH_2 from dehydrogenation of parent $\text{H}_3\text{NH}_2\text{BH}_2\text{NBH}_3$, as well.^[16]

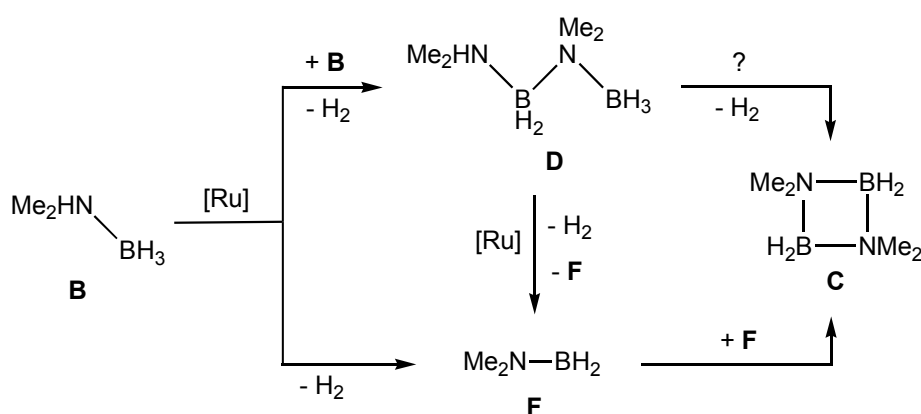


As for the dehydrogenation of **A**, **2** is the only ruthenium species initially detected by ^{31}P NMR spectroscopy. Furthermore, dehydrocoupling of **B** catalyzed by **2** (0.1 mol%), gives virtually the same results as compared with **1** (Figure 1), suggesting that **2** represents the catalyst resting state in the rapid dehydrogenation regime. However, a new ruthenium species quickly evolves, as observed by ^{31}P and ^{11}B NMR spectroscopy, which could be isolated in 70 % yield upon reaction of **1** with 2.3 equiv **B** [Eq. (2)]. This compound was assigned to $[\text{Ru}(\text{H})(\text{PMe}_3)(\text{PNP}^{\text{BH}_2\text{NMe}_2})]$ (**3a**) with a rare M–N–B–H four-membered borametallacycle.^[17] The hydrogen atoms bound to boron could be assigned by ^{11}B - ^1H HETCOR NMR spectroscopy and feature a strongly reduced coupling constant for the bridging ($^1J(\text{H},\text{B}) = 50$ Hz) compared with the terminal hydride ($^1J(\text{H},\text{B}) = 113$ Hz), as derived by selectively proton decoupled ^{11}B NMR spectra. Furthermore, the terminal hydride bound to ruthenium is considerably shifted to higher field compared with **2** ($\Delta\delta(\text{C}_6\text{D}_6) = 4.9$ ppm), indicating the reduced *trans*-influence of the bridging hydride. At higher temperatures, both the PNP phosphorous atoms and the B–H hydrides coalesce. However, the terminal Ru–H hydride is not broadened, suggesting exchange of B–H_{bridge} and B–H_{terminal} by borane rotation around the B–N_{PNP} bond without B–N_{PNP} rupture. Activation parameters for this process were estimated by ^{31}P NMR line shape analysis ($\Delta H^\ddagger = 70.9$ kJ mol⁻¹; $\Delta S^\ddagger = -2.6$ kJ mol⁻¹ K⁻¹). Furthermore, the reaction of **1** with **A** (3.2 equiv) gives parent complex $[\text{Ru}(\text{H})(\text{PMe}_3)(\text{PNP}^{\text{BH}_2\text{NH}_2})]$ (**3b**) in high yield by ^{31}P , ^1H , and ^{11}B NMR spectroscopy. Analytically pure **3a** was tested for

¹⁶ P. M. Zimmermann, A. Paul, Z. Zhang, C. B. Musgrave, *Inorg. Chem.* **2009**, *48*, 1069.

¹⁷ a) G. Fachinetti, C. Floriani, M. Mellini, S. Merlino, *J. Chem. Soc. Chem. Commun.* **1976**, 300; b) P. Binger, F. Sandmeyer, C. Krüger, *Organometallics* **1995**, *14*, 2969; c) M. D. Fryzuk, B. A. MacKay, S. A. Johnson, B. O. Patrick, *Angew. Chem.* **2002**, *114*, 3861; *Angew. Chem. Int. Ed.* **2002**, *41*, 3709. d) A. C. Hillier, T. Fox, H. W. Schmalle, H. Berke, *J. Organomet. Chem.* **2003**, *669*, 14.

dehydrogenation of **B**. Quantitative dehydrocoupling to **C** is observed (2 mol% **3a**), with catalytic activities (TOF 1.5 h⁻¹) as found for the slow dehydrogenation regime with precatalyst **1**. Likewise, **3a** slowly dehydrogenates **A**. No conversion of **3a** to **3b** by exchange of Me₂NBH₂ vs. H₂NBH₂ was observed, confirming the inertness of the B–N_{PNP} bond. The possible formation of **3a/3b** was examined by DFT methods. Relatively low barriers were found for catalyst deactivation by trapping of **1** with aminoboranes R₂NBH₂ (R = H: $\Delta G^\ddagger = 12.8$ kcal mol⁻¹; R = Me: $\Delta G^\ddagger = 15.7$ kcal mol⁻¹). While Me₂NBH₂ (**F**) was observed by ¹¹B NMR spectroscopy, parent H₂NBH₂ is a highly reactive molecule rapidly forming polymeric, insoluble products^[6] Consequently, higher steady state concentration of **F**, compared with H₂NBH₂, could explain the considerably higher TON's obtained for **A** with respect to **B** in the rapid dehydrocoupling regime. Furthermore, the higher TON's for **B** dehydrogenation from the fast catalytic regime at higher substrate loadings (Figure 1) are in agreement with the kinetics of intermediate **F** formation (vide supra).



Scheme 2. Mechanistic model for the dehydrocoupling of **B** to **C**.

1.3.3 Conclusion

From these results a mechanism for **B** dehydrocyclization is proposed (Scheme 2). Upon initial metal catalyzed dehydrogenation of **B**, coupling to **D** competes with release of **F**, which cyclizes towards **C**. Catalytic dehydrogenation of **D** results in B–N bond scission and ultimately cyclization of **F**, as well. Alternatively, direct metal-centered dehydrocyclization of **D** towards **C** is likely to compete with the latter pathway. Unfortunately, quantitative kinetic analysis to answer this question was hampered by underlying catalyst deactivation. Hence, our conclusions are:

- 1) All dehydrogenation and B–N coupling steps, except for aminoborane cyclodimerization, are metal-centered.
- 2) Head-to-tail dehydrocoupling to linear dimer **D** is a viable pathway. This had been proposed earlier for thermal and Rh-catalyzed dehydrogenation and is most likely operative with [TiCp₂], [Rh(PiBu₃)₂]⁺, and Cu-carbene catalysts, but was dismissed in a computational study.^[5a] If this result can be generalized to other amine-boranes, it provides a mechanistic rationale for the formation of linear aminoborane polymers instead of polyborazine.^[3a,4j]
- 3) For Ru catalyst **1**, deactivation proceeds via formation of a rare, four-membered Ru–N–B–H metallacycle, providing valuable information for further catalyst design. Its high thermal stability and the dehydrogenation of **A** with **3a** suggest, that **F** does not dissociate from **3a** during the reaction.

Further studies will focus on the catalytic cycle to unfold the full mechanistic picture of extraordinarily fast amine-borane dehydrogenation with Ru-amide complexes.

1.3.4 Experimental details and syntheses

Materials and Synthetic Methods. All experiments were carried out under an atmosphere of argon using Schlenk and glove-box techniques. The solvents were dried over Na/benzophenone/tetraglyme (benzene) or Na/benzophenone (THF), distilled under argon and deoxygenated prior to use. *d*₆-Benzene and *d*⁸-toluene were dried by distillation from Na/K alloy and deoxygenated by three *freeze-pump-thaw* cycles. H₃NBH₃ (**A**) and Me₂HNBH₃ (**B**) were purchased from Aldrich and sublimed prior to use. [Ru(H)PMe₃(PNP)] (**1**) and [Ru(H)₂PMe₃(PNP^H)] (**2**) were prepared as reported earlier.¹⁸ **2** was used as a solution in situ from hydrogenation of **1** with H₂, as isolation of **2** leads to partial H₂ loss.

Analytical Methods. Elemental analyses were obtained from the Microanalytical Laboratory of Technische Universität München. The IR spectra were recorded on a Jasco FT/IR-460 PLUS spectrometer as nujol mulls between KBr plates. NMR spectra were recorded on Jeol Lambda 400 and Bruker DPX 500 spectrometers and were calibrated to the residual proton resonance and the natural abundance ¹³C resonance of the solvent (*d*₆-benzene, δ_H = 7.16 and

¹⁸ M. Käß, A. Friedrich, M. Drees, S. Schneider *Angew. Chem.* **2009**, *121*, 922.

$\delta_C = 128.06$ ppm; d_8 -toluene, $\delta_H^{\text{Me}} = 2.09$ and $\delta_C^{\text{Me}} = 20.40$ ppm). ^{31}P NMR and ^{11}B NMR chemical shifts are reported relative to external phosphoric acid and BF_3 etherate (δ 0.0 ppm), respectively. Signal multiplicities are abbreviated as: s (singlet), d (doublet), t (triplet), vt (virtual triplet), sp (septet), m (multiplet), br (broad). Hydride exchange in **3a** was studied by VT- ^{31}P NMR at 161.83 MHz. The rate was derived by lineshape fitting using the program WinDNMR and activation parameters obtained by an Eyring plot (Figure S4).¹⁹

$[\text{Ru}(\text{H})\text{PMe}_3\{\mu\text{-H}\}\text{HB}(\text{NMe}_2)\text{N}(\text{CH}_2\text{CH}_2\text{P}^i\text{Pr}_2)_2\}]$ (**3a**): **B** (10.8 mg; 183.3 μmol ; 2.3 equiv.) is added to a solution of **1** (38.5 mg; 79.8 μmol) in THF (1 mL). After 30 min. at RT the solvent is evaporated i. vac. The residue is extracted with pentanes, filtered and evaporated. The sticky crude product is dissolved in benzene (5 mL), filtered and the solvent sublimed off over night to give solid orange-brown **3a** (30 mg; 55.6 μmol ; 70 %). Anal. Calcd. for $\text{C}_{21}\text{H}_{54}\text{BN}_2\text{P}_3\text{Ru}$ (539.48): C, 46.75; H, 10.09; N, 5.19. Found: C, 47.34; H, 10.71; N, 4.81. NMR (d_6 -benzene, r.t., [ppm]) ^1H NMR (399.8 MHz): $\delta = 3.38 - 3.20$ (br m, 1H, NCH_2), 3.28 - 3.03 (br m, 2H, NCH_2 , PCH_2), 2.54 (s, 6H, $\text{BH}_2\text{N}(\text{CH}_3)_2$), 2.30 - 2.15 (m, 2H, PCH_2 , NCH_2), 2.15 - 2.05 (m, 1H, NCH_2), 1.98 - 1.87 (m, 1H, PCH), 1.77 (sp, $^3J(\text{H,H}) = 7.9$ Hz, 4H, 3 x PCH , BH), 1.40 (dd, $^3J(\text{H,H}) = 7.0$ Hz, $^3J(\text{H,P}) = 11.0$ Hz, 4H, CH_3 , PCH_2), 1.31 (dd, $^3J(\text{H,H}) = 7.0$ Hz, $^3J(\text{H,P}) = 11.0$ Hz, 3H, CH_3), 1.29 (d, $^2J(\text{H,P}) = 7.3$ Hz, 9H, $\text{P}(\text{CH}_3)_3$), 1.14 (dd, $^3J(\text{H,H}) = 7.0$ Hz, $^3J(\text{H,P}) = 11.0$ Hz, 4H, CH_3 , PCH_2), 1.07 (m, 6H, CH_3), 1.02 (m, 6H, CH_3), 0.94 (t, 3H, $^3J(\text{H,H}) = ^3J(\text{H,P}) = 8.0$ Hz, CH_3), -8.02 (br, 1H, $\text{Ru}(\mu\text{-H})\text{B}$), -13.55 (q, $^2J(\text{H,P}) = 24.8$ Hz, 1H, RuH). $^{13}\text{C}\{^1\text{H}\}$ NMR (100.53 MHz): $\delta = 60.7$ (d, $^2J(\text{C,P}) = 5.0$ Hz, NCH_2), 58.1 (s, NCH_2), 46.5 (s, $\text{BH}_2\text{N}(\text{CH}_3)_2$), 29.0 (dd, $^1J(\text{C,P}) = 12.3$ Hz, $^3J(\text{C,P}) = 3.5$ Hz, PCH), 28.7 (dd, PCH , superimposed with $\text{P}(\text{CH}_3)_3$ signal), 28.6 (d, $^1J(\text{C,P}) = 23.4$ Hz, $\text{P}(\text{CH}_3)_3$), 27.5 (dd, $^1J(\text{C,P}) = 13.1$ Hz, $^3J(\text{C,P}) = 3.0$ Hz, PCH_2), 26.0 (dd, $^1J(\text{C,P}) = 8.8$ Hz, $^3J(\text{C,P}) = 5.4$ Hz, PCH), 25.8 (dd, $^1J(\text{C,P}) = 15.1$ Hz, $^3J(\text{C,P}) = 4.0$ Hz, PCH_2), 25.2 (dd, $^1J(\text{C,P}) = 11.1$ Hz, $^3J(\text{C,P}) = 5.8$ Hz, PCH), 20.0 (d, $^2J(\text{C,P}) = 7.3$ Hz, CH_3), 19.7 (d, $^2J(\text{C,P}) = 6.5$ Hz, 2 x CH_3), 19.6 (d, $^2J(\text{C,P}) = 5.0$ Hz, CH_3), 19.5 (d, $^2J(\text{C,P}) = 5.0$ Hz, CH_3), 19.1 (d, $^2J(\text{C,P}) = 4.6$ Hz, CH_3), 16.7 (d, $^2J(\text{C,P}) = 5.4$ Hz, CH_3), 16.2 (d, $^2J(\text{C,P}) = 5.8$ Hz, CH_3). $^{31}\text{P}\{^1\text{H}\}$ NMR (161.83 MHz): $\delta = 79.3$ (dd, $^2J(\text{P,P}) = 253.4$ Hz, $^2J(\text{P,P}) = 27.0$ Hz, P^iPr_2), 76.7 (dd, $^2J(\text{P,P}) = 253.4$ Hz, $^2J(\text{P,P}) = 27.0$ Hz, P^iPr_2), 5.6 (t, $^2J_{\text{PP}} = 27.0$ Hz, $\text{P}(\text{CH}_3)_3$). ^{11}B NMR (128.27 MHz): $\delta = -10.4$ (dd, $^1J(\text{H,B}) = 113$ Hz, $^1J(\text{H,B}) = 50$ Hz). Assignments were

¹⁹ Reich, H. J. WinDNMR: Dynamic NMR Spectra for Windows *J. Chem. Educ. Software* **3D2**.

B Results and Discussion

confirmed by ^1H COSY, ^1H - ^{13}C HMQC, ^{11}B - ^1H HETCOR and selectively ^1H decoupled ^{11}B NMR spectroscopy.

Reaction of 1 with A: **A** (8.3 mg; 268.9 μmol ; 3.2 equiv.) is added to a solution of **1** (40.3 mg; 83.5 μmol) in THF (3 mL). After 3 days at RT the solvent is evaporated i. vac. The residue is extracted with pentanes, filtered and evaporated to give a yellow-brown solid (40.0 mg). ^{31}P , ^1H , and ^{11}B NMR spectra indicate the formation of $[\text{Ru}(\text{H})\text{PMe}_3\{(\mu\text{-H})\text{HB}(\text{NH}_2)\text{N}(\text{CH}_2\text{CH}_2\text{P}^i\text{Pr}_2)_2\}]$ (**3b**) as main product, which could not be obtained analytically pure by recrystallization or column chromatography. Selected NMR signals of **3b** (d_6 -benzene, r.t., [ppm]) ^1H NMR (399.8 MHz): $\delta = -7.57$ (br, 1H, Ru($\mu\text{-H}$)B), -13.61 (q, $^2J_{\text{HP}} = 24.0$ Hz, 1H, RuH). $^{31}\text{P}\{^1\text{H}\}$ NMR (161.83 MHz): $\delta = 82.1$ ($P^i\text{Pr}_2$), 79.5 ($P^i\text{Pr}_2$), 4.7 (t, $^2J_{\text{PP}} = 26.7$ Hz, $P(\text{CH}_3)_3$). ^{11}B NMR (128.27 MHz): $\delta = -17.5$ (br).

Reaction of 3a with A: **A** (1.5 mg; 48.6 μmol ; 1.2 equiv.) is added to a solution of **3a** (42.0 μmol) in THF (0.5 mL). A white solid immediately precipitates and H_2 evolution is observed. The reaction mixture is stirred at room temperature over 3 days and monitored by ^{11}B NMR. During this time **3a** remains the only ruthenium species observed by ^{11}B and ^{31}P NMR.

Reaction of B with C: **B** (28.5 mg; 483.7 μmol ; 4.6 equiv.) is added to a solution of **C** (105.2 μmol) in THF (0.5 mL). No reaction was observed by ^{11}B NMR over 1 week at room temperature.

1.3.5 NMR Spectra

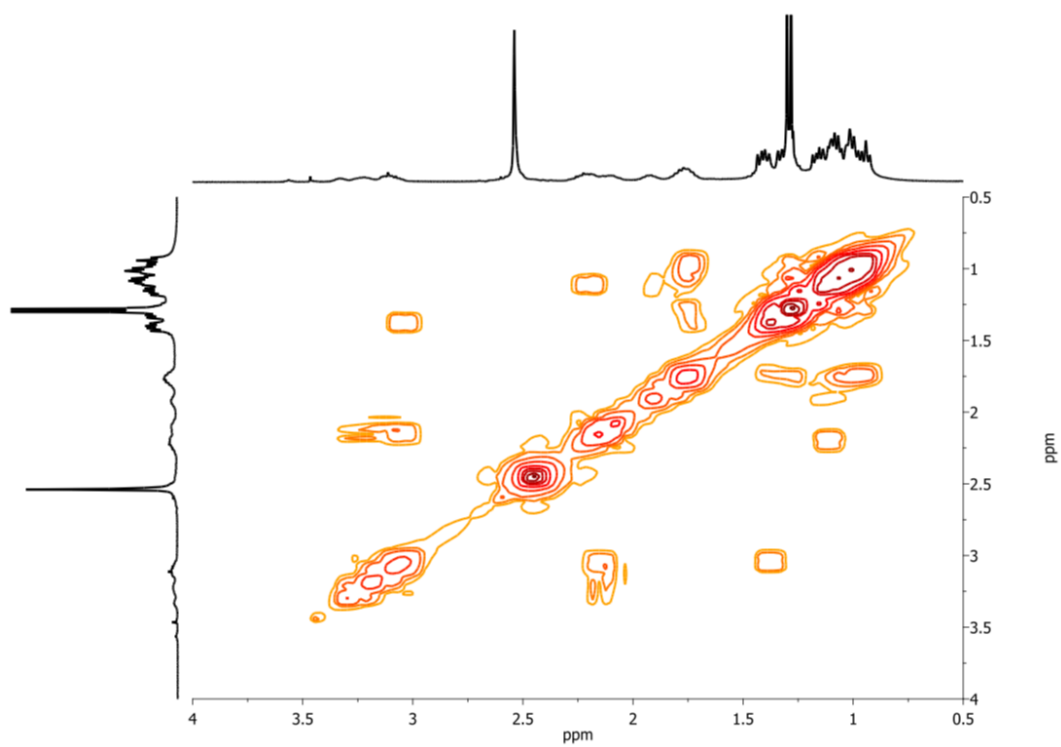


Figure S1. ^1H COSY spectrum of **3a** in d_6 -benzene.

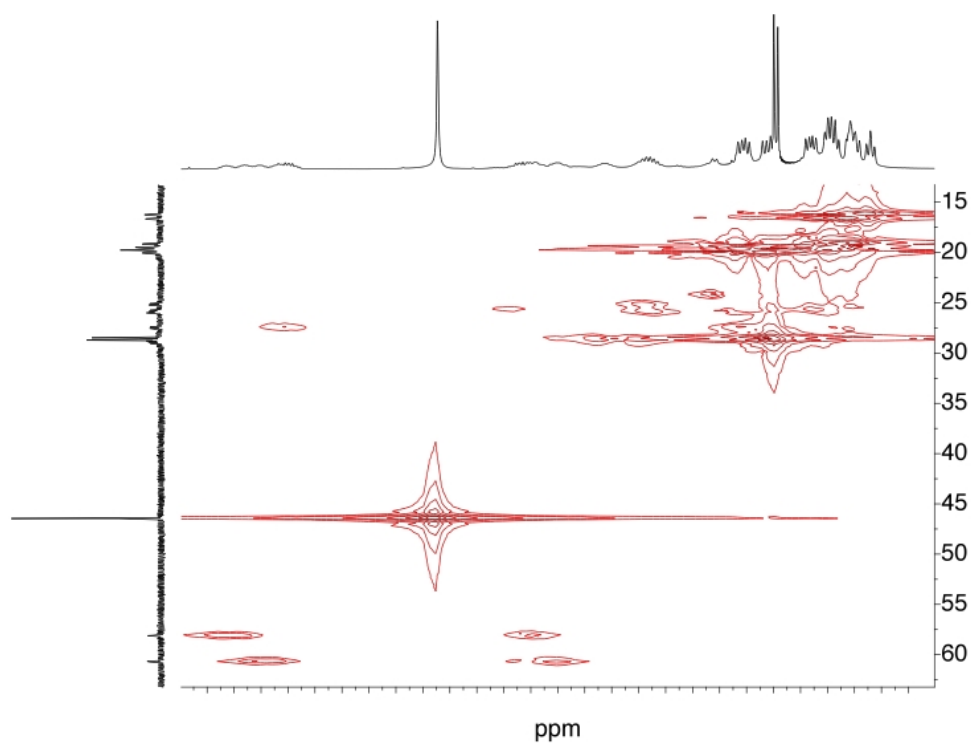


Figure S2. ^1H - ^{13}C HMQC spectrum of **3a** in d_6 -benzene.

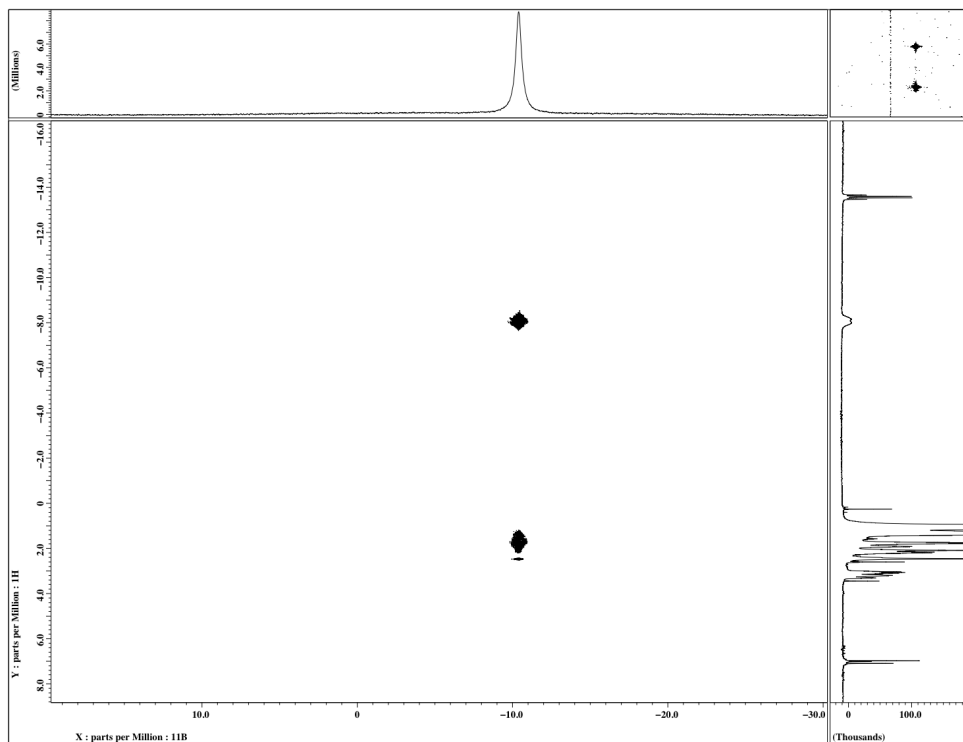


Figure S3. ^{11}B - ^1H HETCOR NMR spectrum of **3a** in d_8 -toluene.

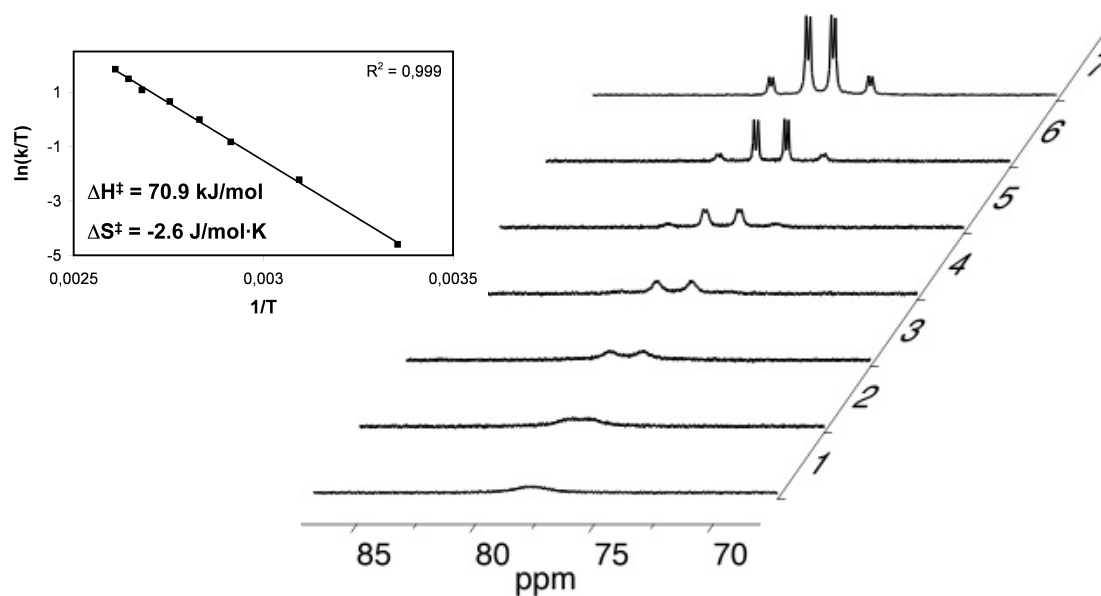


Figure S4. VT- ^{31}P NMR spectra of **3a** in d_8 -toluene; 7: 50 °C, 6: 60 °C, 5: 70 °C, 4: 80 °C, 3: 90 °C, 2: 100 °C, 1: 110 °C. Insert: Eyring plot derived from lineshape fitting.

1.3.6 Catalytic protocols

Safety warning: Dehydrocoupling of amine-boranes with catalysts **1** or **2** quickly evolves large amounts of H₂. Therefore, the reaction should be carried out in a well vented fume-hood and the release of pressure from the reaction vessel has to be assured!

Volumetric monitoring: **B** is dissolved in 2.5 mL THF. The vessel is stoppered with a fresh, tight-fitting rubber septum and connected to an up-turned, water-filled graduated cylinder via a thin cannula. 0.5 mL of a solution of **1**, **2** or **3a** in THF is quickly added via syringe. Results are displayed in Figure 1.

NMR Monitoring: **B** (16.0 mg; 271.6 μmol) in 0.25 mL THF is added via syringe to a solution of **1** (2.6 mg; 5.4 μmol) or **3a** (2.9 mg; 5.4 μmol) in 0.25 mL THF (2.0 mol-%), respectively, in a septum-cap NMR tube. The reaction was monitored by ¹¹B NMR. H₂ pressure release was ensured through the pierced NMR tube septum. Results are displayed in Figures S5 and S6.

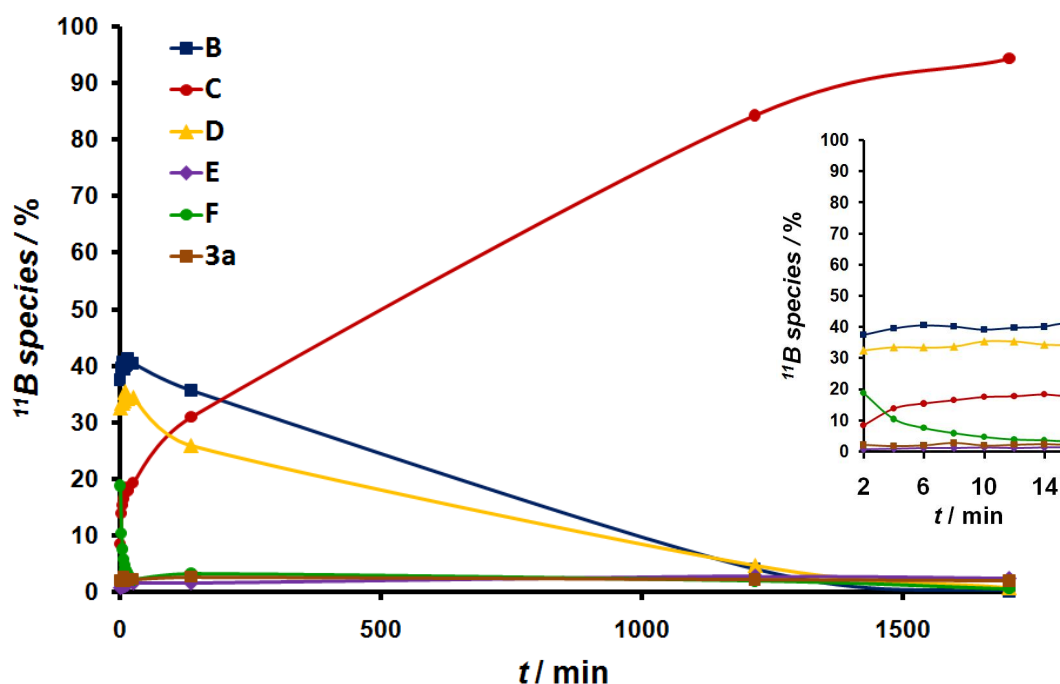


Figure S5. Time course of of **B** (0.54 M in THF) dehydrocoupling with catalyst **1** (2 mol-%) at room temperature in an NMR tube.

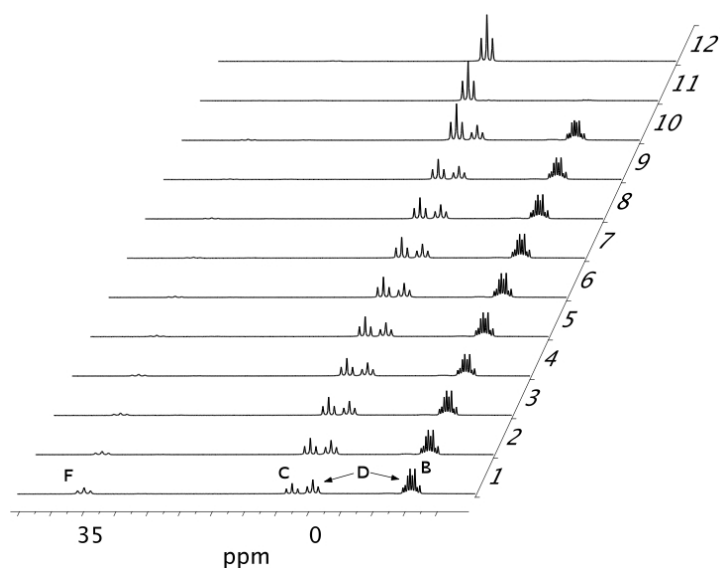


Figure S6. ^{11}B NMR spectra of **B** (0.54 M in THF) dehydrocoupling with catalyst **1** (2 mol-%) at room temperature in a vented NMR tube; 1: 2 min, 2: 4 min, 3: 6 min, 4: 8 min, 5: 10 min, 6: 12 min, 7: 14 min, 8: 16 min, 9: 27 min, 10: 138 min, 11: 1218 min, 12: 1705 min.

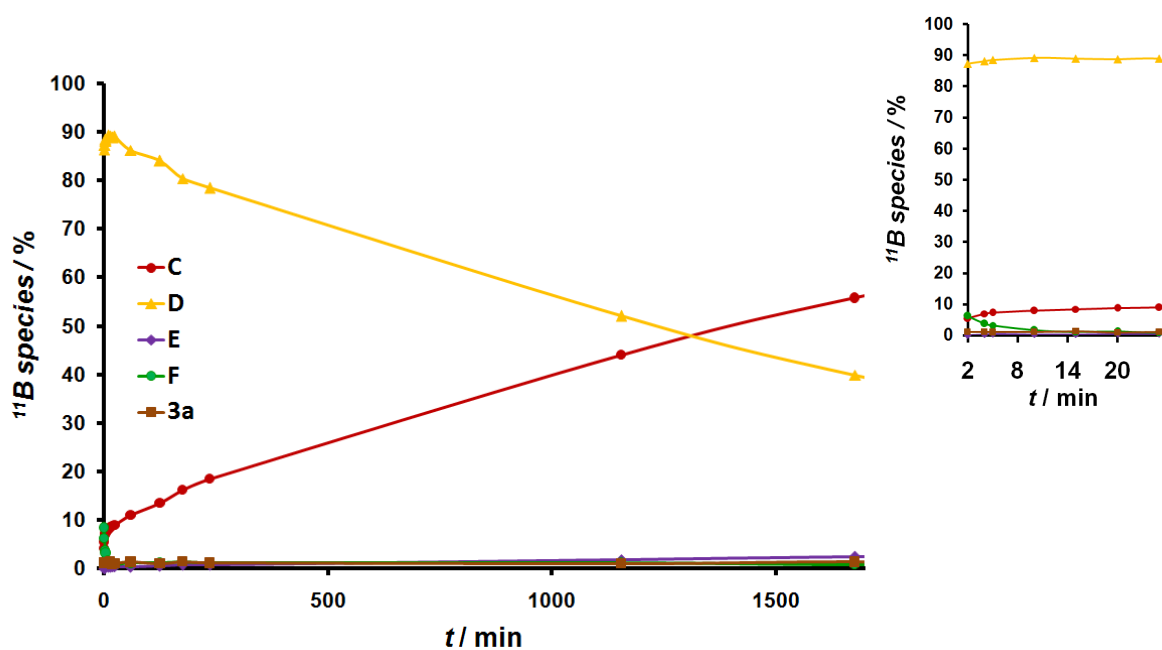


Figure S7. Time course of of **D** (0.54 M in THF) dehydrocoupling with catalyst **1** (2 mol-%) at room temperature in an NMR tube. Quantitative conversion to **C** was observed after 3d under these conditions.

1.3.7 Computational results

The following theoretical studies were performed with the program package Gaussian-03.²⁰ The thermochemistry of **B** dehydrocoupling was calculated with the composite method G3MP2.²¹ The structure reported for Me₂HNH₂BMe₂NBH₃ (**D**) represents the most stable conformer with respect to rotation around the central N-B bond. Reactions of [Ru(H)PMe₃(PNP)] (**1**) with R₂HNBH₃ (**A**: R = H; **B**: R = Me) were studied by DFT methods using a slightly simplified model bearing PMe₂ substituents on the pincer ligand instead of P^{*i*}Pr₂, to save computational time. The hybrid functional B3LYP was utilized with Hay's and Wadt's ECP and corresponding basis set for ruthenium and the basis set 6-31G* for all other atoms.^{22,23,24} Minima and transition states were distinguished by the number of imaginary frequencies (ground states: 0, transition states: 1). The transition states were found using the Berny algorithm as implemented in Gaussian03.²⁵ Energy values are reported for standard conditions (298.15 K, 1 bar atmospheric pressure) in the gas-phase.

²⁰ Frisch, M. J.; Trucks, G. W.; Schlegel, H. B.; Scuseria, G. E.; Robb, M. A.; Cheeseman, J. R.; Montgomery Jr., J. A.; Vreven, T.; Kudin, K. N.; Burant, J. C.; Millam, J. M.; Iyengar, S. S.; Tomasi, J.; Barone, V.; Mennucci, B.; Cossi, M.; Scalmani, G.; Rega, N.; Petersson, G. A.; Nakatsuji, H.; Hada, M.; Ehara, M.; Toyota, K.; Fukuda, R.; Hasegawa, J.; Ishida, M.; Nakajima, T.; Honda, Y.; Kitao, O.; Nakai, H.; Klene, M.; Li, X.; Knox, J. E.; Hratchian, H. P.; Cross, J. B.; Bakken, V.; Adamo, C.; Jaramillo, J.; Gomperts, R.; Stratmann, R. E.; Yazyev, O.; Austin, A. J.; Cammi, R.; Pomelli, C.; Ochterski, J. W.; Ayala, P. Y.; Morokuma, K.; Voth, G. A.; Salvador, P.; Dannenberg, J. J.; Zakrzewski, V. G.; Dapprich, S.; Daniels, A. D.; Strain, M. C.; Farkas, O.; Malick, D. K.; Rabuck, A. D.; Raghavachari, K.; Foresman, J. B.; Ortiz, J. V.; Cui, Q.; Baboul, A. G.; Clifford, S.; Cioslowski, J.; Stefanov, B. B.; Liu, G.; Liashenko, A.; Piskorz, P.; Komaromi, I.; Martin, R. L.; Fox, D. J.; Keith, T.; Al-Laham, M. A.; Peng, C. Y.; Nanayakkara, A.; Challacombe, M.; Gill, P. M. W.; Johnson, B.; Chen, W.; Wong, M. W.; Gonzalez, C.; Pople, J. A. *Gaussian03 Rev. D.01*; Gaussian Inc.: Wallingford, CT, **2004**.

²¹ (a) Curtiss, L. A.; Redfern, P. C.; Raghavachari, K.; Rassolov, V.; Pople, J. A. *J. Chem. Phys.* **1999**, *110*, 4703. (b) Curtiss, L. A.; Raghavachari, K.; Redfern, P. C.; Rassolov, V. J.; Pople, A. *J. Chem. Phys.* **1998**, *109*, 7764.

²² (a) Lee, C. Y.; Parr, R. G. *Phys. Rev. B* **1988**, *37*, 785. (b) Vosko, S. H. W. L.; Nusair, M. *Can. J. Phys.* **1980**, *58*, 1200. (c) Becke, A. D. *J. Chem. Phys.* **1993**, *98*, 5648. (d) Stephens, P. J. D.; Chabalowski, C. F.; Frisch, M. J. *J. Phys. Chem.* **1994**, *98*, 11623.

²³ Hay, P. J.; Wadt, W. R. *J. Chem. Phys.* **1985**, *82*, 299.

²⁴ Hehre, W. J.; Ditchfield, R.; Pople, J. A. *J. Chem. Phys.* **1972**, *56*, 2257.

²⁵ Schlegel, H. B. *J. Comput. Chem.* **1982**, *3*, 214.

Thermochemistry of C formation

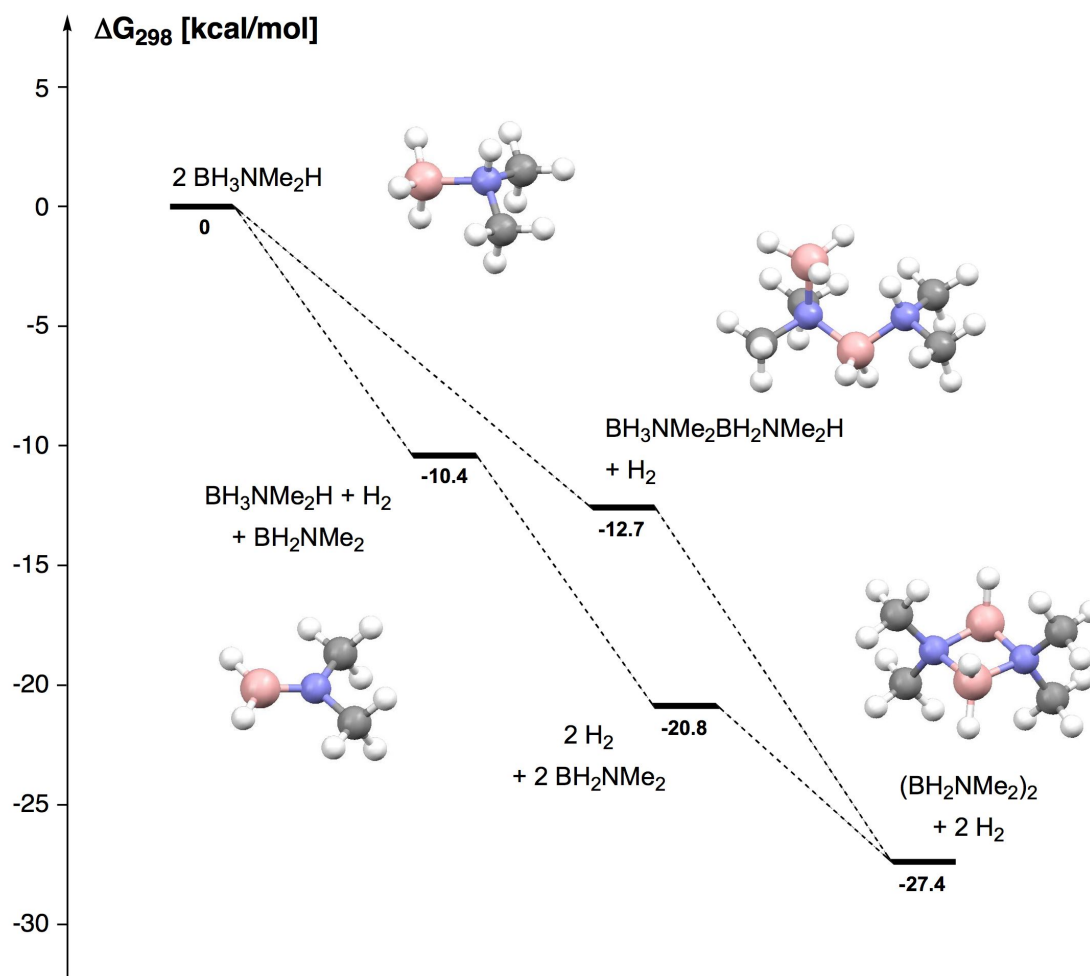


Figure S8. Thermodynamics of stepwise **B** dehydrocoupling via **D** and **F**, respectively, (G3MP2).

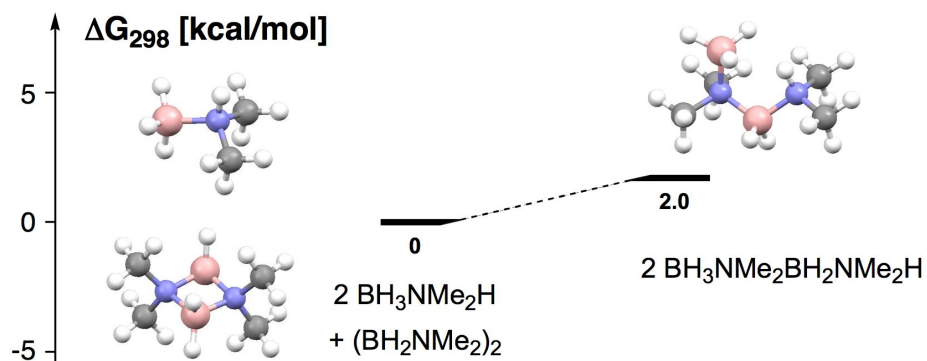


Figure S9. Thermodynamics of **B** and **C** vs. diborazane **D** (G3MP2).

Coordinates and G3MP2 thermochemical energy values for Me_2HNBH_3 (**B**), Me_2NBH_2 (**F**), H_2 , $\text{Me}_2\text{HNBH}_2\text{NMe}_2\text{BH}_3$ (**D**) and $(\text{BH}_2\text{NMe}_2)_2$ (**C**) see Supporting Information for this article under <http://dx.doi.org/10.1002/chem.200901372>.

Formation of **3a/b**

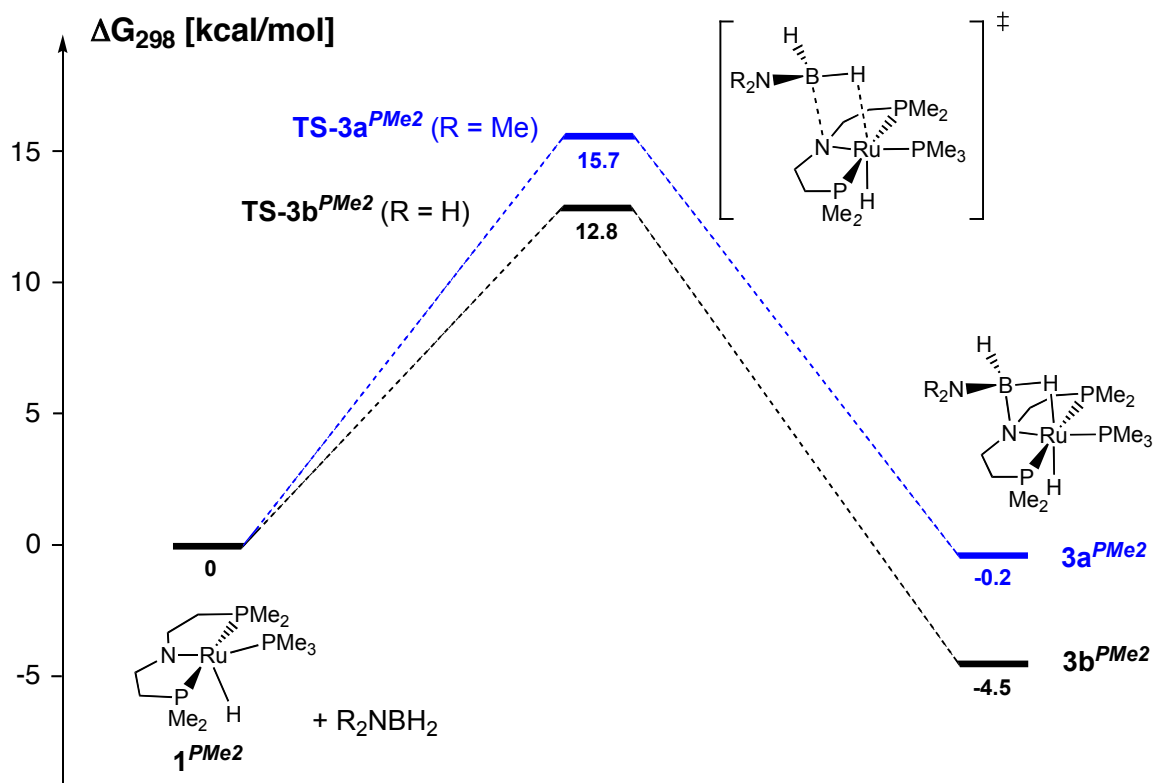


Figure S10. DFT calculated pathways for aminoborane addition to Ru-PNP complex **1**^{PMe2}

Coordinates and Energies for

BH_2NH_2 ,

BH_2NMe_2 ,

$[\text{Ru}(\text{H})\text{PMe}_3\{\text{N}(\text{CH}_2\text{CH}_2\text{PMe}_2)_2\}]$ (**1**^{PMe2}),

$[\text{Ru}(\text{H})\text{PMe}_3\{(\mu\text{-H})\text{HB}(\text{NH}_2)\text{N}(\text{CH}_2\text{CH}_2\text{PMe}_2)_2\}]$ (**TS-3b**^{PMe2}),

$[\text{Ru}(\text{H})\text{PMe}_3\{(\mu\text{-H})\text{HB}(\text{NMe}_2)\text{N}(\text{CH}_2\text{CH}_2\text{PMe}_2)_2\}]$ (**TS-3a**^{PMe2}),

$[\text{Ru}(\text{H})\text{PMe}_3\{(\mu\text{-H})\text{HB}(\text{NH}_2)\text{N}(\text{CH}_2\text{CH}_2\text{PMe}_2)_2\}]$ (**3b**^{PMe2}),

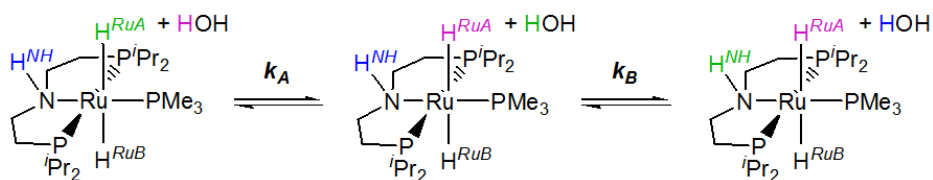
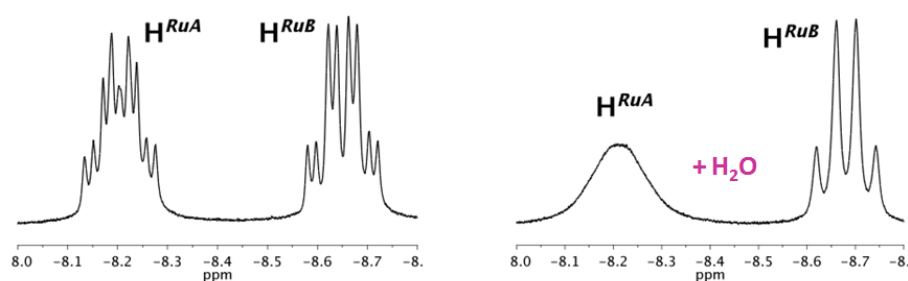
$[\text{Ru}(\text{H})\text{PMe}_3\{(\mu\text{-H})\text{HB}(\text{NMe}_2)\text{N}(\text{CH}_2\text{CH}_2\text{PMe}_2)_2\}]$ (**3a**^{PMe2}) see Supporting Information for this article under <http://dx.doi.org/10.1002/chem.200901372>.

1.4 Highly Stereoselective Proton/Hydride-Exchange: Assistance of Hydrogen-Bonding for the Heterolytic Splitting of H₂

This chapter originated the following publication:

A. Friedrich, M. Drees, J. Schmedt auf der Günne, S. Schneider

J. Am. Chem. Soc. **2009**, *131*, 17552.



1.4.1 Introduction

The heterolytic activation of H₂ is of great importance both in biological systems (e.g., hydrogenases) and catalytic ionic hydrogenations.^[1] For hydrogenations of carbonyl groups, ruthenium catalysts with primary amino ligands have been found to exhibit extraordinary activities.^[2] This ‘NH-effect’ was attributed to a bifunctional mechanism with rate determining heterolytic hydrogen splitting by intramolecular proton transfer from a η^2 -H₂ ligand to a basic amido ligand, but calculated barriers for this step turned out to be too high compared with experimental results.^[3] Furthermore, the acceleration of catalytic rates by alkali alkoxide cocatalysts, protic solvents, and hydrogenation products points towards the involvement of hydrogen bridging in bifunctional H₂-activation,^[4] which was confirmed computationally.^[5,4h] However, the body of experimental data, which allows for quantification and precise mechanistic interpretation of this observation, remains very limited,^[6] and most recently kinetic studies suggested direct proton transfer as originally proposed to be operative in the absence of base.^[7]

¹ Kubas, G. J. *Chem. Rev.* **2007**, *107*, 4152.

² (a) Noyori, R.; Ohkuma, T. *Angew. Chem. Int. Ed.* **2001**, *40*, 40. (b) Clapham, S. E.; Hadzovic, A.; Morris, R. H. *Coord. Chem. Rev.* **2004**, *248*, 2201. (c) Muñiz, K. *Angew. Chem. Int. Ed.* **2005**, *44*, 6622. (d) Samec, J. S. M.; Bäckvall, J.-E.; Andersson, P. G.; Brandt, P. *Chem. Soc. Rev.* **2006**, *35*, 237. (e) Ito, M.; Ikariya, T. *Chem. Commun.* **2007**, 5134.

³ Abdur-Rashid, K.; Clapham, S. E.; Hadzovic, A.; Harvey, J. N.; Lough, A. J.; Morris, R. H. *J. Am. Chem. Soc.* **2002**, *124*, 15104.

⁴ (a) Hartmann, R.; Chen, P. *Angew. Chem. Int. Ed.* **2001**, *40*, 3581 (b) Ito, M.; Hirakawa, M.; Murata, K.; Ikariya, T. *Organometallics* **2001**, *20*, 379.. (c) Rautenstrauch, V.; Hoang-Cong, X.; Churland, R.; Abdur-Rashid, K.; Morris, R. H. *Chem. Eur. J.* **2003**, *9*, 4954. (d) Sandoval, C. A.; Ohkuma, T.; Muñiz, K.; Noyori, R. *J. Am. Chem. Soc.* **2003**, *125*, 13490. (e) Abbel, R.; Abdur-Rashid, K.; Faatz, M.; Hadzovic, A.; Lough, A. J.; Morris, R. H. *J. Am. Chem. Soc.* **2005**, *127*, 1870. (f) Hamilton, R. J.; Bergens, S. H. *J. Am. Chem. Soc.* **2006**, *128*, 13700. (g) Baratta, W.; Siega, K.; Rigo, P. *Chem. Eur. J.* **2007**, *13*, 7479. (h) Hadzovic, A.; Song, D.; MacLaughlin, C. M.; Morris, R. H. *Organometallics* **2007**, *26*, 5987.

⁵ Hedberg, C.; Källström, K.; Arvidsson, P. I.; Brandt, P.; Andersson, P. G. *J. Am. Chem. Soc.* **2005**, *127*, 15083.

⁶ (a) Casey, C. P.; Johnson, J. B.; Singer, S. W.; Cui, Q. *J. Am. Chem. Soc.* **2005**, *127*, 3100. (b) Heiden, Z. A.; Rauchfuss, T. B. *J. Am. Chem. Soc.* **2009**, *131*, 3593.

⁷ Zimmer-De Iuliis, M.; Morris, R. H. *J. Am. Chem. Soc.* **2009**, *131*, 11263.

1.4.2 Results and discussion

Ir and Ru complexes with PNP pincer ligand $\text{HN}(\text{CH}_2\text{CH}_2\text{P}^i\text{Pr}_2)_2$ (*HPNP*) have been utilized as catalysts for hydrogenation of ketones and imines,^[8] and cooperative, pyridine based PNP ligands are active catalysts in acceptorless alcohol dehydrogenation.^[9] Recently, we presented the dehydrocoupling of borane-amine adducts catalyzed by amido complex $[\text{Ru}(\text{H})\text{PMe}_3(\text{PNP})]$ (**1**).^[10] **1** reversibly both eliminates and adds H_2 , forming equilibria with $[\text{Ru}(\text{H})\text{PMe}_3\{\text{N}(\text{CHCHP}^i\text{Pr}_2)(\text{CH}_2\text{CH}_2\text{P}^i\text{Pr}_2)\}]$ (**2**) and $[\text{Ru}(\text{H})_2\text{PMe}_3(\text{HPNP})]$ (**3**), respectively.^[10a] Amino complex **3** features a trans-dihydride configuration with only one hydride in close proximity to the internal N–H acid, representing an ideal probe to study hydrogen exchange processes of the syn H–N–Ru–H moiety referenced against the second hydride.

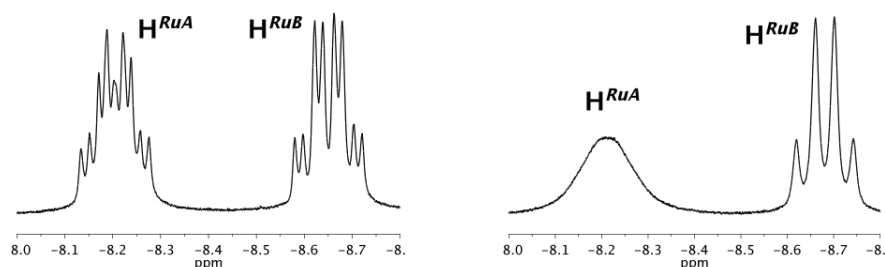


Figure 1. Hydride region of the ^1H NMR spectrum of **3** (*left*) and of **3** with 2 equiv. H_2O (*right*).

The ^1H NMR spectrum of complex **3** in d_8 -THF (Figure 1, *left*) exhibits two sharp signals in the hydride region at -8.20 (H^{RuA}) and -8.65 ppm (H^{RuB}). H^{RuA} can be assigned to the hydride adjacent to the PNP N–H proton (H^{NH}) by ^1H nuclear Overhauser effect NMR spectroscopy

⁸ (a) Abdur-Rashid, K. US 2005/0107638A1. (b) Clarke, Z. E.; Maragh, P. T.; Dasgupta, T. P.; Gusev, D. G.; Lough, A. J.; Abdur-Rashid, K. *Organometallics* **2006**, *25*, 4113. (c) Chen, X.; Jia, W.; Guo, R.; Graham, T. W.; Gullons, M. A.; Abdur-Rashid, K. *Dalton Trans.* **2009**, 1407.

⁹ (a) Zhang, J.; Gandelman, M.; Shimon, L. J. W.; Rozenberg, H.; Milstein, D. *Organometallics* **2004**, *23*, 4026. (b) Zhang, J.; Leitun, G.; Ben-David, Y.; Milstein, D. *J. Am. Chem. Soc.* **2005**, *127*, 10840. (c) Gunanathan, C.; Ben-David, Y.; Milstein, D. *Science* **2007**, *317*, 790. (d) Gunanathan, C.; Shimon, L. J. W.; Milstein, D. *J. Am. Chem. Soc.* **2009**, *131*, 3146.

¹⁰ (a) Käß, M.; Friedrich, A.; Drees, M.; Schneider, S. *Angew. Chem. Int. Ed.* **2009**, *48*, 905. (b) Friedrich, A.; Drees, A.; Schneider, S. *Chem. Eur. J.*, **2009**, *15*, 10339.

(NOESY). To account for possible chemical exchange of H^{RuA} with H^{NH} the NOE signals were calibrated with proton distances obtained from a density functional theory (DFT) model of **3**. In the calculated structure, the $H^{RuA}\cdots H^{NH}$ distance ($d_A = 2.64 \text{ \AA}$) is very close to the distances between H^{RuB} and two C-H protons on the pincer backbone ($d_{B1} = 2.60$; $d_{B2} = 2.81 \text{ \AA}$), which are equivalent on the NMR timescale. A comparison of the distances ($d_A^{-6}/d_B^{-6} = 1.14$)^[11] with the integrals of the respective NOESY ($\tau_m = 1 \text{ s}$) cross peaks ($I_A/I_B = 1.13$) suggests negligible H^{RuA}/H^{NH} chemical exchange on the experimental time scale. Accordingly, H_2 elimination from **3** proceeds very slowly and full dehydrogenation towards **1** under vacuum at room temperature takes several hours.

The addition of 2 equiv. water to a sample of **3** in d^8 -THF results in broadening of the hydride signals and breakdown of the H^{RuA} - H^{RuB} J -coupling (Figure 1, right).^[12] The hydride chemical shift differences with respect to dry samples are very small ($\Delta\delta(H^{RuA}) = 0.01 \text{ ppm}$; $\Delta\delta(H^{RuB}) = 0.03 \text{ ppm}$), which would be in agreement with Ru-H/ H_2O proton exchange via short lived dihydrogen complexes.^[13] Accordingly, below $-50 \text{ }^\circ\text{C}$ exchange is slow on the NMR time scale giving two sharp hydride signals with similar T_1^{min} (H^{RuA} : 154 ms (191 K) and H^{RuB} : 172 ms (191 K) at 400 MHz) that are typical for terminal hydride ligands.^[14] Addition of molecular sieves to this NMR sample resulted in full restoration of the “dry” ^1H NMR spectrum. Most significantly, at room temperature, the broadening of the H^{RuA} signal was considerably larger than for H^{RuB} , pointing toward very different exchange rates, as was further substantiated by T_1 measurements: Above $-50 \text{ }^\circ\text{C}$, apparent T_1 values derived from

¹¹ The value of d_B (2.70 \AA) was obtained by averaging d_{B1} and d_{B2} over $\langle d^{-3} \rangle^{-1/3}$; D. Neuhaus, M. P. Williamson, in *The Nuclear Overhauser Effect in Structural and Conformational Analysis*, 2nd ed., WILEY-VCH, New York 2000.

¹² Small amounts ($\sim 5 \%$) of $[\text{Ru}(\text{OH})(\text{H})\text{PMe}_3(\text{HPNP})]$ (**4**) are also observed.

¹³ (a) Crabtree, R. H.; Siegbahn, P. E. M.; Eisenstein, O.; Rheingold, A. L.; Koetzle, T. F. *Acc. Chem. Res.* **1996**, *29*, 348. (b) Custelcean, R.; Jackson, J. E. *Chem. Rev.* **2001**, *101*, 1963. (c) Papish, E. T.; Magee, M. P.; Norton, J. R. in *Recent Advances in Hydride Chemistry*; Peruzzini, M., Poli, R., Eds.; Elsevier: Amsterdam, 2001, pp. 39. (d) Jacobsen, H.; Berke, H. in *Recent Advances in Hydride Chemistry*; Peruzzini, M., Poli, R., Eds.; Elsevier: Amsterdam, 2001, pp. 89. (e) Epstein, L. M.; Belkova, N. V.; Shubina, E. S. in *Recent Advances in Hydride Chemistry*; Peruzzini, M., Poli, R., Eds.; Elsevier: Amsterdam, 2001, pp. 391. (f) Bakhmutov, V. I. *Eur. J. Inorg. Chem.* **2005**, 245.

¹⁴ Crabtree, R. H. *Acc. Chem. Res.* **1990**, *23*, 95.

B Results and Discussion

inversion recovery for H^{RuA} dropped as a result of rapid exchange, contrasting sharply with H^{RuB} (see chapter B1.4.4).

Proton exchange rates of H_2O (4.25 equiv.) with H^{RuA} ($k_A = 337(20) \text{ L mol}^{-1} \text{ s}^{-1}$) and H^{NH} ($k_B = 8.0(4) \text{ L mol}^{-1} \text{ s}^{-1}$) in d_8 -THF were derived by 1H 2D exchange spectroscopy (EXSY) combined with simultaneous fitting of several 2D spectra at different mixing times (Scheme 1).^[15,16] This method offers the opportunity to study simultaneous multisite exchange over a wide dynamic range of exchange rates without isotope effect inherent in H/D exchange kinetics. The k_A value is surprisingly high considering the low acidity of water in such a nonpolar solvent. Most intriguingly, within experimental errors no direct exchange of H_2O with H^{RuB} was found. Stereoselective dihydrogen bonding has been observed previously, e.g., for $[Re(cis-H)_2(CO)(NO)(trans-PR_3)_2]$ with alcohols, and was attributed to different relative ligand hydricities and steric effects.^[17] However, H^{RuA} and H^{RuB} are in very similar steric environments, and the trans dihydride configuration suggests comparable basicities of the hydride ligands. Therefore, the highly site-selective hydride/ H_2O exchange and large exchange rate of H^{RuA} can best be rationalized in terms of directing H^{NH}/OH_2 hydrogen bonding. To further probe for the influence of the amine proton, the nitrogen atom was blocked by methylation (chapter B1.4.4). Addition of 2 equiv. of H_2O to $[Ru(H)_2PMe_3(MePNP)]$ (**5**; $MePNP = MeN(CH_2CH_2P^iPr_2)_2$) in d_8 -THF did not result in considerable broadening of either of the two hydride signals, and mutual J -coupling is retained. Finally, the H_2O exchange rates with the hydrides of **5** as derived by 1H 2D EXSY NMR ($0.07(3) \text{ Lmol}^{-1}\text{s}^{-1}$ and $0.03(2) \text{ Lmol}^{-1}\text{s}^{-1}$) are very similar to each other and about four orders of magnitude smaller than k_A , supporting the idea that stereoselective H^+/H^- exchange in **3** is directed by H^{NH} .^[18]

¹⁵ (a) Perrin, C. L.; Dwyer, T. J. *Chem. Rev.* **1990**, *90*, 935. (b) Sweeney, Z. K.; Polse, J. L.; Andersen, R. A.; Bergman, R. G.; Kubinec, M. G. *J. Am. Chem. Soc.* **1997**, *119*, 4543.

¹⁶ Rate laws which are first order in H^{H_2O} and in H^{RuA} or H^{NH} are in agreement with the asymmetric magnetization exchange matrix.

¹⁷ Messmer, A.; Jacobsen, H.; Berke, H. *Chem. Eur. J.* **1999**, *5*, 3341.

¹⁸ H^+/H^+ exchange involving amine N-H and water O-H (k_B) could occur directly with N-H hydrogen-bonded water without Ru-H involvement: the slow exchange (0.14 s^{-1}) of H^{RuA} with H^{RuB} can best be explained by amine inversion upon such H^{NH} exchange with water.

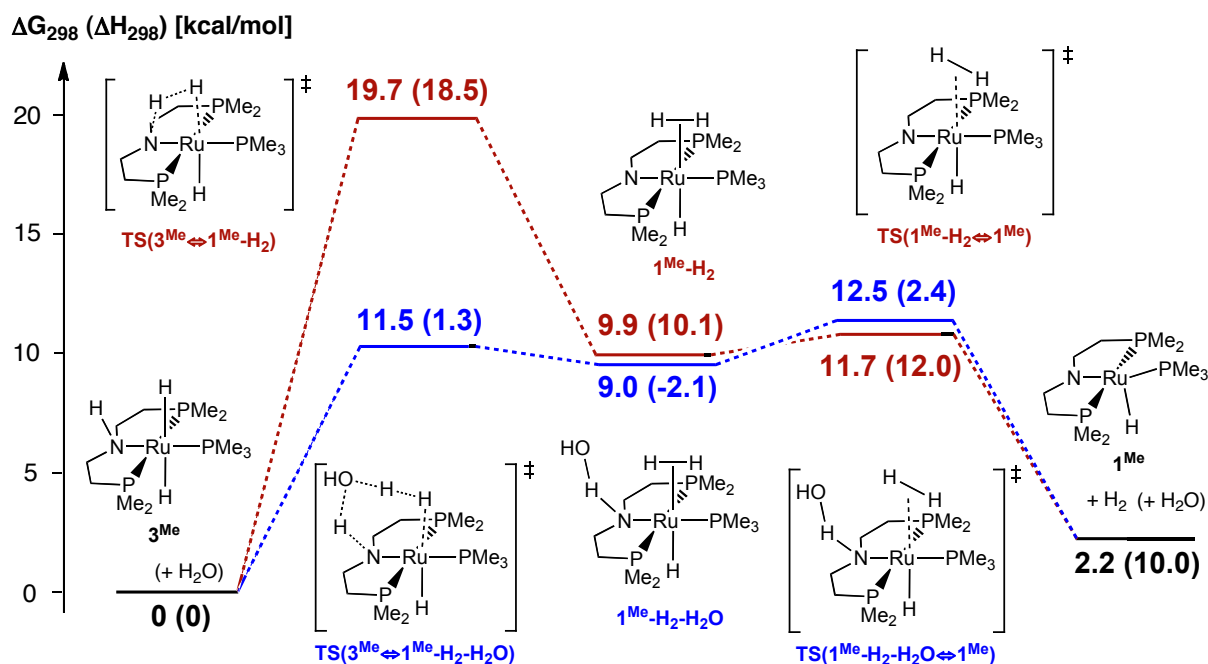


Figure 2. DFT calculations (B3LYP/6-31+G**) for heterolytic hydrogen splitting in THF (blue) with and (red) without water assistance.^[19]

Since the intermediate dihydrogen complex that accounts for H^+/H^- exchange should be on the reaction path of H_2 activation by **1** as well, these results suggest that water lowers the barrier of heterolytic hydrogen splitting. Therefore, H_2 addition to model complex **1**^{Me} with and without H_2O was examined using DFT calculations (Figure 2). Addition of H_2 to amide **1**^{Me} is slightly exergonic ($\Delta\text{G} = -2.2$ kcal/mol). The water-free mechanism exhibits a barrier of $\Delta\text{G}^\ddagger = 9.8$ kcal/mol for rate-determining proton transfer from an H_2 -ligand to nitrogen in four-membered transition state $\text{TS}(\mathbf{3}^{\text{Me}} \rightleftharpoons \mathbf{1}^{\text{Me}}\text{-H}_2)$. In contrast, hydrogen bonding of the amido and the H_2 ligands with water via six-membered-ring transition state $\text{TS}(\mathbf{3}^{\text{Me}} \rightleftharpoons \mathbf{1}^{\text{Me}}\text{-H}_2\text{-H}_2\text{O})$ lowers this barrier by $\Delta\Delta\text{G}^\ddagger = 8.2$ kcal/mol, in agreement with our proton exchange experiments.^[19] Overall, the computed reaction profile compares well with calculations by Brandt, Andersson and co-workers⁵ on alcohol-assisted hydrogen activation with diamine diphosphine model system $[\text{Ru}(\text{trans-H})_2(\text{cis-PH}_3)_2(\text{H}_2\text{NCH}_2\text{CH}_2\text{NH}_2)]$.

¹⁹ $\mathbf{3}^{\text{Me}}\text{-H}_2\text{O}$ with water hydrogen-bonded to H^{NH} was found to be slightly endergonic with respect to $\mathbf{3}^{\text{Me}}$ ($\Delta\text{G} = +2.0$ kcal/mol; $\Delta\text{H} = -7.5$ kcal/mol; chapter B1.4.6).

1.4.3 Conclusion

The unusual stereoselectivity of H⁺/H⁻ exchange and the computational results strongly emphasize the role of hydrogen bonding networks with Brønsted acids as weak as H₂O for heterolytic H₂ splitting by ruthenium amide hydrogenation catalysts. In view of the ubiquitous availability of water, this mechanism might be relevant both for catalysis and biological heterolytic H₂ activation.

1.4.4 Experimental details and syntheses

Materials and Methods. All experiments were carried out under an atmosphere of argon using Schlenk and glove-box techniques. *d*⁸-THF was dried by distillation from Na/K alloy and deoxygenated by three freeze-pump-thaw cycles. Water was deoxygenated by three freeze-pump-thaw cycles prior to use. [Ru(H)PMe₃(PNP)] (**1**) was synthesized as reported earlier.^[20] [Ru(H)₂PMe₃(HPNP)] (**3**) was prepared in situ from reaction of **1** with H₂ in a *J-Young* NMR tube. For NMR exchange measurements the tube was subsequently evacuated and backfilled with Argon. NMR spectra were recorded on Jeol Lambda 400, Bruker Avance III 400, and Bruker DPX 500 spectrometers and calibrated to the residual proton resonance. *T*₁ measurements were performed by the inversion-recovery method with relaxation delays set to 5-10 times the expected *T*₁ times. ¹H 2D EXSY NMR spectra were obtained at 300 K in *d*⁸ THF using the BRUKER pulse sequence *noesyph* with d1 set to 2s.

Synthesis of [Ru(H)₂PMe₃(MePNP)] (5). MeOTf (42.3 mg; 0.258 mmol) is added dropwise to a vigorously stirred solution of **1** (104.3 g; 0.216 mmol) in pentane (5 mL) at r.t. and a yellow solid precipitates immediately. After filtration the residue is washed with pentane (2 x 5 mL) and dried *in vacuo* to give [RuH(PMe₃)OTf(MePNP)]: NMR (C₆D₆, r.t., [ppm]) ¹H NMR (399.8 MHz): δ = -27.20 (q, ²J_{HP} = 25.0 Hz, 1H, RuH), 0.83-0.89 (m, 12H, CHCH₃), 1.10 (dd, ³J_{HH} = 6.1 Hz, ³J_{HP} = 12.2 Hz, 6H, CHCH₃), 1.30 + 1.25-1.31 (d + m, ²J_{HP} = 8.6 Hz, 15H, P(CH₃)₃ + CHCH₃), 1.40-1.48 (m, 2H), 1.76-1.85 (m, 4H), 1.96 (s, 3H, NCH₃), 1.96-2.03 (m, 2H), 2.24 (sp, ³J_{HH} = 7.3 Hz, 2H, CHCH₃), 2.35-2.47 (m, 2H, NCH₂). ³¹P{¹H} NMR (161.83 MHz): δ = 61.4 (d, ²J_{PP} = 28.7 Hz, PⁱPr₂), 11.4 (t, ²J_{PP} = 28.7 Hz, P(CH₃)₃). ¹⁹F{¹H} NMR (376.17 MHz): δ = -77.4 (s, SO₃CF₃). [RuH(PMe₃)OTf(MePNP)] is redissolved in THF (10 mL) and NaH (23.8 g; 0.992 mmol) is added. After 5 h at room

²⁰ Käß, M.; Friedrich, A.; Drees, M.; Schneider, S. *Angew. Chem.* **2009**, *121*, 922.

temperature the solvent is evaporated *in vacuo* and the residue is extracted with pentanes. Evaporation of the filtrate gives **5** as a bright yellow solid. Yield starting from **1**: 59.0 mg (0.118 mmol; 55 %). Anal. calcd. for C₂₀H₅₀NP₃Ru (498.61): C, 48.18; H, 10.11; N, 2.81. Found: C 48.59; H, 9.83; N, 2.54. IR (cm⁻¹) ν = 1911 (w, Ru-H_{sym}), 1556 (s, Ru-H_{as}). NMR (C₆D₆, r.t., [ppm]) ¹H NMR (399.8 MHz): δ = -8.31 (ddt, ²J_{HH} = 7.3 Hz, ²J_{HP} = 17.1 Hz, ²J_{HP} = 29.3 Hz, 1H, RuH), -7.43 (ddt, ²J_{HH} = 7.3 Hz, ²J_{HP} = 16.5 Hz, ²J_{HP} = 31.1 Hz, 1H, RuH), 1.13-1.18 (m, 12H, CHCH₃), 1.31 (d, ²J_{HP} = 7.3 Hz, 9H, P(CH₃)₃), 1.35 (m, ²J_{HP} = 7.3 Hz, 2H, PCH₂), 1.44 (dd, ³J_{HH} = 7.3 Hz, ³J_{HP} = 13.4 Hz, 6H, CHCH₃), 1.65 (m, 2H, PCH₂), 1.70 (dd, ³J_{HH} = 7.3 Hz, ³J_{HP} = 14.6 Hz, 6H, CHCH₃), 1.98 (sp, ³J_{HH} = 7.3 Hz, 4H, CHCH₃ + NCH₂), 2.07 (sp, ³J_{HH} = 7.3 Hz, 2H, CHCH₃), 2.22 (s + m, 5H, NCH₃ + NCH₂). ¹³C-{¹H} NMR (100.6 MHz): δ 16.4 (t, J_{CP} = 2.0 Hz, CHCH₃), 19.4 (t, J_{CP} = 3.5 Hz, CHCH₃), 19.7 (t, J_{CP} = 2.5 Hz, CHCH₃), 20.3 (t, J_{CP} = 4.0 Hz, CHCH₃), 24.6 (dt, ¹J_{CP} = 8.0 Hz, ³J_{CP} = 2.0 Hz, CHCH₃), 25.5 (dt, ¹J_{CP} = 6.5 Hz, ³J_{CP} = 3.0 Hz, PCH₂), 27.9 (t, J_{CP} = 11.1 Hz, ³J_{CP} = 2.7 Hz, CHCH₃), 30.2 (dt, ¹J_{CP} = 24.1 Hz, ³J_{CP} = 3.0 Hz, P(CH₃)₃), 54.05 (s, NCH₃), 65.3 (dt, ³J_{CP} = 5.0 Hz, ³J_{CP} = 1.0 Hz, NCH₂). ³¹P-{¹H} NMR (161.83 MHz): δ = 85.1 (d, ²J_{PP} = 34.7 Hz, P^tPr₂), 14.5 (t, ²J_{PP} = 34.7 Hz, P(CH₃)₃). Assignments were confirmed by ¹H-¹H COSY and ¹H-¹³C HMQC.

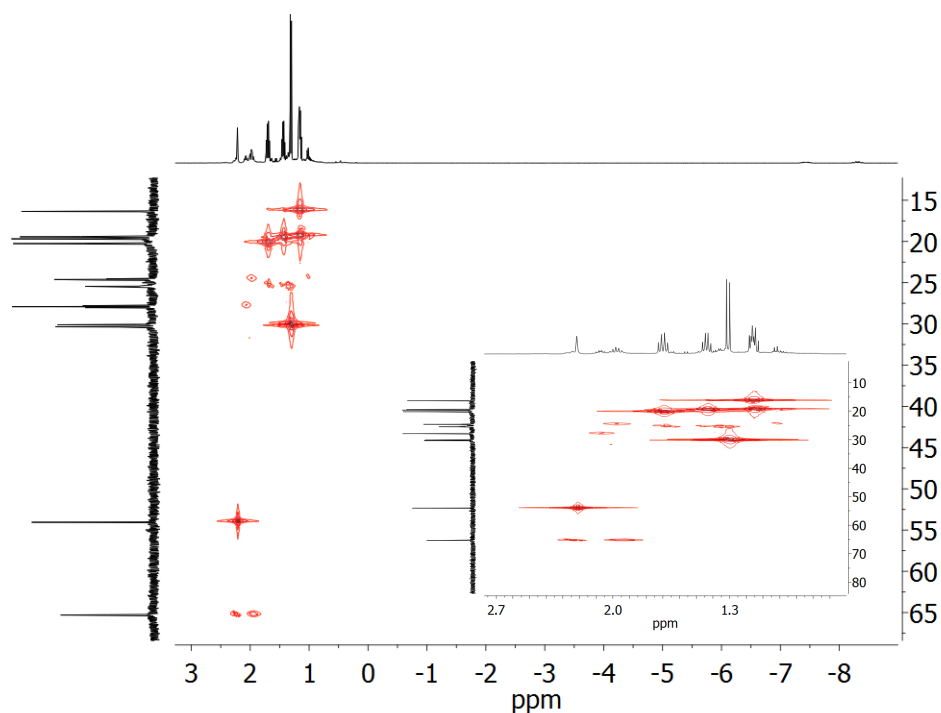


Figure S1. ¹H-¹³C HMQC NMR of **5** in benzene.

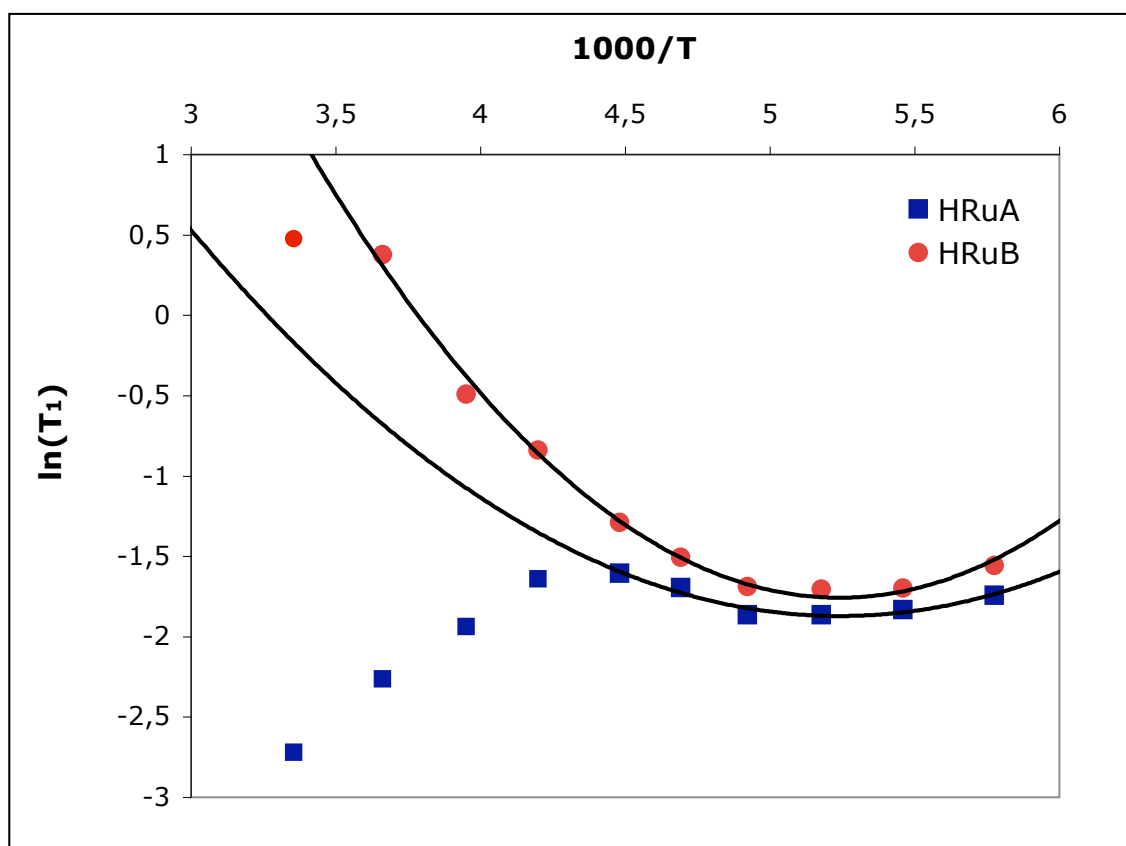


Figure S2. Plot of $\ln(T_1)$ vs $1/T$ (recorded at 400 MHz) of the two hydride signals H^{RuA} (■) and H^{RuB} (●) of **3** in the presence of 2 equiv. H_2O .

1.4.5 1H 2D EXSY NMR measurements

Mixing times (τ_m) of 500 and 1000 ms were used for **3** in dry d^8 -THF and for **5** in d^8 -THF with H_2O (2 equiv.). For **3** with 2 - 5 equiv. H_2O in d^8 -THF, τ_m was varied over a wide range (0.01, 0.1, 0.5, 1, 10, 100, 500, and 1000 ms) to account for the largely different exchange rates. Typical spectra are shown in Figures S3 – S5. Intensities were determined by integration of the exchange cross-peaks and diagonal peaks. In the next step, magnetization exchange rate constants were determined using two different approaches which are based on the peak intensities not the lineshapes in 2D EXSY spectra. In case of **5** the situation is simplified by the fact that the processes to be investigated have similarly slow rates, so analysis can be done following the eigen-values eigenvectors method²¹ implemented in EXSY

²¹ Perrin, C. L.; Gipe, R. K. *J. Am. Chem. Soc.* **1984**, *106*, 4036.

Calc developed by Mestrelab Research.²² In case of **3** several processes with rate constants differing several orders of magnitudes take place. In such a situation a simple iterative scheme which considers the intensities of several 2D EXSY spectra at different mixing times is indicated,²³ which was implemented in a home-written Fortran90 program which allows non-linear least square fitting using the MINUIT routines from the CERN library. The program minimizes the sum of the difference between experimental and calculates intensities of all peaks at different mixing times. If all peaks are given the same weight, small deviations in the diagonal peaks (for example the intense water peak) distort the fitted curves tremendously. For this reason, the residuals of each peak intensity were normalized on the square root of maximum intensity occurring in the time series of each peak. Nine times more weight was given to off-diagonal peaks than to diagonal peaks. The best-fit result is displayed in Figure S6 and the magnetization rate matrix in Table S1. The fit is numerically stable with acceptable correlation coefficients. Conversion to reaction rate constants for exchange of H^{H_2O} with H^{RuA} (k_A) and H^{NH} (k_B), respectively, were calculated assuming second order rate laws for the forward and reverse reactions:

$$r_1 = r_{-1} = k_1 \cdot [\text{H}^{RuA}] \cdot [\text{H}^{H_2O}] = k_{-1} \cdot [\text{H}^{RuA}] \cdot [\text{H}^{H_2O}]$$

$$r_2 = r_{-2} = k_2 \cdot [\text{H}^{NH}] \cdot [\text{H}^{H_2O}] = k_{-2} \cdot [\text{H}^{NH}] \cdot [\text{H}^{H_2O}]$$

$$k_A = k_1 \cdot [\text{H}^{H_2O}] = k_A' = k_{-1} \cdot [\text{H}^{RuA}]$$

$$k_B = k_2 \cdot [\text{H}^{H_2O}] = k_B' = k_{-2} \cdot [\text{H}^{NH}]$$

²² (a) www.mestrelab.com (b) Lu, J.; Ma, D.; Hu, J.; Tang, W.; Zhu, D. *J. Chem. Soc., Dalton Trans.* **1998**, 2267. (c) Zolnai, Z.; Juranic, N.; Vikić-Topić, D.; Macura, S. *J. Chem. Inf. Comput. Sci.* **2000**, *40*, 611.

²³ Hawkes, G. E.; Lan, L.Y.; Randall, E.W.; Sales, K.D.; Aoime, S. *J. Magn. Reson.* **1985**, *65*, 173.

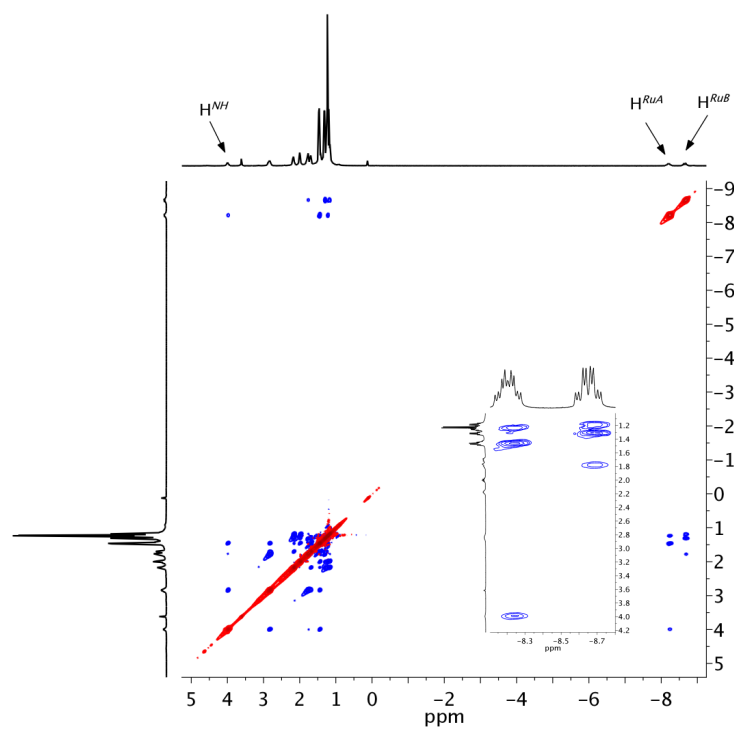


Figure S3. ¹H EXSY NMR of **3** in dry THF ($\tau_m = 1000$ ms).

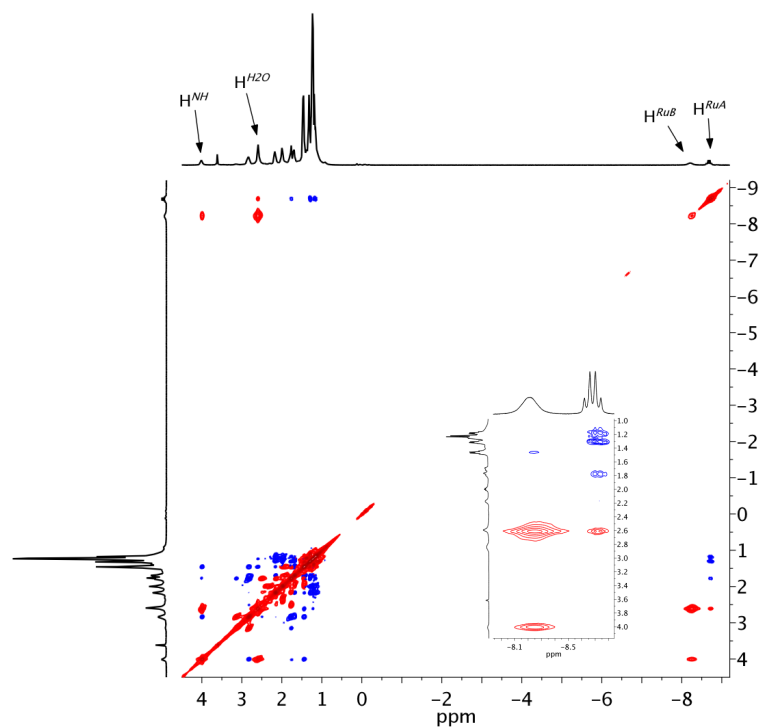


Figure S4. Typical ¹H EXSY NMR of **3** in the presence of 2 equiv. H₂O in THF ($\tau_m = 500$ ms).

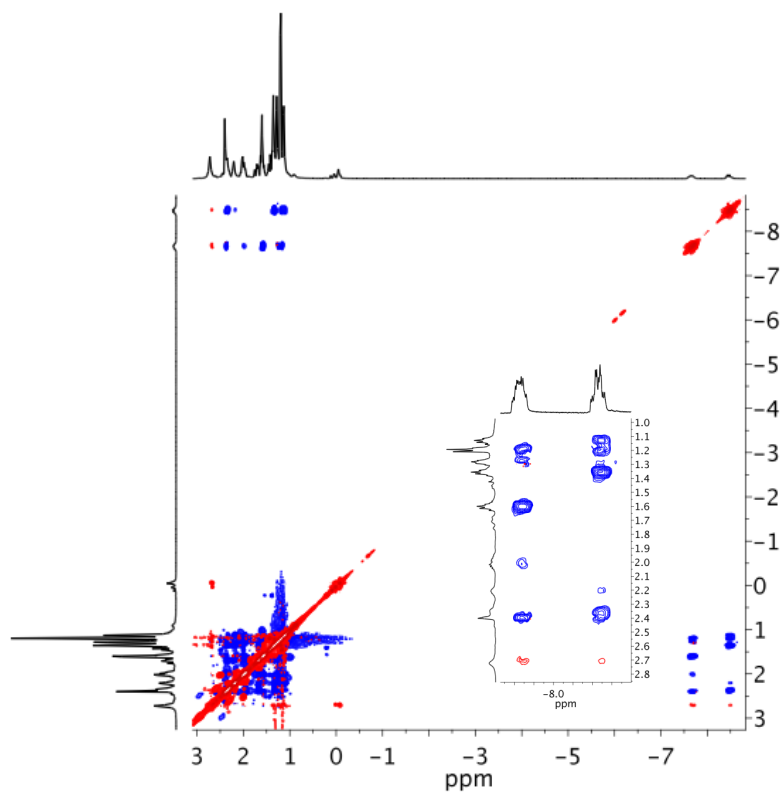


Figure S5. Typical ^1H EXSY NMR of **5** with 2 equiv. H_2O in THF ($\tau_m = 1000$ ms).

Table S1. Magnetization exchange rate matrix for **3** with H_2O (4.25 equiv.).

	H^{NH}	$\text{H}^{\text{H}_2\text{O}}$	H^{RuHA}	H^{RuHB}
H^{RuHB}	0 s^{-1}	0 s^{-1}	0.131 s^{-1}	--
H^{RuHA}	0.042 s^{-1}	16.5 s^{-1}	--	0.155 s^{-1}
$\text{H}^{\text{H}_2\text{O}}$	3.45 s^{-1}	--	154 s^{-1}	0 s^{-1}
H^{NH}	--	0.416 s^{-1}	0 s^{-1}	0 s^{-1}

Table S2. Reaction rate constant matrix for **3** with H_2O (4.25 equiv.).

	H^{NH}	$\text{H}^{\text{H}_2\text{O}}$	H^{RuHA}	H^{RuHB}
H^{RuHB}	0 s^{-1}	0 s^{-1}	0.131 s^{-1}	--
H^{RuHA}	0.042 s^{-1}	$320 \text{ Lmol}^{-1}\text{s}^{-1}$	--	0.155 s^{-1}
$\text{H}^{\text{H}_2\text{O}}$	$7.91 \text{ Lmol}^{-1}\text{s}^{-1}$	--	$354 \text{ Lmol}^{-1}\text{s}^{-1}$	$0 \text{ Lmol}^{-1}\text{s}^{-1}$
H^{NH}	--	$8.11 \text{ Lmol}^{-1}\text{s}^{-1}$	0 s^{-1}	0 s^{-1}

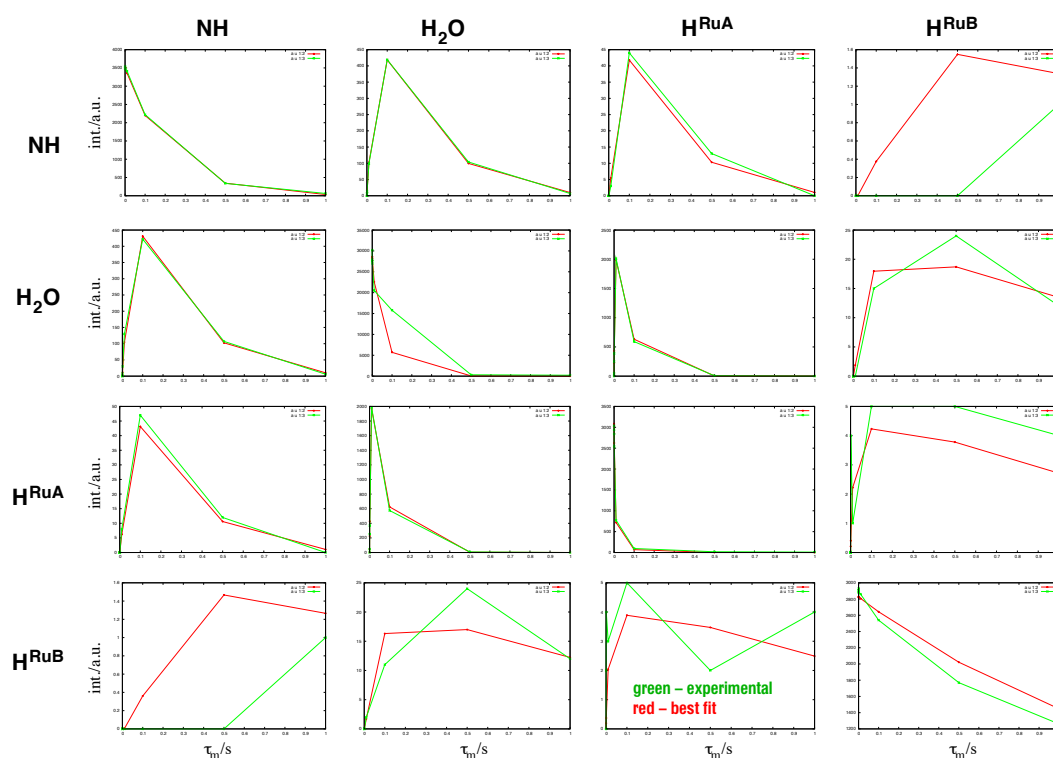


Figure S6. Magnetization exchange curves of H^{H_2O} , H^{RuA} , H^{RuB} , and H^{NH} of **3** with H_2O (4.25 equiv.); green: experimental data, red: simulated data; all curves are scaled to the maximum intensity found in the time series of the respective peak.

1.4.6 Computational results

Reactions of $[Ru(H)_2PMe_3(PNP^H)]$ (**3**) with H_2O were studied by DFT methods using a slightly simplified model bearing PMe_2 substituents on the pincer ligand (3^{Me} : $[Ru(H)_2PMe_3\{HN(CH_2CH_2PMe_2)_2\}]$ instead of P^iPr_2 , to save computational time. The hybrid functional B3LYP was utilized with Hay's and Wadt's ECP and corresponding basis set for ruthenium and the basis set 6-31+G** for all other atoms.^[24,25,26] The solvent influence was introduced applying the PCM model. Optimized structures, coordinates and energy values of 3^{Me} , $TS(3^{Me} \leftrightarrow 1^{Me}-H_2)$, $1^{Me}-H_2$, $TS(1^{Me}-H_2 \leftrightarrow 1^{Me})$, 1^{Me} for water free and water-assisted H_2 activation are available free of charge via the Internet at <http://pubs.acs.org>.

²⁴ (a) Lee, C. Y.; Parr, R. G. *Phys. Rev. B* **1988**, *37*, 785. (b) Vosko, S. H. W. L.; Nusair, M. *Can. J. Phys.* **1980**, *58*, 1200. (c) Becke, A. D. *J. Chem. Phys.* **1993**, *98*, 5648. (d) Stephens, P. J. D.; Chabalowski, C. F.; Frisch, M. J. *J. Phys. Chem.* **1994**, *98*, 11623.

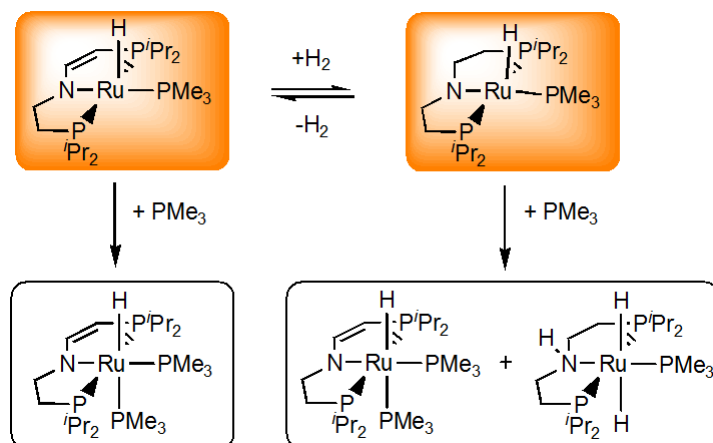
²⁵ Hay, P. J.; Wadt, W. R. *J. Chem. Phys.* **1985**, *82*, 299.

²⁶ Hehre, W. J.; Ditchfield, R.; Pople, J. A. *J. Chem. Phys.* **1972**, *56*, 2257.

1.5 Ruthenium Complexes with Cooperative PNP-Pincer Amine, Amido, Imine, and Enamido Ligands: Facile Ligand Backbone Functionalization Processes

This chapter originated the following publication:

A. Friedrich, M. Drees, M. Käß, E. Herdtweck, S. Schneider,
Inorg. Chem. **2010**, *49*, 5482.



1.5.1 Abstract

The quantitative formation of enamido complex $[\text{Ru}(\text{H})\text{PMe}_3(\text{PNP}')] (\mathbf{3}; \text{PNP}' = \text{N}(\text{CHCHP}^i\text{Pr}_2)(\text{CH}_2\text{CH}_2\text{P}^i\text{Pr}_2))$ from the reaction of $[\text{RuCl}_2\text{PMe}_3(\text{HPNP})] (\mathbf{5}; \text{HPNP} = \text{HN}(\text{CH}_2\text{CH}_2\text{P}^i\text{Pr}_2)_2)$ with an excess of base ($\text{KO}t\text{Bu}$) can be explained by β -hydride migration from an intermediate amido complex $[\text{RuClPMe}_3(\text{PNP})] (\mathbf{6}; \text{PNP} = \text{N}(\text{CH}_2\text{CH}_2\text{P}^i\text{Pr}_2)_2)$. Resulting imine complex $[\text{RuCl}(\text{H})\text{PMe}_3(\text{PNP}^*)] (\mathbf{7}; \text{PNP}^* = \text{N}(\text{CHCH}_2\text{P}^i\text{Pr}_2)(\text{CH}_2\text{CH}_2\text{P}^i\text{Pr}_2))$ could be independently synthesized and gives $\mathbf{3}$ with $\text{KO}t\text{Bu}$. A computational examination of the reversible double H_2 addition and elimination equilibria of enamide $\mathbf{3}$, amido complex $[\text{Ru}(\text{H})\text{PMe}_3(\text{PNP})] (\mathbf{1})$ and amine complex $[\text{Ru}(\text{H})_2\text{PMe}_3(\text{HPNP})] (\mathbf{2})$ explains, why $[\text{Ru}(\text{H})_2\text{PMe}_3(\text{PNP}^*)] (\mathbf{8})$ is not observed experimentally. The distinctly different molecular and electronic structures of related complexes $\mathbf{1}$ and $\mathbf{3}$, which feature a Y-shaped distorted trigonal-bipyramid (Y-TBP) for amide $\mathbf{1}$, but T-shaped TBP for enamide $\mathbf{3}$, respectively, can be attributed to considerably reduced $\text{N} \rightarrow \text{M}$ π -donation for the PNP' ligand due to delocalization of the N -lone pair into the unsaturated pincer backbone. The resulting low-lying LUMO of $\mathbf{3}$ explains its Lewis-acidic behaviour, as documented by the formation of octahedral complex $[\text{RuH}(\text{PMe}_3)_2(\text{PNP}')] (\mathbf{14})$ upon addition of PMe_3 . In comparison, the reaction of $\mathbf{1}$ with PMe_3 gives a mixture of $\mathbf{2}$ and $\mathbf{14}$ via a base assisted hydrogen elimination pathway. On the other hand, with electrophiles, such as MeOTf , predominant N -methylation is observed for both $\mathbf{1}$ and $\mathbf{3}$ producing $[\text{RuH}(\text{OTf})\text{PMe}_3(\text{MePNP})] (\mathbf{11})$ and $[\text{RuH}(\text{OTf})\text{PMe}_3(\text{MePNP}')] (\mathbf{12})$, respectively. This reactivity of $\mathbf{3}$ contrasts with pyridine-based cooperative pincer analogues, and can be attributed to the high flexibility of the aliphatic PNP' pincer ligand. The structural and reactivity patterns place this novel ligand between the parent PNP and aromatic pincer ligands.

1.5.2 Introduction

Terminal π -donating ligands, such as amides, were for a long time considered unsuitable for late transition metals owing to the *hard* ligand and *soft* metal mismatch. In fact, the high electron count of metal centers with $d^n \geq d^6$ results in distinctly different properties as compared with electron poor metal amido complexes,^[1] and repulsive filled-filled π -interactions of the nitrogen free electron pair with metal d -electrons strongly determine the reactivity of this compound class.^[2,3] Owing to the pronounced ligand nitrogen centered reactivity, such as the high basicity and nucleophilicity,^[4] late transition metal amido complexes are ideal compounds to examine metal-ligand cooperativity. Cooperating ligands are directly involved in reversible chemical transformations of metal complexes. This concept has recently attracted considerable interest to accelerate absolute and relative rates of bond activation reactions aimed at improving activity and selectivity in catalysis.^[5] As a prominent example, Noyori and Ohkuma introduced ruthenium amido catalysts for the hydrogenation and transfer hydrogenation of carbonyl groups, for which a bifunctional mechanism has been

¹ (a) Bryndza, H. E.; Tam, W. *Chem. Rev.* **1988**, *88*, 1163-1188. (b) Fryzuk, M. D.; Montgomery, C. D. *Coord. Chem. Rev.* **1989**, *95*, 1-40. (c) Roundhill, D. M. *Chem. Rev.* **1992**, *92*, 1-27. (d) Fulton, J. R.; Holland, A. W.; Fox, D. J.; Bergman, R. G. *Acc. Chem. Res.* **2002**, *35*, 44-56. (e) Gunnoe, T. B. *Eur. J. Inorg. Chem.* **2007**, 1185-1203.

² Caulton, K. G. *New J. Chem.* **1994**, *18*, 25-41.

³ Alternatively, the nitrogen centered nucleophilicity has been attributed to the high M-N σ -bond polarity: Holland, P. L.; Andersen, R. A.; Bergman, R. G. *Comments Inorg. Chem.* **1999**, *21*, 115-129.

⁴ (a) Park, S.; Rheingold, A. L.; Roundhill, D. M. *Organometallics* **1991**, *10*, 615-623. (b) Fulton, J. R.; Bouwkamp, M. W.; Bergman, R. G. *J. Am. Chem. Soc.* **2000**, *122*, 8799-8800. (c) Büttner, T.; Breher, F.; Grützmacher, H. *Chem. Commun.* **2004**, 2820-2821. (d) Maire, P.; Breher, F.; Schönberg, H.; Grützmacher, H. *Organometallics* **2005**, *24*, 3207-3218. (e) Büttner, T.; Geier, J.; Frison, G.; Harmer, J.; Calle, C.; Schweiger, A.; Schönberg, H.; Grützmacher, H. *Science* **2005**, *307*, 235-238. (f) Marziale, A. N.; Herdtweck, E.; Eppinger, J.; Schneider, S. *Inorg. Chem.* **2009**, *48*, 3699-3709. (g) Askevold, B.; Friedrich, A.; Buchner, M. R.; Marziale, A. N.; Herdtweck, E.; Schneider, S. manuscript in preparation.

⁵ Some recent reviews: (a) Rowlands, G. J. *Tetrahedron* **2001**, *57*, 1865-1882. (b) Grützmacher, H. *Angew. Chem.* **2008**, *120*, 1838-1842; *Angew. Chem. Int. Ed.* **2008**, *47*, 1814-1818. (c) Grotjahn, D. B. *Dalton Trans.* **2008**, 6497-6508. (d) Park, Y. J.; Park, J.-W.; Jun, C.-H. *Acc. Chem. Res.* **2008**, *41*, 222-234. (e) van der Vlugt, J. I.; Reek, J. N. H. *Angew. Chem.* **2009**, *121*, 8990-9004; *Angew. Chem. Int. Ed.* **2009**, *48*, 8832-8846.

proposed with concerted transfer of a nitrogen bound proton and a hydride to the substrate.^[6] Subsequent H₂ activation is accomplished by direct or acid catalyzed proton transfer from a dihydrogen ligand to the amido moiety.^[7] More recently, bifunctional ruthenium amido catalysts were also successfully applied in the reverse reaction: the acceptorless dehydrogenation of organic and inorganic substrates, such as alcohols, formic acid, or borane amines.^[8,9,10] These reactions are of great interest for applications both in synthesis and hydrogen storage.^[11]

As a fundamental reactivity of late transition metal amido complexes, such compounds bearing β -hydrogen atoms typically suffer from low thermodynamic stability, owing to decomposition towards metal hydrides by imine extrusion.^[1a,b,12] Accordingly, ruthenium imine complexes have been identified as deactivation products from Noyori-type

⁶ (a) Noyori, R.; Ohkuma, T. *Angew. Chem.* **2001**, *113*, 40-75; *Angew. Chem. Int. Ed.* **2001**, *40*, 40-73. (b) Clapham, S. E.; Hadzovic, A.; Morris, R. H. *Coord. Chem. Rev.* **2004**, *248*, 2201-2237. (c) Muñiz, K. *Angew. Chem.* **2005**, *117*, 6780-6785; *Angew. Chem. Int. Ed.* **2005**, *44*, 6622-6627. (d) Samec, J. S. M.; Bäckvall, J.-E.; Andersson, P. G.; Brandt, P. *Chem. Soc. Rev.* **2006**, *35*, 237-248.

⁷ (a) Abdur-Rashid, K.; Clapham, S. E.; Hadzovic, A.; Harvey, J. N.; Lough, A. J.; Morris, R. H. *J. Am. Chem. Soc.* **2002**, *124*, 15104-15118. (b) Sandoval, C. A.; Ohkuma, T.; Muñiz, K.; Noyori, R. *J. Am. Chem. Soc.* **2003**, *125*, 13490-13503. (c) Friedrich, A.; Drees, M.; Schmedt auf der Günne, J.; Schneider, S. *J. Am. Chem. Soc.* **2009**, *131*, 17552-17553.

⁸ Zhao, J.; Hartwig, J. F. *Organometallics* **2005**, *24*, 2441-2446.

⁹ Morris, D. J.; Clarkson, G. J.; Wills, M. *Organometallics* **2009**, *28*, 4133-4140.

¹⁰ (a) Blaquiere, N.; Diallo-Garcia, S.; Gorelsky, S. I.; Black, D. A.; Fagnou, K. *J. Am. Chem. Soc.* **2008**, *130*, 14034-14035. (b) Käß, M.; Friedrich, A.; Drees, M.; Schneider, S. *Angew. Chem.* **2009**, *121*, 922-924; *Angew. Chem. Int. Ed.* **2009**, *48*, 905-907. (c) Friedrich, A.; Drees, M.; Schneider, S. *Chem. Eur. J.* **2009**, *15*, 10339-10342.

¹¹ (a) Hamid, M. H. S. A.; Slatford, P. A.; Williams, J. M. J. *Adv. Synth. Catal.* **2007**, *349*, 1555-1575. (b) Boddien, A.; Loges, B.; Junge, H.; Beller, M. *ChemSusChem* **2008**, *1*, 751-758. (c) Bower, J. F.; Kim, I. S.; Patman, R. L.; Krische, M. J. *Angew. Chem.* **2009**, *121*, 36-48; *Angew. Chem. Int. Ed.* **2009**, *48*, 34-46. (d) Friedrich, A.; Schneider, S. *ChemCatChem* **2009**, *1*, 72-73. (e) Johnson, T. C.; Morris, D. J.; Wills, M. *Chem. Soc. Rev.* **2010**, *39*, 81-88.

¹² (a) Diamond, S. E.; Mares, F. *J. Organomet. Chem.* **1977**, *142*, C55-C57. (b) Hartwig, J. F. *J. Am. Chem. Soc.* **1996**, *118*, 7010-7011. (c) Hartwig, J. F.; Richards, S.; Barañano, D.; Paul, F. *J. Am. Chem. Soc.* **1996**, *118*, 3626-3633. (d) Wagaw, S.; Rennels, R. A.; Buchwald, S. L. *J. Am. Chem. Soc.* **1997**, *119*, 8451-8458.

hydrogenation catalysts.^[13] Furthermore, the reverse reaction, i.e., hydride migration to a metal bound imine, defines an important elementary step in catalytic imine hydrogenation.^[6b] However, despite of the high relevance of frequently observed β -hydride elimination in late transition metal amido chemistry only few mechanistic studies have been published, contrasting sharply with β -H elimination in alkyl complexes.^[14,15]

We have recently presented the use of amido complex [Ru(H)PMe₃(PNP)] (**1**; PNP = N(CH₂CH₂PⁱPr₂)₂) as highly efficient catalyst for borane-amine dehydrogenation.^[10b,c] Furthermore, iridium and ruthenium complexes with amine ligand HPNP (HN(CH₂CH₂PⁱPr₂)₂) are highly active catalysts for the hydrogenation and transfer hydrogenation of R₂C=E (E = O, NR) double bonds.^[16] Complex **1** can be synthesized from amine complex [Ru(H)₂PMe₃(HPNP)] (**2**) upon H₂ elimination,^[10b,7c] and **2** results from the reaction of enamide [Ru(H)PMe₃(PNP')] (**3**; PNP' = N(CHCHPⁱPr₂)(CH₂CH₂PⁱPr₂)) with excess H₂. Furthermore, it was shown for the double hydrogen addition and elimination equilibria of **1**, **2**, and **3** to be reversible (Scheme 1), demonstrating the two-fold cooperativity of the pincer ligand. While the oxidation of amine ligands with hydrogen acceptors (e.g. O₂) or electrochemical oxidation of amines are well studied, acceptorless dehydrogenation

¹³ Abbel, R.; Abdur-Rashid, K.; Faatz, M.; Hadzovic, A.; Lough, A. J.; Morris, R. H. *J. Am. Chem. Soc.* **2005**, *127*, 1870-1882.

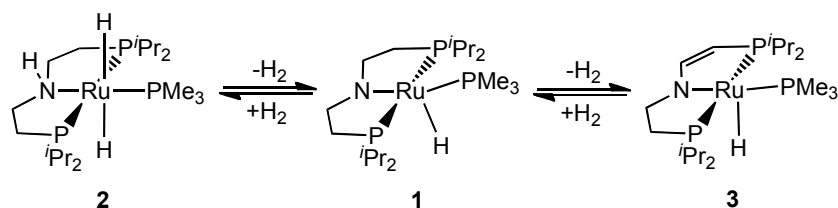
¹⁴ (a) Mayer, J. M.; Curtis, C. J.; Bercaw, J. E. *J. Am. Chem. Soc.* **1983**, *105*, 2651-2660. (b) Hartwig, J. F. *J. Am. Chem. Soc.* **1996**, *118*, 7010-7011. (c) Tsai, Y.-C.; Johnson, M. J. A.; Mindiola, D. J.; Cummins, C. C. *J. Am. Chem. Soc.* **1999**, *121*, 10426-10427. (d) Zhao, J.; Hesslink, H.; Hartwig, J. F. *J. Am. Chem. Soc.* **2001**, *123*, 7220-7227. (e) Zhao, P.; Hartwig, J. F. *J. Am. Chem. Soc.* **2005**, *127*, 12066-12073. (f) Matas, I.; Campora, J.; Palma, P.; Alvarez, E. *Organometallics* **2009**, *28*, 6515-6523.

¹⁵ (a) Collman, J. P.; Hegedus, L. S.; Norton, J. R.; Finke, R. G. In *Principles and Applications of Organotransition Metal Chemistry*, University Science Books, Sausalito, CA, **1987**. (b) Crabtree, R. H. In *The Organometallic Chemistry of the Transition Metals*, 3rd ed., Wiley-Interscience, New York, NY, **2001**. (c) Niu, S.; Hall, M. B. *Chem. Rev.* **2000**, *100*, 353-405.

¹⁶ (a) Clarke, Z. E.; Maragh, P. T.; Dasgupta, T. P.; Gusev, D. G.; Lough, A. J.; Abdur-Rashid, K. *Organometallics* **2006**, *25*, 4113-4117. (b) Amoroso, D.; Graham, T. W.; Guo, R.; Tsang, C.-W.; Abdur-Rashid, K. *Aldrichim Acta* **2008**, *41*, 15-26. (c) Chen, X.; Jia, W.; Guo, R.; Graham, T. W.; Gullons, M. A.; Abdur-Rashid, K. *Dalton Trans.* **2009**, 1407-1410.

B Results and Discussion

remains scarcely investigated.^[17] Therefore, we were interested in elucidating the mechanism for formation of **3**.



Scheme 1. H₂ elimination/addition reactions of amine, amido, and enamido complexes **2**, **1**, and **3**.

In this paper, we report a combined experimental and computational study to clarify the C-H activation processes in the PNP pincer backbone. These results can serve as a model for imine hydrogenation and, more specifically, comprise valuable information for the design of future cooperative ligands in catalysis. We will first present a plausible mechanism for the pincer backbone C-H activation processes. Since the new enamido type PNP' ligand of **3** is on first sight similar to the parent PNP amido ligand, further emphasis will be put into the examination of the PNP- and PNP'- *d*⁶ ruthenium complex electronic structures (Figure 1). This comparison reveals that the reactivity, particularly with nucleophiles, can be controlled by ligand backbone de/hydrogenation as a consequence of tunable π -donation of the cooperating ligand.

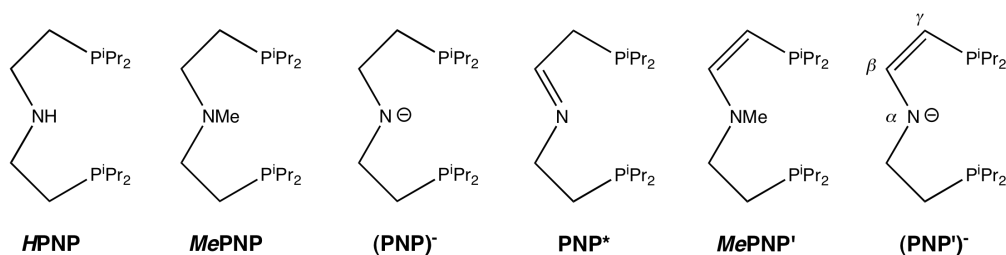


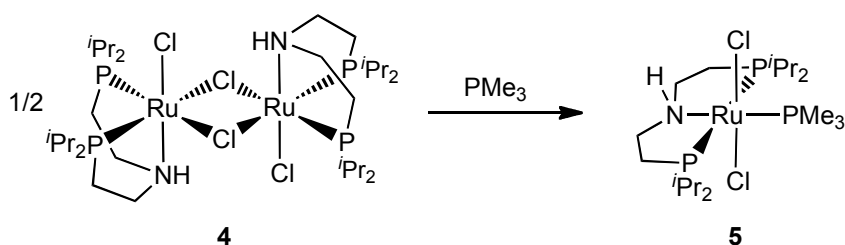
Figure 1. Nomenclature for the PNP pincer ligands used throughout this paper.

¹⁷ Keene, R. F. *Coord. Chem. Rev.* **1999**, *187*, 121-149.

1.5.3 Results and discussion

Metal-ligand cooperativity: Formation of PNP enamido complex

Starting from commercially available [(Cymene)RuCl₂]₂, precursor complex [RuCl₂PMe₃(HPNP)] (**5**) is easily prepared in almost quantitative yield by ligand substitution and subsequent reaction of chloro-bridged dimer [RuCl₂(HPNP)]₂ (**4**) with PMe₃ (Scheme 2), as reported earlier.^[10b] The molecular structures of **4** and **5** in the solid state could be derived by single-crystal X-ray diffraction (Figures 2 and 3, Table 1), confirming the structural assignments on the basis of solution NMR spectroscopy.^[18] A comparison of the molecular structures demonstrates the capability of the *iso*-propyl substituted HPNP ligand to bind both facially and meridionally to the metal. Facial coordination as in **4** permits dimerization via chloro bridges to allow for coordinative saturation of the ruthenium(II) center. The close proximity of N1 and the terminal chloride Cl1 suggests further stabilization by N...H...Cl hydrogen bonding. The structural parameters of **4** in the crystal strongly resemble those of [RuCl₂{HN(CH₂CH₂PPh₂)₂}].^[19] The molecular structure of **5** features octahedrally coordinated ruthenium and a *trans*-dichloride configuration with small distortions mainly caused by the pincer bite angle (P1-Ru-P2 163.04(3)°), which is in the typical range for the meridionally bound HPNP ligand.^[4f,20]



Scheme 2. Synthesis of complex **5**.

¹⁸ The molecular structure of **4** has recently been depicted in a patent without structural details reported: Abdur-Rashid, K.; Graham, T.; Tsang, C.-W.; Chen, X.; Guo, R.; Jia, W.; Amoroso, D.; Sui-Seng, C. WO2008/141439.

¹⁹ Walther, D.; Klobes, O.; Stollenz, M.; Imhof, W.; Gørls, H. Private communication to the Cambridge Structural Database, **2003**.

²⁰ (a) Friedrich, A.; Ghosh, R.; Kolb, R.; Herdtweck, E.; Schneider, S. *Organometallics* **2009**, *28*, 708-718. (b) Meiners, J.; Friedrich, A.; Herdtweck, E.; Schneider, S. *Organometallics* **2009**, *28*, 6331-6338.

We previously reported that the reaction of **5** with KO^tBu (> 3 equiv.) gives enamide **3** in quantitative yield (Scheme 3). The reaction is rapid with an immediate color change to the deep green product observed at room temperature. No intermediates are detected by ³¹P NMR, and only incomplete conversion is obtained with smaller amounts of base. As a likely pathway for the formation of **3**, initial dehydrohalogenation of **5** to chloroamide complex [RuClPMe₃(PNP)] (**6**) is followed by β-hydride migration to give imine complex [RuCl(H)PMe₃(PNP*)] (**7**; PNP* = N(CHCH₂PⁱPr₂)(CH₂CH₂PⁱPr₂)). Deprotonation of **7** at the expectedly acidic γ-carbon atom (Figure 1) would then result in **3**. To check for this pathway, imine intermediate **7** was synthesized by HCl addition to **3** in isolated yields around 50 %. Complex **7** is quantitatively deprotonated by KO^tBu to give enamido complex **3**, supporting our proposed mechanism. Finally, reactions of **7** with 1 equiv HCl or **3** with excess HCl give **5** selectively. ³¹P, ¹H, and ¹³C NMR spectra of **7** confirm the C₁ symmetry and meridional arrangement of the PNP* pincer ligand. The two chelate ³¹P NMR signals exhibit a typical *trans* ²J_{PP} coupling constant (281 Hz), and the mutual *trans*-configuration of the hydrido and the chloro ligands was confirmed by ¹H NOESY NMR. This structural assignment of **7** is further supported by X-ray diffraction. However, the crystal was disordered with respect to the position of the N=C double bond in the pincer backbone, preventing a detailed structural discussion (chapter B1.5.7).

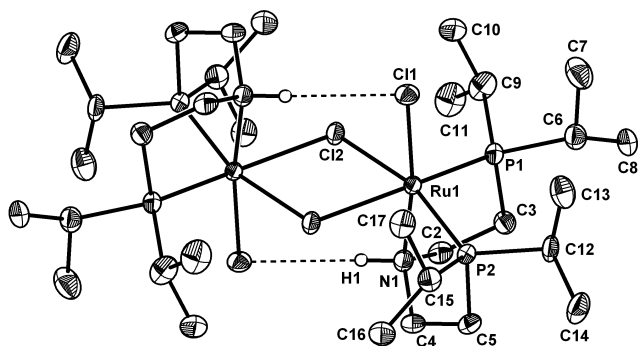


Figure 2. DIAMOND plot of **4** in the crystal with thermal ellipsoids drawn at the 50% probability level. Hydrogen atoms other than H1 are omitted for clarity.

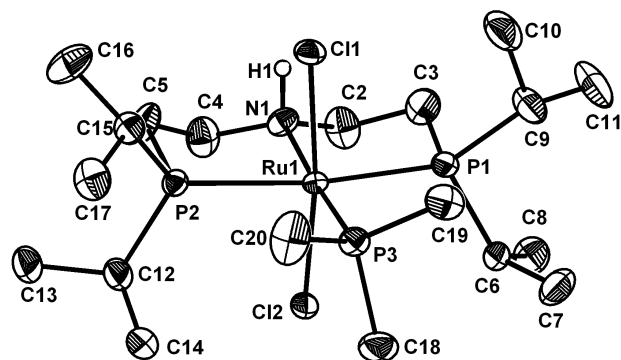


Figure 3. DIAMOND plot of **5** in the crystal with thermal ellipsoids drawn at the 50 % probability level. Hydrogen atoms other than H1 are omitted for clarity.

Table 1. Selected bond lengths and bond angles of **4** and **5** in the crystal.

	4	5
Bond Lengths (Å)		
Ru1–Cl1	2.442(1)	2.4312(7)
Ru1–Cl2	2.472(1)	2.4309(6)
Ru1–Cl2 ⁱ	2.478(1)	–
Ru1–N1	2.113(4)	2.186(2)
Ru1–P1	2.261(1)	2.3897(8)
Ru1–P2	2.274(1)	2.3838(8)
Ru1–P3	–	2.2627(8)
Bond Angles (°)		
N1–Ru1–P3	–	177.13(6)
P1–Ru1–P2	98.05(5)	163.04(3)

ⁱ symmetry operation for equivalent atoms (-x, -y, -z)

Milstein and co-workers have shown that PNP pincer complexes of the type $[\text{RuH}(\text{CO})\text{Cl}\{\text{NC}_5\text{H}_3\text{-2-CH}_2\text{PR}_2\text{-6-CH}_2\text{ER}'_2\}]$ ($\text{R} = \textit{i}\text{Pr}, \textit{t}\text{Bu}; \text{ER}'_2 = \text{NEt}_2, \text{P}^i\text{Pr}_2$) can be deprotonated at the pincer backbone in benzylic position to give $[\text{RuH}(\text{CO})\{\text{NC}_5\text{H}_3\text{-2-CHPR}_2\text{-6-CH}_2\text{ER}'_2\}]$,^[21] which is a highly active catalyst for carbonyl group hydrogenation, acceptorless alcohol dehydrocoupling, and water oxidation.^[21,22] For these reactions, mechanisms have been proposed, where reversible proton transfer at the pincer backbone is a decisive step in the catalytic cycles. Furthermore, ligand cooperativity was demonstrated for both H_2 and benzene addition to $[\text{Ir}(\text{COE})\{\text{NC}_5\text{H}_3\text{-2-CH}_2\text{P}^i\text{Pr}_2\text{-6-CHP}^i\text{Pr}_2\}]$, where proton shifts to the deprotonated benzylic position of the pincer ligand was observed upon H–H and C–H bond activation.^[23] Benzylic deprotonation of such pyridine based PNP pincer complexes was further reported for nickel, platinum, and copper complexes.^[24] Similarly, the facile double deprotonation of iridium bis(picoyl)amine complex $[\text{Ir}\{\text{HN}(\text{CH}_2\text{Py})_2\}(\text{cod})]^+$ (cod = cyclooctadiene) in benzylic position to give $[\text{Ir}\{\text{N}(\text{CHPy})(\text{CH}_2\text{Py})(\text{cod})\}]$ is stabilized by delocalization of the negative charge with the pyridyl substituent.^[25] In this context, complex **3** represents an aliphatic analogue, suggesting that the aromaticity as in pyridine based pincer ligands does not define a general prerequisite for such proton shift reactions.

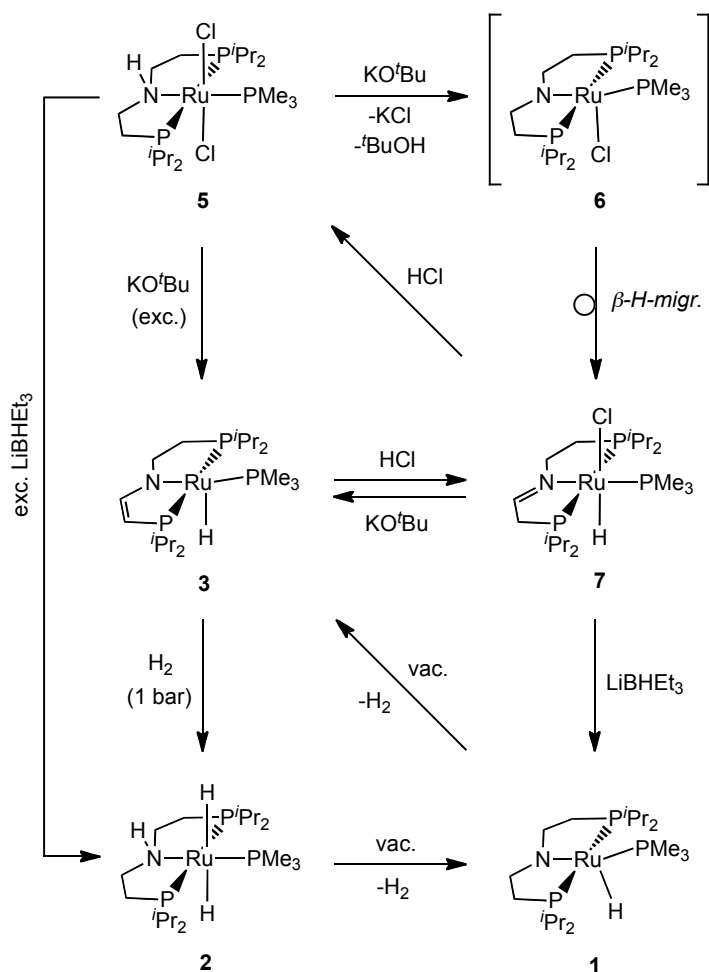
²¹ (a) Zhang, J.; Leitus, G.; Ben-David, Y.; Milstein, D. *J. Am. Chem. Soc.* **2005**, *127*, 10840-10841. (b) Zhang, J.; Leitus, G.; Ben-David, Y.; Milstein, D. *Angew. Chem.* **2006**, *118*, 1131-1133; *Angew. Chem. Int. Ed.* **2006**, *45*, 1113-1115.

²² (a) Gunanathan, C.; Ben-David, Y.; Milstein, D. *Science* **2007**, *317*, 790-792. (b) Kohl, S. W.; Weiner, L.; Schwartsburd, L.; Konstantinovski, L.; Shimon, L. J. W.; Ben-David, Y.; Iron, M. A.; Milstein, D. *Science* **2009**, *324*, 74-77.

²³ (a) Ben-Ari, E.; Leitus, G.; Shimon, L. J. W.; Milstein, D. *J. Am. Chem. Soc.* **2006**, *128*, 15390-15391. (b) Iron, M. A.; Ben-Ari, E.; Cohen, R.; Milstein, D. *Dalton Trans.* **2009**, 9433-9439. (c) Zeng, G.; Guo, Y.; Li, S. *Inorg. Chem.* **2009**, *48*, 10257-10263.

²⁴ (a) Vuzman, D.; Poverenov, E.; Shimon, L. J. W.; Diskin-Posner, Y.; Milstein, D. *Organometallics* **2008**, *27*, 2627-2634. (b) van der Vlugt, J. I.; Lutz, M.; Pidko, E. A.; Vogt, D.; Spek, A. L. *Dalton Trans.* **2009**, 1016-1023. (c) van der Vlugt, J. I.; Pidko, E. A.; Vogt, D.; Lutz, M.; Spek, A. L. *Inorg. Chem.* **2009**, *48*, 7513-7515.

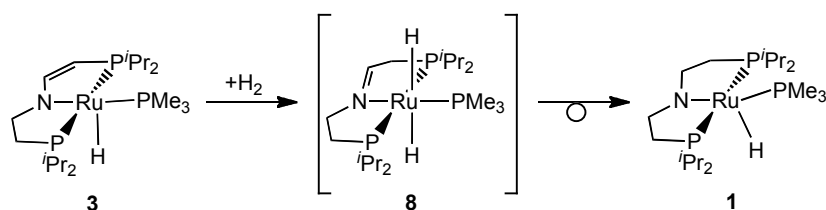
²⁵ (a) Tejel, C.; Ciriano, M. A.; del Río, M. P.; Hettterscheid, D. G. H.; Tschlis i Spithas, N.; Smits, J. M. M.; de Bruin, B. *Chem. Eur. J.* **2008**, *14*, 10932-10936. (b) Tejel, C.; del Río, M. P.; Ciriano, M. A.; Reijerse, E. J.; Hartl, F.; Zálíš, S.; Hettterscheid, D. G. H.; Tschlis i Spithas, N.; de Bruin, B. *Chem. Eur. J.* **2009**, *15*, 11878-11889.



Scheme 3. Syntheses of PNP enamido (**3**), amido (**1**), amine (**2**), and imine (**7**) complexes.

Metal-ligand cooperativity: Reversible double H₂ elimination/addition

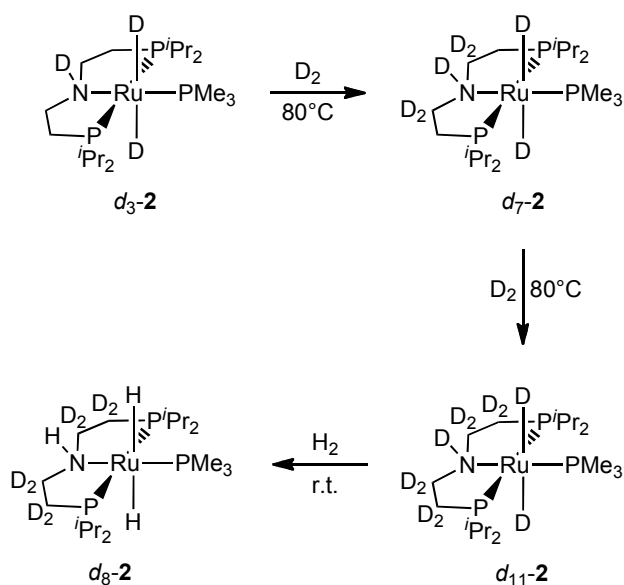
As a major difference with Milstein's pyridine based system, **1**, **2**, and **3** formally exhibit two functional groups in the pincer backbone (the amine group and the ethylene bridge), which are capable of promoting bifunctional heterolytic hydrogen activation, allowing for the reversible addition of 2 equiv of H₂ to **3** (Scheme 1). For the conversion of **3** to **1**, dihydrido imine complex [Ru(H)₂PMe₃(PNP*)] (**8**) seems to be a likely intermediate after proton transfer from H₂ initially binding at the free coordination site of **3** to the γ-carbon atom (Scheme 4). However, we could not find spectroscopic evidence for this compound. Furthermore, the reaction of **7** with Li[BHET₃] gives amido complex **1** in high yield (Scheme 3), suggesting that **8** might be unstable with respect to the formation of amido isomer **1**.



Scheme 4. Possible intermediate **8** for hydrogenation of **3** to **1**.

The hydrogen elimination/addition equilibria (Scheme 1) were examined by H/D exchange experiments. Selectively deuterated $[\text{Ru}(\text{D})_2\text{PMe}_3\{\text{DN}(\text{CH}_2\text{CH}_2\text{P}^i\text{Pr}_2)_2\}]$ ($d_3\text{-2}$) can be prepared by reaction of **1** with D_2 at room temperature. Under these reaction conditions, no incorporation of deuterium into the pincer backbone is observed within 18 hours. Upon heating of $d_3\text{-2}$ to 80°C under D_2 , slow H/D exchange of the PNP pincer backbone protons vs deuterium is observed with slightly different rates for the NCH_2 ($k = 0.51 \text{ h}^{-1}$; 80°C) and PCH_2 ($k = 0.03 \text{ h}^{-1}$; 80°C) groups, respectively (Scheme 5 and Figure 4). Finally, exposure of the fully backbone deuterated isotopomer $[\text{Ru}(\text{D})_2\text{PMe}_3\{\text{DN}(\text{CD}_2\text{CD}_2\text{P}^i\text{Pr}_2)_2\}]$ ($d_{11}\text{-2}$) to H_2 at room temperature results in rapid D/H exchange of the Ru–D and N–D protons ($t_{1/2} < 5 \text{ min}$; r.t.), giving $[\text{Ru}(\text{H})_2\text{PMe}_3\{\text{HN}(\text{CD}_2\text{CD}_2\text{P}^i\text{Pr}_2)_2\}]$ ($d_8\text{-2}$). Interestingly, both hydride ligands exhibit the same rates of exchange, which cannot be simply explained by reversible Ru–H/N–H syn H_2 elimination/addition. Therefore, a 2D ^1H NOESY spectrum of **2** in $d_8\text{-THF}$ under H_2 (1 bar) was obtained (chapter B1.5.6). The spectrum features exchange cross peaks of the two hydride ligands with each other and of the hydride, which is adjacent to the PNP N–H proton, with H_2 . This result is in agreement with Ru–H/N–H syn H_2 elimination/addition and scrambling of the two hydride ligands, e.g. via amine inversion.^[26] On the contrary, Ru–H/ H_2 exchange upon phosphine dissociation should not be stereoselective and give exchange cross peaks of H_2 with *both* hydride ligands.

²⁶ In the presence of water, we proposed for O–H/N–H proton exchange of **2** to account for amine inversion. However, sharp ^1H NMR signals for the Ru–H protons during reaction monitoring suggest the absence of water in the sample (reference 7c).



Scheme 5. H/D exchange experiments.

Precise evaluation of the H/D exchange kinetic data is hampered by superimposition of pincer backbone ^1H signals with other peaks (Figure 4). However, comparison of the relative rates for Ru–H and N–H vs pincer backbone C–H H/D exchange provides valuable information: H/D exchange for the pincer backbone protons exhibits sizable activation energies, with a slightly higher barrier for the PCH₂ as compared to the NCH₂ group. Most importantly, no stereoselectivity for the diastereotopic NCH₂ and PCH₂ protons of **2** is found, respectively, indicating that the exchange proceeds via a C_{2v} symmetric intermediate, such as imine complex **8**.^[27] Furthermore, these barriers are considerably higher as compared with exchange of the Ru–H and N–H moieties.

²⁷ Owing to the considerably different rates for Ru–H, NCH₂, and PCH₂ H/D exchange, respectively, secondary isotope effects can be neglected.

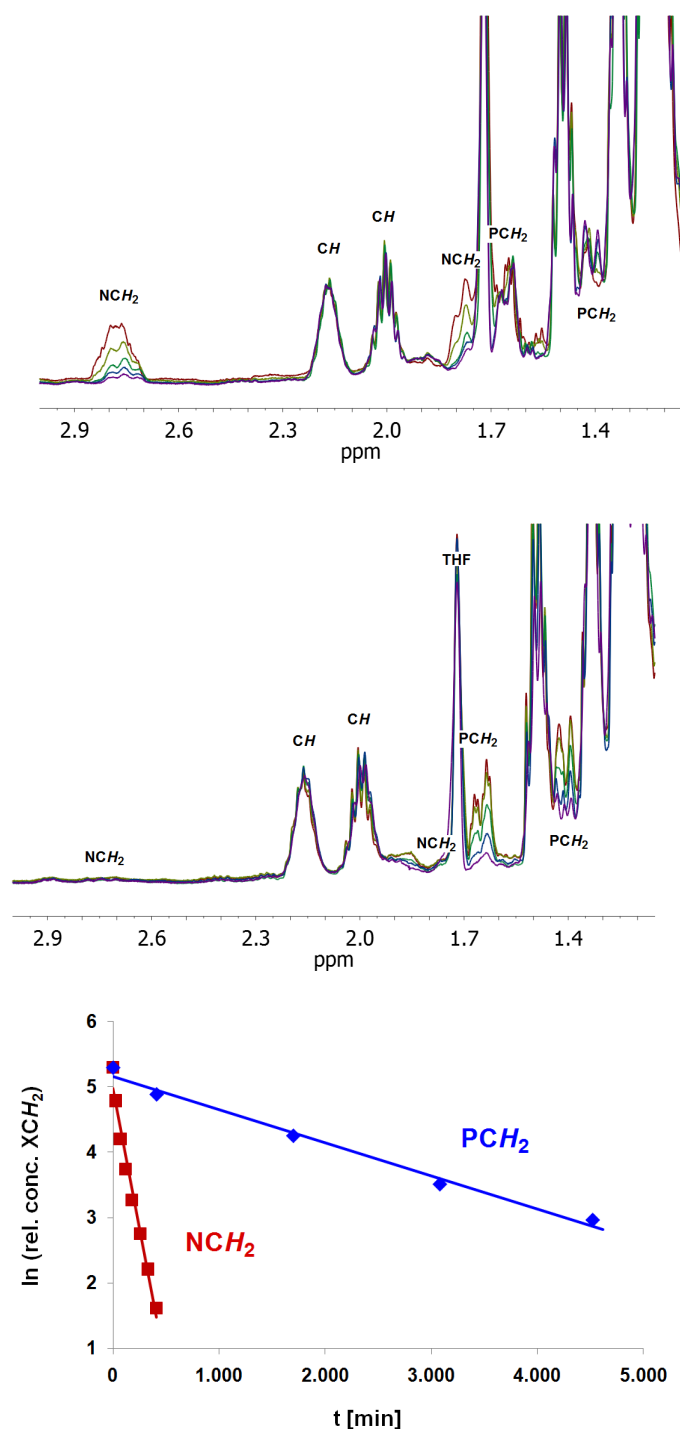


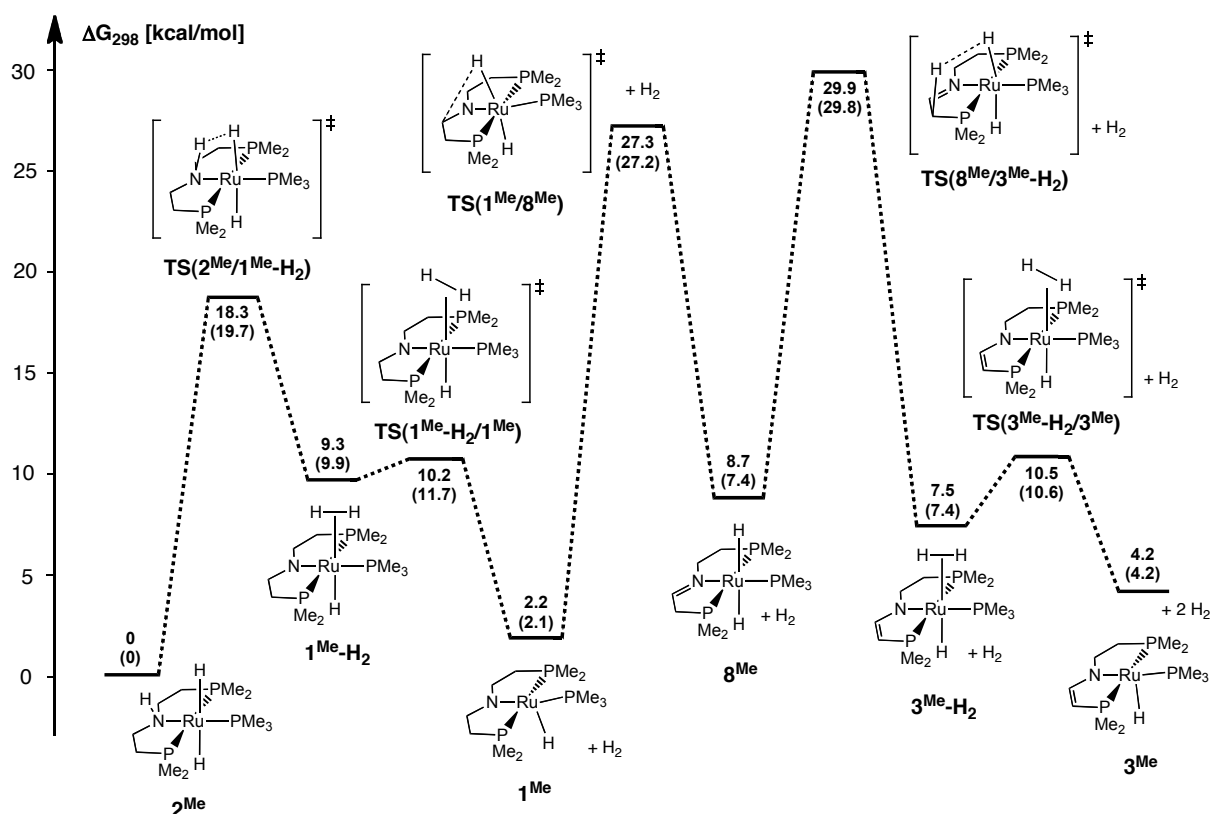
Figure 4. Top: Progress of NCH_2 H/D exchange of $d_3\text{-2}$ monitored by ^1H NMR in $d_8\text{-THF}$ (1 bar D_2 , 80 °C) after 0 min (red), 30 min (light green), 70 min (green), 120 min (blue), and 180 min (purple). **Center:** Progress of PCH_2 H/D exchange of $d_7\text{-2}$ monitored by ^1H NMR in $d_8\text{-THF}$ (1 bar D_2 , 80 °C) after 410 min (red), 660 min (light green), 1700 min (green), 3080 min (blue), and 4520 min (purple). **Bottom:** First order kinetic plots for NCH_2 (2.8 ppm) and PCH_2 (1.65 ppm) ^1H NMR peak integrals.

To gain further insight into the interconversion of **1**, **2**, and **3** and the possible involvement of **8**, DFT calculations (B3LYP/6-31+G**) on a somewhat simpler model with PMe₂ instead of PⁱPr₂ substituents on the pincer ligand were carried out. The barriers for the elementary steps of the sequence $2^{\text{Me}} \rightleftharpoons \text{TS}(2^{\text{Me}}/1^{\text{Me}}\text{-H}_2) \rightleftharpoons 1^{\text{Me}}\text{-H}_2 \rightleftharpoons \text{TS}(1^{\text{Me}}\text{-H}_2/1^{\text{Me}}) \rightleftharpoons 1^{\text{Me}} \rightleftharpoons \text{TS}(1^{\text{Me}}/8^{\text{Me}}) \rightleftharpoons 8^{\text{Me}} \rightleftharpoons \text{TS}(8^{\text{Me}}/3^{\text{Me}}\text{-H}_2) \rightleftharpoons 3^{\text{Me}}\text{-H}_2 \rightleftharpoons \text{TS}(3^{\text{Me}}\text{-H}_2/3^{\text{Me}}) \rightleftharpoons 3^{\text{Me}}$ are displayed in Scheme 6. Gusev and co-workers recently examined hydrogen shift reactions in the backbone of related PCP ruthenium pincer complexes.^[28] The proposed mechanism was composed of a sequence of α - and β -H migration reactions, interconverting ruthenium(II) olefin hydrido, carbene hydrido, and alkyl isomers. Most interestingly, the authors showed that the four-coordinate 14-electron alkyl intermediates exhibit an energetically low lying triplet ground state resulting in very low barriers of isomerisation.^[29] However, in contrast to that system in the present case all intermediates are formally 18- or 16-electron complexes, respectively. Accordingly, single-point calculations for all ground state geometries in the triplet state resulted in higher energies by 44-74 kcal/mol (chapter B1.5.8).^[30] Therefore, it is reasonable to assume for all reactions to be located on a singlet potential energy surface (PES).

²⁸ Kuznetsov, V. F.; Abdur-Rashid, K.; Lough, A. J.; Gusev, D. G. *J. Am. Chem. Soc.* **2006**, *128*, 14388-14396.

²⁹ A rare example of a square-planar ruthenium(II) complex with a triplet ground state: Watson, L. A.; Ozerov, O. V.; Pink, M.; Caulton, K. G. *J. Am. Chem. Soc.* **2003**, *125*, 8426-8427.

³⁰ Even for four-coordinate, square-planar complex [RuCl{N(CH₂CH₂PⁱBu₂)₂}] a singlet ground state was found experimentally: Askevold, B.; Khusniyarov, M. M.; Herdtweck, E.; Meyer, K.; Schneider, S. *submitted*.



Scheme 6. DFT results for the mechanism of H₂ elimination (2 equiv.) from **2**^{Me} in the gas phase (energies for PCM solvent correction in parantheses).

Overall, elimination of two equivalents of H₂ from **2**^{Me} via **1**^{Me} to **3**^{Me} was calculated to be almost thermoneutral with $\Delta G_{2-1} = +2.2$ and $\Delta G_{1-3} = +2.0$ kcal/mol, respectively. Hydrogen elimination from amine **2**^{Me} to amide **1**^{Me} proceeds via proton transfer from the N-H moiety to a ruthenium bound hydride with a moderate barrier (18.3 kcal/mol) followed by almost barrierless H₂ loss of dihydrogen complex **1**^{Me}-H₂ (0.9 kcal/mol).^[10b] This result is in qualitative agreement with the H/D exchange experiments at room temperature. For the **1**^{Me} \rightleftharpoons **3**^{Me} branch of the H₂-elimination sequence, dihydrodo imine complex [Ru(H)₂PMe₃(PNP*)] (**8**^{Me}) was found to be a minimum on the PES but unstable with respect to both loss of dihydrogen towards enamide **3** ($\Delta G_{8-3} = -4.5$ kcal/mol) and isomerization to amide **1** ($\Delta G_{8-1} = -6.5$ kcal/mol). Hence, thermodynamics explain why **8** cannot not be detected as an intermediate experimentally. The sizable calculated barriers for **TS**(**8**^{Me}/**3**^{Me}-H₂) and **TS**(**1**^{Me}/**8**^{Me}) are in agreement with the slow H/D exchange found for the pincer backbone protons. Furthermore, the higher calculated barrier for **TS**(**8**^{Me}/**3**^{Me}-H₂) over **TS**(**1**^{Me}/**8**^{Me}) ($\Delta\Delta G^\ddagger = 2.6$ kcal/mol) provide an explanation for the higher experimental rate of NCH₂ over PCH₂ H/D exchange, since both hydride ligands of **2** undergo H/D exchange with higher rates

than backbone C-H activation. As for H₂-elimination from amido dihydrogen complex **1**^{Me}-H₂, elimination from enamido dihydrogen intermediate **3**^{Me}-H₂ proceeds with a very small barrier ($\Delta G_{\text{TS3-H}_2/3}^\ddagger = 3.0$ kcal/mol) to complete the sequence **2**^{Me} \rightleftharpoons **1**^{Me}-H₂ \rightleftharpoons **1**^{Me} + H₂ \rightleftharpoons **8**^{Me} + H₂ \rightleftharpoons **3**^{Me}-H₂ + H₂ \rightleftharpoons **3**^{Me} + 2 H₂. Our theoretical results demonstrate, that the pincer ligand N-H and C-H activation processes via proton shifts to hydride ligands and β -hydrogen migration are thermally accessible even without predissociation of one of the pincer ligand ‘arms’.

We have shown earlier, that Brønsted acids, such as water, can catalyze the formation of dihydrogen complex **1**^{Me}-H₂ by hydrogen bonding with the amine and the hydride ligands.^[7c] Likewise, Iron, Milstein, and co-workers recently reported theoretical results suggesting that water considerably lowers the barrier of oxidative proton transfer from a benzylic methylene group to the metal in a pyridine based PNP-iridium complex.^[23b] Therefore, acceleration of the right branch of the **2**^{Me} \rightleftharpoons **1**^{Me} \rightleftharpoons **3**^{Me} sequence by trace amounts of Brønsted acids, such as water, cannot be fully excluded. However, from the slow H₂ loss from **1** at room temperature reported earlier,^[10b] a first order half life of approx $t_{1/2} \approx 9$ d ($k \approx 0.0036$ h⁻¹) can be estimated. Hence, the corresponding barrier ($\Delta G^\ddagger \approx 28$ kcal/mol) is in good agreement with the calculated barriers for the model **TS(1**^{Me}/**8**^{Me}) and **TS(8**^{Me}/**3**^{Me}-H₂). Furthermore, the sharp ¹H NMR peaks observed for the hydride ligands during H/D exchange experiments indicate the absence of water.^[7c] Therefore, Brønsted acid catalysis was not examined theoretically for this step.

In contrast to dihydrido imine complex **8**, hydrido chloro imine **7** could be isolated and fully characterized. The preference for imine isomer **7** is accounted to the reduced hydridicity of the hydride ligand owing to the smaller *trans*-influence of the chloride ligand as compared to dihydride **8**. Ground-state destabilization of the imine hydride by a strong *trans*-ligand to the hydride might therefore be an important structural feature for Noyori-type hydrogenation catalysts to prevent rapid catalyst deactivation by imine formation.^[13]

Enamido (3) vs. amido (1) complex: Comparison of the Structures.

The facile synthesis of enamide **3** is particularly interesting since enamido ligand PNP' was unknown prior to this template synthesis.^[31] Therefore, a comparison of the molecular and electronic structures could provide valuable information to rationalize the reactivities (*vide infra*) of the related PNP amido and enamido complexes.

Despite the high relevance of five-coordinate 16-electron ruthenium(II) hydrido amido complexes like **1** in hydrogenation reactions with Noyori-Morris-type catalysts,^[31] only very few examples have been structurally characterized by X-ray diffraction.^[7a,32] Suitable single crystals of **1** were grown by slow cooling of a pentane solution to -40 °C (Fig. 5 and Table 2).

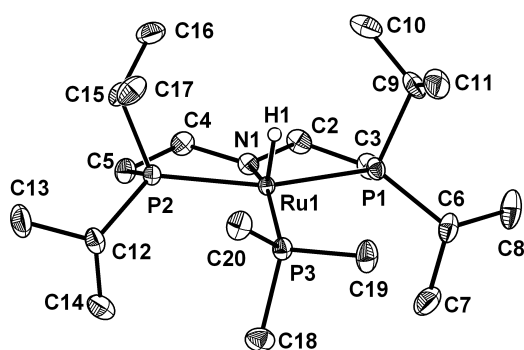


Figure 5. DIAMOND plot of **1** in the crystal with thermal ellipsoids drawn at the 50% probability level. Hydrogen atoms other than H1 are omitted for clarity.

³¹ Monoanionic PN enamido ligands with an aliphatic chelate backbone have been reported: (a) Braunstein, P.; Pietsch, J.; Chauvin, Y.; Mercer, S.; Saussine, L.; DeCian, A.; Fischer, J. *J. Chem. Soc. Dalton Trans.* **1996**, 3571-3574. (b) Coleman, K. S.; Green, M. L. H.; Pascu, S. I.; Rees, N. H.; Cowley, A. R.; Rees, L. H. *J. Chem. Soc., Dalton Trans.* **2001**, 3384-3395. (c) Pascu, S. I.; Anderson, G. D. W.; Green, M. L. H.; Green, J. C.; Rees, N. H.; Cowley, A. R. *Inorg. Chim. Acta* **2006**, 359, 3677-3692. (d) Wang, Z.-X.; Wang, L. *Chem. Commun.* **2007**, 2423-2425.

³² (a) Haack, K.-J.; Hashiguchi, S.; Fujii, A.; Ikariya, T.; Noyori, R. *Angew. Chem.* **1997**, 109, 297-300; *Angew. Chem. Int. Ed. Engl.* **1997**, 36, 285-288. (b) Fryzuk, M. D.; Petrella, M. J.; Coffin, R. C.; Patrick, B. O. *C. R. Chimie* **2002**, 5, 451-460. (c) Watson, L. A.; Coalter III, J. N.; Ozerov, O.; Pink, M.; Huffman, J. C.; Caulton, K. G. *New J. Chem.* **2003**, 27, 263-273. (d) Li, T.; Churlaud, R.; Lough, A. J.; Abdur-Rashid, K.; Morris, R. H. *Organometallics* **2004**, 23, 6239-6247. (e) Çelenligil-Çetin, R.; Watson, L. A.; Guo, C.; Foxman, B. M.; Ozerov, O. V. *Organometallics* **2005**, 24, 186-189. (f) Boubekeur, L.; Ulmer, S.; Ricard, L.; Mézailles, N.; Le Floch, P. *Organometallics* **2006**, 25, 315-317. (g) Zhang, G.; Leitius, J.; Ben-David, Y.; Milstein, D. *Angew. Chem.* **2006**, 118, 1131-1133; *Angew. Chem. Int. Ed.* **2006**, 45, 1113-1115. (h) Hadzovic, A.; Song, D.; MacLaughlin, C. M.; Morris, R. H. *Organometallics* **2007**, 26, 5987-5999.

Table 2. Selected bond lengths and bond angles of **1** in the crystal and in the DFT models (B3LYP/6-31+G**) of **1** and **3**.

	1	1^{DFT}	3^{DFT}
Bond Lengths (Å)			
Ru1–H	1.49(2)	1.59	1.59
Ru1–N1	2.023(1)	2.07	2.13
Ru1–P1	2.3077(3)	2.36	2.37
Ru1–P2	2.2996(4)	2.36	2.43
Ru1–P3	2.2629(4)	2.34	2.32
Bond Angles (°)			
H1–Ru1–P3	76.0(7)	79.7	84.6
H1–Ru1–N1	124.8(7)	119.1	102.5
N1–Ru1–P3	159.12(3)	161.1	172.6
P1–Ru1–P2	160.57(1)	160.5	159.0

The high quality of the diffraction data allowed for independent location and refinement of the hydride ligand. The coordination polyhedron around the metal can best be described as a Y-shaped distorted trigonal-bipyramid (Y-TBP) with N1, H1, and P3 defining the equatorial ligands and with distortion from the ideal TBP arising from the small H1–Ru–P3 angle (76.0(7)°) and large H1–Ru–N1 (124.8(7)°) and N1–Ru–P3 (159.12(3)°) angles. Such Y-TBP coordination polyhedra are typically found for diamagnetic five-coordinate d^6 complexes with one strongly π -donating ligand in *trans*-position to the smallest bond angle, such as in [IrCl(H)Me(PCy₃)₂] or [Ir(^{*i*}Pr)₂{N(SiMe₂CH₂PPh₂)₂}].^[33] The Y-TBP conformation is preferred over T-shaped distortion owing to stabilization of the amide nitrogen lone pair p-

³³ (a) Werner, H.; Höhn, A.; Dziallas, M. *Angew. Chem.* **1986**, *98*, 1112-1114; *Angew. Chem. Int. Ed. Engl.* **1986**, *25*, 1090-1092. (b) Fryzuk, M. D.; McNeil, P. A.; Ball, R. G. *J. Am. Chem. Soc.* **1986**, *108*, 6414-6416.

orbital by interaction with the empty metal d_{xy} orbital (Figure 6).^[34] However, some deformation of the Y-TBP towards T-shaped (*viz.* square pyramidal, SP) geometry in **1** most likely arises from steric interactions of the PMe_3 ligand with the pincer ^iPr substituents, as suggested by a space filling model. Similarly, the Ru-N1 distance (2.023(1) Å) points towards increased steric crowding, as compared with $[\text{RuH}(\text{HNCMe}_2\text{CMe}_2\text{NH}_2)(\text{PPh}_3)_2]$ (Ru-N_{amide} = 1.967(1) Å),^[7a] but is considerably shorter compared with amine complex **5** (Ru-N1 = 2.186(2) Å).

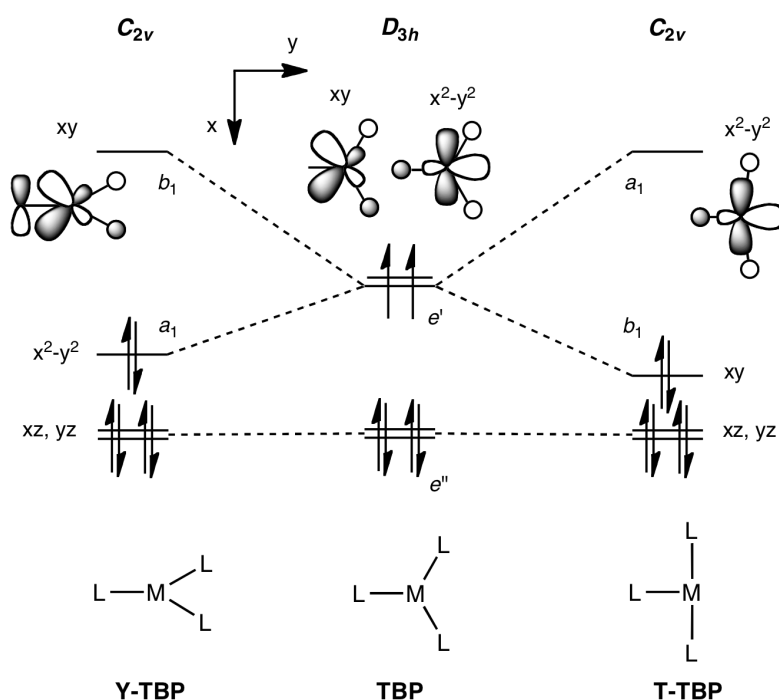


Figure 6. Qualitative Walsh diagram illustrating the splitting of the degenerate e' orbitals in trigonal-bipyramidal (TBP) geometry upon Y-shaped and T-shaped distortion, respectively. Interaction of the LUMO in the Y-TBP case with a single-faced π -donor is indicated. Axial ligands of the TBP are omitted for clarity. Please note that the orbital denotations refer to the coordinate system of the TBP structure (D_{3h}).

Since enamide **3** could not be crystallized to date, full models of **1** and **3** were calculated by DFT methods (B3LYP/6-31+G**). The structure of **1** agrees reasonably well with the

³⁴ (a) Thorn, D. L.; Hoffmann, R. *New J. Chem.* **1979**, *3*, 39-45. (b) Riehl, J. F.; Jean, Y.; Eisenstein, O.; Pélessier, M. *Organometallics* **1992**, *11*, 729-737. (c) Jean, Y. In *Molecular Orbitals of Transition Metal Complexes*, Oxford University Press, Oxford, **2005**.

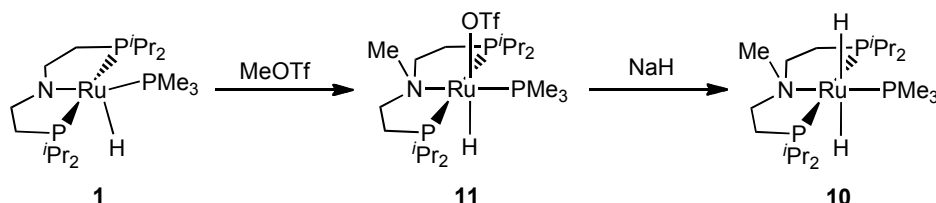
experimental data from X-ray diffraction (Table 2).^[35] Furthermore, the structural parameters around the metal centers of the optimized geometries of **1** and **3** are only marginally different compared with the simpler, PMe_2 -substituted models used in section 2.1. Analysis of the frontier orbitals confirms the simple qualitative picture described above (chapter B1.2.8). The HOMO of **1** is mostly represented by the metal $d_{x^2-y^2}$ orbital, while the LUMO is composed of contributions by the metal d_{xy} orbital and the nitrogen p -orbital, further increasing the HOMO-LUMO gap. In contrast to **1**, **3** exhibits a structure much closer to SP coordination of the metal with the hydride ligand in apical position, as documented by the H1–Ru–N1 (**1**^{DFT}: 120.9 °; **3**^{DFT}: 102.5 °) and N1–Ru–P3 angles (**1**^{DFT}: 159.8 °; **3**^{DFT}: 172.6 °), respectively. Accordingly, the frontier orbital diagram shows the typical features of the T-TBP geometry with a low-lying LUMO, having a high $d_{x^2-y^2}$ contribution (chapter B1.2.8). The smaller HOMO-LUMO gap of **3** is further expressed in the different colours of red **1** and green **3**, respectively. The notably different structures of strongly related complexes **1** and **3** can be rationalized in terms of π -donation by the PNP chelate: While the electronic and molecular structures of **1** point towards strong $\text{N} \rightarrow \text{M}$ π -donation, in case of **3** they suggest highly reduced $\text{N} \rightarrow \text{M}$ π -donation, owing to delocalization of the N -lone pair by conjugation with the $\text{C}=\text{C}$ double bond in the enamido ligand. Accordingly, the HOMO of **3** exhibits a strong contribution of a $\text{C}=\text{C}$ γ -carbon atom p -orbital. Furthermore, the Wiberg Bond Indices (WBI's) of the Ru–N bonds (**1**: 0.50; **3**: 0.37) and of the ligand backbone N–C (**1**: 1.02; **3**: 1.31) and C–C (**1**: 1.02; **3**: 1.60) bonds of **1** as compared with the dehydrogenated branch of **3** support reduced amide to metal π -bonding and N–C–C π -delocalization in **3**. In this context, enamido ligand PNP' can be considered as a transition between strongly π -donating alkylamido ligand PNP and acceptor N -substituted, moderately π -donating amido pincer ligands, such as silylamides $\text{N}(\text{SiMe}_2\text{CH}_2\text{PR}_2)_2$ or arylamides $\text{N}(\text{C}_6\text{H}_4\text{-2-PR}_2)_2$, respectively.^[36,37]

³⁵ In a preliminary communication, we had reported DFT models of **1** and **3** on the B3LYP/6-31+G** level of theory (ref. 10b). There the optimized geometry of **1** adopted a slightly different conformation of the chelate ethylene bridges as compared with the experimentally derived molecular structure. However, the bond lengths and angles around the metal are in good agreement with the calculated structure presented here, which reflects the same conformation as the structural model from X-ray diffraction and represents the global minimum.

³⁶ (a) Liang, L.-C. *Coord. Chem. Rev.* **2006**, 250, 1152-1177. (b) Whited, M. T.; Grubbs, R. H. *Acc. Chem. Res.* **2009**, 42, 1607-1616.

Enamido (3) vs. amido (1) complex: Comparison of Reactivities.

The tunable π -donating ability of the PNP ligands, which is displayed in the electronic and molecular structures, should also be expressed in the chemical reactivity of **1** and **3**. Therefore, their reactivities with electrophiles and nucleophiles were examined exemplarily by reactions with MeOTf and PMe_3 , respectively.



Scheme 7. Synthesis of amine complex **10**.^[7c]

Owing to the high electron density at the nitrogen atom, pronounced *N*-centered nucleophilicity can be expected for amido complexes of transition metals with high *d*-electron counts. Accordingly, stoichiometric C-N coupling of d^8 amides with carbon electrophiles is well established.^[4a,f] Furthermore, in Hartwig-Buchwald-type C-N cross-coupling, amine reductive elimination by nucleophilic attack of an amido ligand at the aryl electrophile defines the selectivity determining step.^[38] In a preliminary communication, we recently reported the synthesis of ruthenium(II) dihydride $[\text{Ru}(\text{H})_2\text{PMe}_3(\text{MePNP})]$ (**10**; $\text{MePNP} = \text{MeN}(\text{CH}_2\text{CH}_2\text{P}^i\text{Pr}_2)_2$) starting from **1** by *N*-methylation with MeOTf and subsequent salt metathesis with NaH (Scheme 7).^[7c] The molecular structure of **10** in the solid state (Figure 7 and Table 3) confirms the structural assignments of **10** in solution, viz. the meridional arrangement of the *MePNP* chelate ligand and the *trans*-dihydride configuration. The longer Ru–N1 distance (2.270(2) Å) in **10**, as compared with **5** (Ru–N1: 2.186(2) Å) is compensated by shorter Ru–P_{PNP} bonds (**10**: 2.3011(4) Å; **5**: 2.3897(8) and 2.3838(8) Å) possibly reflecting increased backbonding to the phosphines in the more electron rich dihydride.

³⁷ For further references *c.f.* [4f] and [20a].

³⁸ (a) Hartwig, J. F. *Acc. Chem. Res.* **1998**, *31*, 852-860. (b) Hartwig, J. F. *Synlett* **2006**, 1283-1294. (c) Corbet, J.-P.; Mignani, G. *Chem. Rev.* **2006**, *106*, 2651-2710. (d) Hartwig, J. F. *Inorg. Chem.* **2007**, *46*, 1936-1947.

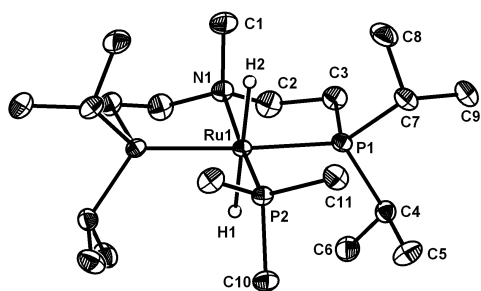


Figure 7. DIAMOND plot of **10** in the crystal with thermal ellipsoids drawn at the 50% probability level. Hydrogen atoms other than H1 and H2 are omitted for clarity. N1, Ru1 and H1 define a crystallographic mirror plane.

Table 3. Selected bond lengths and bond angles of **10** in the crystal.

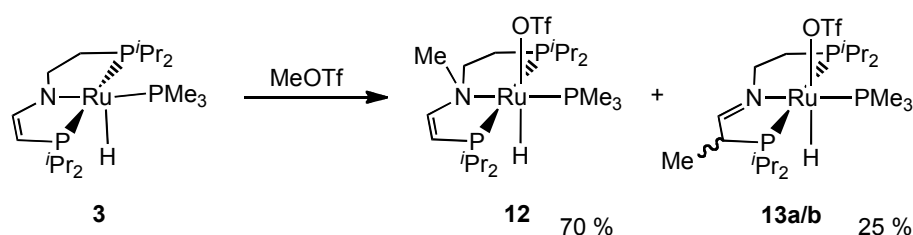
Bond Lengths (Å)			
Ru1–P1	2.3011(4)	Ru1–N1	2.270(2)
Ru1–P1 ⁱ	2.3011(4)	Ru1–P2	2.2373(5)
Bond angles (°)			
N1–Ru1–P1	82.29(1)	P1–Ru1–P1 ⁱ	163.40(2)
N1–Ru1–P1 ⁱ	82.29(1)	N1–Ru1–P2	174.32(4)
P1–Ru1–P2	97.98(1)	P1 ⁱ –Ru1–P2	97.98(1)

ⁱ symmetry operation for equivalent atoms ($x, \frac{1}{2}-y, z$)

The *N*-centered reactivity of **1** with electrophiles reflects the shape of the HOMO and the NPA charge of the nitrogen atom ($-0.67e$). However, for enamide **3** two centres, i.e., the nitrogen atom (NPA charge: $-0.65e$) and the γ -carbon atom (NPA charge: $-0.81e$), exhibit considerable contributions to the HOMO (chapter B1.5.8). Hence, electrophiles could attack at either of the two sites. In analogy to the backbone-saturated complex [RuH(OTf)PMe₃(*MePNP*)] (**11**), complex [RuH(OTf)PMe₃(*MePNP'*)] (**12**; *MePNP'* = MeN(CHCHPⁱPr₂)(CH₂CH₂PⁱPr₂)) is obtained from the reaction of **3** with MeOTf upon *N*-methylation in isolated yields around 40 % (Scheme 8). Monitoring the reaction by ³¹P NMR reveals that besides of **12** (~70 %) two major side products are formed accounting for around

B Results and Discussion

20 % (**13a**), and 5 % (**13b**) yield, respectively (Figure 8). Like enamine complex **12**, both side products exhibit an asymmetric PNP ligand with typical $^2J_{PP}$ *trans* coupling constants of 262 Hz (**13a**) and 261 Hz (**13b**), respectively.^[39] Furthermore, both exhibit one hydride signal and a signal assignable to an N=C-H imine proton. While **13a** and **13b** could not be isolated, the spectroscopic data is in agreement with an assignment to the two diastereomeric imine complexes, resulting from nucleophilic attack of MeOTf at the enamido γ -carbon atom. Interestingly, van der Vlugt *et al.* recently reported, that the reaction of pyridine based PNP pincer complex [Cu{C₅H₃N(2-CH₂PⁱBu₂)(5-CHPⁱBu₂)}] (**A**) with MeOTf results in C-methylation in 71 % isolated yield, i.e., the reversed selectivity compared with **3**.^[24c] As for **3**, for this aromatic analogue the authors indicated a larger NPA charge on γ -C- than on the N-atom. Therefore, the different selectivities of **3** and **A** suggest, that the reaction with electrophiles is not only controlled by charge but also by kinetic arguments, such as the higher flexibility of the PNP' ligand which enables pyramidalization of the nitrogen atom compared with the planar pyridine based PNP ligands.



Scheme 8. Reaction of enamido complex **3** with MeOTf.

³⁹ Selected spectroscopic data of **13a**: NMR (C₆D₆, r.t., [ppm]) ¹H NMR (399.8 MHz): δ = -24.76 (q, $^2J_{HP}$ = 23.2 Hz, 1H, RuH), 3.16 (s, 3H, CHCH₃), 7.40 (dd, $^3J_{HP}$ = 23.5 Hz, $^4J_{HP}$ = 5.9 Hz, 1H, N=CH). ³¹P {¹H} NMR (161.83 MHz): δ = 78.0 (dd, $^2J_{PP}$ = 262.4 Hz, $^2J_{PP}$ = 28.8 Hz, CHPⁱPr₂), 71.1 (dd, $^2J_{PP}$ = 262.4 Hz, $^2J_{PP}$ = 28.8 Hz, CH₂PⁱPr₂), 8.5 (t, $^2J_{PP}$ = 28.8 Hz, P(CH₃)₃). Spectroscopic data of **13b**: NMR (C₆D₆, r.t., [ppm]) ¹H NMR (399.8 MHz): δ = -24.76 (q, $^2J_{HP}$ = 23.2 Hz, 1H, RuH), 3.21 (s, 3H, CHCH₃), 7.62 (dd, $^3J_{HP}$ = 21.1 Hz, $^4J_{HP}$ = 5.6 Hz, 1H, N=CH). ³¹P {¹H} NMR (161.83 MHz): δ = 72.5 (dd, $^2J_{PP}$ = 260.6 Hz, $^2J_{PP}$ = 29.0 Hz, PⁱPr₂), 69.3 (dd, $^2J_{PP}$ = 260.6 Hz, $^2J_{PP}$ = 29.0 Hz, PⁱPr₂), 9.3 (t, $^2J_{PP}$ = 29.0 Hz, P(CH₃)₃).

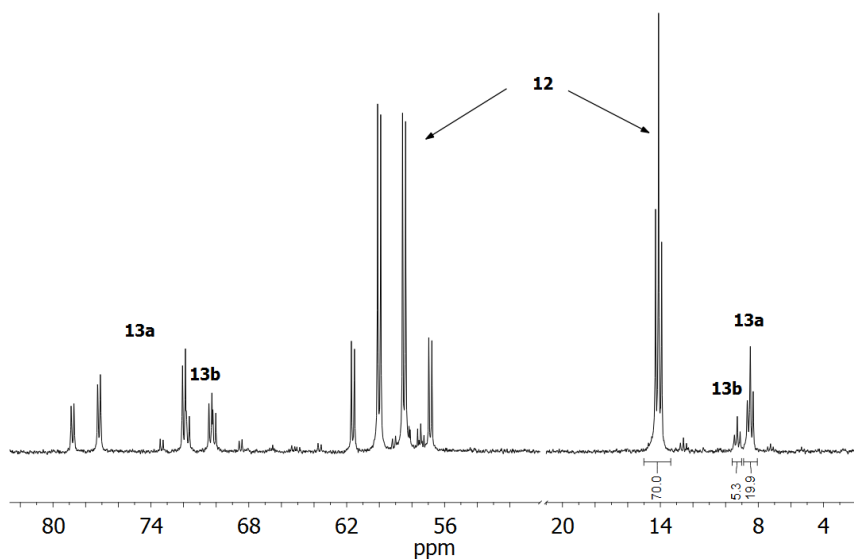


Figure 8. Representative ^{31}P NMR spectrum of the reaction of **3** with MeOTf in benzene.

Multinuclear NMR spectroscopic data for **12** is in agreement with the structure depicted in equation 2, with a meridional arrangement of the *MePNP'* chelate ($^2J_{\text{pp}} = 262$ Hz), a mutual *trans*-configuration of the hydride (^1H : -25.92 ppm) and triflate ligands, and an *N*-bound methyl group (^1H : 2.28 ppm). This structural assignment was confirmed by X-ray diffraction in the solid state (Figure 9 and Table 4). The triflate anion is loosely bound to the metal center (Ru–O1 2.356(1) Å). The *MePNP'* ligand exhibits a short C=C (C2–C3 1.341(3) Å) and a long C–C (C4–C5 1.426(3) Å) bond on the respective “arms” of the chelate backbone. However, the relatively short C4–C5 single bond length points towards some disorder in the crystal structure as observed for imine complex **7** (vide supra).

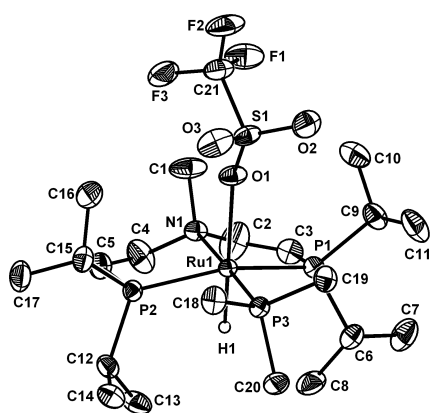


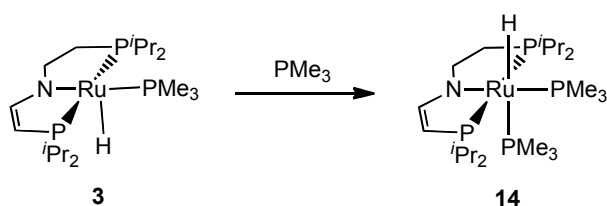
Figure 9. DIAMOND plot of **12** in the crystal with thermal ellipsoids drawn at the 50% probability level. Hydrogen atoms other than H1 are omitted for clarity.

B Results and Discussion

Table 4. Selected bond lengths and bond angles of **12** in the crystal.

Bond Lengths (Å)			
Ru1–P1	2.3348(5)	Ru1–N1	2.249(2)
Ru1–P2	2.3194(5)	Ru1–P3	2.2579(5)
C2–C3	1.341(3)	C4–C5	1.426(3)
Bond Angles (°)			
N1–Ru1–P3	178.87(4)	P1–Ru1–P2	154.31(2)
N1–Ru1–P1	82.08(4)	N1–Ru1–P2	82.71(4)
P1–Ru1–P3	98.01(2)	P2–Ru1–P3	96.81(2)

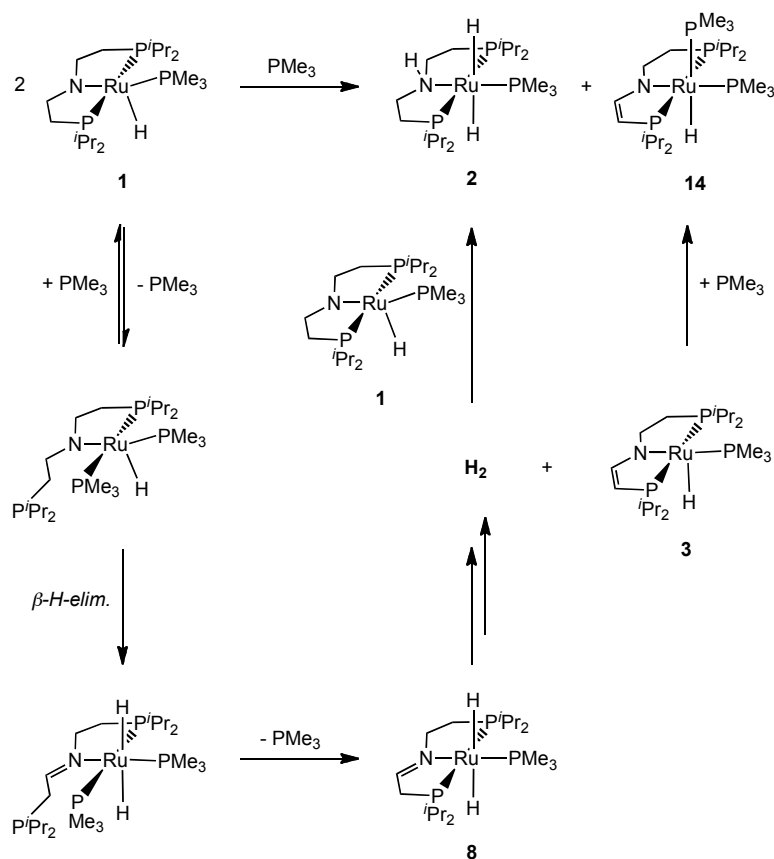
Regarding the reactivity of **3** with nucleophiles, the relatively low-lying, metal centred LUMO suggests Lewis-acidic behaviour of the ruthenium atom for this complex. Therefore, this reactivity of **3** was probed by reaction with PMe_3 . Accordingly, the octahedral diphosphine complex $[\text{RuH}(\text{PMe}_3)_2(\text{PNP}')] (\mathbf{14})$ is obtained in quantitative yield (Scheme 9). The $^2J_{\text{pp}}$ coupling constants of the four ^{31}P signals, the hydride chemical shift (-10.30 ppm) and the large $^2J_{\text{HP}}$ coupling constant of the hydride with a PMe_3 ligand (88 Hz) are in agreement with a meridional coordination of the PNP' chelate and mutual *cis* arrangement of the two PMe_3 ligands.



Scheme 9. Reaction of enamido complex **3** with MeOTf.

Owing to the large HOMO-LUMO gap of amido complex **1**, a different reactivity with nucleophiles can be expected as compared with **3**. In fact, upon addition of PMe_3 to **1** no immediate reaction is observed but considerable broadening of all ^{31}P NMR signals, i.e. the pincer ligand, coordinated PMe_3 , and free PMe_3 , respectively. Monitoring the sample by ^{31}P

NMR over 2 days reveals complete conversion to an equimolar mixture of amine complex **2** and amid **14**, but no intermediates could be detected. This result can be explained by the following proposed mechanism (Scheme 10): The broadening of the ^{31}P NMR signals indicates rapid exchange of free PMe_3 with the coordinated phosphine ligands. This exchange process could open up a pathway for β -hydride migration with lower barriers, as compared with **1** in the absence of PMe_3 (*vide ultra*), because the NCH_2 protons of a dissociated pincer ‘arm’ could adopt a more favorable conformation in the transition state. The thermodynamic instability of resulting imine **8** towards H_2 -elimination was discussed in section 1.2. Finally, eliminated H_2 adds to amide **1** and **3** is trapped by PMe_3 to give the observed mixture of **2** and **14**. This interpretation suggests that nucleophiles might generally reduce the stability of chelate stabilized late metal amides towards β -hydride migration. Most importantly, the simple change in saturation of the PNP chelate backbone strongly alters the reactivity towards nucleophiles, attributable to the change in $\text{N}\rightarrow\text{Ru}$ π -donation of the amido function.



Scheme 10. Reaction of amido complex **1** with PMe_3 and proposed mechanism.

1.5.4 Concluding remarks

Cooperative behaviour of the *N*-functionality in late transition metal amido complexes has been well examined and utilized, e.g., for Noyori-type hydrogenations. More recently, with pyridine-based amido pincer complexes, the chelate backbone cooperativity afforded new catalytic alcohol functionalization reactions. In this context, the present aliphatic PNP ruthenium system offers unusual twofold metal-ligand cooperativity, both at the nitrogen atom and the ligand backbone. This reactivity is highly useful for easy pincer ligand functionalization, and for bifunctional bond activation reactions, e.g., of H₂.

Access to backbone ethylene-bridge functionalization is provided by the formation of enamido complex **3** from **5** and KO*t*Bu. Independent synthesis suggests imine complex **7**, to be an intermediate in this reaction, which is formed by β -hydride migration from **6** and undergoes reversible γ -C deprotonation towards **3**. Both amide **1** and enamide **3** exhibit distinct *N*-centered reactivity with electrophiles, e.g., MeOTf, which distinguishes **3** from similar, pyridine-based, aromatic pincer complexes, attributable to the high flexibility of the aliphatic analogon. However, while **3** reacts with PMe₃ to octahedral complex **14**, **1** gives a mixture of **2** and **14** via a β -hydride migration pathway. This considerably different reactivity of **3** vs. **1** with nucleophiles nicely demonstrates the weaker π -donation by the new enamido type ligand PNP' of **3**, as compared to amido ligand PNP, which is further expressed in their molecular structures. Therefore, with respect to electronic properties we tend to categorize the PNP' ligand in the series of known amido pincer ligands between the strongly basic dialkylamido PNP ligand and the disilylamido ligands N(SiMe₂CH₂PR₂)₂. In this context, the preparation of doubly unsaturated, anionic ligands, such as N(CHCHPR₂)₂ would be desirable to bridge the gap towards weakly π -donating PNP pincer ligands like the diphosphinoarylamides N(C₆H₄PR₂)₂.

The quantumchemical examination of bifunctional reversible H₂ addition/elimination of enamido complex **3**, amido complex **1**, and amine complex **2** explains, why imine intermediate **8** is not observed experimentally. In comparison, imine complex **7** can be isolated, attributable to the weaker *trans*-influence of the chloride ligand in **7**. Hence, the *trans*-dihydride configuration might generally stabilize Noyori-Morris-type (de)hydrogenation catalysts against deactivation to an imine complex. Experimental and theoretical results suggest β -hydride migration to the metal and proton transfer to hydride ligands with sizable barriers as mechanism for the **3** \rightleftharpoons **1** \rightleftharpoons **8** \rightleftharpoons **2** reaction sequence. We

have no evidence for predissociation of a pincer phosphine ‘arm’ to be necessary for this process.

1.5.5 Experimental details and syntheses

Materials and Methods. All experiments were carried out under an atmosphere of argon using Schlenk and glove-box techniques. Benzene and THF were dried over Na/benzophenone, distilled under argon and deoxygenated prior to use. Pentane was dried and deoxygenated by passing through columns packed with activated alumina and Q5, respectively. Deuterated solvents were dried by distillation from Na/K alloy (C_6D_6 and d_8 -THF), and deoxygenated by three *freeze-pump-thaw* cycles. KO^tBu was purchased from VWR and sublimed prior to use. 1M HCl solution in Et₂O (Aldrich), LiBHET₃ (1M solution in THF) (ACROS), H₂ (5.0, Westfalen), and D₂ (99.96, ISOTECH) were used as purchased. **1**, **3**, and **10** were prepared as reported earlier.^[7c,10b]

Analytical Methods. Elemental analyses were obtained from the Microanalytical Laboratory of Technische Universität München. The IR spectra were recorded on a Jasco FT/IR-460 PLUS spectrometer as nujol mulls between KBr plates. NMR spectra were recorded on Jeol Lambda 400 and Bruker Avance III 400 NMR spectrometers at room temperature and were calibrated to the residual proton resonance and the natural abundance ¹³C resonance of the solvent (C_6D_6 , $\delta_H = 7.16$ and $\delta_C = 128.06$ ppm; d_8 -THF, $\delta_H = 1.72$ and 3.57 ppm, $\delta_C = 25.3$ and 67.4 ppm). ³¹P NMR chemical shifts are reported relative to external phosphoric acid (δ 0.0 ppm). Signal multiplicities are abbreviated as: s (singlet), d (doublet), t (triplet), q (quartet), sept (septet), m (multiplet), br (broad).

Synthesis of [RuHCl(PMe₃)(PNP^{})] (7).* **3** (0.127 g; 0.264 mmol) is dissolved in THF (10 mL) and a solution of HCl in Et₂O (1 M; 264 μ L; 0.264 mmol) is added via syringe at room temperature. The color immediately changes to brownish yellow. After 5 min at room temperature the solvent is evaporated *in vacuo* to give a yellow-brown oil. The residue is dissolved in THF and pentane (5 mL) is added. After crystallization over night at -35°C the precipitate is filtered off to give **7** as a yellow solid. Yield: 0.068 g (0.132 mmol; 50 %). Small amounts of [RuHCl(PMe₃)(PNP^H)] (< 2 %) were detected by ¹H and ³¹P NMR. Anal. Calcd for C₁₉H₄₅ClNP₃Ru (517.02): C, 44.14; H, 8.77; N, 2.71. Found: C, 45.05; H, 9.34; N, 2.53. IR (cm⁻¹) $\nu = 1957$ (s, Ru-H), 1616 (m, C=N). NMR (C_6D_6 , r.t., [ppm]) ¹H NMR (399.8 MHz): δ -19.20 (dt, ²J_{HP} = 26.5 Hz, ²J_{HP} = 22.2 Hz, 1H, Ru-H), 0.79 (dd, ³J_{HP} = 11.8 Hz, ³J_{HH} = 6.7 Hz, 3H, CHCH₃), 0.96 (dd, ³J_{HP} = 11.6 Hz, ³J_{HH} = 6.9 Hz, 3H, CHCH₃), 1.02 (dd, ³J_{HP} =

B Results and Discussion

15.7 Hz, $^3J_{\text{HH}} = 7.6$ Hz, 3H, CHCH₃), 1.07 (dd, $^3J_{\text{HP}} = 14.5$ Hz, $^3J_{\text{HH}} = 6.9$ Hz, 3H, CHCH₃), 1.11 (dd, $^3J_{\text{HP}} = 10.5$ Hz, $^3J_{\text{HH}} = 7.1$ Hz, 3H, CHCH₃), 1.23 (dd, $^3J_{\text{HP}} = 10.7$ Hz, $^3J_{\text{HH}} = 7.0$ Hz, 3H, CHCH₃), 1.42 (d, $^2J_{\text{HP}} = 7.8$ Hz, 9H, P(CH₃)₃), 1.54 (dd, $^3J_{\text{HP}} = 13.3$ Hz, $^3J_{\text{HH}} = 7.4$ Hz, 3H, CHCH₃), 1.62 (dd, $^3J_{\text{HP}} = 14.3$ Hz, $^3J_{\text{HH}} = 7.1$ Hz, 3H, CHCH₃), 1.66-1.89 (m, 2H, CH(CH₃)₂ + 2H, PCH₂CH₂N), 1.96 (ddt, $^2J_{\text{HP}} = 17.9$ Hz, $^3J_{\text{HH}} = 8.5$ Hz, $^4J_{\text{HP}} = 2.5$ Hz, 1H, PCH₂CHN), 2.14 (m, 1H, CH(CH₃)₂), 2.60-2.76 (m, 1H, CH(CH₃)₂ + 1H, PCH₂CHN), 3.11 (m, 1H, NCH₂), 3.62 (m, 1H, NCH₂), 7.30 (dd, $^3J_{\text{HP}} = 21.5$ Hz, $^4J_{\text{HP}} = 3.8$ Hz, 1H, N=CH). ¹³C {¹H} NMR (100.6 MHz): δ 17.9 (s, CHCH₃), 18.3 (dd, $^2J_{\text{CP}} = 3.8$ Hz, $^4J_{\text{CP}} = 1.8$ Hz, CHCH₃), 18.8 (dd, $^2J_{\text{CP}} = 2.7$ Hz, $^4J_{\text{CP}} = 1.9$ Hz, CHCH₃), 19.0 (d, $^2J_{\text{CP}} = 6.5$ Hz, CHCH₃), 19.1 (s, CHCH₃), 19.6 (d, $^2J_{\text{CP}} = 5.0$ Hz, CHCH₃), 20.1 (d, $^2J_{\text{CP}} = 5.8$ Hz, CHCH₃), 20.2 (d, $^2J_{\text{CP}} = 2.3$ Hz, CHCH₃), 24.7 (dd, $^1J_{\text{CP}} = 14.6$ Hz, $^3J_{\text{CP}} = 2.7$ Hz, PCH₂CH₂N), 24.9 (dt, $^1J_{\text{CP}} = 24.6$ Hz, $^3J_{\text{CP}} = 2.7$ Hz, P(CH₃)₃), 26.2 (dd, $^1J_{\text{CP}} = 20.4$ Hz, $^3J_{\text{CP}} = 1.5$ Hz, CH(CH₃)₂), 26.4 (dd, $^1J_{\text{CP}} = 19.6$ Hz, $^3J_{\text{CP}} = 1.1$ Hz, CH(CH₃)₂), 27.0 (ddd, $^1J_{\text{CP}} = 8.1$ Hz, $^3J_{\text{CP}} = 5.8$ Hz, $^3J_{\text{CP}} = 1.2$ Hz, CH(CH₃)₂), 27.5 (ddd, $^1J_{\text{CP}} = 7.7$ Hz, $^3J_{\text{CP}} = 6.6$ Hz, $^3J_{\text{CP}} = 1.2$ Hz, CH(CH₃)₂), 35.1 (dd, $^1J_{\text{CP}} = 15.0$ Hz, $^3J_{\text{CP}} = 4.2$ Hz, PCH₂CHN), 60.4 (dd, $^2J_{\text{CP}} = 6.5$ Hz, $^3J_{\text{CP}} = 1.1$ Hz, NCH₂), 163.2 (dd, $^2J_{\text{CP}} = 6.9$ Hz, $^3J_{\text{CP}} = 1.9$ Hz, N=CH). ³¹P {¹H} NMR (161.8 MHz): δ 75.2 (dd, $^2J_{\text{PP}} = 30$ Hz, $^2J_{\text{PP}} = 281$ Hz, PⁱPr₂), 66.9 (dd, $^2J_{\text{PP}} = 30$ Hz, $^2J_{\text{PP}} = 281$ Hz, PⁱPr₂), 9.4 (t, $^2J_{\text{PP}} = 30$ Hz, P(CH₃)₃). Assignments were confirmed by ¹H COSY, ¹H NOESY, ¹H-¹³C HETCOR (chapter B1.5.6), and ¹³C {¹H} DEPT spectra.

Synthesis of [RuH(PMe₃)OTf(MePNP')] (**12**). MeOTf (0.060 g; 0.366 mmol) is added dropwise to a vigorously stirred solution of **3** (154.0 mg; 0.320 mmol) in benzene (5 mL) at rt. The color immediately changes from deep green to brown and a small amount of pentane is added to precipitate some oily contents. After filtration the solvent is removed *in vacuo* to give 0.192 mg of the greenish brown raw product with 70 % of **12** determined by ³¹P-NMR. The residue is washed with pentane (3 x 5 mL) and dried *in vacuo* to give **12** as an analytically pure pale yellow solid. Yield: 0.080 g (0.124 mmol; 39 %). Anal. Calcd for C₂₁H₄₇F₃NO₃P₃RuS (644.65): C, 39.13; H, 7.35; N, 2.17; F, 8.84; S, 4.97. Found: C, 38.76; H, 7.30; N, 2.11; F, 8.9; S, 4.82. IR (cm⁻¹) ν = 2143 (s, Ru-H), 1639 (s, C=C). NMR (C₆D₆, r.t., [ppm]) ¹H NMR (399.8 MHz): δ = -25.92 (q, $^2J_{\text{HP}} = 23.8$ Hz, 1H, RuH), 0.76 (dd, $^3J_{\text{HH}} = 6.8$ Hz, $^3J_{\text{HP}} = 11.7$ Hz, 3H, CHCH₃), 0.85 (m, 6H, CHCH₃), 0.95 (dd, $^3J_{\text{HH}} = 7.1$ Hz, $^3J_{\text{HP}} = 13.7$ Hz, 3H, CHCH₃), 1.10 (dd, $^3J_{\text{HH}} = 6.6$ Hz, $^3J_{\text{HP}} = 10.0$ Hz, 3H, CHCH₃ + 1H, PCH₂), 1.18 (dd, $^3J_{\text{HH}} = 7.1$ Hz, $^3J_{\text{HP}} = 12.0$ Hz, 3H, CHCH₃), 1.40-1.52 (m, 6H, CHCH₃ + 1H, PCH₂), 1.49 (d, $^2J_{\text{HP}} = 8.5$ Hz, 9H, P(CH₃)₃), 1.67-1.81 (m, 2H, CH(CH₃)₂ + 1H, NCH₂), 2.02 (dm, 1H, NCH₂),

2.15-2.25 (m, 2H, $\text{CH}(\text{CH}_3)_2$), 2.28 (s, 3H, NCH_3), 5.22 (d, $^3J_{\text{HH}} = 6.1$ Hz, 1H, PCH), 5.45 (ddt, $^3J_{\text{HP}} = 27.4$ Hz, $^3J_{\text{HH}}/^4J_{\text{HP}} = 6.4$ Hz, $^4J_{\text{HP}} = 1.7$ Hz, 1H, NCH). ^{13}C $\{^1\text{H}\}$ NMR (100.6 MHz): δ 17.9 (dd, $^2J_{\text{CP}} = 2.6$ Hz, $^4J_{\text{CP}} = 1.5$ Hz, CHCH_3), 18.2 (d, $^2J_{\text{CP}} = 0.7$ Hz, CHCH_3), 18.6 (d, $^2J_{\text{CP}} = 0.9$ Hz, CHCH_3), 18.8 (s, CHCH_3), 19.1 (d, $^2J_{\text{CP}} = 3.3$ Hz, CHCH_3), 19.3 (d, $^2J_{\text{CP}} = 4.8$ Hz, CHCH_3), 19.4 (s, CHCH_3), 19.5 (d, $^2J_{\text{CP}} = 1.4$ Hz, CHCH_3), 22.4 (dt, $^1J_{\text{CP}} = 14.8$ Hz, $^3J_{\text{CP}} = 0.9$ Hz, PCH_2), 25.7 (dd, $^1J_{\text{CP}} = 24.4$ Hz, $^3J_{\text{CP}} = 3.2$ Hz, $\text{CH}(\text{CH}_3)_2$), 25.8 (dt, $^1J_{\text{CP}} = 26.8$ Hz, $^3J_{\text{CP}} = 2.8$ Hz, $\text{P}(\text{CH}_3)_3$), 27.2 (ddd, $^1J_{\text{CP}} = 18.6$ Hz, $^3J_{\text{CP}} = 6.1$ Hz, $^3J_{\text{CP}} = 1.4$ Hz, $\text{CH}(\text{CH}_3)_2$), 27.2 (dt, $^1J_{\text{CP}} = 5.8$ Hz, $^3J_{\text{CP}} = 1.3$ Hz, $\text{CH}(\text{CH}_3)_2$), 28.9 (dd, $^1J_{\text{CP}} = 23.2$ Hz, $^3J_{\text{CP}} = 2.6$ Hz, $\text{CH}(\text{CH}_3)_2$), 46.7 (s, NCH_3), 63.2 (dt, $^2J_{\text{CP}} = 6.2$ Hz, $^3J_{\text{CP}} = 1.1$ Hz, NCH_2), 120.8 (q, $^1J_{\text{CF}} = 319.5$ Hz, SO_3CF_3), 121.5 (ddd, $^1J_{\text{CP}} = 22.3$ Hz, $^3J_{\text{CP}} = 3.1$ Hz, $^3J_{\text{CP}} = 1.5$ Hz, PCH), 157.5 (ddd, $^2J_{\text{CP}} = 11.1$ Hz, $^3J_{\text{CP}} = 2.7$ Hz, $^3J_{\text{CP}} = 1.1$ Hz, NCH). ^{31}P $\{^1\text{H}\}$ NMR (161.83 MHz): $\delta = 60.7$ (dd, $^2J_{\text{PP}} = 261.7$ Hz, $^2J_{\text{PP}} = 30.7$ Hz, CHP^iPr_2), 57.5 (dd, $^2J_{\text{PP}} = 261.7$ Hz, $^2J_{\text{PP}} = 30.7$ Hz, $\text{CH}_2\text{P}^i\text{Pr}_2$), 14.0 (t, $^2J_{\text{PP}} = 30.7$ Hz, $\text{P}(\text{CH}_3)_3$). ^{19}F NMR (376.17 MHz): $\delta = -77.5$ (s, SO_3CF_3). Assignments were confirmed by ^1H COSY, ^1H - ^{13}C HMQC (chapter B1.5.6), and ^1H $\{\text{sel. } ^{31}\text{P}\}$ NMR spectra.

Reaction of 7 with KO^tBu. Potassium *tert*-butoxide (0.004 g; 0.038 mmol) is added to a solution of **7** (0.020 g; 0.039 mmol) in 0.4 mL THF in a *J-Young*-NMR tube. The suspension immediately changes the color to deep green and **3** is observed as the only product by ^{31}P NMR.

Reaction of 7 with HCl. HCl in Et_2O (1 M; 42 μL ; 0.042 mmol) is added to a solution of **7** (0.021 g; 0.041 mmol) in 0.4 mL THF in a septum cap NMR tube. **5** is exclusively observed by ^{31}P NMR.

Reaction of 7 with LiBHET₃. Addition of LiBHET_3 in THF (1 M; 10 μL ; 0.010 mmol) to a solution of **7** (0.006 g; 0.012 mmol) in 0.4 mL THF in a septum cap NMR tube results in a red suspension. **1** is observed as the only product by ^{31}P NMR.

Reaction of 5 with LiBHET₃. LiBHET_3 in THF (1 M; 400 μL ; 0.400 mmol; 18 equiv.) is added to a solution of **5** (0.012 g; 0.022 mmol) in 0.4 mL THF in a septum cap NMR tube. **2** is observed as product by ^{31}P NMR exclusively.

[RuH(PMe₃)₂(PNP')] (14) Method A: To a suspension of **5** (0.082 g; 0.148 mmol) and potassium *tert*-butoxide (0.059 g; 0.526 mmol; 3.6 equiv.) in THF (10 mL) a solution of PMe_3 in THF (1 M; 160 μL ; 0.160 mmol) is added via syringe at room temperature. The dark green color immediately changes to pale brown. After 5 min at room temperature the solvent is

B Results and Discussion

evaporated *in vacuo* to give a pale brown solid. After filtration with pentane (10 mL) the filtrate is evaporated and the residue is dried over night, redissolved in pentane (10 mL) and filtrated again. Evaporation of the filtrate gives **14** as a pale brown solid. Yield: 0.071 g (0.128 mmol; 86 %). Anal. Calcd for $C_{22}H_{53}NP_4Ru$ (556.63): C, 47.47; H, 9.60; N, 2.52. Found: C, 47.48; H, 9.72; N, 2.50. IR (cm^{-1}) $\nu = 1968$ (s, Ru-H). NMR (C_6D_6 , r.t., [ppm]) 1H NMR (399.8 MHz): δ -10.30 (dq, $^2J_{HP} = 87.7$ Hz, $^2J_{HP} = 26.2$ Hz, 1H, Ru-H), 1.00-1.10 (m, 9H, $CHCH_3$), 1.14-1.19 (m, 3H, $CHCH_3$), 1.16 (d, $^2J_{HP} = 4.9$ Hz, 9H, $P(CH_3)_3$), 1.27 (d, $^2J_{HP} = 6.8$ Hz, 9H, $P(CH_3)_3$), 1.31-1.46 (m, 12H, $CHCH_3$), 1.46-1.52 (m, 1H, PCH_2), 1.58-1.67 (m, 1H, PCH_2), 1.88 (dsept, $^2J_{HP} = 2.4$ Hz, $^3J_{HH} = 7.2$ Hz, 2H, $CH(CH_3)_2$), 2.08 (sept, $^3J_{HH} = 6.7$ Hz, 1H, $CH(CH_3)_2$), 2.27 (dsept, $^2J_{HP} = 3.4$ Hz, $^3J_{HH} = 7.2$ Hz, 1H, $CH(CH_3)_2$), 3.10-3.21 (m, 2H, NCH_2), 3.56 (d, $^3J_{HH} = 4.8$ Hz, 1H, PCH), 7.28 (ddt, $^3J_{HP} = 38.2$ Hz, $^3J_{HH}/^4J_{HP} = 4.9$ Hz, $^4J_{HP} = 1.4$ Hz, 1H, NCH). ^{13}C $\{^1H\}$ NMR (100.6 MHz, $[D_6]$ benzene, 25°C): ^{13}C - $\{^1H\}$ NMR (100.6 MHz): δ 19.2 (s, $CHCH_3$), 19.3 (s, $CHCH_3$), 19.8 (s, $CHCH_3$), 19.9 (s, $CHCH_3$), 20.2 (s, $CHCH_3$), 20.6 (d, $^2J_{CP} = 4.1$ Hz, $CHCH_3$), 20.9 (s, $CHCH_3$), 22.1 (d, $^2J_{CP} = 4.9$ Hz, $CHCH_3$), 23.0 (d, $^1J_{CP} = 13.5$ Hz, $P(CH_3)_3$), 27.9 (ddd, $^1J_{CP} = 24.2$ Hz, $^3J_{CP} = 9.4$ Hz, $^3J_{CP} = 2.6$ Hz, $CH(CH_3)_2$), 28.5 (d, $^1J_{CP} = 22.3$ Hz, $P(CH_3)_3$ + superimposed $CH(CH_3)_2$), 29.1 (ddd, $^1J_{CP} = 25.7$ Hz, $^3J_{CP} = 5.7$ Hz, $^3J_{CP} = 1.9$ Hz, $CH(CH_3)_2$), 29.7 (d, $^1J_{CP} = 16.9$ Hz, PCH_2), 30.6 (dt, $^1J_{CP} = 13.1$ Hz, $^3J_{CP} = 5.8$ Hz, $CH(CH_3)_2$), 53.6 (dd, $^2J_{CP} = 5.3$ Hz, $^3J_{CP} = 2.1$ Hz, NCH_2), 66.3 (dd, $^1J_{CP} = 40.3$ Hz, $^3J_{CP} = 5.2$ Hz, PCH), 161.9 (d, $^2J_{CP} = 20.9$ Hz, NCH). ^{31}P $\{^1H\}$ NMR (161.8 MHz): δ 72.3 (ddd, $^2J_{PP} = 224.3$ Hz, $^2J_{PP} = 24.8$ Hz, $^2J_{PP} = 17.8$ Hz, P^iPr_2), 67.2 (ddd, $^2J_{PP} = 224.3$ Hz, $^2J_{PP} = 24.8$ Hz, $^2J_{PP} = 17.8$ Hz, P^iPr_2), 3.2 (q, $^2J_{PP} = 24.8$ Hz, N-Ru- PMe_3), -19.6 (q, $^2J_{PP} = 17.8$ Hz, H-Ru- PMe_3). Assignments were confirmed by 1H COSY, 1H - ^{13}C HMQC NMR spectra (chapter B1.5.6).

Method B: **3** (0.095 g; 0.198 mmol) is dissolved in THF (10 mL) and a solution of PMe_3 in THF (1 M; 200 μ L; 0.200 mmol) is added via syringe at room temperature. The color immediately changes from dark green to pale orange. After 10 min at room temperature the solvent is evaporated *in vacuo* to give a pale brown solid. Yield: 0.109 g (0.196 mmol; 99 %). Spectroscopic data (1H NMR, ^{13}C NMR, ^{31}P NMR) is identical with *Method A*.

Reaction of 1 with PMe_3 . PMe_3 in THF (1 M; 60 μ L; 0.060 mmol) is added to a solution of **1** (0.010 g; 0.021 mmol) in 0.4 mL d_8 -THF in a septum-NMR tube. The reaction is monitored by ^{31}P and 1H NMR at rt. An increase of an equimolar mixture of **2** and **14** is detected until complete conversion of **1** after 24 h.

H/D exchange studies. A solution of **1** (11.2 mg; 23.2 μmol ; 52 mM) in d_8 -THF and benzene as internal standard was frozen in a *J-Young*-NMR tube, evacuated, and backfilled with D_2 (1 bar). After quantitative formation of $[\text{Ru}(\text{D})_2\text{PMe}_3\{\text{DN}(\text{CH}_2\text{CH}_2\text{P}^i\text{Pr}_2)_2\}]$ (d_3 -**2**) was observed by ^1H NMR (18 h; r.t.), H/D exchange in the pincer backbone was studied by heating this sample to 80°C and monitoring the progress of the reaction by ^1H NMR. Upon complete conversion to $[\text{Ru}(\text{D})_2\text{PMe}_3\{\text{DN}(\text{CD}_2\text{CD}_2\text{P}^i\text{Pr}_2)_2\}]$ (d_{11} -**2**), D_2 was exchanged with H_2 (1 bar) to measure D/H exchange at r.t. giving $[\text{Ru}(\text{H})_2\text{PMe}_3\{\text{HN}(\text{CD}_2\text{CD}_2\text{P}^i\text{Pr}_2)_2\}]$ (d_8 -**2**).

1.5.6 NMR spectra

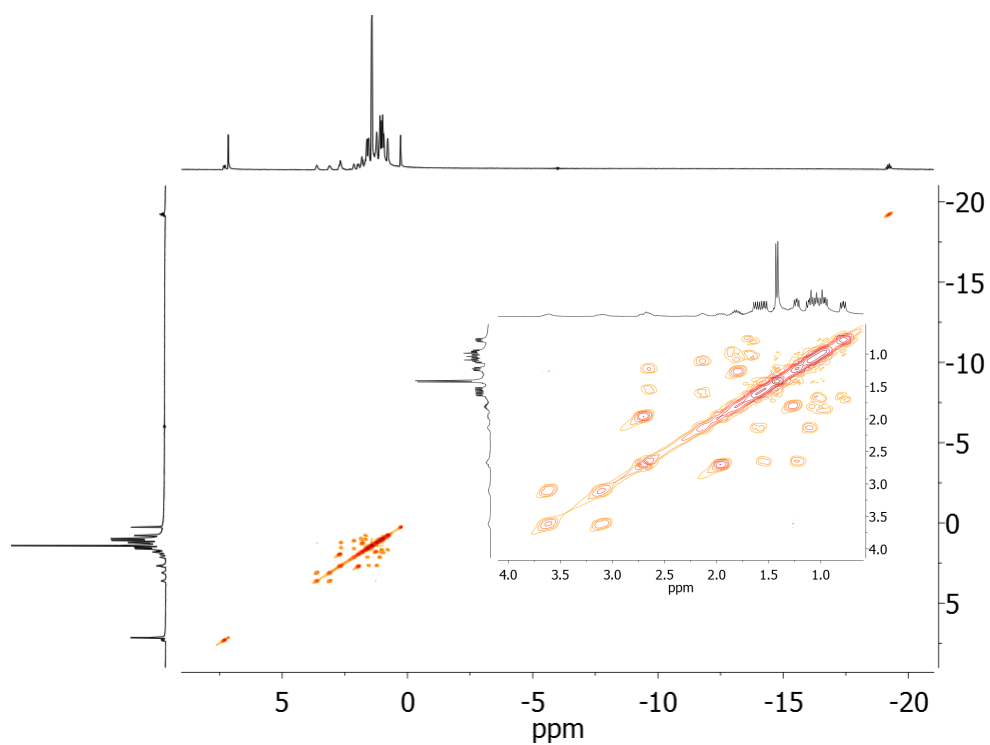


Figure S1. ^1H COSY NMR of **7** in benzene.

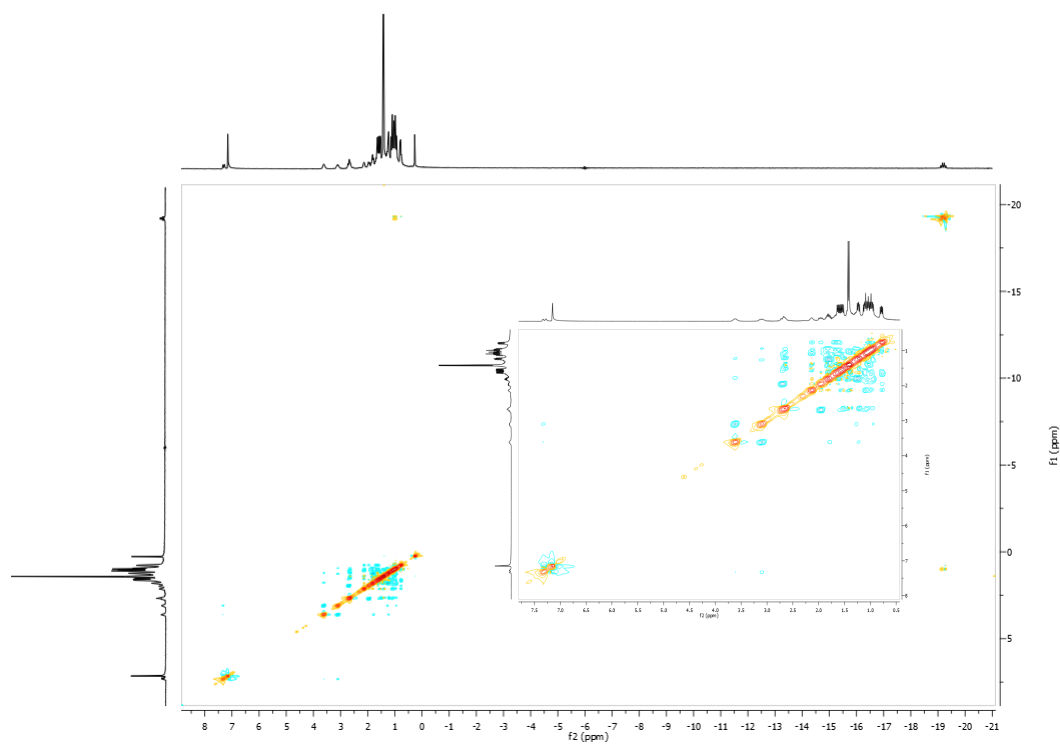


Figure S2. ^1H NOESY NMR of **7** in benzene.

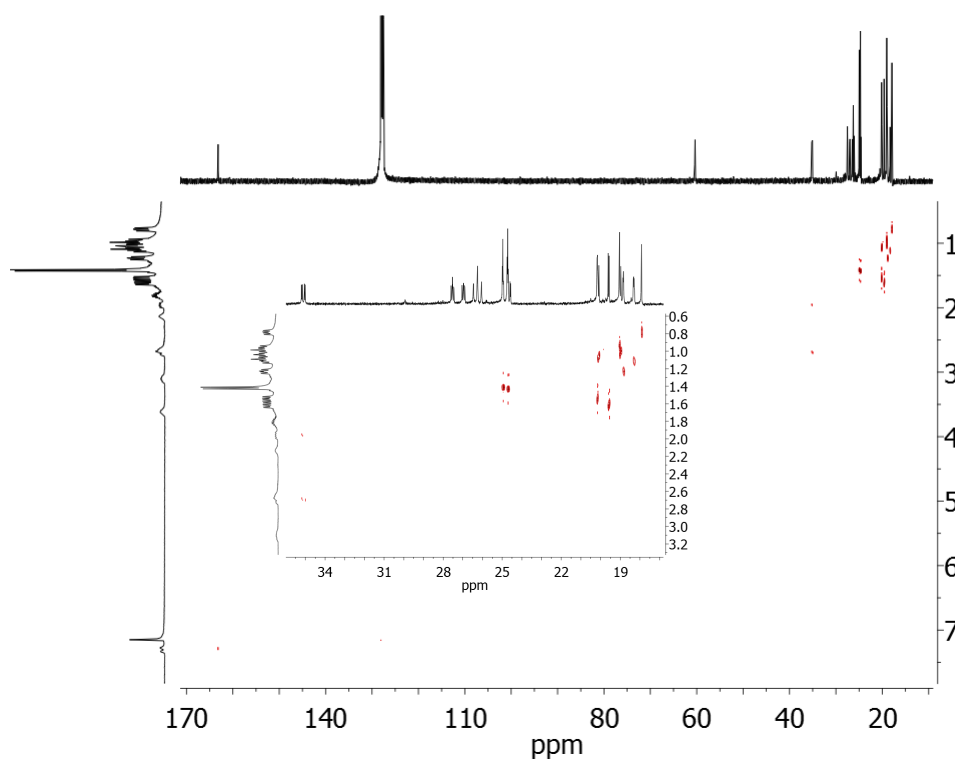


Figure S3. ^{13}C ^1H HETCOR NMR of **7** in benzene.

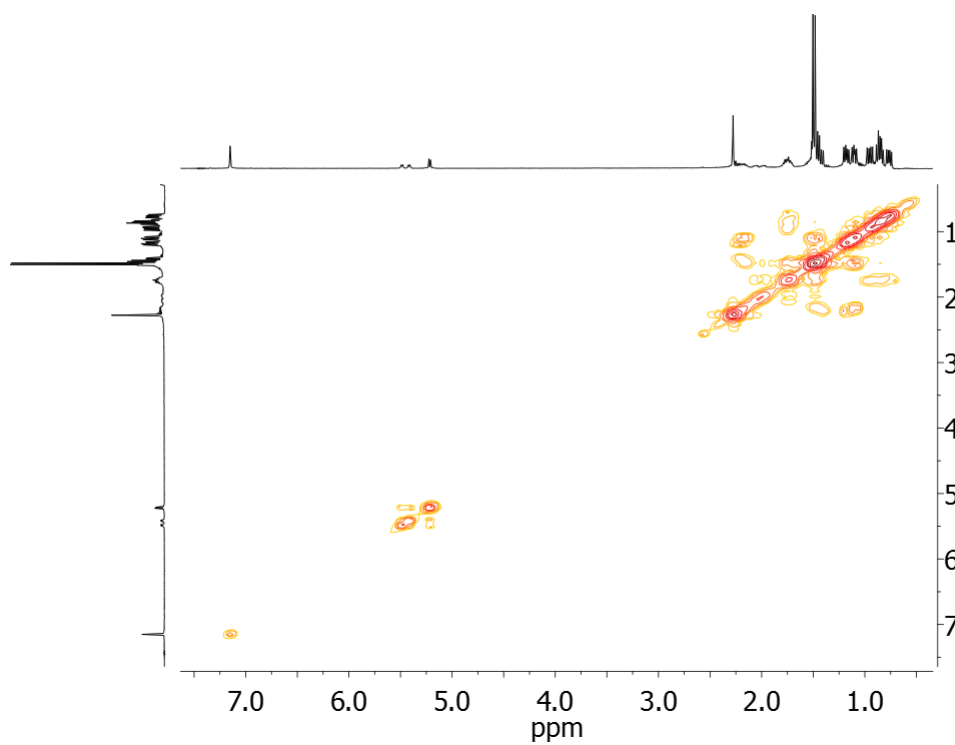


Figure S4. ^1H COSY NMR of **12** in benzene.

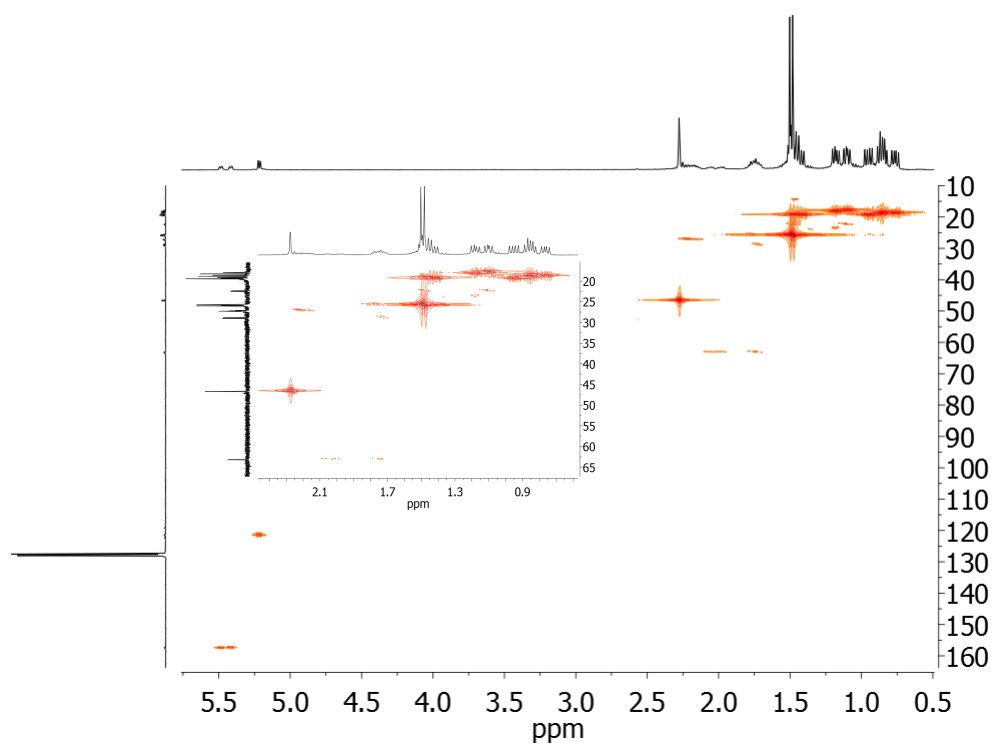


Figure S5. ^1H - ^{13}C HMQC NMR of **12** in benzene.

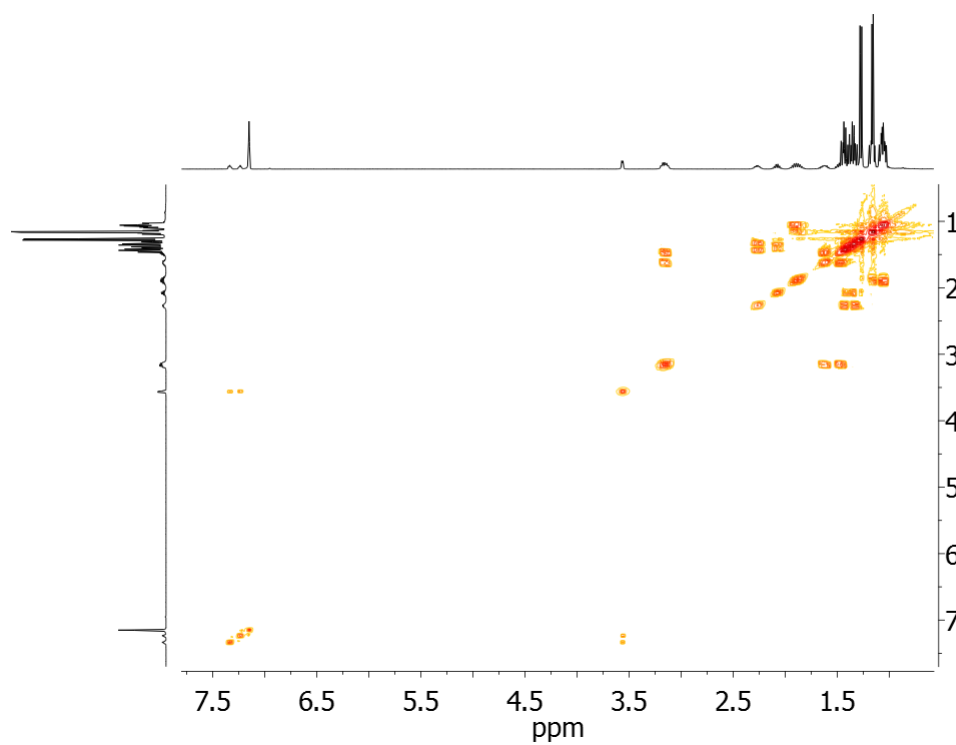


Figure S6. ^1H COSY NMR of **14** in benzene.

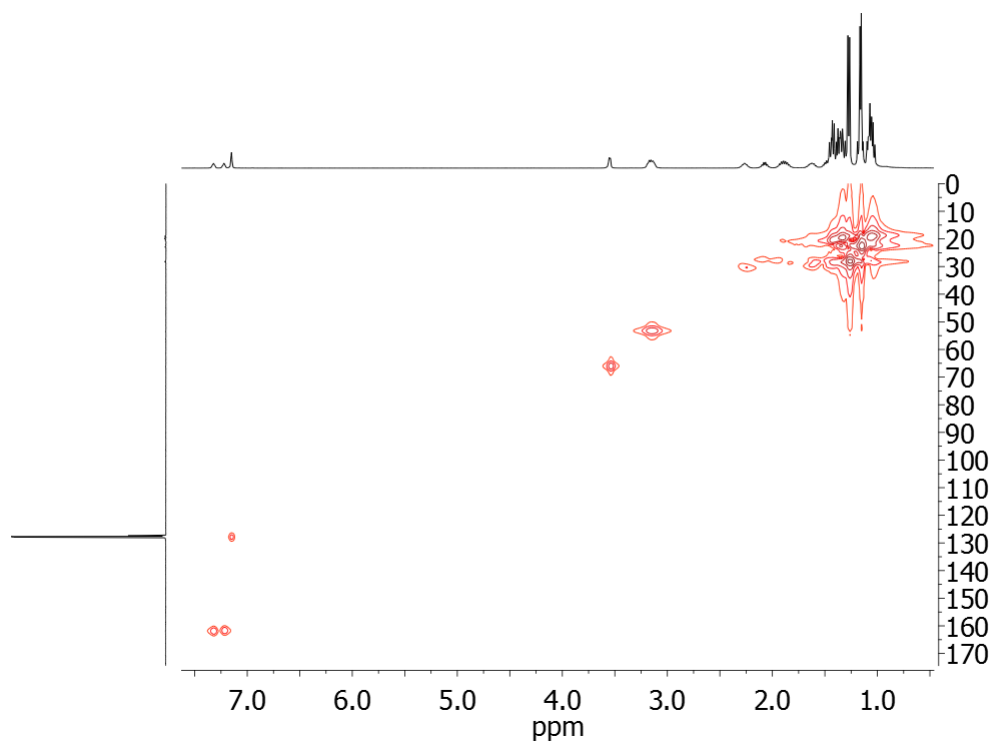


Figure S7. ^1H - ^{13}C HMQC NMR of **14** in benzene.

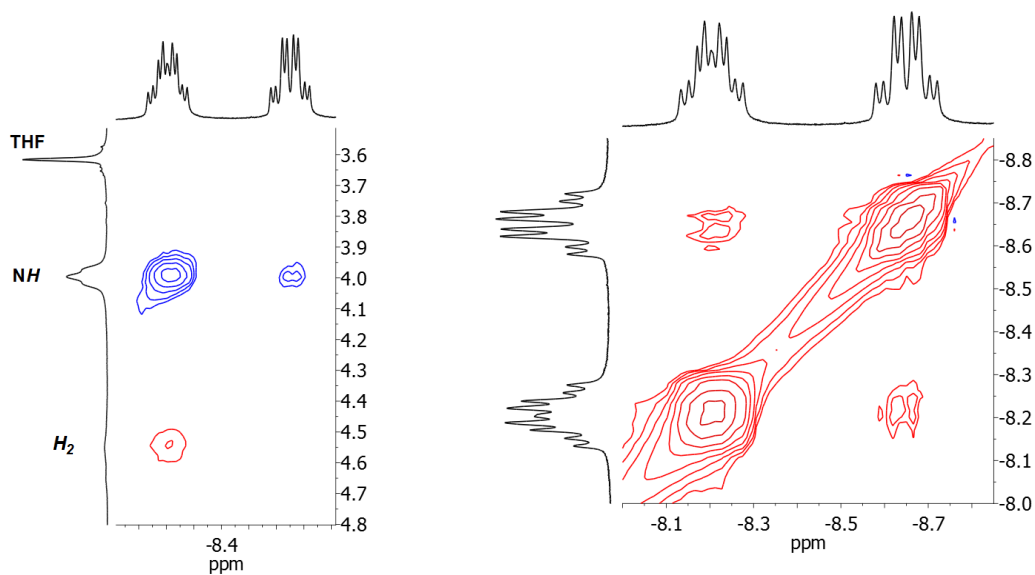


Figure S8. Expansions from the 2D ^1H NOESY NMR spectrum of **2** in d_8 -THF under H_2 (1 bar).

1.5.7 Crystallographic details

X-Ray Crystal Structure Determinations. **1:** Crystal data and details of the structure determination: formula: $C_{19}H_{46}NP_3Ru$; $M_r=482.55$; crystal color and shape: red needle, crystal dimensions= $0.08 \times 0.10 \times 0.51$ mm; crystal system: monoclinic; space group $P2_1/c$ (no. 14); $a=14.3777(4)$, $b=9.9139(3)$, $c=17.8316(5)$ Å; $\beta=103.5144(14)^\circ$; $V=2471.32(12)$ Å³; $Z=4$; μ ($Mo_{K\alpha}$)= 0.831 mm⁻¹; $\rho_{calcd}=1.297$ g cm⁻³; Θ range= $1.46-25.35$; data collected: 113 859; independent data [$I_o > 2\sigma(I_o)$]/all data/ R_{int}]: 4518/4363/0.025; data/restraints/parameters: 4518/0/401; $R1$ [$I_o > 2\sigma(I_o)$]/all data]: 0.0140/0.0148; $wR2$ [$I_o > 2\sigma(I_o)$]/all data]: 0.0348/0.0357; GOF=1.066; $\Delta\rho_{max/min}$: 0.34/-0.33 e Å⁻³. **4:** Crystal data and details of the structure determination: formula: $C_{32}H_{74}Cl_4N_2P_4Ru_2$; $M_r=954.75$; crystal color and shape: yellow prism, crystal dimensions= $0.30 \times 0.51 \times 0.51$ mm; crystal system: monoclinic; space group $P2_1/n$ (no. 14); $a=12.4756(4)$, $b=13.7853(4)$, $c=13.0588(4)$ Å; $\beta=105.114(3)^\circ$; $V=2168.17(12)$ Å³; $Z=2$; μ ($Mo_{K\alpha}$)= 1.115 mm⁻¹; $\rho_{calcd}=1.462$ g cm⁻³; Θ range= $6.04-25.35$; data collected: 24 182; independent data [$I_o > 2\sigma(I_o)$]/all data/ R_{int}]: 2219/2602/0.039; data/restraints/parameters: 2602/0/207; $R1$ [$I_o > 2\sigma(I_o)$]/all data]: 0.0368/0.0498; $wR2$ [$I_o > 2\sigma(I_o)$]/all data]: 0.0718/0.0808; GOF=1.220; $\Delta\rho_{max/min}$: 0.61/-0.49 e Å⁻³. **5:** Crystal data and details of the structure determination: formula: $C_{19}H_{46}Cl_2NP_3Ru$; $M_r=553.45$; crystal color and shape: light orange fragment, crystal dimensions= $0.23 \times 0.28 \times 0.38$ mm; crystal system: triclinic; space group $P\bar{1}$ (no. 2); $a=9.9919(5)$, $b=10.4067(5)$, $c=13.1852(6)$ Å; $\alpha=104.037(2)$, $\beta=100.273(2)$, $\gamma=101.193(2)^\circ$; $V=1267.66(11)$ Å³; $Z=2$; μ ($Mo_{K\alpha}$)= 1.024 mm⁻¹; $\rho_{calcd}=1.450$ g cm⁻³; Θ range= $3.19-25.35$; data collected: 66 371; independent data [$I_o > 2\sigma(I_o)$]/all data/ R_{int}]: 4423/4478/0.047; data/restraints/parameters: 4478/0/246; $R1$ [$I_o > 2\sigma(I_o)$]/all data]: 0.0342/0.0344; $wR2$ [$I_o > 2\sigma(I_o)$]/all data]: 0.0915/0.0919; GOF=1.250; $\Delta\rho_{max/min}$: 1.33/-0.77 e Å⁻³. **10:** Crystal data and details of the structure determination: formula: $C_{20}H_{50}NP_3Ru$; $M_r=498.59$; crystal color and shape: yellow fragment, crystal dimensions= $0.33 \times 0.41 \times 0.43$ mm; crystal system: orthorhombic; space group $Pnma$ (no. 62); $a=12.7484(6)$, $b=19.6938(9)$, $c=10.1107(5)$ Å; $V=2538.4(2)$ Å³; $Z=4$; μ ($Mo_{K\alpha}$)= 0.812 mm⁻¹; $\rho_{calcd}=1.305$ g cm⁻³; Θ range= $2.26-25.48$; data collected: 70 205; independent data [$I_o > 2\sigma(I_o)$]/all data/ R_{int}]: 2252/2376/0.031; data/restraints/parameters: 2376/0/132; $R1$ [$I_o > 2\sigma(I_o)$]/all data]: 0.0167/0.0183; $wR2$ [$I_o > 2\sigma(I_o)$]/all data]: 0.0448/0.0473; GOF=1.126; $\Delta\rho_{max/min}$: 0.34/-0.32 e Å⁻³. **12:** Crystal data and details of the structure determination: formula: $C_{21}H_{47}F_3NO_3P_3RuS$; $M_r=644.65$; crystal color and shape: yellow fragment, crystal dimensions= $0.41 \times 0.46 \times 0.51$

mm; crystal system: monoclinic; space group $P2_1/n$ (no. 14); $a=10.2224(5)$, $b=19.1971(10)$, $c=15.5142(8)$ Å; $\beta=103.351(2)^\circ$; $V=2962.2(3)$ Å³; $Z=4$; μ (Mo_{K α})=0.803 mm⁻¹; $\rho_{\text{calcd}}=1.446$ g cm⁻³; Θ range=1.72–25.32; data collected: 80 411; independent data [$I_o>2\sigma(I_o)$ /all data/ R_{int}]: 5218/5387/0.025; data/restraints/parameters: 5387/0/310; $R1$ [$I_o>2\sigma(I_o)$ /all data]: 0.0200/0.0209; $wR2$ [$I_o>2\sigma(I_o)$ /all data]: 0.0493/0.0501; GOF=1.092; $\Delta\rho_{\text{max/min}}$: 0.45/-0.46 e Å⁻³. CCDC 761695 (1), 761696 (4), 761697 (5), 761698 (10), and 761699 (12) contain the supplementary crystallographic data for this paper. These data can be obtained free of charge from The Cambridge Crystallographic Data Centre via www.ccdc.cam.ac.uk/data_request/cif.

Compound 1

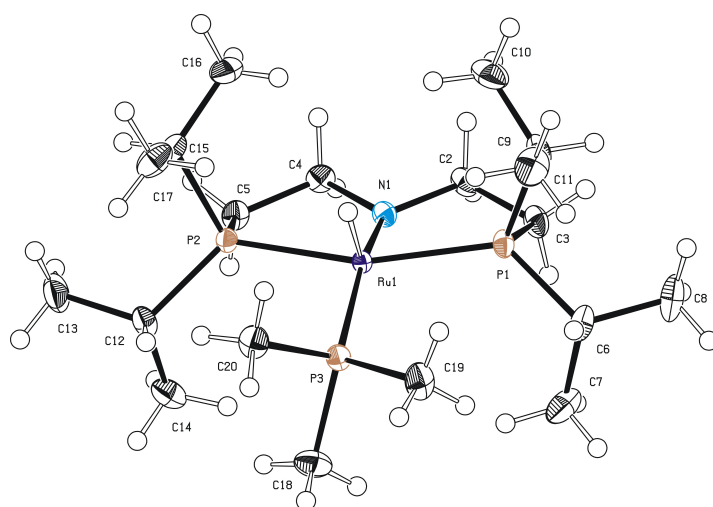


Figure S9. PLATON plot of **1** in the crystal with thermal ellipsoids drawn at the 50 % probability level.

Operator:	*** Herdtweck ***
Molecular Formula:	C ₁₉ H ₄₆ N P ₃ Ru
Crystal Color / Shape	Red needle
Crystal Size	Approximate size of crystal fragment used for data collection: 0.08 × 0.10 × 0.51 mm
Molecular Weight:	482.55 a.m.u.
F ₀₀₀ :	1024
Systematic Absences:	h0l: l≠2n; 0k0: k≠2n
Space Group:	Monoclinic $P 2_1/c$ (I.T.-No.: 14)

B Results and Discussion

Cell Constants:	Least-squares refinement of 9689 reflections with the programs "APEX suite" and "SAINT" [1,2]; theta range $1.46^\circ < \theta < 25.35^\circ$; Mo($K\alpha$); $\lambda = 71.073$ pm $a = 1437.77(4)$ pm $b = 991.39(3)$ pm $\beta = 103.5144(14)^\circ$ $c = 1783.16(5)$ pm $V = 2471.32(12) \cdot 10^6$ pm ³ ; $Z = 4$; $D_{\text{calc}} = 1.297$ g cm ⁻³ ; Mos. = 0.71
Diffraction:	Kappa APEX II (Area Diffraction System; BRUKER AXS); rotating anode; graphite monochromator; 50 kV; 40 mA; $\lambda = 71.073$ pm; Mo($K\alpha$)
Temperature:	(-150±1) °C; (123±1) K
Measurement Range:	$1.46^\circ < \theta < 25.35^\circ$; h: -17/17, k: -11/11, l: -21/21
Measurement Time:	2 × 2.50 s per film
Measurement Mode:	measured: 15 runs; 5163 films / scaled: 15 runs; 5163 films φ - and ω -movement; Increment: $\Delta\varphi/\Delta\omega = 0.50^\circ$; dx = 35.0 mm
LP - Correction:	Yes [2]
Intensity Correction	No/Yes; during scaling [2]
Absorption Correction:	Multi-scan; during scaling; $\mu = 0.831$ mm ⁻¹ [2]
	Correction Factors: $T_{\text{min}} = 0.6556$ $T_{\text{max}} = 0.7452$
Reflection Data:	118116 reflections were integrated and scaled 4257 reflections systematic absent and rejected 113859 reflections to be merged 4518 independent reflections 0.025 R_{int} : (basis F_o^2) 4518 independent reflections (all) were used in refinements 4363 independent reflections with $I_o > 2\sigma(I_o)$ 99.9 % completeness of the data set 401 parameter full-matrix refinement 11.3 reflections per parameter
Solution:	Direct Methods [3]; Difference Fourier syntheses
Refinement Parameters:	In the asymmetric unit: 24 Non-hydrogen atoms with anisotropic displacement parameters

	46 Hydrogen atoms with isotropic displacement parameters	
Hydrogen Atoms:	All hydrogen atom positions were found in the difference map calculated from the model containing all non-hydrogen atoms. The hydrogen positions were refined with individual isotropic displacement parameters.	
Atomic Form Factors:	For neutral atoms and anomalous dispersion [4]	
Extinction Correction:	no	
Weighting Scheme:	$w^{-1} = \sigma^2(F_o^2) + (a*P)^2 + b*P$ with a: 0.0156; b: 1.3392; P: $[\text{Maximum}(0 \text{ or } F_o^2) + 2*F_c^2]/3$	
Shift/Err:	Less than 0.001 in the last cycle of refinement:	
Resid. Electron Density:	+0.34 e ⁻ /Å ³ ; -0.33 e ⁻ /Å ³	
R1:	$\Sigma(F_o - F_c) / \Sigma F_o $	
[F _o > 4σ(F _o); N=4363]:		= 0.0140
[all reflctns; N=4518]:		= 0.0148
wR2:	$[\Sigma w(F_o^2 - F_c^2)^2 / \Sigma w(F_o^2)^2]^{1/2}$	
[F _o > 4σ(F _o); N=4363]:		= 0.0348
[all reflctns; N=4518]:		= 0.0357
Goodness of fit:	$[\Sigma w(F_o^2 - F_c^2)^2 / (\text{NO-NV})]^{1/2}$	
		= 1.066
Remarks:	Refinement expression $\Sigma w(F_o^2 - F_c^2)^2$	

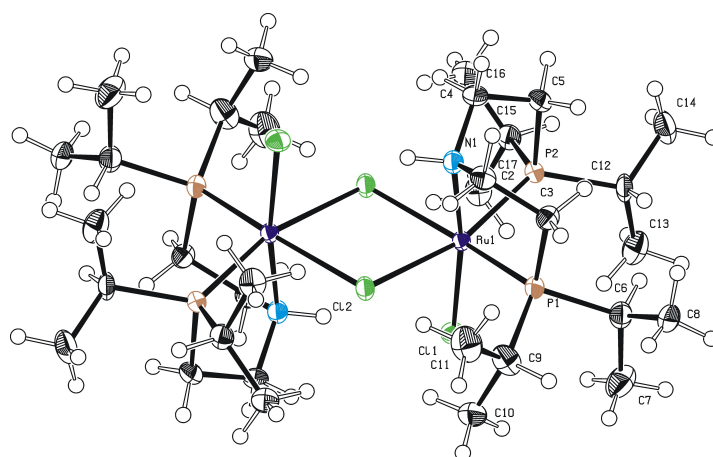
Compound 4

Figure S10. PLATON plot of **4** in the crystal with thermal ellipsoids drawn at the 50 % probability level.

B Results and Discussion

Operator:	*** Herdtweck / Wahl ***
Molecular Formula:	C ₃₂ H ₇₄ Cl ₄ N ₂ P ₄ Ru ₂
Crystal Color / Shape	Yellow prism
Crystal Size	Approximate size of crystal fragment used for data collection: 0.30 × 0.51 × 0.51 mm
Molecular Weight:	954.75 a.m.u.
F ₀₀₀ :	992
Systematic Absences:	h0l: h+l≠2n; 0k0: k≠2n
Space Group:	Monoclinic <i>P</i> 2 ₁ / <i>n</i> (I.T.-No.: 14)
Cell Constants:	Least-squares refinement of 32853 reflections with the program "CRYSTALIS" [1a]; theta range 2.95° < θ < 32.74°; Mo(K $\bar{\alpha}$); λ = 71.073 pm <i>a</i> = 1247.56(4) pm <i>b</i> = 1378.53(4) pm β = 105.114(3)° <i>c</i> = 1305.88(4) pm <i>V</i> = 2168.17(12) · 10 ⁶ pm ³ ; <i>Z</i> = 2; <i>D</i> _{calc} = 1.462 g cm ⁻³
Diffractometer:	Xcalibur™3; κ -CCD (Area Diffraction System; OXFORD DIFFRACTIONS); sealed tube, graphite monochromator; 50 kV; 40 mA; λ = 71.073 pm; Mo(K $\bar{\alpha}$)
Temperature:	(-120±1) °C; (153±1) K
Measurement Range:	6.04° < θ < 25.35°; h: -15/15, k: -16/16, l: -15/15
Measurement Time:	5 s per film
Measurement Mode:	measured: 9 sets; 1328 films / scaled: 9 sets; 1328 films φ - and ω -movement; Increment: $\Delta\varphi/\Delta\omega$ = 1.00°; dx = 50.0 mm
LP - Correction:	Yes [1]
Intensity Correction:	No/Yes; during scaling [1a]
Absorption Correction:	No/Yes; during scaling; μ = 1.115 mm ⁻¹ [1a]
Reflection Data:	62046 reflections were integrated 27859 reflections rejected – overlapped 9480 reflections rejected (resolution limits 20.40 Å to 0.83 Å) 525 reflections systematic absent and rejected 24182 reflections to be merged

	0.0388	R_{int} : (basis F_o^2)	
	2602	independent reflections (all) were used in refinements	
	2219	independent reflections with $I_o > 2\sigma(I_o)$	
	65.5 %	completeness of the data set	
	207	parameter full-matrix refinement	
	12.6	reflections per parameter	
Solution:	Direct Methods [2]; Difference Fourier syntheses		
Refinement Parameters:	In the asymmetric unit:		
	22 Non-hydrogen atoms with anisotropic displacement parameters		
Hydrogen Atoms:	In the difference map(s) calculated from the model containing all non-hydrogen atoms, not all of the hydrogen positions could be determined from the highest peaks. For this reason, the hydrogen atoms were placed in calculated positions ($d_{\text{N-H}} = 93$ pm; $d_{\text{C-H}} = 98, 99, 100$ pm). Isotropic displacement parameters were calculated from the parent carbon atom ($U_{\text{H}} = 1.2/1.5 U_{\text{C/N}}$). The hydrogen atoms were included in the structure factor calculations but not refined.		
Atomic Form Factors:	For neutral atoms and anomalous dispersion [3]		
Extinction Correction:	no		
Weighting Scheme:	$w^{-1} = \sigma^2(F_o^2) + (a * P)^2 + b * P$		
	with a: 0.0123; b: 7.8625; P: $[\text{Maximum}(0 \text{ or } F_o^2) + 2 * F_c^2] / 3$		
Shift/Err:	Less than 0.001 in the last cycle of refinement:		
Resid. Electron Density:	$+0.61 e_0 / \text{\AA}^3$; $-0.49 e_0 / \text{\AA}^3$		
R1:	$\Sigma(F_o - F_c) / \Sigma F_o $		
$[F_o > 4\sigma(F_o)$; N=2219]:			= 0.0368
[all reflctns; N=2602]:			= 0.0498
wR2:	$[\Sigma w(F_o^2 - F_c^2)^2 / \Sigma w(F_o^2)^2]^{1/2}$		
$[F_o > 4\sigma(F_o)$; N=2219]:			= 0.0718
[all reflctns; N=2602]:			= 0.0808
Goodness of fit:	$[\Sigma w(F_o^2 - F_c^2)^2 / (\text{NO} - \text{NV})]^{1/2}$		
			= 1.220
Remarks:	Refinement expression $\Sigma w(F_o^2 - F_c^2)^2$		
	Integration with the " CP RRPTWIN" option		

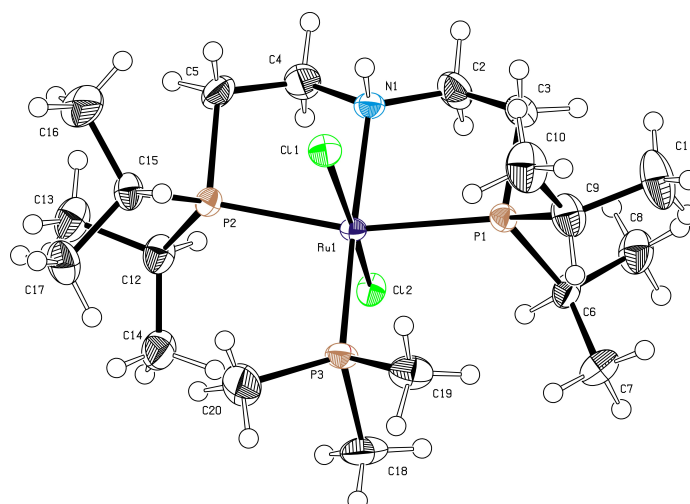
Compound 5

Figure S11. PLATON plot of **5** in the crystal with thermal ellipsoids drawn at the 50 % probability level.

Operator:	*** Herdtweck ***	
Molecular Formula:	C ₁₉ H ₄₆ Cl ₂ N P ₃ Ru	
Crystal Color / Shape	Light orange fragment	
Crystal Size	Approximate size of crystal fragment used for data collection: 0.23 × 0.28 × 0.38 mm	
Molecular Weight:	553.45 a.m.u.	
F ₀₀₀ :	580	
Systematic Absences:	none	
Space Group:	Triclinic $P\bar{1}$ (I.T.-No.: 2)	
Cell Constants:	Least-squares refinement of 9536 reflections with the programs "APEX suite" and "SAINT" [1,2]; theta range $3.19^\circ < \theta < 25.35^\circ$; Mo(K α); $\lambda = 71.073$ pm $a = 999.19(5)$ pm $\alpha = 104.037(2)^\circ$ $b = 1040.67(5)$ pm $\beta = 100.273(2)^\circ$ $c = 1318.52(6)$ pm $\gamma = 101.193(2)^\circ$ $V = 1267.66(11) \cdot 10^6$ pm ³ ; $Z = 2$; $D_{\text{calc}} = 1.450$ g cm ⁻³ ; Mos. = 0.73)	

Diffraction:	Kappa APEX II (Area Diffraction System; BRUKER AXS); rotating anode; graphite monochromator; 40 kV; 40 mA; $\lambda = 71.073$ pm; Mo($K\alpha$)
Temperature:	(-120±1) °C; (153±1) K
Measurement Range:	$3.19^\circ < \theta < 25.35^\circ$; h: -12/12, k: -12/12, l: -15/15
Measurement Time:	2 × 5 s per film
Measurement Mode:	measured: 12 runs; 5962 films / scaled: 12 runs; 5962 films φ - and ω -movement; Increment: $\Delta\varphi/\Delta\omega = 0.50^\circ$; dx = 35.0 mm
LP - Correction:	Yes [2]
Intensity Correction	No/Yes; during scaling [2]
Absorption Correction:	Multi-scan; during scaling; $\mu = 1.024$ mm ⁻¹ [2] Correction Factors: $T_{\min} = 0.6531$ $T_{\max} = 0.7452$
Reflection Data:	66572 reflections were integrated and scaled 201 rejected (theta-cutoff to a resolution of 6.50-0.83 Å) 66371 reflections to be merged 4478 independent reflections 0.047 R_{int} : (basis F_o^2) 4478 independent reflections (all) were used in refinements 4423 independent reflections with $I_o > 2\sigma(I_o)$ 96.6 % completeness of the data set 246 parameter full-matrix refinement 18.2 reflections per parameter
Solution:	Direct Methods [3]; Difference Fourier syntheses
Refinement Parameters:	In the asymmetric unit: 26 Non-hydrogen atoms with anisotropic displacement parameters
Hydrogen Atoms:	In the difference map(s) calculated from the model containing all non-hydrogen atoms, not all of the hydrogen positions could be determined from the highest peaks. For this reason, the hydrogen atoms were placed in calculated positions ($d_{\text{C-H}} = 98, 99, 100$ pm; $d_{\text{N-H}} = 93$ pm). Isotropic displacement parameters were calculated from the parent carbon atom ($U_{\text{H}} = 1.2/1.5 U_{\text{C}}$; $U_{\text{H}} = 1.2 U_{\text{N}}$). The

B Results and Discussion

hydrogen atoms were included in the structure factor calculations but not refined.

Atomic Form Factors:	For neutral atoms and anomalous dispersion [4]
Extinction Correction:	no
Weighting Scheme:	$w^{-1} = \sigma^2(F_o^2) + (a * P)^2 + b * P$ with a: 0.0490; b: 1.2956; P: $[\text{Maximum}(0 \text{ or } F_o^2) + 2 * F_c^2] / 3$
Shift/Err:	Less than 0.001 in the last cycle of refinement:
Resid. Electron Density:	+1.33 e ₀ /Å ³ ; -0.77 e ₀ /Å ³
R1:	$\Sigma(F_o - F_c) / \Sigma F_o $
[F _o > 4σ(F _o); N=4423]:	= 0.0342
[all reflctns; N=4478]:	= 0.0344
wR2:	$[\Sigma w(F_o^2 - F_c^2)^2 / \Sigma w(F_o^2)^2]^{1/2}$
[F _o > 4σ(F _o); N=4423]:	= 0.0915
[all reflctns; N=4478]:	= 0.0919
Goodness of fit:	$[\Sigma w(F_o^2 - F_c^2)^2 / (\text{NO} - \text{NV})]^{1/2}$ = 1.250
Remarks:	Refinement expression $\Sigma w(F_o^2 - F_c^2)^2$

Compound 7

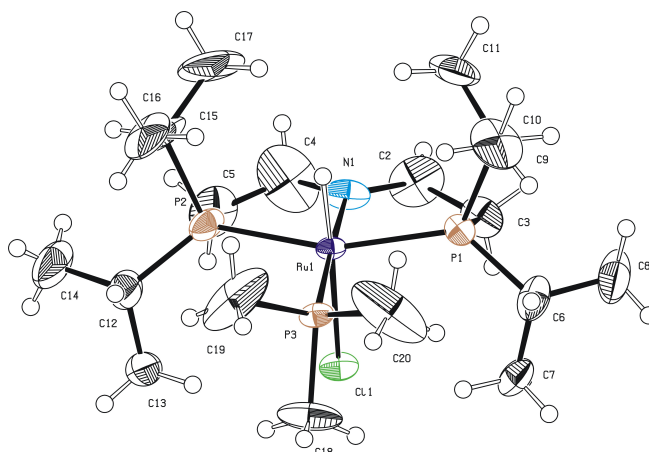


Figure S12. PLATON plot of **7** in the crystal with thermal ellipsoids drawn at the 50 % probability level.

Operator:	*** Herdtweck ***
Molecular Formula:	C ₁₉ H ₄₅ Cl N P ₃ Ru
Crystal Color / Shape	Yellow fragment

Molecular Weight:	516.99 a.m.u.		
Systematic Absences:	h0l: l \neq 2n; 0k0: k \neq 2n		
Space Group:	Monoclinic	<i>P</i> 2 ₁ / <i>c</i>	(I.T.-No.: 14)
Cell Constants:	<i>a</i> =	1183.31(8) pm	
	<i>b</i> =	1503.29(10) pm	β = 105.512(4) $^\circ$
	<i>c</i> =	1508.50(11) pm	
	<i>V</i> = 2585.6(18) · 10 ⁶ pm ³ ; <i>Z</i> = 4		
Diffractionmeter:	Kappa APEX II (Area Diffraction System; BRUKER AXS); rotating anode; graphite monochromator; 50 kV; 40 mA; λ = 71.073 pm; Mo(K α ⁻)		
Temperature:	(-150 \pm 1) $^\circ$ C;	(123 \pm 1) K	
Remarks:	Refinements aborted due to severe disorder in the PNP-pincer ligand		

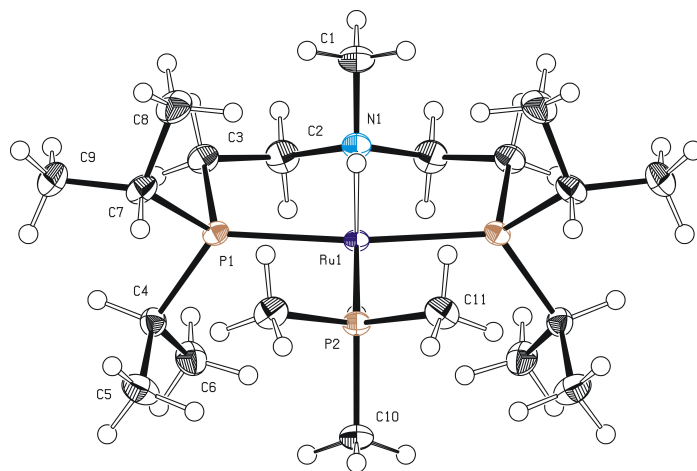
Compound 10

Figure S13. PLATON plot of **10** in the crystal with thermal ellipsoids drawn at the 50 % probability level.

Operator:	*** Herdtweck ***
Molecular Formula:	C ₂₀ H ₅₀ N P ₃ Ru
Crystal Color / Shape	Yellow fragment
Crystal Size	Approximate size of crystal fragment used for data collection: 0.33 × 0.41 × 0.43 mm
Molecular Weight:	498.59 a.m.u.

B Results and Discussion

F ₀₀₀ :	1064
Systematic Absences:	0kl: k+l≠2n; hk0: h≠2n
Space Group:	Orthorhombic <i>P nma</i> (I.T.-No.: 62)
Cell Constants:	Least-squares refinement of 9066 reflections with the programs "APEX suite" and "SAINT" [1,2]; theta range 2.26° < θ < 25.48°; Mo(K $\bar{\alpha}$); λ = 71.073 pm <i>a</i> = 1274.84(6) pm <i>b</i> = 1969.38(9) pm <i>c</i> = 1011.07(5) pm <i>V</i> = 2538.4(2) · 10 ⁶ pm ³ ; <i>Z</i> = 4; <i>D</i> _{calc} = 1.305 g cm ⁻³ ; Mos. = 0.71
Diffraction:	Kappa APEX II (Area Diffraction System; BRUKER AXS); rotating anode; graphite monochromator; 50 kV; 40 mA; λ = 71.073 pm; Mo(K $\bar{\alpha}$)
Temperature:	(-150±1) °C; (123±1) K
Measurement Range:	2.26° < θ < 25.48°; h: -15/15, k: -23/23, l: -11/11
Measurement Time:	2 × 5 s per film
Measurement Mode:	measured: 11 runs; 3964 films / scaled: 11 runs; 3964 films φ- and ω-movement; Increment: Δφ/Δω = 0.50°; dx = 50.0 mm
LP - Correction:	Yes [2]
Intensity Correction	No/Yes; during scaling [2]
Absorption Correction:	Multi-scan; during scaling; μ = 0.812 mm ⁻¹ [2] Correction Factors: T _{min} = 0.6549 T _{max} = 0.7452
Reflection Data:	74905 reflections were integrated and scaled 4700 reflections systematic absent and rejected 70205 reflections to be merged 2376 independent reflections 0.031 R _{int} : (basis <i>F</i> _o ²) 2376 independent reflections (all) were used in refinements 2252 independent reflections with <i>I</i> _o > 2σ(<i>I</i> _o) 97.7 % completeness of the data set 132 parameter full-matrix refinement 18.0 reflections per parameter

Solution:	Direct Methods [3]; Difference Fourier syntheses	
Refinement Parameters:	In the asymmetric unit: 15 Non-hydrogen atoms with anisotropic displacement parameters 2 Hydrogen atoms with isotropic displacement parameters	
Hydrogen Atoms:	In the difference map(s) calculated from the model containing all non-hydrogen atoms, not all of the hydrogen positions could be determined from the highest peaks. For this reason, the hydrogen atoms were placed in calculated positions ($d_{C-H} = 98, 99, 100$ pm). Isotropic displacement parameters were calculated from the parent carbon atom ($U_H = 1.2/1.5 U_C$). The hydrogen atoms were included in the structure factor calculations but not refined. The hydride atoms were found and allowed to refine freely.	
Atomic Form Factors:	For neutral atoms and anomalous dispersion [4]	
Extinction Correction:	no	
Weighting Scheme:	$w^{-1} = \sigma^2(F_o^2) + (a * P)^2 + b * P$ with a: 0.0214; b: 1.3854; P: $[\text{Maximum}(0 \text{ or } F_o^2) + 2 * F_c^2] / 3$	
Shift/Err:	Less than 0.002 in the last cycle of refinement:	
Resid. Electron Density:	+0.34 $e^- / \text{\AA}^3$; -0.32 $e^- / \text{\AA}^3$	
R1:	$\Sigma(F_o - F_c) / \Sigma F_o $	
$[F_o > 4\sigma(F_o)$; N=2252]:		= 0.0167
[all reflctns; N=2376]:		= 0.0183
wR2:	$[\Sigma w(F_o^2 - F_c^2)^2 / \Sigma w(F_o^2)^2]^{1/2}$	
$[F_o > 4\sigma(F_o)$; N=2252]:		= 0.0448
[all reflctns; N=2376]:		= 0.0473
Goodness of fit:	$[\Sigma w(F_o^2 - F_c^2)^2 / (\text{NO-NV})]^{1/2}$ = 1.126	
Remarks:	Refinement expression $\Sigma w(F_o^2 - F_c^2)^2$	

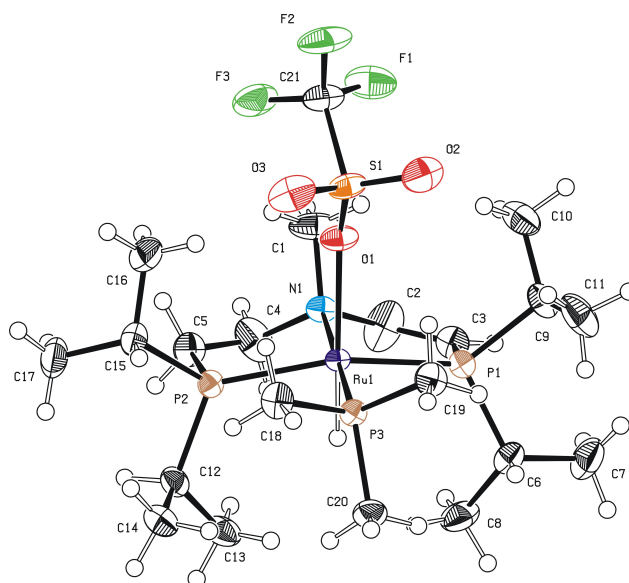
Compound 12

Figure S14. PLATON plot of **12** in the crystal with thermal ellipsoids drawn at the 50 % probability level.

Operator:	*** Herdtweck ***
Molecular Formula:	C ₂₁ H ₄₇ F ₃ N O ₃ P ₃ Ru S
Crystal Color / Shape	Yellow fragment
Crystal Size	Approximate size of crystal fragment used for data collection: 0.41 × 0.46 × 0.51 mm
Molecular Weight:	644.65 a.m.u.
F ₀₀₀ :	1344
Systematic Absences:	h0l: h+l≠2n; 0k0: k≠2n
Space Group:	Monoclinic <i>P</i> 2 ₁ / <i>n</i> (I.T.-No.: 14)
Cell Constants:	Least-squares refinement of 9349 reflections with the programs "APEX suite" and "SAINT" [1,2]; theta range 1.72° < θ < 25.32°; Mo(Kα ⁻); λ = 71.073 pm a = 1022.24(5) pm b = 1919.71(10) pm β = 103.351(2)° c = 1551.42(8) pm V = 2962.2(3) · 10 ⁶ pm ³ ; Z = 4; D _{calc} = 1.446 g cm ⁻³ ; Mos. = 0.71

Diffractometer:	Kappa APEX II (Area Diffraction System; BRUKER AXS); rotating anode; graphite monochromator; 50 kV; 40 mA; $\lambda = 71.073$ pm; Mo($K\alpha$)
Temperature:	(-100±1) °C; (173±1) K
Measurement Range:	$1.72^\circ < \theta < 25.32^\circ$; h: -12/12, k: -23/23, l: -18/18
Measurement Time:	2 × 2.50 s per film
Measurement Mode:	measured: 8 runs; 3027 films / scaled: 8 runs; 3027 films φ - and ω -movement; Increment: $\Delta\varphi/\Delta\omega = 0.50^\circ$; dx = 40.0 mm
LP - Correction:	Yes [2]
Intensity Correction	No/Yes; during scaling [2]
Absorption Correction:	Multi-scan; during scaling; $\mu = 0.803$ mm ⁻¹ [2] Correction Factors: $T_{\min} = 0.6126$ $T_{\max} = 0.7452$
Reflection Data:	81790 reflections were integrated and scaled 1379 reflections systematic absent and rejected 80411 reflections to be merged 5387 independent reflections 0.025 R_{int} : (basis F_o^2) 5387 independent reflections (all) were used in refinements 5218 independent reflections with $I_o > 2\sigma(I_o)$ 99.5 % completeness of the data set 310 parameter full-matrix refinement 17.4 reflections per parameter
Solution:	Direct Methods [3]; Difference Fourier syntheses
Refinement Parameters:	In the asymmetric unit: 33 Non-hydrogen atoms with anisotropic displacement parameters
Hydrogen Atoms:	In the difference map(s) calculated from the model containing all non-hydrogen atoms, not all of the hydrogen positions could be determined from the highest peaks. For this reason, the hydrogen atoms were placed in calculated positions ($d_{\text{C-H}} = 95, 98, 99, 100$ pm; $d_{\text{H-H}} = 154$ pm). Isotropic displacement parameters were calculated from the parent carbon atom ($U_{\text{H}} = 1.2/1.5 U_{\text{C}}$; $U_{\text{H}} = 1.2$

B Results and Discussion

	U _{tr}). The hydrogen atoms were included in the structure factor calculations but not refined.
Atomic Form Factors:	For neutral atoms and anomalous dispersion [4]
Extinction Correction:	no
Weighting Scheme:	$w^{-1} = \sigma^2(F_o^2) + (a*P)^2 + b*P$ with a: 0.0186; b: 2.5092; P: [Maximum(0 or F_o^2) + 2* F_c^2]/3
Shift/Err:	Less than 0.001 in the last cycle of refinement:
Resid. Electron Density:	+0.45 e ₀ /Å ³ ; -0.46 e ₀ /Å ³
R1:	$\Sigma(F_o - F_c) / \Sigma F_o $
[$F_o > 4\sigma(F_o)$; N=5218]:	= 0.0200
[all reflctns; N=5387]:	= 0.0209
wR2:	$[\Sigma w(F_o^2 - F_c^2)^2 / \Sigma w(F_o^2)^2]^{1/2}$
[$F_o > 4\sigma(F_o)$; N=5218]:	= 0.0493
[all reflctns; N=5387]:	= 0.0501
Goodness of fit:	$[\Sigma w(F_o^2 - F_c^2)^2 / (\text{NO} - \text{NV})]^{1/2}$ = 1.092
Remarks:	Refinement expression $\Sigma w(F_o^2 - F_c^2)^2$ Checkcif: PLAT360_ALERT_2_C Short C(sp3)-C(sp3) Bond C4-C5 1.43 Ang. [9]

Crystallographic references:

- [1] APEX suite of crystallographic software. APEX 2 Version 2008.4. Bruker AXS Inc., Madison, Wisconsin, USA (2008).
- [1a] CrysAlis Data Collection Software and Data Processing Software for Oxford Xcalibur diffractometer, Version 1.171, Oxford Diffraction Ltd., Oxfordshire, United Kingdom, (2005).
- [2] SAINT, Version 7.56a and SADABS Version 2008/1. Bruker AXS Inc., Madison, Wisconsin, USA (2008).
- [3] Altomare, A.; Cascarano, G.; Giacovazzo, C.; Guagliardi, A.; Burla, M. C.; Polidori, G.; Camalli M. "SIR92", *J. Appl. Cryst.* **1994**, 27, 435-436.
- [4] International Tables for Crystallography, Vol. C, Tables 6.1.1.4 (pp. 500-502), 4.2.6.8 (pp. 219-222), and 4.2.4.2 (pp. 193-199), Wilson, A. J. C., Ed., Kluwer Academic Publishers, Dordrecht, The Netherlands, 1992.
- [5] Sheldrick, G. M. "SHELXL-97", University of Göttingen, Göttingen, Germany, (1998).
- [6] Spek, A. L. "PLATON", A Multipurpose Crystallographic Tool, Utrecht University, Utrecht, The Netherlands, (2009).
- [7] L. J. Farrugia, "WinGX (Version 1.70.01 January 2005)", *J. Appl. Cryst.* **1999**, 32, 837-838.

- [8] a) The Cambridge Structural Database: a quarter of a million crystal structures and rising; Allen, F. H. *Acta Crystallogr.* **2002**, *B58*, 380-388. b) New Software for searching the Cambridge Structural Database and visualizing crystal structures; Bruno, I. J.; Cole, J. C.; Edgington, P. R.; Kessler, M.; Macrae, C. F.; McCabe, P.; Pearson, J.; Taylor, R. *Acta Crystallogr.* **2002**, *B58*, 389-397.
- [9] This shortened bond distance is indicative for a partial (~10%) but not resolvable disorder of the C=C double bond.

1.5.8 Computational results

DFT calculations. All calculations were performed with GAUSSIAN-03 Rev. C.02 using the density functional/Hartree-Fock hybrid model Becke3LYP and the split valence double- ζ (DZ) basis set 6-31+G**.^[40,41,42] The Ru atoms were described with a Stuttgart-RSC-ECP with a DZ description of the valence electrons.^[43] Geometry optimizations were run without symmetry or internal coordinate constraints. The optimized structures were verified as being true minima (NImag=0) or transition states (NImag=1) by analysis of negative eigenvalues in vibrational frequency calculations. Thermal corrections were carried out at standard conditions ($T = 298.15$ K, and $P = 1$ atmosphere). NBO analyses were performed with NBO

⁴⁰ Frisch, M. J.; Trucks, G. W.; Schlegel, H. B.; Scuseria, G. E.; Robb, M. A.; Cheeseman, J. R.; Montgomery, Jr., J. A.; Vreven, T.; Kudin, K. N.; Burant, J. C.; Millam, J. M.; Iyengar, S. S.; Tomasi, J.; Barone, V.; Mennucci, B.; Cossi, M.; Scalmani, G.; Rega, N.; Petersson, G. A.; Nakatsuji, H.; Hada, M.; Ehara, M.; Toyota, K.; Fukuda, R.; Hasegawa, J.; Ishida, M.; Nakajima, T.; Honda, Y.; Kitao, O.; Nakai, H.; Klene, M.; Li, X.; Knox, J. E.; Hratchian, H. P.; Cross, J. B.; Bakken, V.; Adamo, C.; Jaramillo, J.; Gomperts, R.; Stratmann, R. E.; Yazyev, O.; Austin, A. J.; Cammi, R.; Pomelli, C.; Ochterski, J. W.; Ayala, P. Y.; Morokuma, K.; Voth, G. A.; Salvador, P.; Dannenberg, J. J.; Zakrzewski, V. G.; Dapprich, S.; Daniels, A. D.; Strain, M. C.; Farkas, O.; Malick, D. K.; Rabuck, A. D.; Raghavachari, K.; Foresman, J. B.; Ortiz, J. V.; Cui, Q.; Baboul, A. G.; Clifford, S.; Cioslowski, J.; Stefanov, B. B.; Liu, G.; Liashenko, A.; Piskorz, P.; Komaromi, I.; Martin, R. L.; Fox, D. J.; Keith, T.; Al-Laham, M. A.; Peng, C. Y.; Nanayakkara, A.; Challacombe, M.; Gill, P. M. W.; Johnson, B.; Chen, W.; Wong, M. W.; Gonzalez, C.; and Pople, J. A.; Gaussian, Inc., Wallingford CT, 2004.

⁴¹ (a) Vosko, S. H.; Wilk, L.; Nusair, M. *Can. J. Phys.* **1980**, *58*, 1200-1211. (b) Lee, C.; Yang, W.; Parr, R. G. *Phys. Rev. B.* **1988**, *37*, 785-789. (c) Becke, A. D. *J. Chem. Phys.* **1993**, *98*, 5648-5652.

⁴² (a) Hehre, W. J.; Ditchfield, R.; Pople, J. A. *J. Chem. Phys.* **1972**, *56*, 2257-2261. (b) Francl, M.M.; Pietro, W.J.; Hehre, W.J.; Binkley, J.S.; Gordon, M.S.; DeFrees D.J. and Pople, J.A. *J. Chem. Phys.* **1982**, *77*, 3654-3665.

⁴³ Dolg, M.; Stoll, H.; Preuss, H.; Pitzer, R.M. *J. Phys. Chem.* **1993**, *97*, 5852-5859.

B Results and Discussion

V3.1 as implemented in GAUSSIAN-03.^[44] Orbital expressions were visualized with GaussView via cube files generated from formatted checkpoint files.^[45]

Coordinates for the optimized geometries of 2^{Me} , $\text{TS}(2^{\text{Me}}/1^{\text{Me}}\text{-H}_2)$, 1^{Me}-H_2 , $\text{TS}(1^{\text{Me}}\text{-H}_2/1^{\text{Me}})$, 1^{Me} , $\text{TS}(1^{\text{Me}}/8^{\text{Me}})$, $\text{TS}(8^{\text{Me}}/3^{\text{Me}}\text{-H}_2)$, 3^{Me}-H_2 , $\text{TS}(3^{\text{Me}}\text{-H}_2/3^{\text{Me}})$, 3^{Me} , **1**, and **3** is free of charge via the internet at <http://pubs.acs.org>.

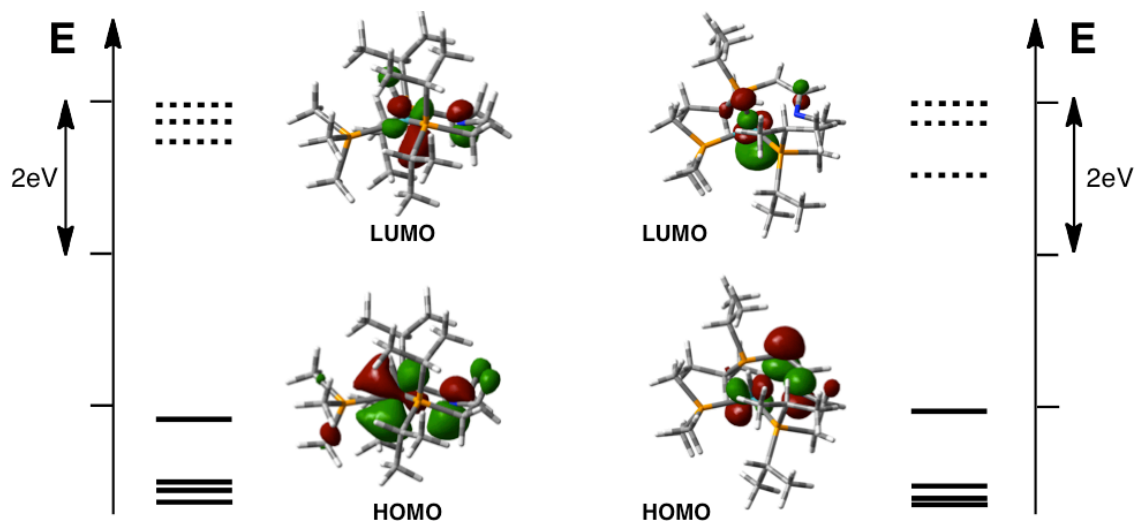


Figure S28. Frontier orbital schemes and graphical HOMO and LUMO representations of **1** (left) and **3** (right), respectively.

Table S13. Single point calculations in the triplet state.

Compound	$E_{\text{singlet}} - E_{\text{triplet}}$ [kcal/mol]
2^{Me}	-68.3
1^{Me}-H_2	-66.6
1^{Me}	-43.5
8^{Me}	-62.3
3^{Me}-H_2	-73.6
3^{Me}	-39.9

⁴⁴ Glendening, E. D.; Reed, A. E.; Carpenter, J. E.; Weinhold, F., NBO Version 3.1.

⁴⁵ Dennington II, R.; Keith, T.; Millam, J. *GaussView V4.1*; Semichem Inc., Shawnee Mission, KS, 2007.

2 Unpublished Results

2.1 The Mechanism of Borane-Amine Dehydrocoupling with Bifunctional Ruthenium Catalysts

A. Friedrich, S. Schneider

2.1.1 Introduction

The dehydrogenation of borane amines, particularly of parent $\text{H}_3\text{N-BH}_3$ (AB), has recently attracted considerable interest owing to the attractiveness of such compounds, both as H_2 -vectors for chemical hydrogen storage and precursors for the synthesis of novel B-N polymeric materials.^[1,2] AB dehydrogenation, a strongly exothermic reaction, has been examined by thermal degradation in the solid state, in solution, and in silico in the gas phase.^[1] However, the onset of H_2 release is difficult to control, rendering this approach less feasible for hydrogen storage.^[3] Furthermore, the polymeric products obtained from thermal AB dehydrocoupling are generally structurally ill-defined solids with varying degrees of dehydrogenation and cross-linking.^[2] Hence, catalysis offers the possibility of control over H_2 -release kinetics and polymer microstructure.

Besides acid,^[4] base,^[5] or frustrated Lewis-pair^[6] catalysis the use of main group^[7] and particularly transition metal (TM) catalysts^[8] for AB dehydrogenation has been extensively

¹ (a) Stephens, F. H.; Pons, V.; Baker, R. T. *DaltonTrans.* **2007**, 2613. (b) Hamilton, C. W.; Baker, R. T.; Staubitz, A.; Manners, I. *Chem. Soc. Rev.* **2009**, *38*, 279. (c) Smythe, N. C.; Gordon, J. C. *Eur. J. Inorg. Chem.* **2010**, 509. (d) Staubitz, A.; Robertson, A. P. M.; Manners, I. *Chem. Rev.* **2010**, *110*, 4079.

² (a) Clark, T. J.; Lee, K.; Manners, I. *Chem. Eur. J.* **2006**, *12*, 8634. (b) Staubitz, A.; Robertson, A. P. M.; Sloan, M. E.; Manners, I. *Chem. Rev.* **2010**, *110*, 4023.

³ Bluhm, M. E.; Bradley, M. G.; Butterick III, R.; Kusari, U.; Sneddon, L. G. *J. Am. Chem. Soc.* **2006**, *128*, 7748.

⁴ Stephens, F. H.; Baker, R. T.; Matus, M. H.; Grant, D. J.; Dixon, D. A. *Angew. Chem.* **2007**, *119*, 760; *Angew. Chem. Int. Ed.* **2007**, *46*, 746.

⁵ Himmelberger, D. W.; Yoon, C. W.; Bluhm, M. E.; Carroll, P. J.; Sneddon, L. G. *J. Am. Chem. Soc.* **2009**, *131*, 14101.

⁶ Miller, A. J. M.; Bercaw, J. E. *Chem. Commun.* **2010**, *46*, 1709.

⁷ Spielmann, J.; Bolte, M.; Harder, S. *Chem. Commun.* **2009**, 6934. (b) Liptrot, D. J.; Hill, M. S.; Mahon, M. F.; MacDougall, D. J. *Chem. Eur. J.* **2010**, *16*, 8508.

⁸ (a) Jaska, C. A.; Temple, K.; Lough, A. J.; Manners, I. *J. Am. Chem. Soc.* **2003**, *125*, 9424. (b) Denney, M. C.; Pons, V.; Hebden, T. J.; Heinekey, D. M.; Goldberg, K. I. *J. Am. Chem. Soc.* **2006**, *128*, 12048. (c) Keaton, R. J.; Blacquiere, J. M.; Baker, R. T. *J. Am. Chem. Soc.* **2007**, *129*, 1844. (d) Cheng, F.; Ma, H.; Li, Y.; Chen, J. *Inorg. Chem.* **2007**, *46*, 788. (e) Fulton, J. F.; Linehan, J. C.; Autrey, T.; Balasubramanian, M.; Chen, Y.; Szymczak, N. K. *J. Am. Chem. Soc.* **2007**, *129*, 11936. (f) Pun, D.; Lobkovsky, E.; Chirik, P. J. *Chem. Commun* **2007**, 3297. (g) Yan, J.-M.; Zhang, X.-B.; Han, S.; Shioyama, H.; Xu, Q. *Angew. Chem.* **2008**, *120*, 2319; *Angew. Chem. Int. Ed.* **2008**, *47*, 2287. (h) Pons, V.; Baker, R. T.; Szymczak, N. K.; Heldebrant, D. J.; Linehan, J. C.; Matus, M. H.;

studied over the last years. However, mechanistic information about TM catalysed AB dehydrocoupling remains scarce. Several stable complexes with coordinated borane-amine adducts, aminoboranes, or dehydrocoupling products via the B-H hydrides could be structurally characterized.^[9,10] This approach provides valuable models for the interaction of the substrate or potential intermediates with catalyst species but no direct mechanistic insights. The mechanism of the highly active catalyst of Goldberg and Heinekey,^[8b] which utilized Brookhart's iridium POCOP pincer complex $[\text{Ir}(\text{H})_2\{\text{C}_6\text{H}_3\text{-}1,3\text{-(OPtBu}_2)_2\}]$,^[11] was probed computationally.^[12] In this study, the release of free aminoborane $\text{H}_2\text{N-BH}_2$ was proposed upon AB dehydrogenation while metal centered B-N coupling was considered to be unlikely. Likewise, for Baker's catalyst,^[8c] a mixture of $[\text{Ni}(\text{COD})_2]$ and Enders' carbene $\text{CN}(\text{Ph})\text{NC}(\text{Ph})\text{NPh}$, a quantumchemical study suggested a mechanism with release of free aminoborane.^[13] $\text{H}_2\text{N-BH}_2$, isoelectronic with ethylene, is a highly reactive molecule which readily oligomerizes in solution even at low temperatures.^[14]

Grant, D. J.; Dixon, D. A. *Chem. Commun.* **2008**, 6597. (i) Blaquiere, N.; Diallo-Garcia, S.; Gorelsky, S. I.; Black, D. A.; Fagnou, K. *J. Am. Chem. Soc.* **2008**, *130*, 14034. (j) Käß, M.; Friedrich, A.; Drees, M.; Schneider, S. *Angew. Chem.* **2009**, *121*, 922; *Angew. Chem. Int. Ed.* **2009**, *48*, 905. (k) Sloan, M. E.; Clark, T. J.; Manners, I. *Inorg. Chem.* **2009**, *48*, 2429. (l) Zahmakiran, M.; Tristany, M.; Philippot, K.; Fajerweg, K.; Özkar, S.; Chaudret, B. *Chem. Commun.* **2010**, 2938. (m) Kim, S.-K.; Han, W.-S.; Kim, T.-J.; Kim, T.-Y.; Nam, S. W.; Mitoraj, M.; Piekos, L.; Michalak, A.; Hwang, S.-J.; Kang, S. O. *J. Am. Chem. Soc.* **2010**, *132*, 9954. (n) Conley, B. L.; Williams, T. J. *Chem. Commun.* **2010**, *46*, 4815.

⁹ Alcaraz, G.; Sabo-Etienne, S. *Angew. Chem.* **2010**, *122*, 7326; *Angew. Chem. Int. Ed.* **2010**, *49*, 7170.

¹⁰ (a) Douglas, T. M.; Chaplin, A. B.; Weller, A. S. *J. Am. Chem. Soc.* **2008**, *130*, 14432. (b) Dallanegra, R.; Chaplin, A. B.; Weller, A. S. *Angew. Chem.* **2009**, *121*, 7007; *Angew. Chem. Int. Ed.* **2009**, *48*, 6875. (c) Douglas, T. M.; Chaplin, A. B.; Weller, A. S.; Yang, X.; Hall, M. B. *J. Am. Chem. Soc.* **2009**, *131*, 15440. (d) Chaplin, A. B.; Weller, A. S. *Angew. Chem.* **2010**, *122*, 473; *Angew. Chem. Int. Ed.* **2010**, *49*, 581. (e) Dallanegra, R.; Chaplin, A. B.; Tsim, J.; Weller, A. S. *Chem Commun.* **2010**, *46*, 3092. (f) Chaplin, A. B.; Weller, A. S. *Inorg. Chem.* **2010**, *49*, 1111. (g) Alcaraz, G.; Vendier, L.; Clot, E.; Sabo-Etienne, S. *Angew. Chem.* **2010**, *122*, 930; *Angew. Chem. Int. Ed.* **2010**, *49*, 918. (h) Yang, C. Y.; Thompson, A. L.; Aldridge, S. *Angew. Chem.* **2010**, *122*, 933; *Angew. Chem. Int. Ed.* **2010**, *49*, 921.

¹¹ Göttker-Schnetmann, I.; White, P.; Brookhart, M. *J. Am. Chem. Soc.* **2004**, *126*, 1804.

¹² Paul, A.; Musgrave, C. B. *Angew. Chem.* **2007**, *119*, 8301; *Angew. Chem. Int. Ed.* **2007**, *46*, 8153.

¹³ Yang, X.; Hall, M. B. *J. Am. Chem. Soc.* **2008**, *130*, 1798.

¹⁴ (a) Kwon, C. T.; McGee, H. A. *Inorg. Chem.* **1970**, *9*, 2458. (b) Wang, J. S.; Geneangel, R. A. *Inorg. Chim. Acta* **1988**, *148*, 185.

the iridium catalyst. This point is of fundamental importance for both hydrogen storage and B-N polymer formation: 1. It possibly provides a rationale that the iridium catalyst produces 1 equiv. H₂ per AB (room temp.) and polyaminoboranes while the nickel catalyst releases more than 2 equiv. H₂ (60 °C) resulting in polyborazine as coupling product. 2. A metal centred B-N coupling process is more likely to enable versatile control over the polymer microstructure by catalyst ligand design.

Some more mechanistic information has been obtained from the dehydrocoupling of Me₂HN-BH₃ (Me₂AB). Since the examination of Me₂AB dehydrocoupling is not hampered by the formation of polymeric, insoluble B-N products it can be easily studied by means of solution ¹¹B NMR. Hence, several groups examined this reaction as a possible general model for borane-amine dehydrogenation.^[8a,e,f,k,9a,b,c,e,17] Although initially dismissed in a computational study for titanocene catalyzed Me₂AB dehydrocyclization,^[18] the involvement of linear diborazane Me₂HN-BH₂-NMe₂-BH₃ as an intermediate was demonstrated for several catalysts spectroscopically, by kinetic studies, and by isolation of metal complexes.^[10c-f,17h,k] The recent synthesis of parent H₃N-BH₂-NH₂-BH₃ further fuels speculation about linear B-N intermediate and product formation for AB dehydrogenation, as well.^[19] In addition, dehydrocoupling of AB or MeH₂N-BH₃ (MeAB) and AB/MeAB co-dehydropolymerization with several catalysts has been shown to give linear and cyclic polyaminoboranes (RHN-BH₂)_n (R = H, Me) of medium to high molecular weight,^[20] pointing towards the relevance of

¹⁷ (a) Jaska, C. A.; Temple, K.; Lough, A. J.; Manners, I. *Chem. Commun.* **2001**, 962. (b) Jaska, C. A.; Manners, I. *J. Am. Chem. Soc.* **2004**, *126*, 1334. (c) Jaska, C. A.; Manners, I. *J. Am. Chem. Soc.* **2004**, *126*, 9776. (d) Chen, Y.; Fulton, J. L.; Linehan, J. C.; Autrey, T. *J. Am. Chem. Soc.* **2005**, *127*, 3254. (e) Clark, T. J.; Russell, C. A.; Manners, I. *J. Am. Chem. Soc.* **2006**, *128*, 9582. (f) Jiang, Y.; Berke, H. *Chem Commun.* **2007**, 3571. (g) Jiang, Y.; Blacque, O.; Fox, T.; Frech, C. M.; Berke, H. *Organometallics* **2009**, *28*, 5493. (h) Friedrich, A.; Drees, M.; Schneider, S. *Chem. Eur. J.* **2009**, *15*, 10339. (i) Rousseau, R.; Schenter, G. K.; Fulton, J. L.; Linehan, J. C.; Linehan, M. K.; Engelhard, M. K.; Autrey, T. *J. Am. Chem. Soc.* **2009**, *131*, 10516. (j) Kawano, Y.; Uruichi, M.; Shimoi, M.; Taki, S.; Kawaguchi, T.; Kakizawa, T.; Ogino, H. *J. Am. Chem. Soc.* **2009**, *131*, 14946. (k) Sloan, M. E.; Staubitz, A.; Clark, T. J.; Russell, C. A.; Lloyd-Jones, G. C.; Manners, I. *J. Am. Chem. Soc.* **2010**, *132*, 3831.

¹⁸ Luo, Y.; Ohno, K. *Organometallics* **2007**, *26*, 3597.

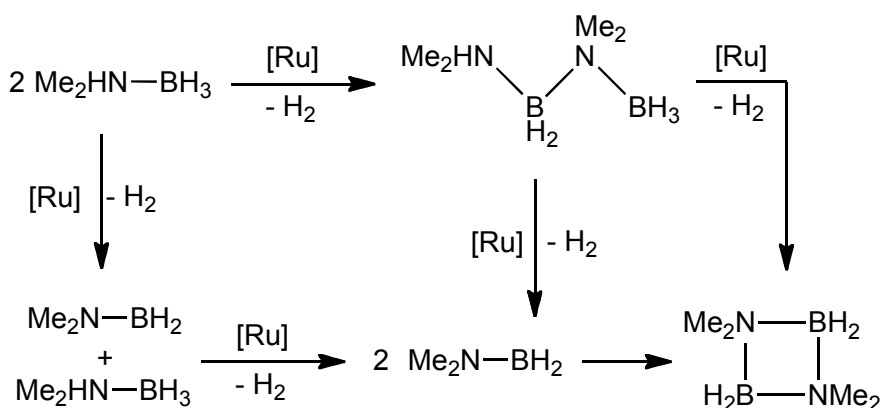
¹⁹ Chen, X.; Zhao, J.-C.; Shore, S. G. *J. Am. Chem. Soc.* **2010**, *132*, 10658.

²⁰ (a) Staubitz, A.; Presa Soto, A.; Manners, I. *Angew. Chem.* **2008**, *120*, 6308; *Angew. Chem. Int. Ed.* **2008**, *47*, 6212. (b) B. L. Dietrich, K. I. Goldberg, D. M. Heinekey, T. Autrey, J. C. Linehan, *Inorg. Chem.* **2008**, *47*, 8583.

linear oligo- and polyborazanes in AB dehydrocoupling, as well. However, the mechanism for the formation of such linear intermediates and products in metal catalyzed AB dehydrocoupling remain unclear.

We recently reported the dehydrocoupling of AB with unprecedented activities utilizing ruthenium amido complex $[\text{RuH}(\text{PMe}_3)(\text{PNP})]$ (**1**, $\text{PNP} = \text{N}(\text{CH}_2\text{CH}_2\text{P}i\text{Pr}_2)$).^[8j] Furthermore, dehydrocoupling of MeAB results in the formation of a high molecular weight polyaminoborane ($M_w \approx 450.000$) with a relatively narrow distribution ($\text{PDI} = 2.6$).^[20c] We further studied the dehydrodimerization of Me₂AB with precatalyst **1**.^[17h] Based on spectroscopic, kinetic, and computational results a mechanistic pathway for the formation of cyclodiaminoborane ($\text{Me}_2\text{N}-\text{BH}_2$)₂ was proposed, suggesting for both Me₂AB dehydrogenation and B-N coupling to be catalyzed (Scheme 2).

Scheme 2. Proposed pathway for Me₂AB dehydrodimerization with precatalyst **1**.^[17h]



Fagnou and co-workers reported comparable activities for AB dehydrogenation using the strongly related amino precatalyst $[\text{Ru}(\text{Cl})_2(i\text{Pr}_2\text{PCH}_2\text{CH}_2\text{NH}_2)_2]$ and 30 equiv. of base ($\text{KO}t\text{Bu}$) as an activator.^[8i] The authors proposed a possible catalytic cycle supported by DFT calculations with release of free $\text{H}_2\text{N}-\text{BH}_2$ by concerted H^+/H^- transfer to a ruthenium amido catalyst species and H_2 elimination from the resulting resulting $\text{Ru}(\text{H})-\text{N}(\text{H})$ hydrido amine species as rate-determining step (r.d.s.). While such a bifunctional mechanism would be in qualitative agreement with the high kinetic isotope effects found with our catalyst upon deuteration of both the N- and the B-termini of AB, some observations remain unaccounted

for: 1. While similarly high barriers were found for H₂-loss from [Ru(H)₂PMe₃(PNP^H)] (**2**, PNP^H = HN(CH₂CH₂PiPr₂)) both experimentally and computationally,^[8j,21] the resulting slow rates are incongruent with the observed rapid borane-amine dehydrogenation. 2. A mechanism with off-catalyst B-N coupling does not explain our observation of linear aminoborane products and intermediates in MeAB and Me₂AB dehydrocoupling.

In this manuscript, we report a comprehensive experimental and computational study to clarify the mechanism of borane-amine dehydrocoupling with our ruthenium amido catalyst system. A catalytic cycle is proposed which fully accounts for the mechanism of AB dehydrogenation and B-N coupling, *both* being catalyst mediated. Most importantly, this outer-sphere, bifunctional mechanism suggests a fundamentally new initial interaction of the catalyst with the substrate via the *N*-terminal protons resulting in a particularly low barrier for the r.d.s.

2.1.2 Results

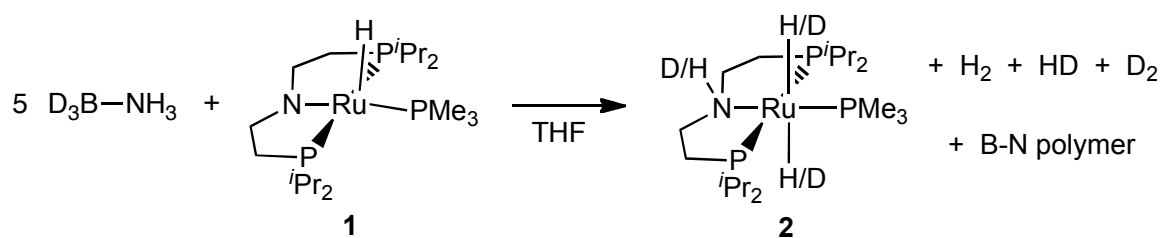
Qualitative mechanistic examinations: H⁺/H⁻ exchange

The interaction of the catalyst with the substrate was probed by monitoring the dehydrogenation of partially deuterated AB with ¹H NMR and by the application of model substrates with blocked *B*- (H₃N-BEt₃) and *N*-termini (Me₃N-BH₃), respectively. Besides of the KIE's, the use of deuterated substrates can further be utilized to examine the hydrogen transfer pathways as a mechanistic probe. For a mechanism with regioselective, concerted H⁺/H⁻ transfer from AB to **1** and intramolecular H₂ elimination from resulting **2**, dehydrogenation of partially deuterated substrates H₃N-BD₃ or D₃N-BH₃ should yield HD exclusively.^[22] However, dehydrocoupling of H₃N-BD₃ with precatalyst **1** (20 mol-%) in a sealed tube reveals the formation of all isotopomers of H₂ (H₂, HD, and D₂) and of **2** with respect to the N-H and both Ru-H hydrogen atoms as judged by ¹H NMR spectra (Scheme 3).

²¹ (a) Friedrich, A.; Drees, M.; Schmedt auf der Günne, J.; Schneider, S. *J. Am. Chem. Soc.* **2009**, *131*, 17552. (b) Friedrich, A.; Drees, M.; Käß, M.; Herdtweck, E.; Schneider, S. *Inorg. Chem.* **2010**, *49*, 5482.

²² H₂-loss from an intermediate amido dihydrogen complex [Ru(H₂)(H)(PMe₃)(PNP)] was calculated to be almost barrierless ($\Delta G^\ddagger = 1.8$ kcal/mol).^[21]

Scheme 3. H/D scrambling during dehydrocoupling of AB with precatalyst **1** in a sealed tube.



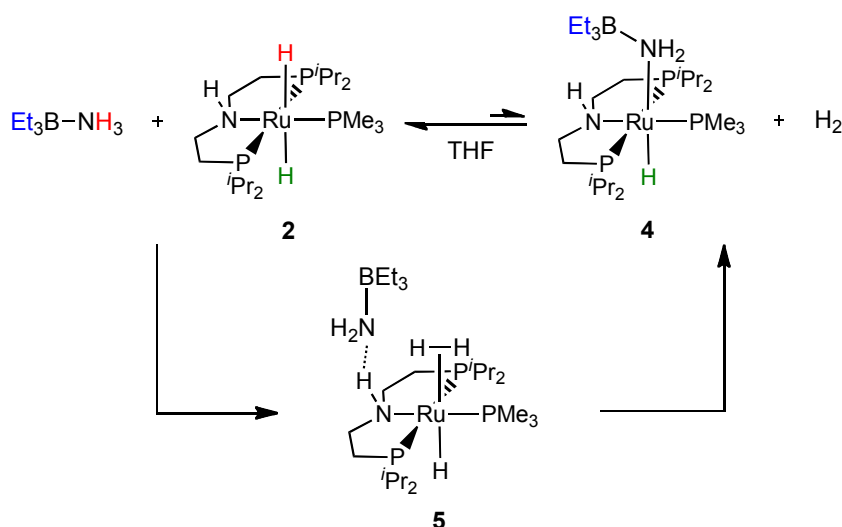
We have recently shown, that Brønstedt acids such as water rapidly exchange protons with one of the hydride ligand in dihydrido amine complex **2**.^[21a] This exchange process is highly stereoselective in favour of the hydride ligand which is in *syn*-position to the N-H proton, owing to considerable stabilization of the transition state by hydrogen bonding with OH_2 .^[23] Therefore, the isotopomeric hydrogen mixture from the sealed $\text{H}_3\text{N-BD}_3$ dehydrogenation experiment could be a result of rapid scrambling of initially formed HD catalyzed by **2** in combination with the boraneamine *N*-terminal Brønstedt acid.

Under an argon atmosphere a mixture of **2** and $\text{H}_3\text{N-BEt}_3$ exhibits a small equilibrium concentration ($< 5 \%$) of a new compound that can be assigned to boraneamido complex $[\text{Ru}(\text{NH}_2\text{-BEt}_3)(\text{H})\text{PMe}_3(\text{PNP}^H)]$ (**4**) (Scheme 4). As in the case of water, a 2D ^1H EXSY NMR spectrum of this mixture reveals stereoselective exchange of the $\text{H}_3\text{N-BEt}_3$ N-H protons with the Ru-H hydride of **2**, which is in *syn*-position to the pincer N-H proton. In comparison, in an equimolar mixture of tertiary amine complex $[\text{Ru}(\text{H})_2\text{PMe}_3(\text{PNP}^{Me})]$ (**3**) with $\text{H}_3\text{N-BEt}_3$ the corresponding boraneamido complex is not observed and no $\text{NH}_3/\text{Ru-H}$ exchange is detected by 2D 1H EXSY NMR on the NMR timescale ($\tau_m = 1 \text{ s}$). Furthermore, an equimolar mixture of **2** with borane amine adduct $\text{Me}_3\text{N-BH}_3$ does not indicate any reaction by ^1H , ^{31}P , and ^{11}B . These results can be explained by protonation of the ruthenium hydride ligand of **2** by the borane-amine resulting in transient dihydrogen complex $[\text{Ru}(\text{H}_2)(\text{H})\text{PMe}_3(\text{PNP}^H)][\text{NH}_2\text{-BEt}_3]$ (**5**, Scheme 4). This intermediate possibly accounts for H/D scrambling. However, H/D scrambling must proceed with much smaller rates than AB dehydrogenation, since considerably different KIE's were found for $\text{H}_3\text{N-BD}_3$ and $\text{D}_3\text{N-BH}_3$, respectively. Again, his interpretation would be in agreement with **2** representing the catalyst resting state and hydride protonation from the substrate *N*-terminus being the r.d.s, while the

²³ Inversion of the ligand backbone by ligand N-H exchange with Brønstedt acid at considerably slower rates ultimately results in exchange of both hydride ligands with the acid.^[21a]

further proton transfer proceeds more rapidly. Accordingly, no interaction of **2** with *B*-terminal hydrogen was found. Furthermore, the stereoselectivity of this exchange and the absence of rapid exchange for **3** strongly indicate stabilization of the borane-amide anion with the pincer ligand secondary amine group, rendering the reaction in Scheme 4 less favorable for **3** both kinetically and thermodynamically.

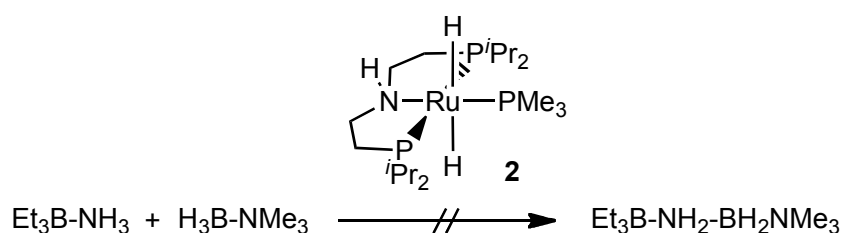
Scheme 4. Reaction of **2** with $\text{H}_3\text{N-BEt}_3$ and proposed mechanism via a dihydrogen complex **5**. Colours indicate selected chemical exchange cross peaks observed by 2D ^1H EXSY NMR.



Qualitative mechanistic examinations: Cross coupling experiment with *N*- and *B*-blocked substrates

A possible pathway for the formation of linear dehydrocoupling products (vide infra) could be the direct catalytic head-to-tail dehydrocoupling of two borane-amine substrate molecules. As a qualitative probe, we therefore run a cross-coupling experiment by mixing $\text{Me}_3\text{N-BH}_3$ and $\text{H}_3\text{N-BEt}_3$ in presence of catalyst **2** (1 mol-%). However, over several hours at room temperature no reaction was observed by ^{11}B NMR (Scheme 5). This result indicates, that proton and hydride transfer from the same substrate molecule to the catalyst are required.

Scheme 5. Cross-coupling experiment of $\text{Me}_3\text{N-BH}_3$ and $\text{H}_3\text{N-BEt}_3$ in the presence of **2**.



Qualitative mechanistic examinations: Aminoborane trapping

The possible release of free aminoborane $\text{H}_2\text{N-BH}_2$ as a step in the mechanism was examined by a trapping experiment with cyclohexene, as proposed by Baker and co-workers.^[8h] AB dehydrocoupling with precatalyst **1** in the presence of cyclohexene (21 equiv. with respect to AB) shows no trapping product in the ^{11}B NMR spectrum within the time frame of the dehydrocoupling reaction (until the starting material is no longer observed by ^{11}B NMR spectroscopy). However, beside small amounts of polyborazine, no signal for borazine was observed in the white suspension, as was always observed without addition of cyclohexene. After 20 h at room temperature, a ^{11}B NMR signal of borazine and a broad peak of $\text{H}_2\text{N-BCy}_2$ at 48.4 ppm appeared, indicating rearrangement processes in the reaction solution. In contrast, AB dehydrocoupling with catalyst **3** in the presence of cyclohexene (21 equiv. with respect to AB) results in the formation of $\text{H}_2\text{N-BCy}_2$ in considerable amounts within the time frame of the dehydrocoupling reaction, evidenced also by the broad ^{11}B NMR peak at 48.4 ppm (Figure S1, B2.1.6). In addition, borazine and small amounts of **A** are detected by ^{11}B NMR spectroscopy, as was found without additional olefin. This result can be interpreted as trapping of free aminoborane, released during AB dehydrogenation with ruthenium catalyst **3**, by a hydroboration of cyclohexene. However, both trapping experiments should be considered with care, due to the observed rearrangement processes in solution and the different reaction conditions compared with H_2 release kinetic experiments. These are particularly very low substrate concentrations, due to solubility properties and the unknown influence of **1** or **3** on catalysing the hydroboration reaction.

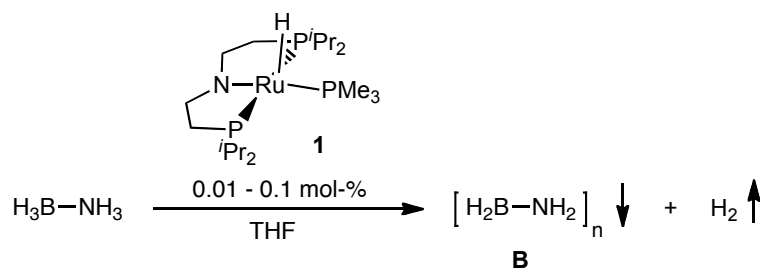
Kinetic studies: Dehydrocoupling of AB with $[\text{RuH}(\text{PMe}_3)(\text{PNP})]$ (**1**)

The kinetics of AB dehydrogenation in THF using amido precatalyst **1** was studied by volumetric measurement of H_2 release with an eudiometer. ^{11}B NMR monitoring of the same reaction in a sealed (*J-Young*) NMR tube reveals considerably slower reaction rates, possibly indicating inhibition upon H_2 build-up. Addition of the catalyst to a solution of AB results in vigorous evolution of H_2 and precipitation of colourless polyaminoborane **B**, which was insoluble in all common organic solvents (vide infra). Upon monitoring AB dehydrocoupling with **1** (20 mol-%) by ^1H NMR amine complex **2** is initially observed, exclusively.^[24] These

²⁴ At higher substrate conversions, catalyst deactivation product $[\text{Ru}(\text{H})(\text{PMe}_3)\{\mu\text{-H}(\text{H})(\text{H}_2\text{N})\text{B}(\text{N}(\text{CH}_2\text{CH}_2\text{P}i\text{Pr}_2)_2)\}]$ (**6**) is also observed by NMR.^[17h]

observation could indicate that **2** represents the catalytic resting state. Ex-situ solution ^{11}B NMR examination reveals full conversion of the substrate and small amounts of **A** and borazine. The latter accounts for the release of slightly more than 1 equiv. of H_2 per substrate. As a general trend, higher catalyst loadings result in the formation of more borazine at identical initial substrate concentrations $[\text{AB}]_0$.

Scheme 6. Dehydrocoupling of AB with precatalyst **1**.



Results with 0.54 M substrate solutions and catalyst loadings of 0.01 and 0.1 mol-%, respectively, had been reported in a preceding communication.^[8j] Turnover numbers (TON) around 8300 and turnover frequencies (TOF) around 20 s^{-1} were obtained, demonstrating the exceptional activities of this system. In the present study the initial substrate concentrations $[\text{AB}]_0$ (0.25 – 2.5 M) and catalyst loadings $[\mathbf{1}]_0$ (0.01 – 0.1 mol-%) were varied over a wider range (Figure 1). As a general trend, the TON can be maximized by raising $[\text{AB}]_0$ and lowering $[\mathbf{1}]_0$. For example, with $[\text{AB}]_0 = 2.5 \text{ M}$ and $[\mathbf{1}]_0 = 1 \cdot 10^{-4} \text{ M}$ a $\text{TON} \geq 10000$ can be achieved. The reaction orders in substrate and catalyst for the H_2 evolution were determined by the initial rate method.^[25,26] Initial rate measurements reveal a first order dependence in catalyst and a broken reaction order in substrate ($[\text{AB}]^{1.7}$). However, reactions with small catalyst loadings and low substrate concentrations indicate a short initiation period. Hence, initial rate measurement will not give information about the reaction at a latter stage.

²⁵ James E. House in *Principles of Chemical Kinetics*, 2nd Edition, Academic Press, **2007**, pp. 83.

²⁶ The concentration of AB was derived by the idealized stoichiometry for the reaction in Scheme 6, which should be a good approximation for low conversions. The small amount of H_2 formation from borazine production has been neglected in this expression.

B Results and Discussion

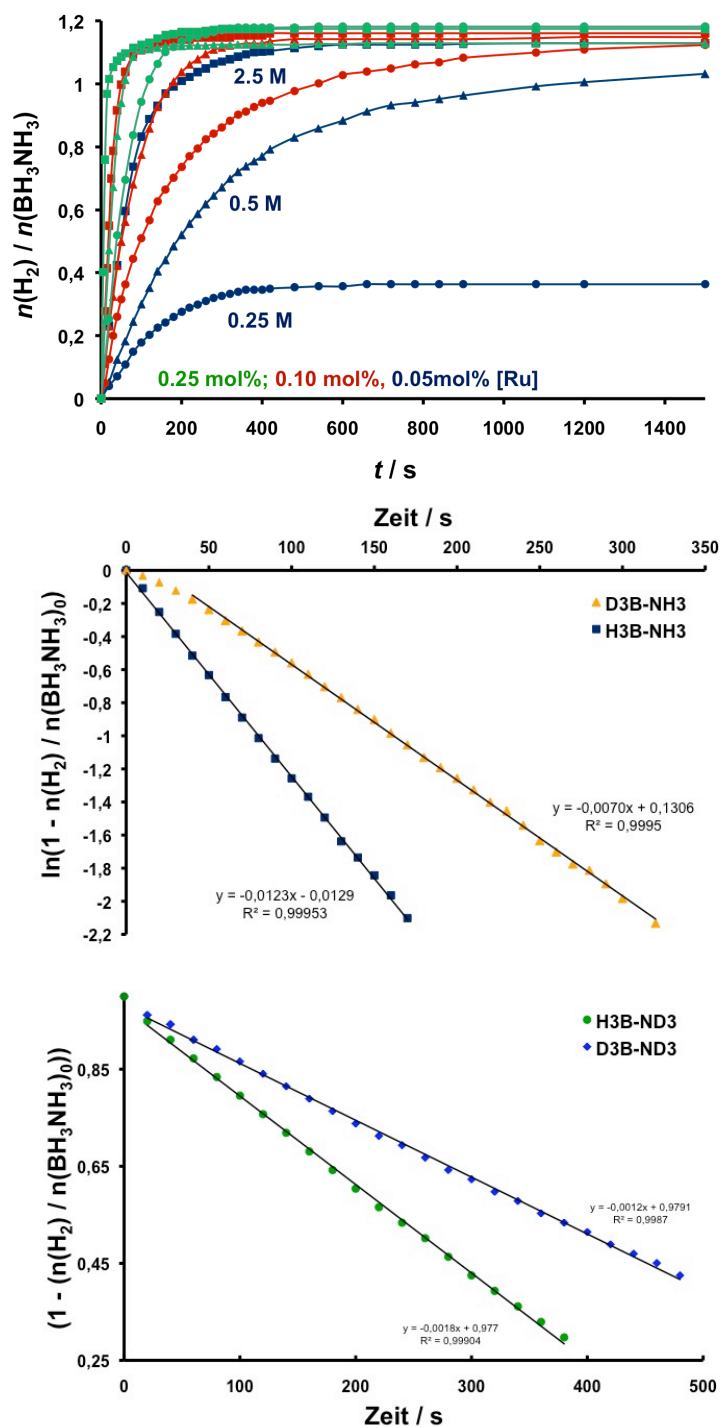


Figure 1. Kinetic plots of AB dehydrogenation using precatalyst **1** (above), first order plot of $\text{H}_3\text{N-BH}_3$ and $\text{H}_3\text{N-BD}_3$ ($[\text{AB}]_0 = 0.54 \text{ M}$; $[\mathbf{1}]_0 = 0.0005 \text{ M}$) dehydrogenation (middle) and zero order plot of $\text{D}_3\text{N-BH}_3$ and $\text{D}_3\text{N-BD}_3$ ($[\text{AB}]_0 = 0.54 \text{ M}$; $[\mathbf{1}]_0 = 0.0005 \text{ M}$) dehydrogenation (bottom).

A plot of $\ln[\text{AB}]$ versus time resulted in linear plots over more than one half-life for a wide range of catalyst and substrate initial concentrations, suggesting first order dependence in

substrate. From the slope of these plots, empirical kinetic constants were derived according to the rate law:

$$r_{\text{H}_2} = k_{\text{obs}} [\text{Ru}]_0 [\text{AB}] \quad (\text{Eq. 1})$$

For the smaller $[\text{AB}]_0$ concentrations (0.25 M and 0.5 M) and higher catalyst loadings (0.25 mol-% and 0.1 mol-%) this evaluation gives congruent results, with k_{obs} around 30(2) $\text{M}^{-1}\text{s}^{-1}$ (Table 1, entries 2, 3, 5, 6). However, for higher $[\text{AB}]_0$ concentrations (2.5 M and 1 M) and lower catalyst loadings (0.05 mol-%), slightly smaller values for k_{obs} are obtained (Table 1). This observation possibly points towards the influence of partial catalyst deactivation on the rate under these conditions. Accordingly, with $[\text{AB}]_0 = 0.25$ M and 0.05 mol-% catalyst loading, conversion of less than 40 % is achieved prior to catalyst deactivation. Catalyst deactivation, which results in formation of aminoborane adduct $[\text{RuH}(\text{PMe}_3)\{\mu\text{-HB}(\text{H})(\text{NH}_2)\text{N}(\text{CH}_2\text{CH}_2\text{P}i\text{Pr}_2)_2\}]$, has been described in a preceding communication.^[17h]

Table 1. Empirical rate constants for AB dehydrogenation with catalyst **1** derived from first order plots according to the rate law $r_{\text{H}_2} = k_{\text{obs}} [\text{Ru}]_0 [\text{AB}]$.

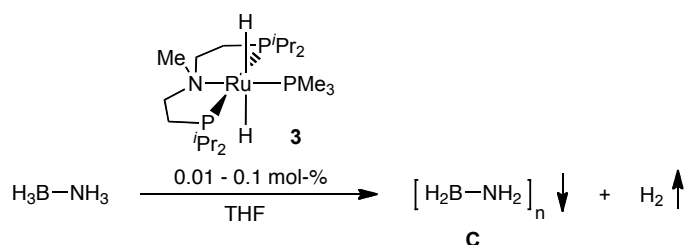
Entry	mol-% 1	$[\text{AB}]_0$ (M)	$[\mathbf{1}]_0$ (M)	k_{obs} ($\text{M}^{-1}\text{s}^{-1}$)
1	0.25	2.5	0.00625	22.8
2	0.25	0.5	0.00125	29.6
3	0.25	0.25	0.000625	32.1
4	0.1	1.0	0.001	20.3
5	0.1	0.5	0.0005	29.7
6	0.1	0.25	0.00025	26.9
7	0.05	2.5	0.00125	13.2
8	0.05	0.5	0.00025	15.0
9	0.05	0.25	0.000125	13.1

In our preceding communication, high kinetic isotope effects (KIE's) for this reaction were estimated employing deuterated substrates on the *B*-terminus, on the *N*-terminus and fully deuterated D_3N-BD_3 .^[8j] The results shall be reevaluated within this more comprehensive study. As for parent H_3N-BH_3 (0.54 M; 0.1 mol-% $[1]_0$), the isotopomer H_3N-BD_3 exhibits first order dependence on substrate after a short initiation period over more than 2 half-lives (Figure 1). From the linear part of the $\ln[AB]$ over time plot, a KIE with $k(H_3N-BH_3) / k(H_3N-BD_3) = 1.8$ was derived.^[27] Interestingly the situation for the *N*-deuterated D_3N-BH_3 and D_3N-BD_3 is different. In both cases, linear $[AB]$ over time plots for 1-2 half-lives suggest a rate law with zero order dependence of H_2 release on substrate concentration (Figure 1). This result indicates a different rate determining step. Therefore, KIE's for these isotopomers referenced to unlabelled H_3N-BH_3 cannot be directly derived. However, a relative KIE for $k(D_3N-BH_3) / k(D_3N-BD_3)$ can be estimated (1.5). Qualitatively, this observation suggests that the rate determining step for H_3N-BH_3 dehydrogenation exhibits a considerably smaller retardation (or higher acceleration) of the rate upon *N*-deuteration, as compared with the rate determining step for the N-D isotopomers.

Kinetic Studies: Dehydrocoupling of AB with $[Ru(H)_2PMe_3(PNP^{Me})]$ (**3**)

Kinetic isotope effects determined for deuteration on both termini of the substrate could be indicative of a bifunctional mechanism, as proposed by Fagnou et al.^[8i] To further probe for cooperativity of the secondary amine functional group of **2** the tertiary amine complex **3**^[21a] was employed as a reference catalyst (Scheme 7). The methylation of the nitrogen atom prohibits N-H hydrogen bonding. Thus, a bifunctional mechanism cannot be operative for this catalyst.

Scheme 7. Dehydrocoupling of AB with precatalyst **3**.



(²⁷) This value is slightly smaller than our original estimate (2.1) where the full plot over 2 half-lives was used.^[8j] However, the present analysis accounts for the initiation period and is therefore more precise.

The addition of **3** to a solution of AB in THF at room temperature results in vigorous evolution of H₂ and precipitation of polymeric dehydrocoupling product **C**. As for precatalyst **1** high turnover numbers (TON ≥ 10000 at [AB]₀ = 2.5 M and [1]₀ = 1•10⁻⁴ M) were observed. However, the volumetrically derived rate of H₂ evolution is considerably lower by about 1-2 orders of magnitude, as compared with precatalyst **1** (Figure 2). Initial rate measurements^[25] reveal first-order dependence in catalyst and second-order dependence in substrate. However, as shown for **1**, reactions with small catalyst loadings and low substrate concentrations indicate a short initiation period. Hence, initial rate measurement will not give information about the reaction at a latter stage. Full kinetic analysis for AB dehydrogenation with **3** is pending. However, preliminary results point towards a rate law with a dependence between zero- and first-order in [AB], suggesting a mechanism with more than one turnover limiting steps.

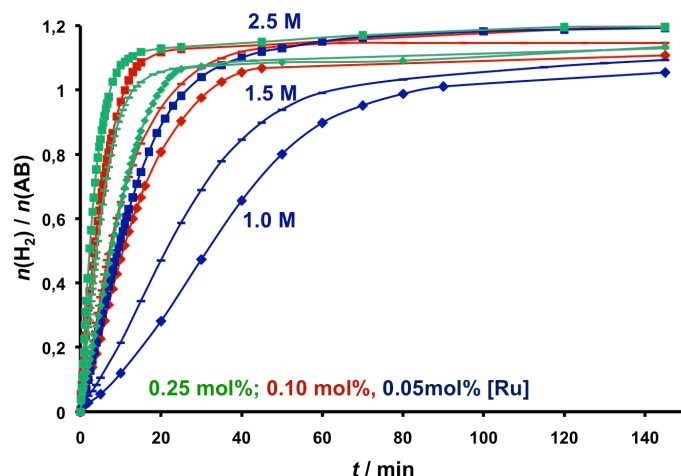


Figure 2. Kinetic plots of AB dehydrogenation using precatalyst **3**.

As for precatalyst **1**, the dehydrocoupling of H₃N-BD₃, D₃N-BH₃, and D₃N-BD₃ was investigated (Figure 3). Similarly, for **3** smaller reaction rates were found in case of *N*-deuterated substrates D₃N-BD₃ and D₃N-BH₃.^[28] As an important difference to **1**, for the *B*-deuterated substrate H₃N-BD₃ no significant isotope effect was observed within experimental errors. This result could indicate that with catalyst **3** only N-H bonds are broken in the r.d.s., rendering mechanisms with B-H activation (e.g. B-H oxidative addition) or concerted B-H/N-H transfer in the r.d.s. implausible.

²⁸ The evaluation of k_H/k_D values for D₃N-BD₃, D₃N-BH₃, H₃N-BD₃ is currently in process.

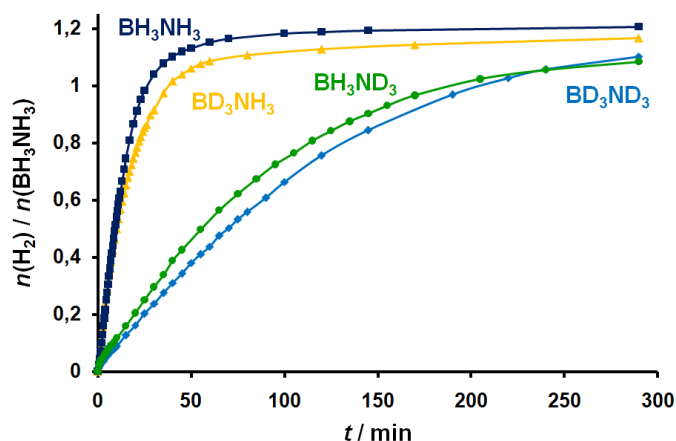


Figure 3. Kinetic plots of AB dehydrogenation in THF at room temperature with partially and fully deuterated substrates using precatalyst **3** (0.05 mol-%; $[AB]_0 = 2.5$ M).

Polymer Characterization

Insolubility of the polymers **B** and **C** inhibits the characterization by solution NMR. Therefore, the polymer was characterized spectroscopically by IR and ^{11}B solid state NMR. Combustion analysis reveals that some solvent adheres to the polymer even after extended drying in vacuo. This observation has been made by Manners and coworkers on iridium POCOP catalyzed AB dehydrocoupling, as well.^[20a,c] Furthermore, the IR spectra of polymers **B** and **C** are virtually identical with the reported product from the iridium catalysed reaction (see B2.1.6 for **C**). For the latter, Staubitz et al. assigned a linear aminoborane structure, $\text{H}_3\text{N}-(\text{BH}_2-\text{NH}_2)_n-\text{BH}_3$ ($n \approx 20$)^[29] and not the originally proposed cyclic pentaaminoborane ($\text{H}_2\text{N}-\text{BH}_2$)₅,^[8b] based on spectroscopic results and comparison with more soluble poly-*N*-methylaminoborane.^[20c] To confirm the supposedly similar structure of the polymers obtained from both ruthenium and iridium catalysis ^{11}B solid state NMR spectroscopy was employed. ^{11}B MAS NMR of **B** displays a very broad peak at 19.5 ppm with a shoulder at 0.44 ppm.^[8j] Hence, Multiple-Quantum Magic-Angle Spinning (MQMAS) experiments were performed to determine the isotropic chemical shift and differentiate between true resonances and second-order quadrupole line shapes. The ^{11}B MQMAS NMR spectrum of **B** (Figure 4) features two signals, one of higher intensity at $\delta_{\text{iso}} = -10.7$ ppm (second-order quadrupolar effect (SOQE) = 1.5 MHz) and one of lower intensity at $\delta_{\text{iso}} = -21.0$ ppm (SOQE = 1.4 MHz). These peaks

²⁹ Combustion analysis of the polymer from dehydrocoupling with catalyst **3** is in good agreement with an empirical formula $\text{H}_3\text{N}-(\text{BH}_2-\text{NH}_2)_{19}-\text{BH}_3 \cdot 0.6$ THF.

indicate two different boron environments present in the polymer, assignable to linear chain BH_2 groups and terminal BH_3 groups, respectively, by comparison with soluble boranes, such as AB ($\delta(^{11}\text{B}) = -23 \text{ ppm}$)^[30] and $\text{H}_3\text{N}-\text{BH}_2-\text{NH}_2-\text{BH}_3$ ($\delta(^{11}\text{B}) = -11.6 \text{ (BH}_2\text{)}$ and $-22.8 \text{ ppm (BH}_3\text{)}$)^[19]. While the ^{11}B spectrum of **B** considerably differs from earlier reports of polyaminoborane,^[31] it is virtually identical with the much better defined polyaminoborane recently prepared by iridium POCOP catalyzed AB dehydrocoupling.^[20c] Therefore, the spectroscopic characterization of **B** confirms, that **1** dehydrocouples AB at the present conditions to give linear polyaminoborane $\text{H}_3\text{N}-(\text{BH}_2-\text{NH}_2)_n-\text{BH}_3$ selectively, with no indications for no cross linking being found. As for the iridium POCOP catalyst, the relative peak intensities indicate a degree of polymerization of around 20, possibly indicating that this chain length defines the solubility of linear polyaminoboranes in THF. However, line shape analysis of broad, unresolved peaks exhibits relatively large uncertainty.^[32] The observation of linear products also suggests, that Me_2AB dehydrogenation, where the linear intermediate $\text{Me}_2\text{HN}-\text{BH}_2-\text{NMe}_2-\text{BH}_3$ is observed provides a reasonable model for AB dehydrogenation, as well.^[10c-f,17h,k]

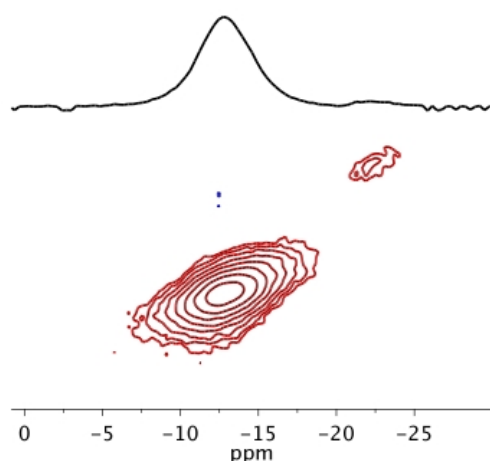


Figure 4. ^{11}B MAS NMR: sheared triple-quantum filtered MQMAS spectrum of the AB dehydrocoupling product with catalyst **1**.

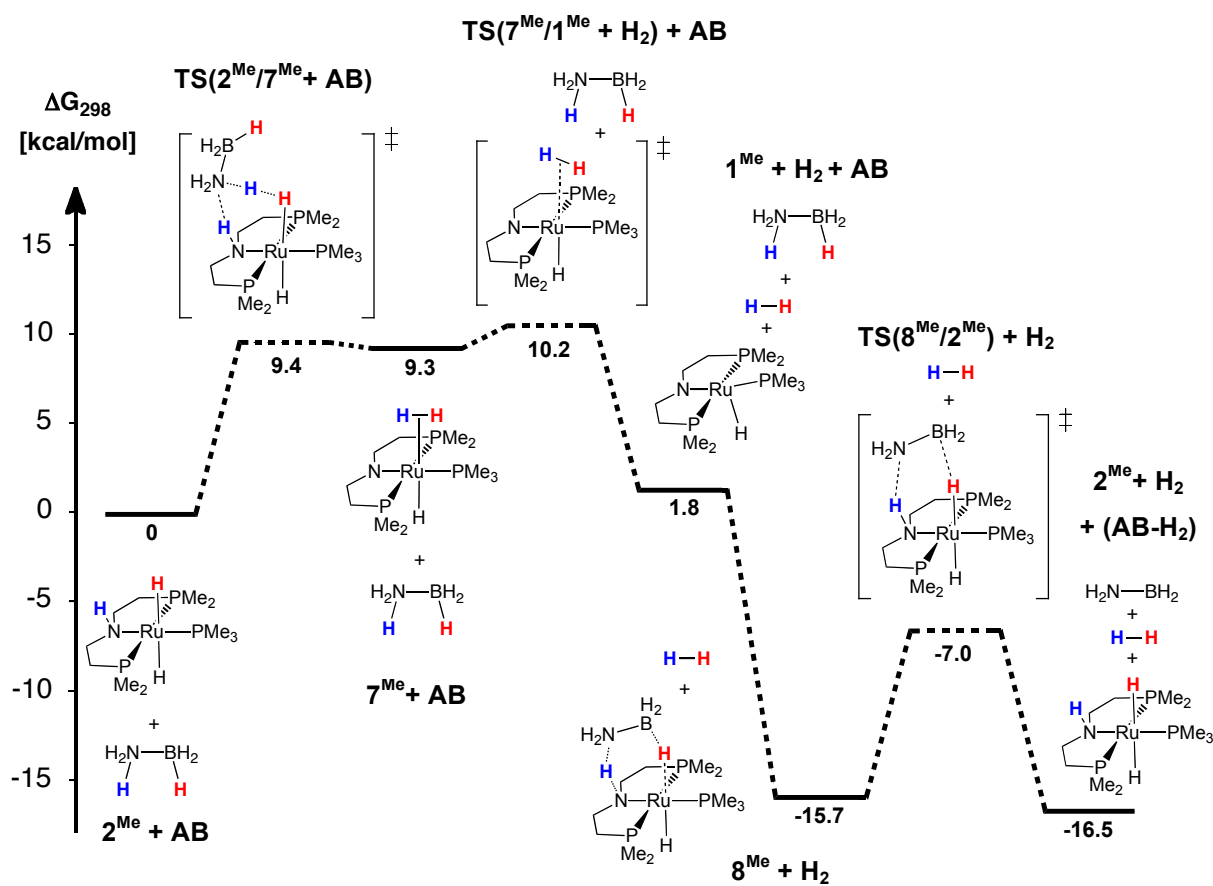
³⁰ The absence of AB in the sample of **B** is evidenced by the ^{11}B MQMAS line-shape.

³¹ (a) Kim, D.-P.; Moon, K.-T.; Kho, J.-G.; Economy, J.; Gervais, C.; Babonneau, F. *Polym. Adv. Technol.* **1999**, *10*, 702. (b) Gervais, C.; Babonneau, F. *J. Organomet. Chem.* **2002**, *657*, 75. (c) Baumann, J.; Baitalov, J.; Wolf, G. *Thermochim Acta* **2005**, *430*, 9.

³² Avadhut, Y. S.; Schneider, D.; Schmedt auf der Günne, J. *J. Magn. Reson.* **2009**, *201*, 1.

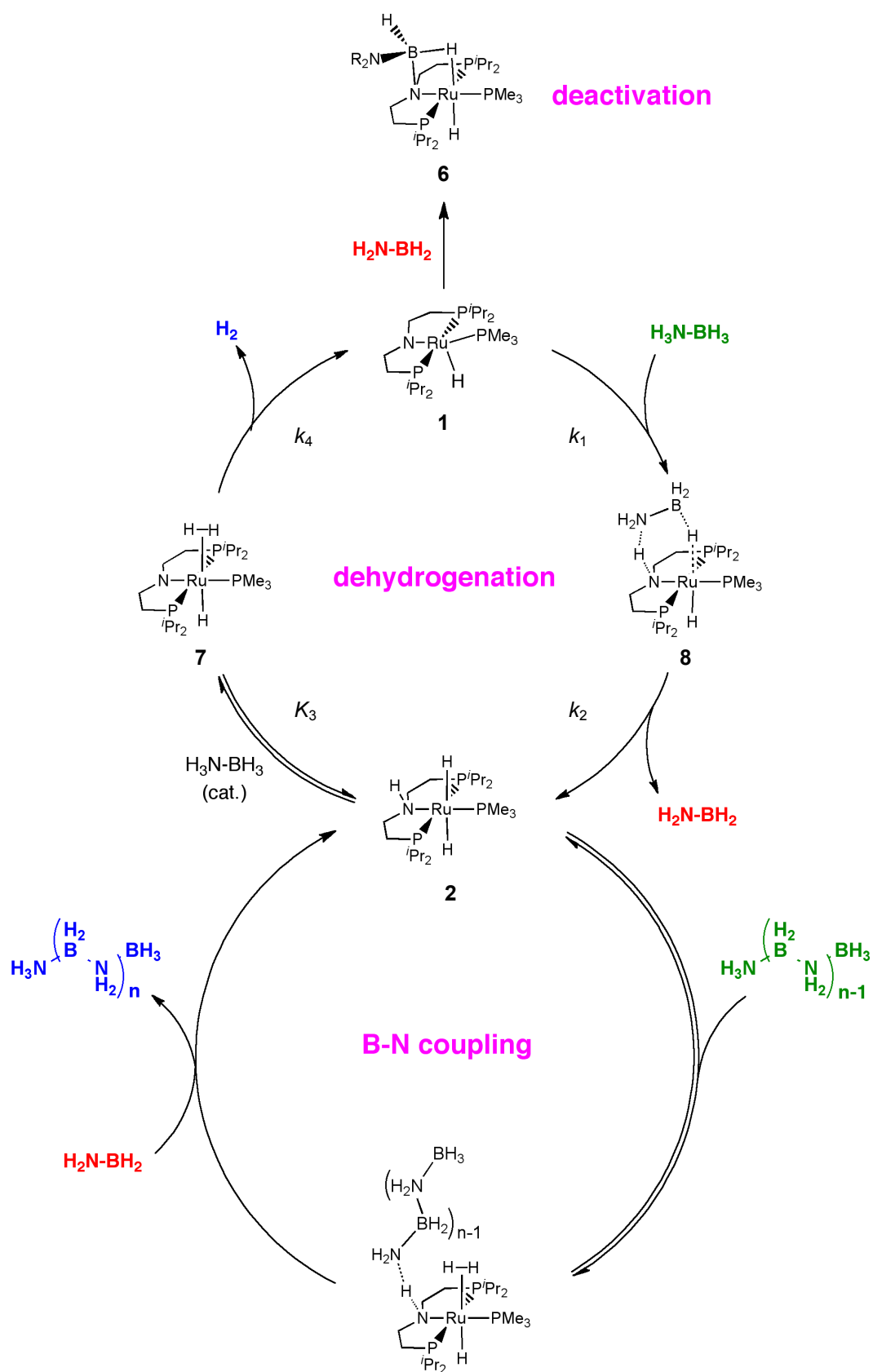
DFT calculations

The spectroscopic results indicate for dehydrocoupling with precatalyst **1**, that **2** represents the catalytic resting state. On the basis of this observation, DFT calculations (B3LYP/6-31+G**) on a slightly simpler model with PMe_2 instead of P^iPr_2 substituents on the pincer ligand were carried out to find a reasonable catalytic cycle. The proposed mechanism for one dehydrogenation cycle, which is described by the sequence $\mathbf{2}^{\text{Me}} + \text{AB} \rightleftharpoons \text{TS}(\mathbf{2}^{\text{Me}}/\mathbf{7}^{\text{Me}} + \text{AB}) \rightleftharpoons \mathbf{7}^{\text{Me}} + \text{AB} \rightleftharpoons \text{TS}(\mathbf{7}^{\text{Me}}/\mathbf{1}^{\text{Me}} + \text{H}_2) + \text{AB} \rightleftharpoons \mathbf{1}^{\text{Me}} + \text{H}_2 + \text{AB} \rightleftharpoons \mathbf{8}^{\text{Me}} + \text{H}_2 \rightleftharpoons \text{TS}(\mathbf{8}^{\text{Me}}/\mathbf{2}^{\text{Me}}) + \text{H}_2 \rightleftharpoons \mathbf{2}^{\text{Me}} + \text{H}_2 + \text{H}_2\text{N-BH}_2$, is displayed in Scheme 8. The first step $\mathbf{2}^{\text{Me}} + \text{AB} \rightleftharpoons \mathbf{7}^{\text{Me}} + \text{AB}$ resembles a proton shuttle between the ruthenium nitrogen and the ruthenium hydride mediated by AB protons. This reaction represents with a barrier of $\Delta G^\ddagger = 9.4$ kcal/mol the calculated r.d.s. of the reaction sequence and is slightly uphill by $\Delta G_r^0 = 9.3$ kcal/mol. Subsequent hydrogen loss from $\mathbf{7}^{\text{Me}}$ to $\mathbf{1}^{\text{Me}} + \text{H}_2$ was calculated to proceed with an even lower barrier ($\Delta G^\ddagger = 0.9$ kcal/mol). Formation of the resulting cyclic aminoborane adduct $\mathbf{8}^{\text{Me}}$ seems to be irreversible with $\Delta G_r^0 = -17.5$ kcal/mol. According to bond distances, the bridging hydride ligand of $\mathbf{8}^{\text{Me}}$ is relatively strongly bonded to both the aminoborane ($D(\text{B-HRu}) = 1.31$ Å) and ruthenium ($D(\text{Ru-HB}) = 1.83$ Å), while the N-H proton of the pincer ligand ($D(\text{H-N}^{\text{PNP}}) = 1.05$ Å) is only weakly hydrogen bonded to the aminoborane ($D(\text{H}_3\text{BH}_2\text{N}\cdots\text{HN}^{\text{PNP}}) = 1.83$ Å). Finally, aminoborane elimination from $\mathbf{8}^{\text{Me}}$ exhibits a slightly smaller barrier ($\Delta G^\ddagger = 8.7$ kcal/mol) than the initial step and is exoergic by only $\Delta G^\ddagger = 0.8$ kcal/mol.

Scheme 8. DFT results for the proposed mechanism of AB dehydrogenation, catalyzed by **2**.

2.1.3 Discussion

The kinetic, spectroscopic, and computational results allow for the proposal of a mechanistic model for AB dehydrogenation, which accounts for the formation of linear aminoboranes. The mechanism can be broken down into two interconnected catalytic cycles (Scheme 9): The upper cycle accounts for AB dehydrogenation with release of H₂ and aminoborane H₂N-BH₂, respectively. Starting from precatalyst **1**, reaction with AB forms borane-amine adduct **8**, which successively gives resting state **2** upon release of aminoborane H₂N-BH₂. These steps have been proposed by Fagnou et al. for bifunctional AB dehydrocoupling, as well.^[81] As a major difference to Fagnou's proposal, we suggest a proton shuttle mechanism for the formation of **7** starting from **2**. Formation of the observed catalyst deactivation product **6**^[17h] can be explained by an off-cycle reaction of **1** with free aminoborane to give the isolable hydride-bridged boraruthenacycle. DFT calculations for the sequence **2** + AB → **7** + AB → **1** + H₂ + AB → **8** + H₂ → **2** + H₂ + H₂N-BH₂ suggests a shallow potential energy surface which is in agreement with the extraordinarily high experimental catalytic rates.

Scheme 9. Proposed catalytic cycle for the dehydrocoupling of AB with precatalyst **1**.

The analytical rate law for H₂ evolution by this proposed mechanism can be derived from the following rate equations and equilibria:

$$r_{\text{H}_2} = k_4 \cdot [\mathbf{7}] \quad (\text{Eq. 2})$$

$$K_3 = k_3 / k_{-3} = ([\mathbf{7}] \cdot [\text{AB}]) / ([\mathbf{2}] \cdot [\text{AB}]) \quad (\text{Eq. 3})$$

$$r_{\text{H}_2} = K_3 \cdot k_4 \cdot [\mathbf{2}] \quad (\text{Eq. 4})$$

$$d[\mathbf{1}] / dt = (K_3 \cdot k_4 \cdot [\mathbf{2}]) - (k_1 \cdot [\text{AB}] \cdot [\mathbf{1}]) \quad (\text{Eq. 5})$$

$$d[\mathbf{8}] / dt = (k_1 \cdot [\mathbf{1}] \cdot [\text{AB}]) - (k_2 \cdot [\mathbf{8}]) \quad (\text{Eq. 6})$$

$$[\text{Ru}] = [\mathbf{1}] + [\mathbf{2}] + [\mathbf{7}] + [\mathbf{8}] \quad (\text{Eq. 7})$$

Reversibility for Eq. 3 seems reasonable, according to our computational results and the spectroscopic examination of H⁺/H⁻ exchange with model borane-amine H₃N-BEt₃. Furthermore, our DFT calculations predict that $(k_3 + k_{-3}) \gg k_4$ and **2** is determined experimentally as resting state in the catalytic cycle. Therefore, we assume quasistationarity for **1** and **8**. Hence, the Bodenstein approximation can be applied to Eq. 5, and Eq. 6 with $d[\mathbf{1}]/dt = 0$ and $d[\mathbf{8}]/dt = 0$, allowing for the derivation of the following rate law:

$$r_{\text{H}_2} = (k_1 \cdot k_2 \cdot K_3 \cdot k_4 \cdot [\text{AB}] [\text{Ru}]) / (k_A \cdot [\text{AB}] + k_B) \quad (\text{Eq. 8})$$

with

$$k_A = (k_1 \cdot k_2 + k_1 \cdot k_2 \cdot K_3 + k_1 \cdot K_3 \cdot k_4)$$

$$k_B = k_2 \cdot K_3 \cdot k_4$$

The first-order dependence in catalyst (Eq. 8) is in agreement with the initial rate data for **1** and also for **3**. Furthermore, for a range of [AB]₀ concentrations, first-order dependence on [AB] was found. Hence, under these conditions $k_A [\text{AB}] \ll k_B$ and the reaction of **1** with AB towards **8** becomes turnover limiting. However, for the highest [AB]₀ concentrations tested, some deviation towards zero-order dependence in [AB] is observed. Hence, under these conditions $k_A [\text{AB}]$ cannot be neglected and the other steps in the postulated cycle, which are all zero-order in [AB] contribute to the overall rate.

For dehydrogenation of the *B*-deuterated isotopomer, first-order dependence in [AB] was found, as well, pointing towards the same turnover limiting step, as for parent AB. The observed normal isotope effect is in qualitative agreement with the expectation for such a step

B Results and Discussion

with a symmetrically bridging μ -hydride ligand in the transition state.³³ However, *N*-terminal deuteration results in a rate law with zero-order dependence in [AB]. Hence, for these isotopomers k_a [AB] \gg k_b must apply. This point can be rationalized with the high N-H/D equilibrium isotope effect (EIE) calculated by DFT ($K_3(\text{BH}_3\text{-NH}_3)/K_3(\text{BH}_3\text{-ND}_3) = 6.1$; $K_3(\text{BH}_3\text{-NH}_3)/K_3(\text{BD}_3\text{-ND}_3) = 3.1$). Under these conditions, the following rate law results:

$$r_{\text{H}_2} = (k_2 \cdot K_3 \cdot k_4 / k_C) [\text{Ru}] \quad (\text{Eq. 9})$$

with

$$k_C = (k_2 + k_2 \cdot K_3 + K_3 \cdot k_4)$$

Assuming that $k_2 \gg (k_2 \cdot K_3 + K_3 \cdot k_4)$, because of the large EIE of K_3 , hydrogen loss from **2** becomes rate determining:

$$r_{\text{H}_2} = K_3 \cdot k_4 \cdot [\text{Ru}] \quad (\text{Eq. 10})$$

which is in agreement with the observation that **2** represents the catalyst resting state under these conditions, as observed by ^1H and ^{31}P NMR spectroscopy.

The lower cycle in Scheme 9 accounts for B-N coupling. While the H_2 release kinetics do not provide information about the actual B-N coupling step, some qualitative observations point towards a metal centered reaction:

1. Dehydrocoupling of Me_2AB shows higher steady-state concentrations of intermediate linear coupling product $\text{Me}_2\text{HN-BH}_2\text{-NMe}_2\text{-BH}_3$ with higher catalyst loadings.
2. All experimental and quantumchemical examinations from other groups suggest the formation of cyclic AB dehydrocoupling products (and ultimately borazine and polyborazine) to result from uncatalyzed aminoborane rearrangement. However, only minor amounts of borazine are observed, which might stem from uncatalyzed aminoborane coupling as a side reaction with higher barriers.

Based on DFT calculations a B-N coupling cycle upon Ru-catalyzed aminoborane insertion into an AB N-H bond with small barriers is proposed. For further chain propagation, oligomeric and polymeric intermediates $\text{H}_3\text{N-(BH}_2\text{-NH}_2)_n\text{-BH}_3$ ($n \geq 1$) can enter the B-N coupling cycle instead of parent AB. Ultimately, for polymers exceeding a critical chain

³³ Based on a B-H stretching vibration around 2350 cm^{-1} the maximum H/D isotope effect for full B-H bond cleavage in AB is expected to be 4.9.

length, low solubility will result in precipitation from solution. In agreement with the report of Staubitz et al., our experimental results indicate that this condition is matched in THF at $n \approx 20$.^[20c]

2.1.4 Conclusions

Our results provide useful informations about important features of ammonia borane dehydrocoupling with bifunctional catalysts. The proposed mechanism with catalytic release of aminoborane upon dehydrogenation of AB and subsequent metal catalyzed B-N coupling route offers the opportunity to control the B-N polymer microstructure by catalyst design. This pathway is fundamentally different to the proposed mechanisms with other catalysts, which rely on:

1. Polyaminoborane formation by metal centered dehydrogenation and B-N coupling without aminoborane release (proposed for Goldberg and Heinekey's catalyst).
2. Release of catalytically dehydrogenated aminoborane and subsequent uncatalyzed aminoborane oligomerization resulting in formation of borazine and polyporazine.

Overall, our ruthenium catalyst can be considered *bifunctional* in the literal and a figurative sense: A bifunctional mechanism is adopted with two functional groups of the catalyst being involved in the turnover limiting steps and the ruthenium compounds incur two separate functions, being catalysts both for dehydrogenation and B-N-coupling.

2.1.5 Experimental details and syntheses

Materials and Methods. All experiments were carried out under an atmosphere of argon using Schlenk and glove-box techniques. Benzene and THF were dried over Na/benzophenone, distilled under argon and deoxygenated prior to use. Pentane was dried and deoxygenated by passing through columns packed with activated alumina and Q5, respectively. Deuterated solvents were dried by distillation from Na/K alloy (C_6D_6 and d^8 -THF), and deoxygenated by three *freeze-pump-thaw* cycles. KO^tBu was purchased from VWR and sublimed prior to use. H_3B-NMe_3 (Aldrich) was used as purchased. **1**, **2** and **3** were prepared as reported earlier.

Analytical Methods. IR spectra were recorded on a Varian FT/IR-670 spectrometer. NMR spectra were recorded on a Bruker Avance III 400 NMR spectrometers and were calibrated to the residual proton resonance and the natural abundance ^{13}C resonance of the solvent (C_6D_6 ,

B Results and Discussion

$\delta_{\text{H}} = 7.16$ and $\delta_{\text{C}} = 128.06$ ppm; d_8 -THF, $\delta_{\text{H}} = 1.72$ and 3.57 ppm, $\delta_{\text{C}} = 25.3$ and 67.4 ppm). ^{31}P NMR chemical shifts are reported relative to external phosphoric acid (δ 0.0 ppm). ^{11}B NMR chemical shifts are reported relative to external BF_3 etherate. Signal multiplicities are abbreviated as: s (singlet), d (doublet), t (triplet), q (quartet), m (multiplet), br (broad).

Synthesis of $\text{H}_3\text{N-BEt}_3$: $\text{NH}_3(\text{g})$ (15 mL) is dried by condensation into a flask with sodium at -78 °C and subsequently condensed *trap-to-trap* to a solution of BEt_3 in THF (20 mL, 20 mmol BEt_3). After warming to room temperature and evaporation of NH_3 the solvent is removed *i. vac.* until a colourless oil remains. Further removal of the solvent at elevated temperatures *i. vac.* leads to product decomposition. Therefore, the crude product, $\text{H}_3\text{N-BEt}_3 \cdot 0.5$ THF, was used as obtained: NMR (C_6D_6 , r.t., [ppm]) ^1H NMR (399.8 MHz): δ 3.44 (2H, m, CH_2^{THF}), 1.96 (3H, br, NH_3), 1.50 (2H, m, CH_2^{THF}), 0.80 (9H, t, $^3J_{\text{HH}} = 7.9$ Hz, CH_3), 0.19 (6H, q, $^3J_{\text{HH}} = 7.9$ Hz, CH_2). ^{11}B NMR (128.3 MHz): δ -5.3. NMR (d^8 -THF, r.t., [ppm]) ^1H NMR (399.8 MHz): δ 3.61 (2H, m, CH_2^{THF}), 3.52 (3H, br, NH_3), 1.77 (2H, m, CH_2^{THF}), 0.74 (9H, t, $^3J_{\text{HH}} = 7.8$ Hz), 0.15 (6H, q, $^3J_{\text{HH}} = 7.8$ Hz). ^{11}B NMR (128.3 MHz): δ -5.9. ^{13}C $\{^1\text{H}\}$ NMR (100.6 MHz): δ 68.2 (s, CH_2^{THF}), 26.4 (s, CH_2^{THF}), 15.4 (br, CH_2), 10.2 (s, CH_3). Assignments were confirmed by ^{13}C $\{^1\text{H}\}$ DEPT NMR.

*Reaction of **2** with $\text{Et}_3\text{B-NH}_3$.* **2** (11.6 mg, 24.0 μmol) is dissolved in dry d_8 -THF in a *J-Young* NMR tube with $\text{BEt}_3\text{NH}_3 \cdot 0.5$ THF (3.0 mg, 19.9 μmol , 0.8 equiv). Small amounts of **5** are observed in the ^1H and ^{31}P NMR spectra. With mixing times of $\tau_{\text{m}} = 500$ ms and 1000 ms cross peaks between the N-H protons of NH_3BEt_3 and the hydride adjacent to the N-H function of **2** were observed in the ^1H 2D EXSY NMR spectra.

*Reaction of **3** with $\text{Et}_3\text{B-NH}_3$.* **3** (10.0 mg, 20.1 μmol) is dissolved in dry d_8 -THF in a *J-Young* NMR tube with $\text{BEt}_3\text{NH}_3 \cdot 0.5$ THF (4.5 mg, 29.8 μmol , 1.5 equiv). With mixing times of $\tau_{\text{m}} = 500$ ms and 1000 ms no exchange peaks between NH_3BEt_3 and the hydrides of **3** were observed in the ^1H 2D EXSY NMR spectra.

*Reaction of **2** with $\text{Et}_3\text{B-NH}_3$ and $\text{H}_3\text{B-NMe}_3$.* $\text{Et}_3\text{B-NH}_3 \cdot 0.5$ THF (8.2 mg, 54.5 μmol) and $\text{H}_3\text{B-NMe}_3$ (3.8 mg, 52.1 μmol) are added to a solution of **2** (0.46 μmol ; 0.9 mol%) in 0.4 mL d_8 -THF in a *J-Young*-NMR tube. Over the course of 24 h no coupling reaction is observed at room temperature by ^{11}B and ^1H NMR spectroscopy.

2.1.6 Kinetic experiments

Catalytic Protocols: In a typical experiment, $\text{H}_3\text{B-NH}_3$ (46.3 mg; 1.5 mmol) is dissolved in THF in a schlenk tube connected to a water-filled graduated cylinder (eudiometer). A solution of catalyst in THF is quickly added via syringe. The volume of collected hydrogen gas is recorded in adequate time spans.

Trapping experiment with 2. Cyclohexene (1.5 mL, 14.8 mmol, 21 eq) is added to a solution of $\text{H}_3\text{N-BH}_3$ (22.0 mg, 0.7 mmol, 0.2 M) in THF (1.5 mL). After addition of **1** (0.7 mol%), the reaction mixture is stirred for 10 min at r.t. in a vented vial. The ^{11}B NMR spectrum of an aliquot of the white suspension shows a broad peak for polyborazylene as the only product. After 24 h a dublet for borazine and a broad singlet at 48.4 ppm appear.

Aminoborane Trapping with 3. Cyclohexene (0.8 mL, 7.9 mmol, 21 eq) is added to a solution of $\text{H}_3\text{N-BH}_3$ (11.5 mg, 0.37 mmol, 0.1 M) in THF (3 mL). After addition of **3** (0.1 mol%) the reaction mixture is stirred for 3.5 h at r.t. in a vented vial. The ^{11}B NMR spectrum of an aliquot of the slightly turbid reaction solution shows beside starting material ($\delta = -21.6$ ppm) signals for borazine ($\delta = 31.1$ ppm), polyborazylene ($\delta = 26.0$ ppm), **A** ($\delta = -5.0$ ppm, -11.0 ppm, -23.0 ppm) and a broad peak at 48.4 ppm, indicating the trapping of free aminoborane by hydroboration of cyclohexene^[8h] (Figure S1).

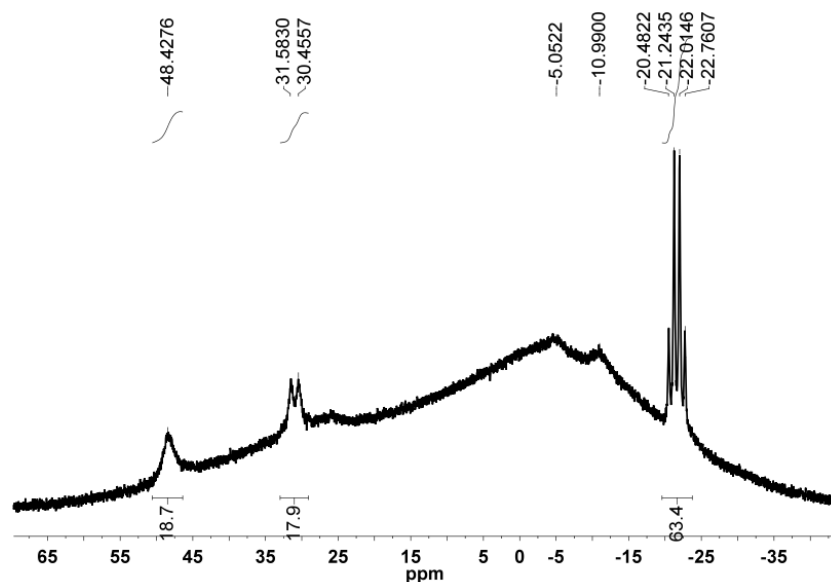


Figure S1. ^{11}B NMR (without baseline correction) of the AB dehydrocoupling (0.1M) with catalyst **3** (0.1 mol%) in THF with 21 equiv. cyclohexene after 3.5 h.

B Results and Discussion

Characterization of the dehydrocoupling product C: A solution of **3** (0.00075 mmol; 0.05 mol%) in 0.3 mL THF is added via syringe to a vigorous stirred solution of H₃B-NH₃ (46.0 mg; 1.490 mmol; 2.5 M) in 0.3 mL THF. After evolution of 1 eq H₂ at rt the suspension is filtered. The white residue is washed with THF (3 x 5mL) and pentane (3 x 5 mL) and dried *i. vac.* Yield: 39.0 mg (1.223 mmol; 82 %; determined by $n(\mathbf{C}) = n(\text{H}_3\text{B-NH}_3) - n(\text{H}_2)$). Anal. Calcd. for H₄BN (28.85): H, 13.98; N, 48.55. Found: H, 13.39; N, 44.46; C, 3.99 from residual solvent. IR (ATR, cm⁻¹): 3298 (s, N-H_{asym}), 3248 (s, N-H_{sym}), 2386-2314 (B-H), 1557 (s).

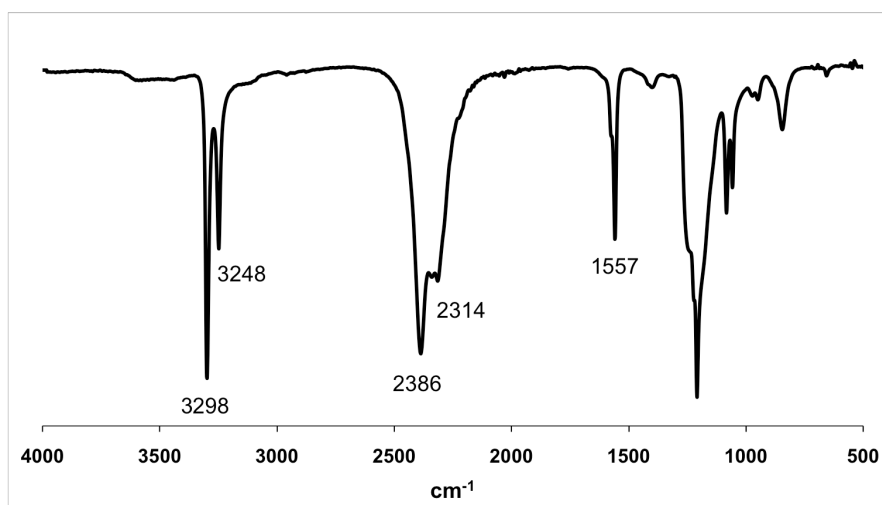


Figure S2. ATR spectra of polymer C.

2.1.7 Computational results

DFT calculations. All calculations were performed with GAUSSIAN-03 Rev. C.02 using the density functional/Hartree-Fock hybrid model Becke3LYP and the split valence double- ζ (DZ) basis set 6-31+G**.^[34,35,36] The Ru atoms were described with a Stuttgart-RSC-ECP with a DZ description of the valence electrons.^[37] Geometry optimizations were run without

⁽³⁴⁾ Frisch, M. J. et al. Gaussian, Inc., Wallingford CT, 2004.

⁽³⁵⁾ (a) Vosko, S. H.; Wilk, L.; Nusair, M. *Can. J. Phys.* **1980**, *58*, 1200-1211. (b) Lee, C.; Yang, W.; Parr, R. G. *Phys. Rev. B.* **1988**, *37*, 785-789. (c) Becke, A. D. *J. Chem. Phys.* **1993**, *98*, 5648-5652.

⁽³⁶⁾ (a) Hehre, W. J.; Ditchfield, R.; Pople, J. A. *J. Chem. Phys.* **1972**, *56*, 2257-2261. (b) Francl, M.M.; Pietro, W.J.; Hehre, W.J.; Binkley, J.S.; Gordon, M.S.; DeFrees D.J. and Pople, J.A. *J. Chem. Phys.* **1982**, *77*, 3654-3665.

⁽³⁷⁾ Dolg, M.; Stoll, H.; Preuss, H.; Pitzer, R.M. *J. Phys. Chem.* **1993**, *97*, 5852.

symmetry or internal coordinate constraints. The optimized structures were verified as being true minima (NImag=0) or transition states (NImag=1) by analysis of negative eigenvalues in vibrational frequency calculations. Thermal corrections were carried out at standard conditions ($T = 298.15$ K, and $P = 1$ atmosphere). Orbital energies were obtained from the Mulliken population analysis. NBO analyses were performed with NBO V3.1 as implemented in GAUSSIAN-03.^[38] Orbital expressions were visualized with GaussView via cube files generated from formatted checkpoint files.^[39]

⁽³⁸⁾ Glendening, E. D.; Reed, A. E.; Carpenter, J. E.; Weinhold, F., NBO Version 3.1.

⁽³⁹⁾ Dennington II, R.; Keith, T.; Millam, J. *GaussView V4.1*; Semichem Inc., Shawnee Mission, KS, **2007**.

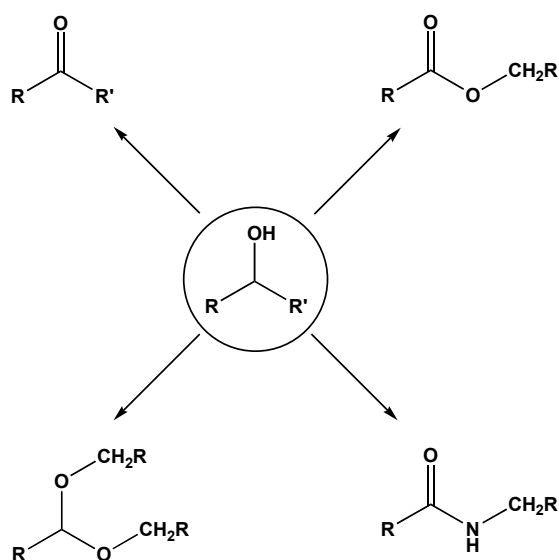
3 Published Review Article

3.1 Acceptorless Dehydrogenation of Alcohols: Perspectives for Synthesis and Hydrogen-Storage

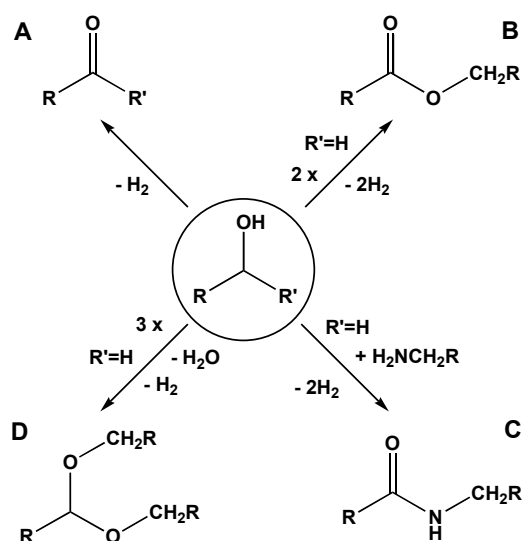
This chapter originated the following publication:

A. Friedrich, S. Schneider

ChemCatChem **2009**, *1*, 72.



The oxidation of alcohols represents an important synthetic route towards carbonyl compounds, such as aldehydes, ketones, or carbonic acid derivatives.^[1] Obtaining high selectivities for these reactions can be challenging, owing to the risk of substrate over-oxidation. Metal catalyzed oxidation permits the use of mild, inexpensive and environmentally benign oxidizing agents, e.g., O₂ or H₂O₂.^[2] Particularly late transition metal catalysts were successfully utilized for aerobic alcohol oxidation.^[2,3] Other mild oxidizing agents used as hydrogen acceptors include ketones,^[4] olefins,^[5] and amine-*N*-oxides.^[6]



Scheme 1. Products from metal catalyzed AAD.

¹ a) M. Hudlicky in *Oxidations in Organic Chemistry*, American Chemical Society, Washington DC, **1990**; b) G. Tojo, M. Fernández in *Oxidation of Alcohols to Aldehydes and Ketones*, Springer, New York, **2006**.

² a) R. A. Sheldon, J. K. Kochi in *Metal-Catalyzed Oxidations of Organic Compounds*, Academic Press, New York, **1981**; b) I. W. C. E. Arends, R. A. Sheldon in *Modern Oxidation Methods*, (Ed: J.-E. Bäckvall), Wiley-VCH, Weinheim, **2004**, pp. 83.

³ a) S.-I. Murahashi, N. Komiya in *Ruthenium in Organic Synthesis*, (Ed: S.-I. Murahashi), Wiley-VCH, Weinheim, **2004**, pp. 53; c) S.-I. Murahashi, N. Komiya in *Modern Oxidation Methods*, (Ed: J.-E. Bäckvall), Wiley-VCH, Weinheim, **2004**, pp. 165.

⁴ S. E. Clapham, A. Hadzovic, R. H. Morris, *Coord. Chem. Rev.* **2004**, 248, 2201.

⁵ Some recent examples: a) P. A. Slatford, M. K. Whittlesley, J. M. J. Williams, *Tetrahedr. Lett.* **2006**, 47, 6787; b) D. Gnanamgari, A. Moores, E. Rajaseelan, R. H. Crabtree, *Organometallics* **2007**, 26, 1226; c) N. A. Owston, A. J. Parker, J. M. J. Williams, *Chem. Comm.* **2008**, 624.

⁶ S. V. Ley, J. Norman, W. P. Griffith, S. P. Marsden, *Synthesis* **1994**, 639.

However, with respect to atom economy it is desirable to dehydrogenate without a hydrogen acceptor by release of H₂. Furthermore, such acceptorless alcohol dehydrogenations (AAD's) are of great current interest for hydrogen storage.^[7] Thermodynamics of AAD demand elevated temperatures and removal of H₂ from the equilibrium.^[8,9] However, based on the principle of microscopic reversibility catalyst systems used in ketone hydrogenation could be suitable for the reverse reaction, as well. Accordingly, several late metal homogeneous and colloidal catalysts have been successfully used for thermal AAD.^[10,11,12]

Generally, secondary alcohols are converted to ketones by AAD (Scheme 1, A).^[10a-g] Likewise, with catalysts, such as [Ru(OC(O)CF₃)₂(CO)(PPh₃)₂]/HOC(O)CF₃ or metal nanoparticles, AAD of primary alcohols to aldehydes was reported (Scheme 1, A, R' = H).^{[10h-}

⁷ B. Loges, H. Junge, B. Spilker, C. Fischer, M. Beller, *Chem. Ing. Tech.* **2007**, 79, 741.

⁸ The dehydrogenation of 2-propanol to acetone and H₂ is endothermic by $\Delta_r H^0 = 69$ kJ/mol: K. B. Wiberg, L. S. Crocker, K. M. Morgan, *J. Am. Chem. Soc.* **1991**, 113, 3447.

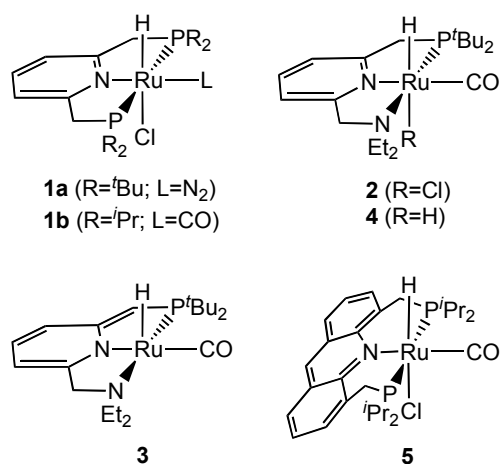
⁹ The entropic contribution (TAS) for a reaction with H₂ release at room temperature is about 8 kcal/mol: M. Pink, O. Eisenstein, *J. Chem. Edu.* **2002**, 79, 1269.

¹⁰ a) H. B. Charman, *J. Chem. Soc. B* **1970**, 548; b) Y. Lin, D. Ma, X. Lu, *Tetrahedron Lett.* **1987**, 28, 3115; c) H. Junge, M. Beller, *Tetrahedron Lett.* **2005**, 46, 1031; d) G. R. A. Adair, J. M. J. Williams, *Tetrahedron Lett.* **2005**, 46, 8233; e) J. van Buijtenen, J. Meuldijk, J. A. J. M. Vekmans, L. A. Hulshof, H. Kooijman, A. L. Spek, *Organometallics* **2006**, 25, 873; f) K. Fujita, N. Tanino, R. Yamaguchi, *Org. Lett.* **2007**, 9, 109; g) H. Junge, B. Loges, M. Beller, *Chem. Commun.* **2007**, 522; h) A. Dobson, S. D. Robinson, *J. Organomet. Chem.* **1975**, 87, C52; i) A. Dobson, S. D. Robinson, *Inorg. Chem.* **1977**, 16, 137; j) C. W. Jung, P. E. Garrou, *Organometallics* **1982**, 1, 658; k) W. K. Rybak, J. J. Ziolkowski, *J. Mol. Catal.* **1981**, 11, 365; l) T. A. Smith, R. P. Aplin, P. M. Maitlis, *J. Organomet. Chem.* **1985**, 291, C13; m) S. Shinoda, H. Itagaki, Y. Saito, *J. Chem. Soc., Chem. Commun.* **1985**, 860; n) H. Itagaki, S. Shinoda, Y. Saito, *Bull. Chem. Soc. Jpn.* **1988**, 61, 2291; o) T. Fujii, Y. Saito, *J. Mol. Catal.* **1991**, 67, 185; p) L.-C. Yang, T. Ishida, T. Yamakawa, S. Shinoda, *J. Mol. Catal. A* **1996**, 108, 87; q) Y. Blum, Y. Shvo, *J. Organomet. Chem.* **1985**, 282, C7; r) J. H. Choi, N. Kim, Y. J. Shin, J. H. Park, J. Park, *Tetrahedron Lett.* **2004**, 45, 4607; s) D. Morton, D. J. Cole-Hamilton, *J. Chem. Soc., Chem Commun.* **1987**, 248. t) D. Morton, D. J. Cole-Hamilton, J. A. Schofield, R. J. Pryce, *Polyhedron* **1987**, 6, 2187. u) D. Morton, D. J. Cole-Hamilton *J. Chem. Soc., Chem Commun.* **1988**, 1154. v) D. Morton, D. J. Cole-Hamilton, I. D. Utuk, M. Paneque-Sosa, M. Lopez-Poveda, *J. Chem. Soc. Dalton Trans.* **1989**, 489.

¹¹ a) S.-I. Murahashi, K. Ito, T. Naota, Y. Maeda, *Tetrahedron Lett.* **1981**, 22, 5327; b) S.-I. Murahashi, T. Naota, K. Ito, Y. Maeda, H. Taki, *J. Org. Chem.* **1987**, 52, 4319; c) Y. R. Lin, X. C. Zhu, Y. F. Zhou, *J. Organomet. Chem.* **1992**, 429, 269; d) J. Zhao, J. F. Hartwig, *Organometallics* **2005**, 24, 2441.

¹² Selective dehydrogenative coupling of methanol to methylacetate: T. Ohnishi, T. Yamakawa, S. Shinoda, *J. Chem. Soc., Dalton Trans.* **1997**, 789.

^{k,s,w-y]} However, formation of esters (Scheme 1, **B**) was observed with ruthenium catalysts like $[\text{RuCl}_2(\text{PPh}_3)_3]$ or $[\text{RuH}_2(\text{PPh}_3)_4]$,^[10l-p,q,11a-b] and AAD of diols usually gives the corresponding lactones.^[11] While the ester could be attributed to a Tishchenko reaction of initially formed aldehyde,^[13] Murahashi *et al.* proposed a pathway via a hemiacetal from the addition of alcohol to the aldehyde.^[11b,13b] In fact, formaldehyde represents an intermediate in ruthenium-catalyzed AAD of methanol to methylformate.^[10m] However, while various AAD catalysts have been reported, systems without acid or base cocatalysts and with high selectivities in primary alcohol AAD remain scarce. Side products, e.g., from aldol reactions, must be suppressed by neutral reaction conditions.^[10v] Furthermore, CO, a strong fuel cell catalyst poison, stemming from aldehyde decarbonylation is particularly detrimental for H₂ storage applications.^[10s-v]



In this context, Milstein and co-workers have recently presented ruthenium AAD catalysts with pyridine based pincer ligands. Complex **1a**, activated with base, is a moderately active catalyst for secondary alcohols, but failed to dehydrogenate primary alcohols.^[14a] A $[\text{Ru}^{\text{II}}(\text{H})_2]/[\text{Ru}^0]$ based catalytic cycle was proposed. Modification of the ligand sphere

¹³ a) H. Horino, T. Ito, A. Yamamoto, *Chem. Lett.* **1978**, 24, 2441; b) N. Menashe, Y. Shvo, *Organometallics* **1991**, 10, 3885; c) T. Seki, T. Nakajo, M. Onaka, *Chem. Lett.* **2006**, 35, 824.

¹⁴ a) J. Zhang, M. Gandelman, L. J. W. Shimon, H. Rozenberg, D. Milstein, *Organometallics* **2004**, 23, 4026; b) J. Zhang, G. Leitius, Y. Ben-David, D. Milstein, *J. Am. Chem. Soc.* **2005**, 127, 10840; c) J. Zhang, G. Leitius, Y. Ben-David, D. Milstein, *Angew. Chem.* **2006**, 118, 1131; *Angew. Chem. Int. Ed.* **2006**, 45, 1113; d) J. Zhang, M. Gandelman, L. J. W. Shimon, D. Milstein, *Dalton Trans.* **2007**, 107; e) C. Gunanathan, Y. Ben-David, D. Milstein, *Science* **2007**, 317, 790; f) C. Gunanathan, D. Milstein, *Angew. Chem* **2008**, 120, 8789; *Angew. Chem. Int. Ed.* **2008**, 47, 8661.

resulted in highly selective AAD of primary alcohols to esters by **1b** and **2** with equimolar amounts of KOH.^[14b,d] Furthermore, benzylic deprotonation of **2** with KO^tBu gives amido complex **3**, as was recently found for other aromatic and aliphatic PNP pincer complexes.^[15] **3** exhibits high activity and selectivity in dehydrocoupling of primary alcohols to esters under base free conditions and ester hydrogenation to the corresponding alcohols.^[14c] Owing to the reversible addition of H₂ to complex **3** giving dihydride **4**, this equilibrium was suggested to be the crucial step in H₂ activation/release. **3** does not catalyze the Tishchenko reaction of benzaldehyde, supporting Murahashi's mechanistic proposal for ester formation. Furthermore, this methodology could be extended towards amide synthesis by dehydrogenative coupling of alcohols and amines (Scheme 1, C).^[14e,16]

In their most recent contribution the Milstein group presented AAD with a new acridine based pincer complex (**5**).^[14f,17] **5** exhibits an interesting molecular structure with a particularly long Ru–N bond and the heterocycle being strongly tilted out of the PNP chelate plane. As for complexes **1b** and **2**, **5** catalyses the dehydrocoupling of primary alcohols to esters in the presence of base. Small amounts of acetal were also found (Scheme 1, D), as was reported earlier in Ru-catalyzed AAD.^[10l-p] Most significantly, without additional base the selectivity is reversed giving acetals in high yield. A pathway for acetal formation was proposed via hydroalkoxylation of an intermediate enolether, which was observed during the reaction. Surprisingly, in contrast to linear aliphatic alcohols, AAD of benzyl alcohol with **5** exclusively gave benzyl benzoate, even under neutral conditions. While the selectivities remain to be fully explained, the unusual structure of **5** could point towards hemilability of the pincer ligand to be an important feature.

Metal catalyzed AAD is an interesting alternative to conventional alcohol oxidation, owing to the mild reaction conditions and unusual coupling products. However, after initial studies more than 30 years ago this method remained strongly neglected. The unprecedented dehydrocoupling of alcohols to acetals in high yield reported by Milstein *et al.* demonstrates that the selectivity of AAD can be controlled by intricate changes in the auxiliary ligand

¹⁵ a) E. Ben-Ari, G. Leitus, L. J. W. Shimon, D. Milstein, *J. Am. Chem. Soc.* **2006**, 128, 15390; b) J. I. van der Vlugt, M. Lutz, E. A. Pidko, D. Vogt, A. L. Spek, *Dalton Trans.* **2009**, 1016-1023; c) M. Käß, A. Friedrich, M. Drees, S. Schneider, *Angew. Chem.* **2009**, 121, 922; *Angew. Chem. Int. Ed.* **2009**, 48, 905.

¹⁶ L. U. Nordstrøm, H. Vogt, R. Madsen, *J. Am. Chem. Soc.* **2008**, 130, 17672.

¹⁷ C. Gunanathan, L. J. W. Shimon, D. Milstein, *J. Am. Chem. Soc.* **2009**, 131, 3146.

sphere. Therefore, the Ru pincer complexes provide a unique opportunity to rationalize the parameters that contribute to AAD selectivity on a mechanistic basis. Other coupling products, e.g. polyesters from diols, or enantioselective AAD define challenging targets for future developments.^[18]

¹⁸ a) D. R. Jensen, J. S. Pugsley, M. S. Sigman, *J. Am. Chem. Soc.* **2001**, 123, 7475; b) E. M. Ferreira, B. M. Stoltz, *J. Am. Chem. Soc.* **2001**, 123, 7725.

C Summary

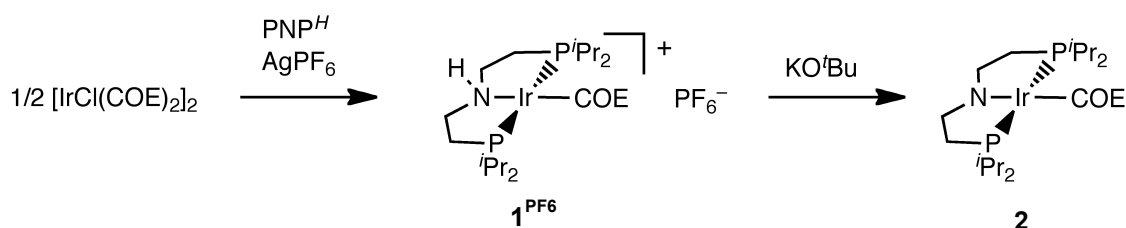
Summary

The coordination chemistry of d^6 ruthenium and d^8 iridium metal amido complexes was examined, with particular emphasis on *cooperative* reactivity in catalysis. The used ethylene bridged tridentate diphosphine amido chelate framework (PNP) uniquely combines M–N *bifunctionality*, as typically found for electron rich transition metal amido complexes, with ligand backbone *cooperativity*. Besides mechanistic information on stoichiometric C–H and H₂ activation, the high potential of the Ru(PNP) platform as catalyst for ionic (de)hydrogenation is presented. Of great current interest both for chemical hydrogen storage and the synthesis of novel inorganic polymeric materials is the dehydrogenation of ammonia borane; detailed studies with Ru(H)PMe₃(PNP), the most active known catalyst to date, suggest a *bifunctional* mechanism for this reaction. The proposed mechanism accounts for structural control of the polymeric B–N coupling product.

1. Reactivity of electron rich M(PNP) (M = Ir, Ru) fragments: E–H (E = C, N, H) bond activation

The ethylene bridged PNP pincer ligand N(CH₂CH₂PⁱPr₂)₂ (PNP) provides synthetic access in high yield to late, electron rich transition metal dialkyl amido complexes. As shown in a preliminary study,^[1] the reaction of the pincer ligand PNP^H (HN(CH₂CH₂PⁱPr₂)₂) with [IrCl(COE)₂]₂ (COE = cyclooctene) and AgPF₆ furnishes iridium(I) amino olefin complex [IrCOE(PNP^H)]PF₆ (**1**^{PF6}). Deprotonation with KO^tBu yields the corresponding amido complex [IrCOE(PNP)] (**2**) (Scheme C-1).

Scheme C-1. Synthesis of Ir^I(PNP) complexes.

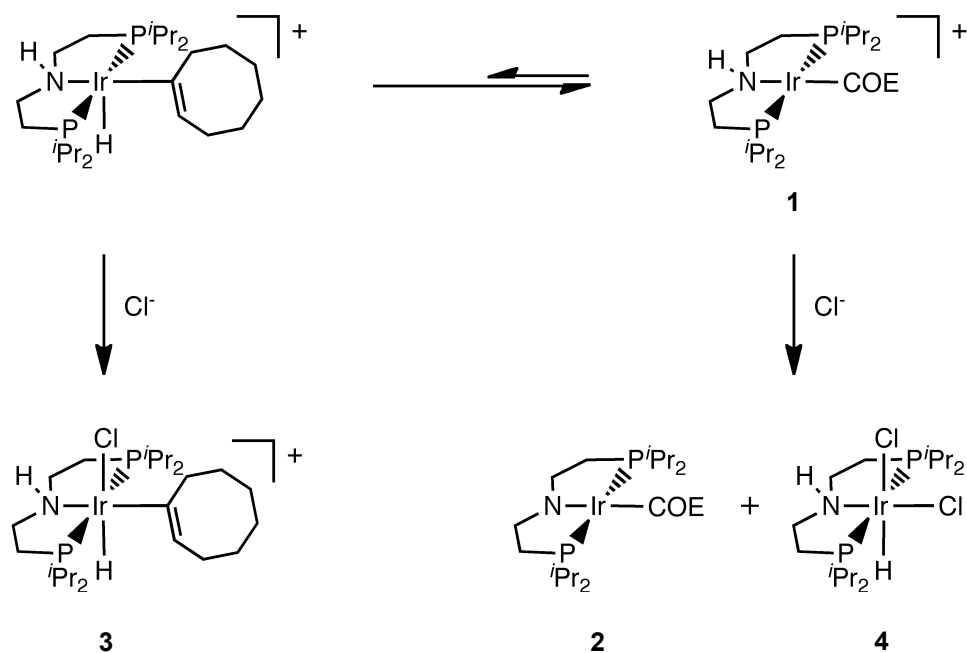


In the present thesis, the reactivity of the Ir^I(PNP) compounds was examined with respect to C–H or N–H bond activation. It was shown that the olefin complex [IrCOE(PNP^H)]⁺ (**1**)

¹ A. Friedrich, *Synthesis and Characterization of Iridium Complexes with chelating Amine and Amido Phosphine Ligands*, Diploma Thesis, TU München, 2007.

exhibits a fast equilibrium with the hydrido cyclooctenyl isomer $[\text{IrH}(\text{C}_8\text{H}_{13})(\text{PNP}^H)]^+$ at room temperature after vinylic C-H activation with a very low barrier. In the presence of chloride, trapping of the vinyl hydride $[\text{IrHCl}(\text{C}_8\text{H}_{13})(\text{PNP}^H)]$ (**3**) is possible (Scheme C-2). However, also N-H activation is initiated by chloride and a mixture of **2**, **3** and $[\text{IrHCl}_2(\text{PNP}^H)]$ (**4**) is observed for the reaction of $[\text{IrCl}(\text{COE})_2]_2$ with PNP^H in nonprotic solvents without chloride anion exchange for the weakly coordinating anions PF_6^- or BPh_4^- . The complex mechanism for the reaction cascade could be fully elucidated by kinetic modelling.^[2] In contrast to the fluxional behavior of **1** the structural rigidity of the corresponding amido complex **2** is attributed to strong olefin binding, which is reinforced by the N-Ir-olefin 3c-4e π -interaction and illustrates the electron-rich character of the Ir(PNP) fragment. Using the olefin ligand as a probe for Ir-N bonding, this interpretation renders **1/2** an interesting system that features switchable C-H activation upon de/protonation of the pincer ligand.

Scheme C-2. Intramolecular vinylic C-H activation proposed for **1** and the reaction with chloride.

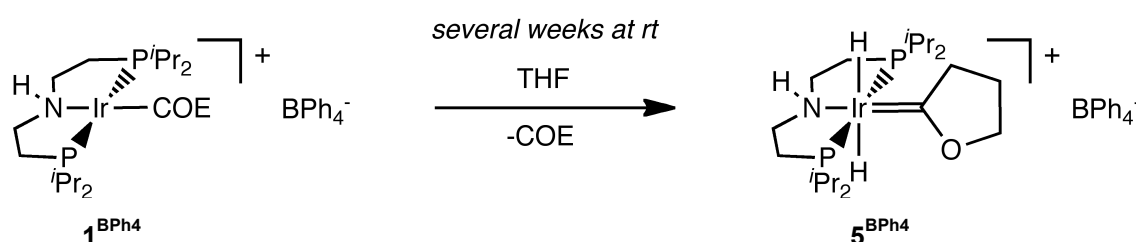


In addition to the described intramolecular C-H activation, the formation of the Fischer-carbene complex $[\text{Ir}(\text{H})_2(=\text{CO}(\text{CH}_2)_3)(\text{PNP}^H)]\text{BPh}_4$ (**5^{BPh4}**) was observed in a saturated THF solution of **1^{BPh4}** after several weeks at room temperature upon α,α -dehydrogenation of THF

² A. Friedrich, R. Ghosh, R. Kolb, E. Herdtweck, S. Schneider, *Organometallics* **2009**, *28*, 708.

(Scheme C-3). Likewise, this result confirmed intermolecular C-H activation with the Ir(PNP) fragment to be possible, although low selectivities were obtained. However, enhanced steric bulk results in lowering the barrier for olefin dissociation, facilitating intermolecular C-H activation with higher selectivities, as recently was shown by Meiners et al.. The replacement of the isopropyl with tert-butyl phosphine groups in the pincer ligand affords selective intermolecular C-H activation to Fischer-carbenes within few hours at room temperature.^[3]

Scheme C-3. Intermolecular C-H Activation of THF with Ir(PNP) fragments (COE = cyclooctene).



The examination of the highly electron rich four-coordinate d^8 dialkylamido complexes yielded important information about M-N bonding and reactivity as potential cooperative catalysts. An expansion to d^6 ruthenium complexes by M. Käß in the group of Dr. S. Schneider offers surprisingly versatile functionalization and access to stable five- and six-coordinate ruthenium(II) amine, amido and enamido complexes starting from [Ru(cymene)Cl₂]₂ and PNP^H.^[4] These ligand functionalization reactions were studied mechanistically in detail in the present thesis. The quantitative formation of enamido complex [Ru(H)PMe₃(PN=P)] (**8**; PN=P = N(CHCHPⁱPr₂)(CH₂CH₂PⁱPr₂)) from the reaction of [RuCl₂PMe₃(PNP^H)] (**7**) with an excess of base can be explained by β -hydride migration from an intermediate amido complex **9** (Scheme C-4).^[5,6] The resulting imine complex [RuCl(H)PMe₃(PN*P)] (**10**; PN*P = N(CHCH₂PⁱPr₂)(CH₂CH₂PⁱPr₂)) could be independently synthesized and gives **8** with KO^tBu.^[6]

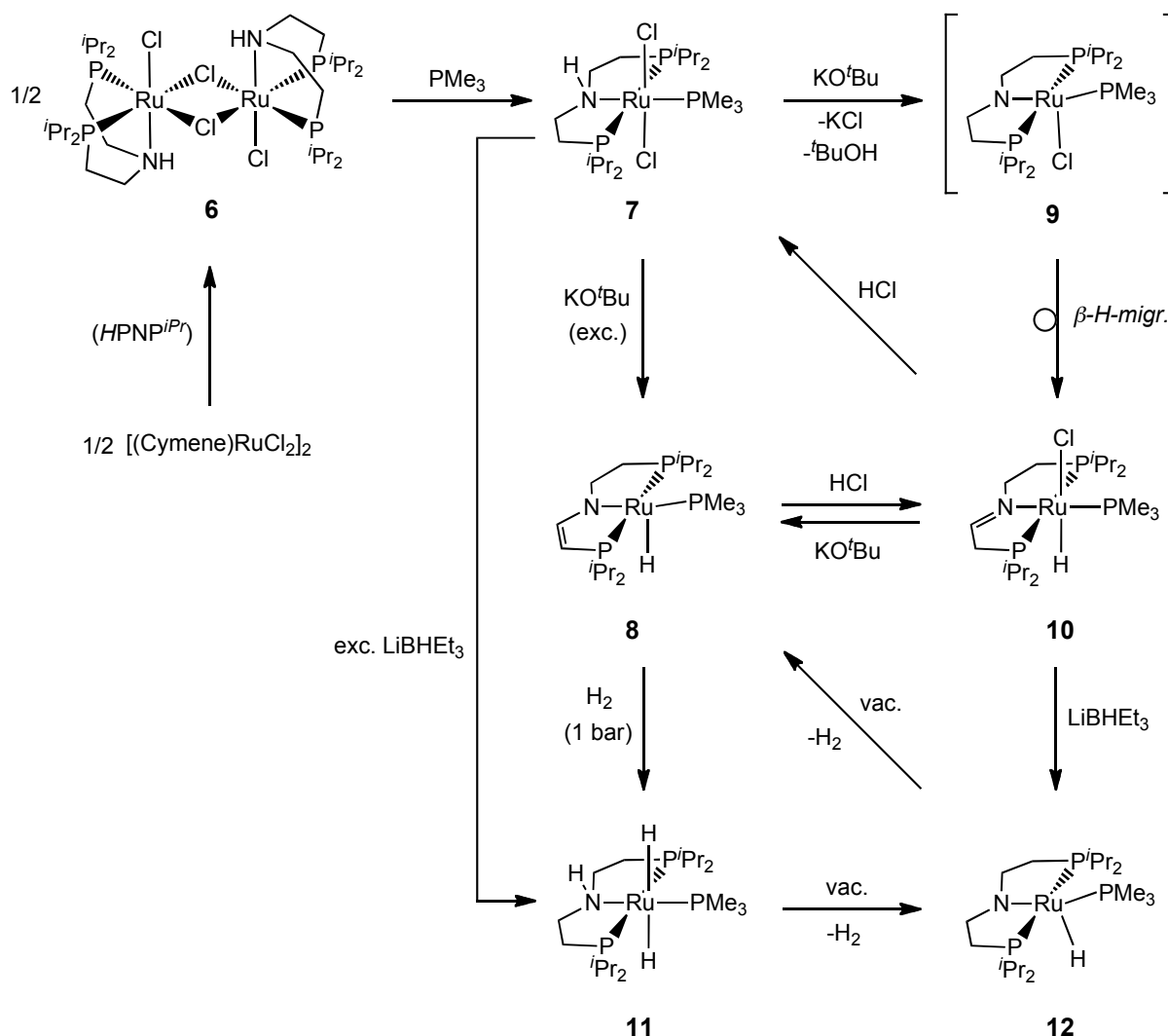
³ J. Meiners, A. Friedrich, E. Herdtweck, S. Schneider, *Organometallics* **2009**, *28*, 6331.

⁴ M. Käß, *Ruthenium Pincer Complexes for acceptorless Alcohol Dehydrogenation and Dehydrocoupling of Ammonia Borane*, Diploma Thesis, TU München, **2008**.

⁵ M. Käß, A. Friedrich, M. Drees, S. Schneider, *Angew. Chem.* **2009**, *121*, 922; *Angew. Chem. Int. Ed.* **2009**, *48*, 905.

⁶ A. Friedrich, M. Drees, M. Käß, E. Herdtweck, S. Schneider, *Inorg. Chem.* **2010**, *49*, 5482.

Scheme C-4. Synthesis of ruthenium(II) PNP-amido, PN=P-enamido, PN*P-imine, and PNP^H-amine complexes.

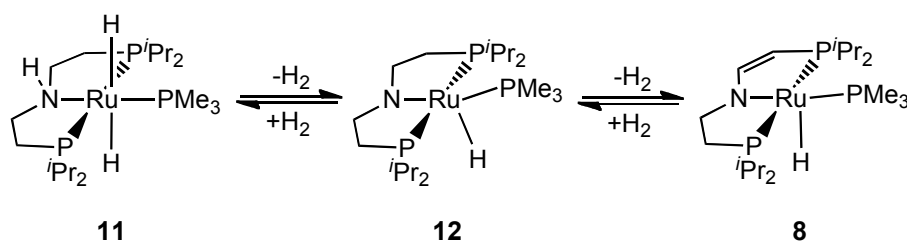


The synthetic potential of the aliphatic Ru(PNP) platform for *cooperative* reactivity is exemplified by the fully reversible addition/elimination of two equivalents of H_2 in the series $11 \rightleftharpoons 12 \rightleftharpoons 8$ (Scheme C-5).^[5] The pincer ligand uniquely combines the well established M–N *bifunctionality* with ligand backbone *cooperativity*, the latter being similar to Milstein's pyridine based PNP ligands.^[7] Most importantly, dehydrogenation of the pincer backbone allows for electronic fine tuning of the ligand π -donor properties, enabling the subtle control of important properties, such as the structure and reactivity of the five-coordinate d^6

⁷ (a) J. Zhang, G. Leitus, Y. Ben-David, D. Milstein, *J. Am. Chem. Soc.* **2005**, *127*, 10840. (b) J. Zhang, G. Leitus, Y. Ben-David, D. Milstein, *Angew. Chem.* **2006**, *118*, 1131; *Angew. Chem. Int. Ed.* **2006**, *45*, 1113.

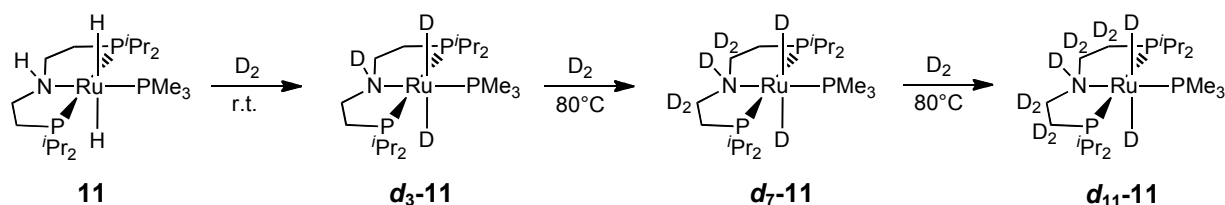
ruthenium complexes **8** and **12** (vide infra). As a major difference with Milstein's pyridine based system, **11** formally exhibits two cooperating functional groups in the pincer backbone - the amine group and the ethylene bridge - which are capable of promoting bifunctional hydrogen activation, allowing for the reversible addition of 2 equiv. of H₂ to **8**.

Scheme C-5. Reversible double H₂ addition/elimination equilibria of **11**, **12**, and **8**.



The mechanism for this equilibrium was examined by H/D labeling studies.^[6] Starting from **11** under an atmosphere of D₂, deuteration of the Ru-H, the N-H, and the pincer backbone protons proceeds in 3 steps, with considerably higher rates for Ru-H and N-H deuteration as compared with pincer backbone H/D exchange (Scheme C-6).

Scheme C-6. Isotomers of **11** observed during successive H/D exchange experiments.



The experimental results were compared with DFT calculations and the observed regioselectivity of H/D exchange is in agreement with the calculated relative barriers for the Ru-H, N-H and C-H activation processes (Figure C-1). The left branch of the reaction sequence (**11**↔**12**) is particularly interesting, as this type of heterolytic H₂ splitting typically represents the rate determining step of the generally accepted mechanism for bifunctional Noyori-type hydrogenation. However, our calculations suggest that H₂ activation by direct intramolecular proton transfer from a η²-H₂ ligand to a basic amido ligand exhibits a relatively high barrier compared with experimental results. Furthermore, the acceleration of catalytic hydrogenation rates by alkali alkoxide cocatalysts, protic solvents, and hydrogenation products points towards the involvement of hydrogen bridging in bifunctional

H₂ activation. However, prior to this work, quantitative experimental studies to clarify this observation were not available.

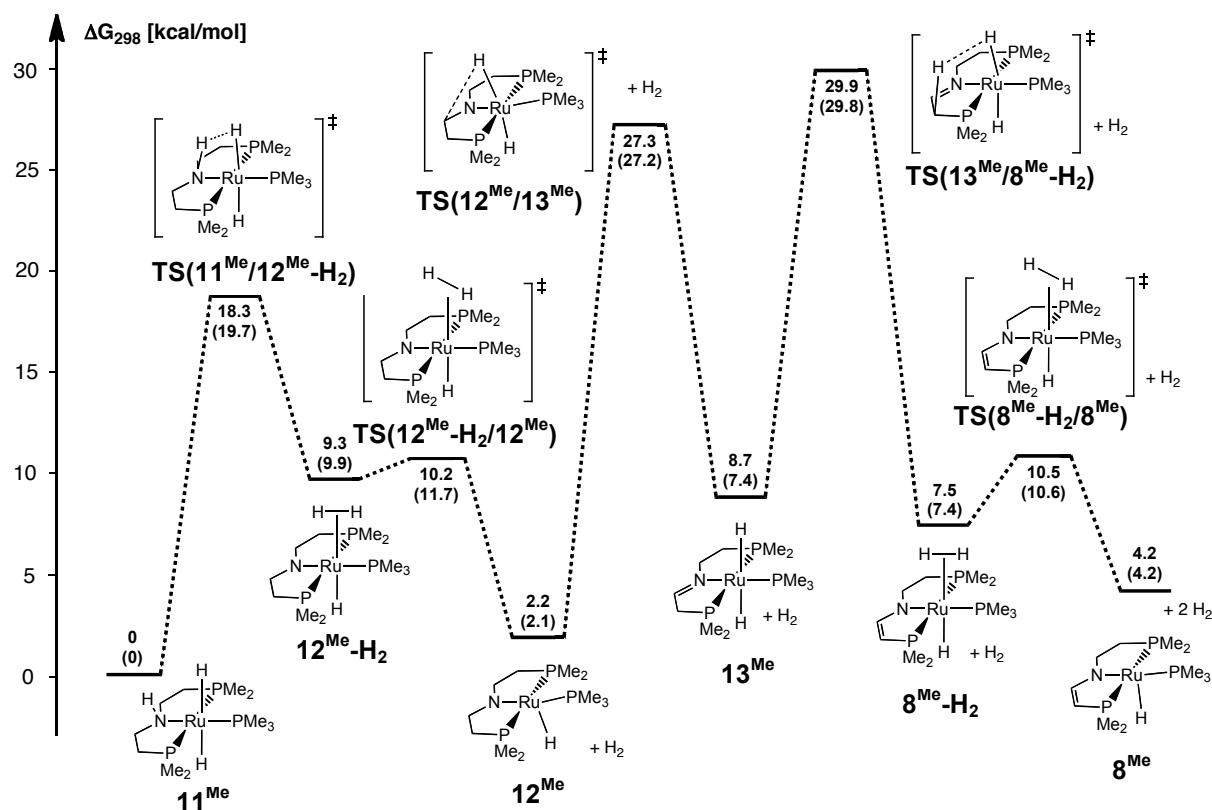


Figure C-1. DFT results (B3LYP/6-31+G**) for the mechanism of H₂ elimination from **11**^{Me} in the gas phase (THF). Free energies in THF (PCM) are given in parantheses.

Narrow ¹H NMR lineshapes and 2D ¹H NOESY NMR spectra suggest for chemical exchange of the N-H and Ru-H functionalities of **11** to be slow on the experimental timescales.^[8] However, the addition of water to a sample of **11** in *d*⁸-THF results in selective broadening of one of the hydride signals and breakdown of mutual hydride *trans* *J*-coupling. Variable temperature *T*₁ measurements suggest stereoselective proton exchange of H₂O with the hydride ligand which is in the proximity of the amine proton. This interpretation could be confirmed and quantified by 2D ¹H EXSY NMR spectroscopy giving high second order exchange rates of H₂O with H^{RuA} and H^{NH} in *d*⁸-THF (Figure C-2). Most intriguingly, no direct exchange of H₂O with H^{RuB} was found. The two hydride ligands are in very similar steric environments and the *trans* dihydride configuration suggests comparable basicities of

⁸ A. Friedrich, M. Drees, J. Schmedt auf der Gönne, S. Schneider, *J. Am. Chem. Soc.* **2009**, *131*, 17552.

the hydride ligands. Therefore, the highly site selective hydride/H₂O exchange can best be rationalized with directing H^{NH}/H₂O hydrogen bonding.

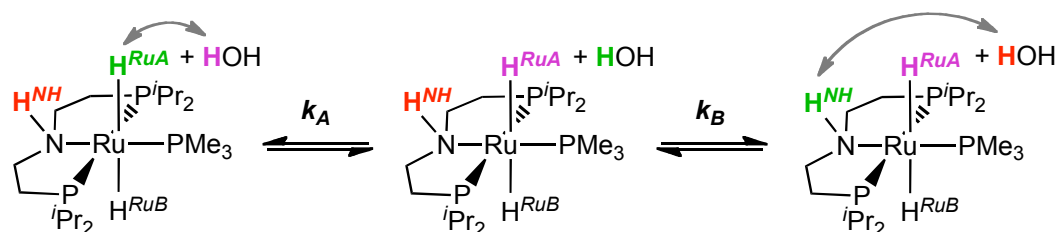


Figure C-2. Exchange of H₂O with H^{RuA} and H^{NH} in amine dihydride complex **11**.

To further probe for the influence of the amine proton, the nitrogen atom was blocked by methylation. H₂O addition to a solution of [Ru(*trans*-H)₂(PMe₃)(PNP^{Me})] (**14**; PNP^{Me} = MeN(CH₂CH₂PⁱPr₂)₂) in *d*⁸-THF results in very slow Ru–H/H₂O proton exchange, which is not stereoselective, fully confirming our mechanistic model. Like for hydrogen addition to amide complex **12** proton/hydride exchange should proceed via the same dihydrogen complex intermediate (**12-H₂**). Therefore, these results suggest that water lowers the barrier of heterolytic hydrogen splitting. DFT calculations confirm this interpretation indicating a lower barrier by $\Delta\Delta G^\ddagger = 8.2$ kcal/mol for water catalyzed hydrogen splitting. This mechanistic study emphasizes the important role of Brønsted acids, such as water or alcohols, for bifunctional, Noyori-type hydrogenation catalysis.

Concerning the right branch of the hydrogen activation sequence in Figure C-1 (**12**↔**8**), comparison of the related PNP and PN=P ligands is of particular interest since the enamido type pincer ligand was not known prior to this work. While the molecular structure of amido complex **12** can best be described by a Y-shaped distorted trigonal-bipyramid, the analogous enamido complex **8** exhibits a structure much closer to square pyramidal coordination. The different molecular structures of **12** and **8** can be attributed to considerably diminished N→Ru π -donation in **8**, owing to delocalization of the *N*-lone pair by conjugation with the C=C double bond in the enamido ligand. The weaker π -donation of the dehydrogenated pincer ligand can be utilized to control the reactivity of the five-coordinate *d*⁶ complexes. The low lying LUMO in square-pyramidal complex **8** is expressed in the different colors of red **12** and green **8** and explains the Lewis-acidic behavior of **8**, as documented by the formation of octahedral complex [RuH(PMe₃)₂(PN=P)] (**15**) upon addition of PMe₃. In comparison, the reaction of **12** with PMe₃ gives a mixture of **11** and **15** via a base-assisted hydrogen elimination pathway.^[6] On the other hand, with electrophiles, such as MeOTf, predominant

N-methylation is observed for both **12** and **8**, giving rise to [RuH(OTf)PMe₃(PNP^{Me})] (**16**) and [RuH(OTf)PMe₃(PN=P^{Me})] (**17**), respectively. C-methylation of **8** occurs only in 25% yield, as determined by ³¹P NMR spectroscopy. This reactivity of **8** contrasts with pyridine-based cooperative pincer analogues where C-methylation is preferential and can be attributed to the high flexibility of the aliphatic PN=P pincer ligand. Overall, the structural and reactivity patterns place this novel enamido ligand PN=P between the strongly π -donating alkylamido PNP ligand and acceptor *N*-substituted, moderately π -donating amido pincer ligands, such as silylamides N(SiMe₂CH₂PR₂)₂ or arylamides N(C₆H₄-2-PR₂)₂. Thermodynamics of the β -hydride migration reactions are strongly dependent on the other ligands bound to the metal, exemplified by the synthesis of complex **10** vs. the instability of elusive complex **13**. Hence, the *trans* dihydride configuration might be an important structural feature to stabilize Noyori-type hydrogenation catalysts against deactivation to an imine complex.

2. Cooperative catalysis

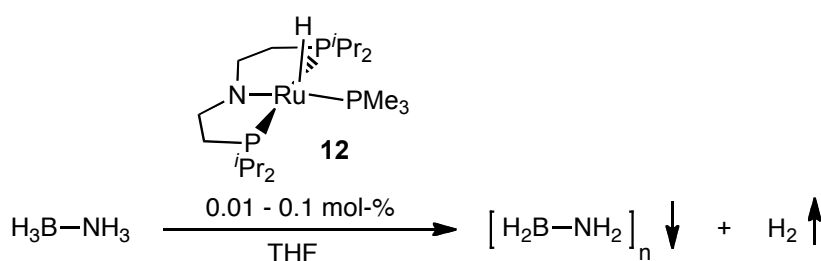
The ruthenium PNP complex **12** exhibits unprecedented activity and turnovers in the dehydrogenation of ammonia borane (H₃N-BH₃ = AB) at room temperature with catalyst loadings as low as 0.01 mol%, marking the most active known homogeneous catalyst to date (Scheme C-7).^[5] Vigorous H₂ evolution from AB is simultaneous with the formation of a white polymer [H₂NBH₂]_n, which turned out to be insoluble in all common organic solvents. Catalyst loadings of 0.1 mol% **12** produce slightly more than 1 equiv. H₂, attributable to quantitative formation of polyaminoborane and small amounts of borazine.

In collaboration with the groups of Ian Manners (University of Bristol) and Jörn Schmedt auf der Günne (Ludwig-Maximilians-Universität München), the polymeric product from AB dehydrocoupling was further examined.^[9] Solid-state ¹¹B-MQ-MAS NMR spectra were recorded to suppress second order quadrupolar effects showing two signals assignable to BH₂ domains and BH₃ end groups in the polymer. No indication for BH or quaternary B moieties were found pointing towards the absence of cross-linking in the polymer, which is in agreement with the reaction stoichiometry. Owing to the lack of solubility, this result could not be correlated with molecular weight information from gel permeation chromatography

⁹ (a) A. Staubitz, M. E. Sloan, A. P. M. Robertson, A. Friedrich, S. Schneider, P. J. Gates, J. Schmedt auf der Günne, I. Manners, *J. Am. Chem. Soc.* **2010**, *132*, 13332. (b) A. Friedrich, S. Schneider, *unpublished*.

(GPC). However, polymerization of MeH₂N-BH₃ (MAB) and copolymerization of AB and MAB with **12** results in a linear polymer with high molecular weight, as shown by ¹¹B-MQ-MAS NMR, GPC, and electrospray mass spectrometry. These results are particularly interesting with respect to the reaction mechanism. Mechanistic information about metal catalyzed amine-borane dehydrogenation remains scarce and all experimental and computational studies suggest the formation of cyclic oligoaminoboranes or borazine derivatives exhibiting only BH₂ and BH functionalities. Therefore, the formation of a linear polymer from AB dehydrocoupling with catalyst **12** exhibiting BH₃ end groups and no BH groups points towards a different reaction mechanism.

Scheme C-7. Dehydrocoupling of AB with precatalyst **12**.



To gain further information, AB dehydrogenation with **12** was examined by kinetic experiments using volumetric measurement of H₂. Initial rate measurements with different catalyst loadings reveal a first-order dependence in **12**. Furthermore, for a wide range of catalyst and substrate initial concentrations also first-order dependence in AB over more than one half-life was suggested and a kinetic isotope effect (KIE) of 1.8 for the dehydrogenation of the *B*-deuterated isotopomer H₃N-BD₃ was derived from ln[AB] over time plots. The observed normal isotope effect is in qualitative agreement with the expectation for a step with a symmetrically bridging μ-hydride ligand in the transition state.^[10] However, the situation for the *N*-deuterated substrates D₃N-BH₃ and D₃N-BD₃ is different. In both cases, a significantly lower reaction rate with zero-order dependence of H₂ release on substrate concentration was observed. Therefore, KIE's for these isotopomers cannot be directly derived by referencing to unlabelled AB. This result indicates a change in the reaction order with a different turnover limiting step for *N*-deuterated substrates. The bifunctional effect of catalyst **12** was

¹⁰ Based on a B-H stretching vibration around 2350 cm⁻¹ the maximum H/D isotope effect for full B-H bond cleavage in AB is expected to be 4.9.

demonstrated by kinetic control experiments with tertiary amine complex $[\text{Ru}(\text{trans-H})_2(\text{PMe}_3)(\text{PNP}^{\text{Me}})]$ (**14**) as catalyst, exhibiting smaller rates in AB dehydrogenation of around two orders of magnitudes.^[9b] These measurements gave some important mechanistic informations:

- 1) reaction monitoring of AB dehydrocoupling with **12** by ^{31}P and ^1H NMR spectroscopy initially shows amine complex **11** exclusively, suggesting for **11** to represent the catalytic resting state.
- 2) The slow rate for H_2 elimination from complex **11**, as similarly found in Fagnou's DFT study,^[11] indicates that a mechanism with spontaneous H_2 elimination from the corresponding amine complex is not the rate determining step. Furthermore, the observed first order dependence of the rate on substrate points towards a different rate determining step.
- 3) The turnover number (TON) is highly dependent on initial substrate concentration $[\text{AB}]_0$. Maximum TON's are achieved for high $[\text{AB}]_0$ concentrations and low catalyst loadings, which is desirable from the point of hydrogen storage to obtain high gravimetric H_2 density.
- 4) Catalyst deactivation is attributed to the formation of $[\text{Ru}(\text{H})(\text{PMe}_3)(\text{H}_2\text{NBH}_2\text{PNP}^{\text{iPr}})]$ (**18a**) with a rare M–N–B–H four membered borametallacycle.^[12] Complex **18a** is not completely inactive in AB dehydrogenation but exhibits catalytic rates which are smaller by some orders of magnitude, as compared with **11** and **12**. The formation of **18a** can be attributed to addition of transient aminoborane $\text{H}_2\text{N-BH}_2$ across the N–Ru bond of **12**. Hence, high $[\text{AB}]_0$ concentrations provides low aminoborane steady-state concentrations.

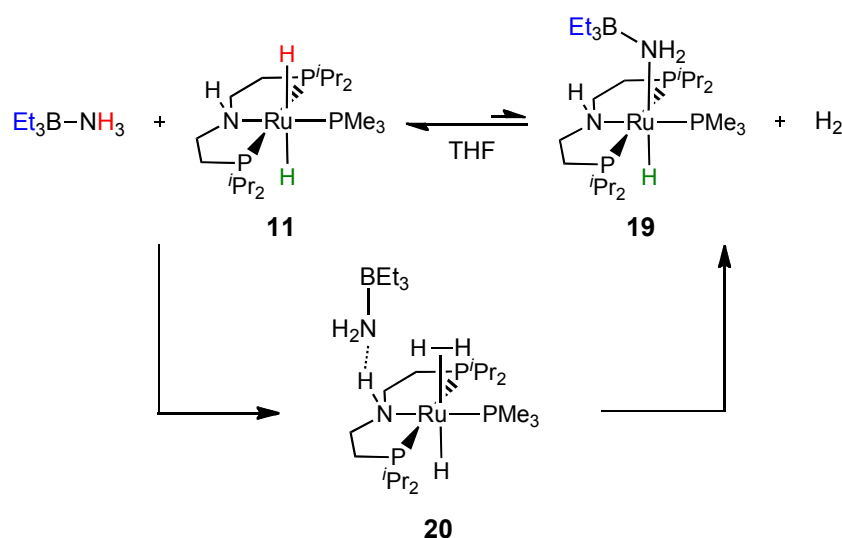
B-terminally blocked $\text{H}_3\text{N-BEt}_3$ was used to study the interaction of the amino group of borane amines with complex **11**, which we propose to represent the catalytic resting state in the borane-amine dehydrocoupling reaction. Upon mixing, a small equilibrium concentration of a new complex is observed by NMR spectroscopy which was assigned to borane-amido complex **19** (Scheme C-8). The equilibrium was further examined applying 2D ^1H EXSY NMR spectroscopy as described for exchange of **11** with other Brønsted acids like water.

¹¹ N. Blaquiere, S. Diallo-Garcia, S. I. Gorelsky, D. A. Black, K. Fagnou, *J. Am. Chem. Soc.* **2008**, *130*, 14034.

¹² A. Friedrich, M. Drees, S. Schneider *Chem. Eur. J.* **2009**, *15*, 10339.

These experiments revealed rapid chemical exchange of complexes **11** and **19** and of the $\text{H}_3\text{N}-\text{BEt}_3$ N-H protons with the Ru-H ligand in syn-position to the pincer ligand N-H proton. Therefore, exchange proceeds via the dihydrogen complex intermediate **20**. On the other hand, N-terminal blocked $\text{Me}_3\text{N}-\text{BH}_3$ showed no reaction with **11** over hours. The cooperativity of the amine function for the formation of a dihydrogen complex intermediate is further demonstrated by the very slow Ru-H/ NH_3 proton exchange in a reaction mixture of $\text{H}_3\text{N}-\text{BEt}_3$ and *N*-methylated catalyst **14** on the NMR time-scale.

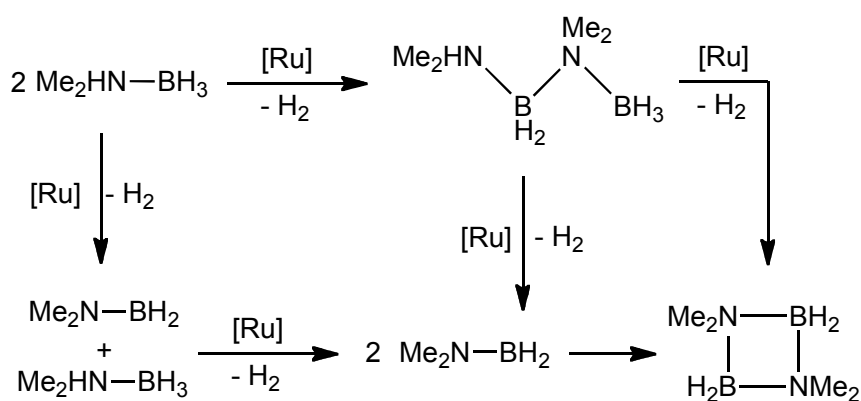
Scheme C-8. Reaction of **11** with $\text{H}_3\text{N}-\text{BEt}_3$ and proposed mechanism via a dihydrogen complex **20**. Colours indicate selected chemical exchange cross peaks observed by 2D ^1H EXSY NMR.



Some more mechanistic information has been obtained from the dehydrocoupling of $\text{Me}_2\text{HN}-\text{BH}_3$ (DMAB). Since the examination of DMAB dehydrocoupling is not hampered by the formation of polymeric, insoluble B-N products, it can be easily studied by means of solution ^{11}B NMR spectroscopy. The reaction proceeds quantitatively with catalysts **11** and **12**, but after high initial rates the reaction considerably slows down prior to complete conversion. This observation can be attributed to more rapid formation of catalyst deactivation product $[\text{Ru}(\text{H})(\text{PMe}_3)(\text{Me}_2\text{NBH}_2\text{PNP})]$ (**18b**), as compared with **18a** during AB dehydrocoupling.^[12] Monitoring the reaction by ^{11}B NMR spectroscopy reveals the formation of transient aminoborane $\text{Me}_2\text{N}-\text{BH}_2$, which rapidly dimerizes. Furthermore, linear diborazane $\text{Me}_2\text{HN}-\text{H}_2\text{B}-\text{Me}_2\text{N}-\text{BH}_3$ is observed as an intermediate. Accordingly, dehydrocyclization of $\text{Me}_2\text{HN}-\text{H}_2\text{B}-\text{Me}_2\text{N}-\text{BH}_3$ with **12** yields the final dehydrocyclization product $(\text{Me}_2\text{N}-\text{BH}_2)_2$ and H_2 quantitatively. The latter reaction most likely proceeds both by direct

dehydrocyclization to $(\text{Me}_2\text{N}-\text{BH}_2)_2$ and diborazane dehydrogenation with $\text{Me}_2\text{N}-\text{BH}_2$ formation, as suggested by ^{11}B NMR spectroscopic reaction monitoring. Spectroscopic kinetics and quantumchemical calculations suggests for the formation of diborazane $\text{Me}_2\text{HN}-\text{H}_2\text{B}-\text{Me}_2\text{N}-\text{BH}_3$ to be a metal catalyzed process as it cannot be attributed to an uncatalyzed rearrangement of transient $\text{Me}_2\text{N}-\text{BH}_2$ with DMAB. For further clarification a control experiment was conducted by mixing *B*-terminally blocked $\text{H}_3\text{N}-\text{BEt}_3$ and *N*-terminally blocked $\text{Me}_3\text{N}-\text{BH}_3$ in the presence of catalyst **11**. However, no B–N coupling was observed pointing out that intermolecular borane-amine head-to-tail dehydrocoupling is not a viable pathway.

Scheme C-9. Mechanistic proposal for DMAB dehydrocyclization with catalysts **11** or **12**.



Based on these results, a mechanism for DMAB dehydrocyclization is proposed, suggesting for both DMAB dehydrogenation and B–N coupling to be catalyzed (Scheme C-9): Initial intramolecular dehydrogenation of DMAB releases aminoborane $\text{Me}_2\text{N}-\text{BH}_2$, which can either react with DMAB in a metal catalyzed process towards the linear diborazane or dimerize with another equivalent of aminoborane to the final product. Catalytic dehydrogenation of the diborazane intermediate results in cyclization or B–N bond scission. The resulting aminoborane monomers quickly dimerize. If these results on DMAB dehydrogenation can be generalized to other amine-boranes, they provide a mechanistic rationale for the formation of linear aminoborane polymers instead of polyborazine, as observed for AB dehydrocoupling with catalyst **12**.

The present kinetic, spectroscopic, and computational results allow for the proposal of a mechanistic model for AB dehydropolymerization, which accounts for the formation of linear aminoboranes. The mechanism can be broken down into two connected catalytic cycles

(Scheme C-10): The upper cycle accounts for AB dehydrogenation with release of H₂ and aminoborane H₂N-BH₂, respectively. Starting from precatalyst **12**, reaction with AB forms borane-amine adduct **21**, which successively gives resting state **11** upon release of aminoborane H₂N-BH₂. These steps have been proposed by Fagnou et al. for bifunctional AB dehydrocoupling, as well.^[11] As a major difference to Fagnou's proposal, we suggest a proton shuttle mechanism for the formation of the dihydrogen complex **22**. DFT calculations for the sequence **11** + AB → **22** + AB → **12** + AB + H₂ → **21** + H₂ → **11** + H₂ + H₂N-BH₂ suggests a shallow potential energy surface which is in agreement with the extraordinarily high experimental catalytic rates. First-order dependence on [AB], found for a wide range of substrate initial concentrations and also for *B*-deuterated AB, would be in agreement with **12** + AB + H₂ → **21** + H₂ to be turnover limiting.^[13] Upon *N*-deuteration of the substrate, other steps in the postulated cycle, which are all zero-order in [AB] contribute to the overall rate. Formation of the observed catalyst deactivation product **18** can be explained by an off-cycle reaction of **12** with free aminoborane to give the isolable hydride-bridged boraruthenacycle.

The lower cycle in Scheme C-10 accounts for B-N coupling. While the H₂-release kinetics do not provide information about the actual B-N coupling step, some qualitative observations point towards a metal centered reaction:

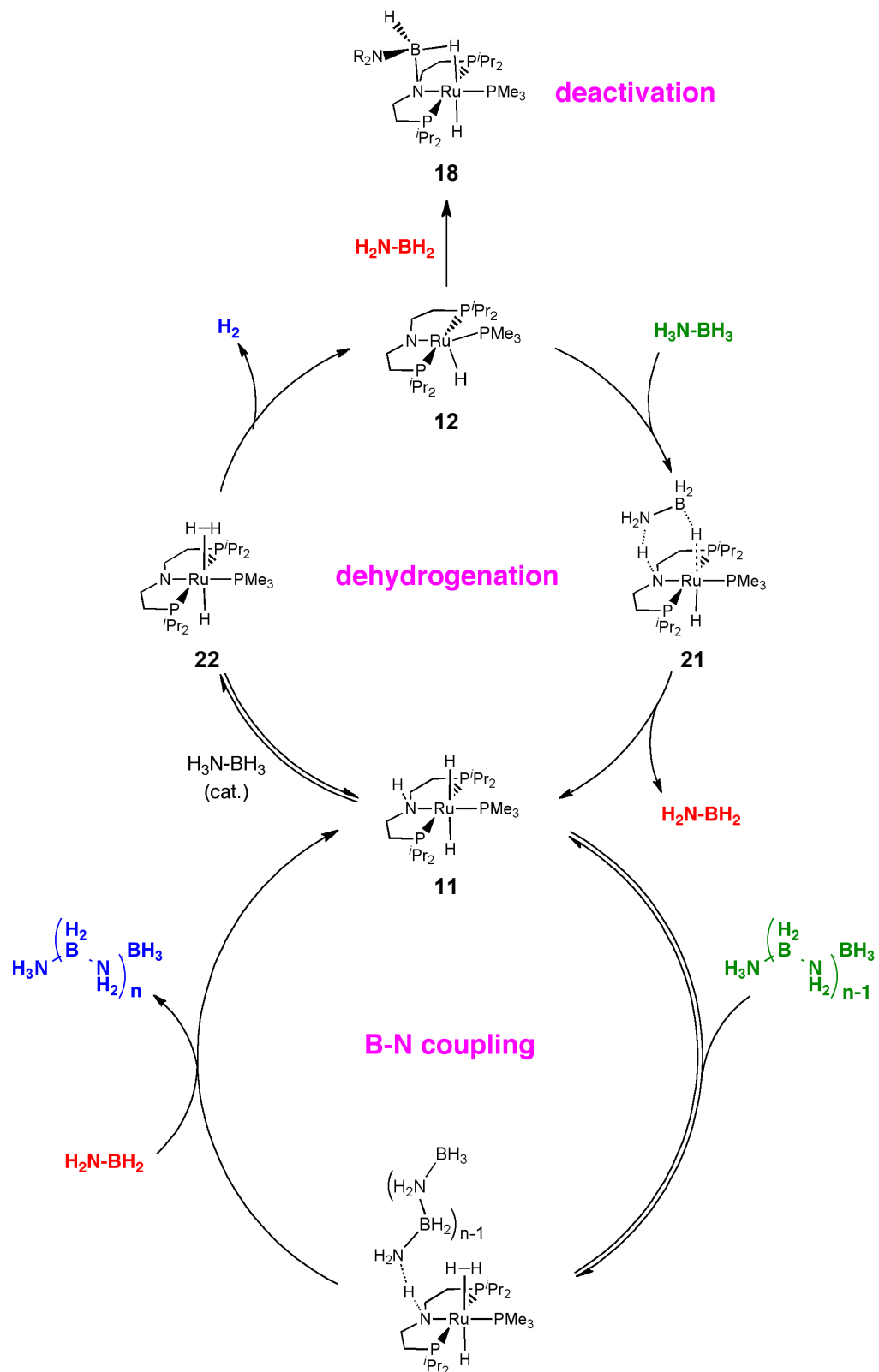
- 1) Dehydrocoupling of Me₂AB shows higher steady-state concentrations of intermediate linear coupling product Me₂HN-BH₂-NMe₂-BH₃ with higher catalyst loadings.
- 2) All experimental and quantumchemical examinations from other groups suggest the formation of cyclic AB dehydrocoupling products (and ultimately borazine and polyborazine) to result from uncatalyzed aminoborane rearrangement. However, only minor amounts of borazine are observed, which might stem from uncatalyzed aminoborane coupling as a side reaction with higher barriers.

Based on DFT calculations a B-N coupling cycle upon Ru-catalyzed aminoborane insertion into an AB N-H bond with small barriers is proposed. For further chain propagation, oligomeric and polymeric intermediates H₃N-(BH₂-NH₂)_{*n*}-BH₃ (*n* ≥ 1) can enter the B-N coupling cycle instead of parent AB. Ultimately, for polymers exceeding a critical chain length, low solubility will result in precipitation from solution. In agreement with the report of

¹³ DFT calculations for the transition state TS(**12** + AB/**21**) are currently in progress.

Staubitz et al., our experimental results indicate that this condition is matched in THF at $n \approx 20$.^[9a]

Scheme C-10. Proposed catalytic cycle for borane-amine dehydrocoupling with catalyst **12**.



Overall, our Ru(PNP)-catalyst can be considered *bifunctional* in the literal and a figurative sense: a bifunctional mechanism is adopted with two functional groups of the catalyst being involved in the turnover limiting steps and the ruthenium compound incurs two separate functions, being catalysts both for dehydrogenation and B-N-coupling. The mechanistic model for extraordinarily rapid borane-amine dehydrogenation with Ru(PNP)-catalysts provides an excellent basis for further catalyst design and an important prerequisite to control of the BN-polymer structure for materials applications. Dehydrocoupling of other polar inorganic substrates, such as borane-phosphine adducts or aminosilanes, could afford interesting new inorganic polymers, e.g. as precursors for semiconducting materials.^[14] In contrast to most other catalysts, amido hydride complex **12** enables dehydrogenation under base free conditions.

¹⁴ (a) T. J. Clarke, K. Lee, I. Manners, *Chem. Eur. J.* **2006**, *12*, 8634. (b) T. Chievers, I. Manners, in *Inorganic Rings and Polymers of the p-Block Elements*, RSC Publishing, Cambridge, **2009**.

D Zusammenfassung

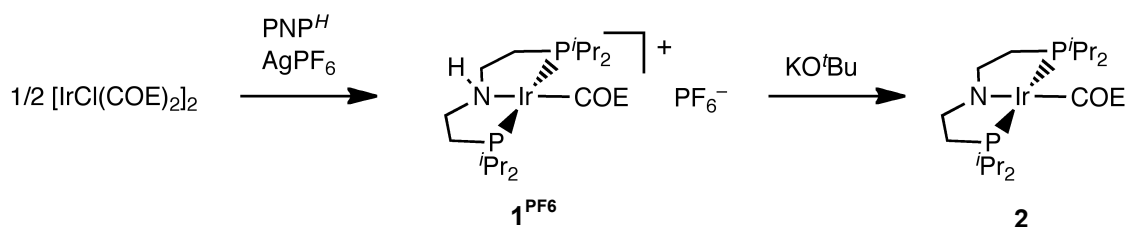
Zusammenfassung

Die Koordinationschemie von d^6 Ruthenium- und d^8 Iridium-Amidkomplexen wurde studiert und insbesondere hinsichtlich *kooperativer* Reaktivität für katalytische Anwendungen untersucht. Das verwendete ethylenverbrückte, dreizählige Diphosphanamid-Chelatgerüst (PNP) vereint auf einzigartige Art und Weise die M-N *Bifunktionalität* von elektronenreichen Übergangsmetall-Amidkomplexen mit *Ligandrückgrat-Kooperativität*. Neben mechanistischen Informationen zu stöchiometrischer C-H und H₂ Aktivierung wird das große Potential der Ru(PNP) Plattform für die katalytische, ionische (De-)Hydrierung demonstriert. Von besonderem Interesse hinsichtlich chemischer Wasserstoffspeicherung und der Synthese neuartiger anorganischer Polymere ist die Boranammin Dehydrierung; detaillierte Studien mit Ru(H)PMe₃(PNP), dem aktuell aktivsten Katalysator, legen hierfür einen *bifunktionalen* Mechanismus nahe. Dieser erklärt die Kontrolle über die Struktur des polymeren B-N Kupplungsprodukts.

1. Reaktivität von elektronenreichen M(PNP) (M = Ir, Ru) Fragmenten: E-H (E = C, N, H) Bindungsaktivierung

Der ethylenverbrückte PNP Pinzettenligand N(CH₂CH₂PⁱPr₂)₂ (PNP) ermöglicht synthetischen Zugang zu späten, elektronenreichen Übergangsmetall-Dialkylamidokomplexen in hohen Ausbeuten. Wie in einer vorausgehenden Untersuchung gezeigt wurde,^[1] führt die Reaktion des Pinzettenliganden PNP^H (HN(CH₂CH₂PⁱPr₂)₂) mit [IrCl(COE)₂]₂ (COE = Cycloocten) und AgPF₆ zum Iridium(I)-Aminoolefinkomplex [IrCOE(PNP^H)]PF₆ (**1**^{PF6}). Deprotonierung mit KO^tBu führt zum entsprechenden Amidokomplex [IrCOE(PNP)] (**2**) (Schema D-1).

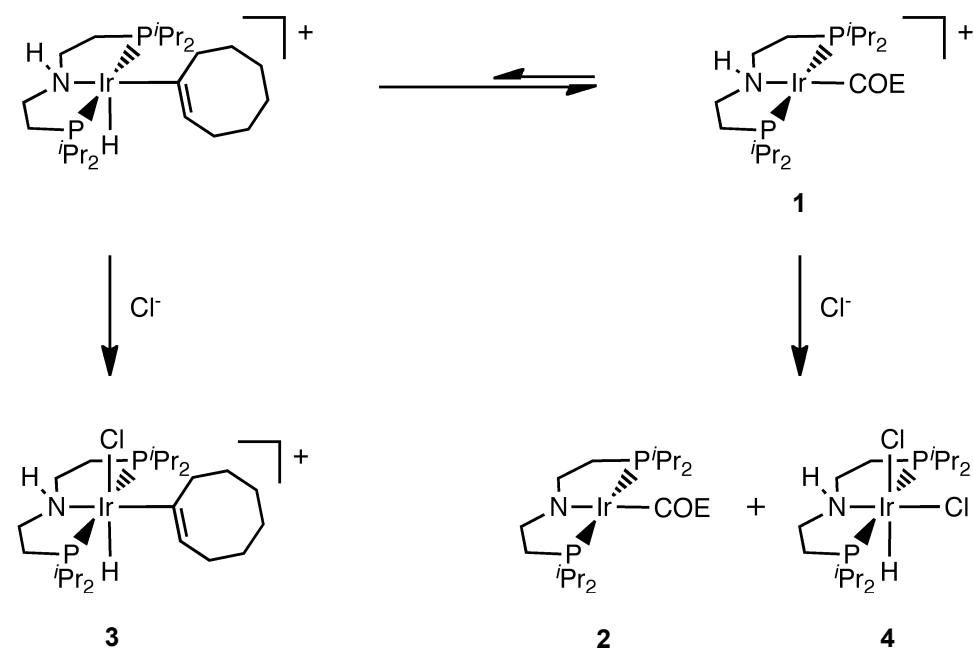
Schema D-1. Synthese von Ir^I(PNP) Komplexen.



¹ A. Friedrich, *Synthese und Charakterisierung von Iridiumkomplexen mit chelatisierten Amin- und Amidophosphanliganden*, Diplomarbeit, TU München, 2007.

In der vorliegenden Arbeit wurde die Reaktivität der Ir^I(PNP) Verbindungen hinsichtlich C-H und N-H Bindungsaktivierungsprozessen untersucht. So zeigt sich, dass der Olefinkomplex [IrCOE(PNP^H)]⁺ (**1**) bei Raumtemperatur im Gleichgewicht mit dem Hydridocyclooctenylisomer [IrH(C₈H₁₃)(PNP^H)]⁺ nach vinyli-scher C-H Aktivierung mit sehr niedriger Barriere steht. In Anwesenheit von Chlorid kann der Vinylhydridokomplex [IrHCl(C₈H₁₃)(PNP^H)] (**3**) abgefangen werden (Schema D-2). Allerdings wird durch Chlorid auch N-H Aktivierung ausgelöst und eine Mischung aus **2**, **3** und [IrHCl₂(PNP^H)] (**4**) wurde bei der Reaktion von [IrCl(COE)₂]₂ mit PNP^H in nichtprotischen Lösungsmitteln ohne Chloridanionenaustausch mit schwach koordinierenden Anionen wie PF₆⁻ oder BPh₄⁻ beobachtet. Der komplexe Mechanismus dieser Reaktionskaskade konnte durch kinetische Modellierung vollständig aufgeklärt werden.^[2] Im Gegensatz zum dynamischen Verhalten von **1** ist die Struktursteifigkeit des entsprechenden Amidokomplexes **2** auf die starke N-Ir-Olefin Dreizentren- π -Wechselwirkung (3c-4e) zurückzuführen und veranschaulicht damit den elektronenreichen Charakter des Ir(PNP) Fragments. Dies macht **1/2** zu einem interessanten System, das eine schaltbare intramolekulare C-H Aktivierung durch De-/Protonierung des Pinzettenliganden ermöglicht.

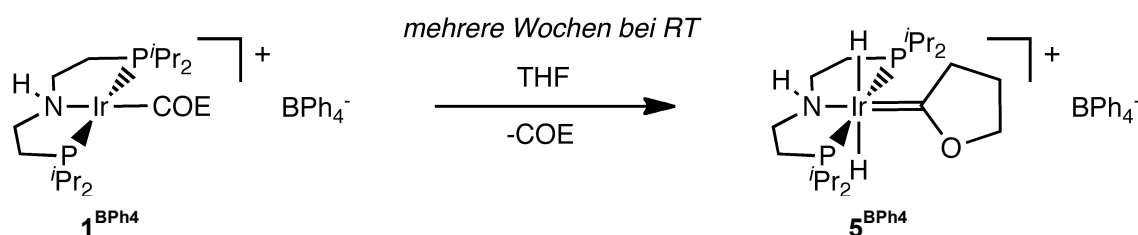
Schema D-2. Vorgeschlagene intramolekulare vinyli-sche C-H Aktivierung für **1** und Reaktion mit Chlorid.



² A. Friedrich, R. Ghosh, R. Kolb, E. Herdtweck, S. Schneider, *Organometallics* **2009**, *28*, 708.

Neben der beschriebenen intramolekularen C-H Aktivierung wurde die Bildung eines Fischer-Carbenkomplexes $[\text{Ir}(\text{H})_2(=\text{CO}(\text{CH}_2)_3)(\text{PNP}^H)]\text{BPh}_4$ (**5^{BPh4}**) durch α,α -Dehydrierung von THF in einer gesättigten THF Lösung von **1^{BPh4}** nach einigen Wochen bei Raumtemperatur beobachtet (Schema D-3). Dieses Ergebnis bestätigt eine ebenso mögliche intermolekulare C-H Aktivierung mit Ir(PNP) Fragmenten, obwohl nur geringe Selektivität erhalten wurde. Sterisch anspruchsvollere Substituenten jedoch senken die Barriere zur Olefin-Dissoziation und erleichtern damit die intermolekulare C-H Aktivierung, verbunden mit höherer Selektivität, wie erst kürzlich von Meiners et al. gezeigt wurde. Der Austausch von Isopropyl- durch tert-Butylphosphangruppen im Pinzettenligand ermöglicht selektive intermolekulare C-H Aktivierung zu Fischer-Carbenen innerhalb weniger Stunden bei Raumtemperatur.^[3]

Schema D-3. Intermolekulare C-H Aktivierung von THF an Ir(PNP) Fragmenten (COE = Cycloocten).



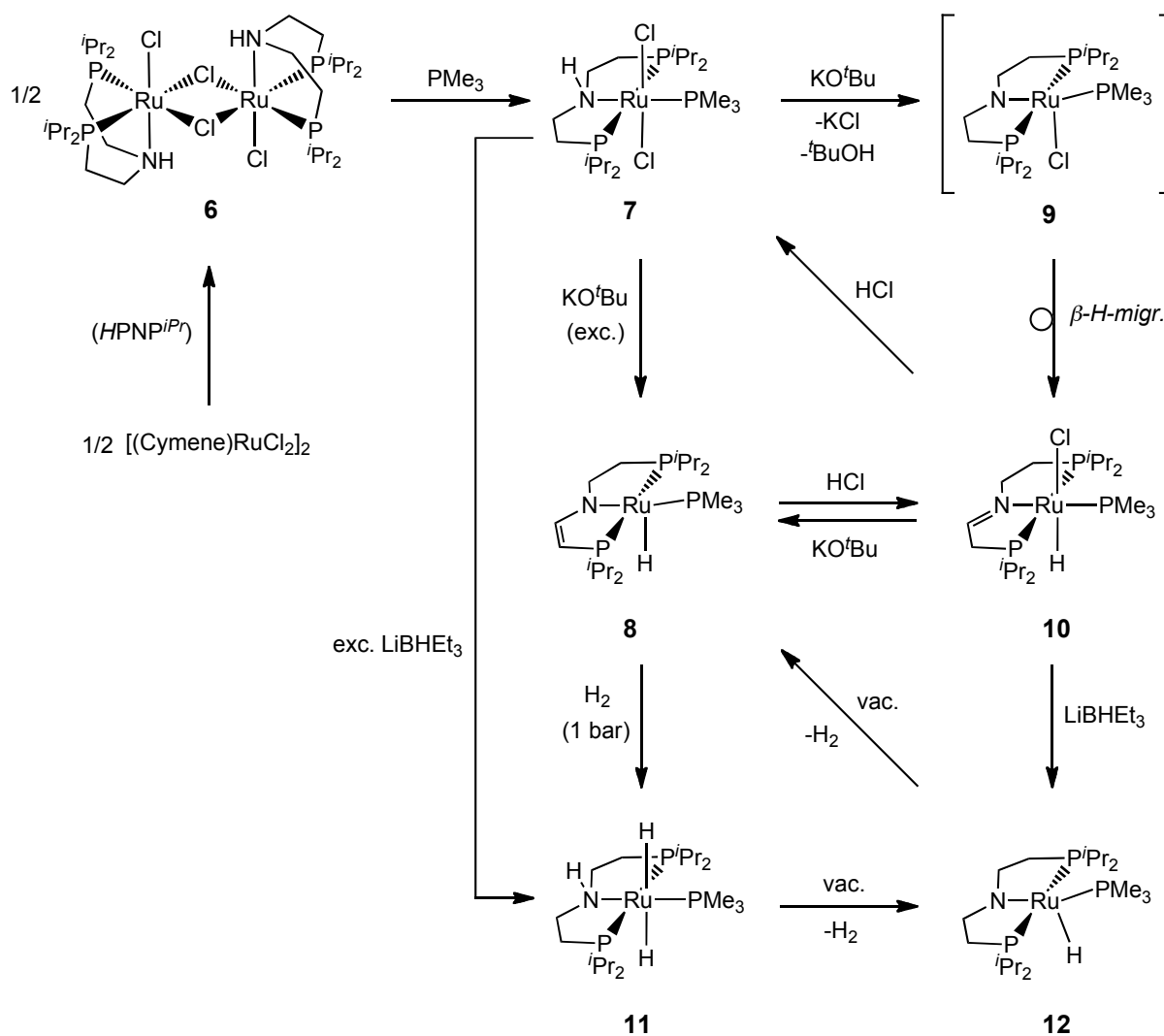
Die Untersuchung der äußerst elektronenreichen, vierfach koordinierten d^8 Dialkylamido-komplexe lieferte wichtige Informationen über M-N Bindung und Reaktivität für den Einsatz als mögliche kooperative Katalysatoren. Eine Erweiterung auf d^6 Rutheniumkomplexe durch M. Käß in der Arbeitsgruppe von Dr. S. Schneider bot eine erstaunlich vielseitige Funktionalisierung und den Zugang zu stabilen fünf- und sechsfach koordinierten Ruthenium(II) Amin, Amido- und Enamidokomplexen, ausgehend von $[\text{Ru}(\text{Cymol})\text{Cl}_2]_2$ und PNP^H .^[4] Zu diesen Ligandfunktionalisierungsreaktionen wurden in der vorliegenden Arbeit detaillierte mechanistische Studien durchgeführt. Die quantitative Bildung von Enamidokomplex $[\text{Ru}(\text{H})\text{PMe}_3(\text{PN}=\text{P})]$ (**8**; $\text{PN}=\text{P} = \text{N}(\text{CHCHP}^i\text{Pr}_2)(\text{CH}_2\text{CH}_2\text{P}^i\text{Pr}_2)$) in der Reaktion von $[\text{RuCl}_2\text{PMe}_3(\text{PNP}^H)]$ (**7**) mit einem Überschuss an Base kann durch β -Hydrid-

³ J. Meiners, A. Friedrich, E. Herdtweck, S. Schneider, *Organometallics* **2009**, *28*, 6331.

⁴ M. Käß, *Ruthenium-Pincer-Komplexe zur akzeptorfreien Dehydrierung von Alkoholen und Dehydrokupplung von Amminboran*, Diplomarbeit, TU München, **2008**.

Migration des intermediär gebildeten Amidokomplex **9** erklärt werden (Schema D-4).^[5,6] Der entstehende Iminkomplex $[\text{RuClHPMe}_3(\text{PN}^*\text{P})]$ (**10**; $\text{PN}^*\text{P} = \text{N}(\text{CHCH}_2\text{P}^i\text{Pr}_2)(\text{CH}_2\text{CH}_2\text{P}^i\text{Pr}_2)$) konnte auf anderem Wege synthetisiert und isoliert werden und reagiert mit KO^tBu zu **8**.^[6]

Schema D-4. Synthese von Ruthenium(II) PNP-Amido-, $\text{PN}=\text{P}$ -Enamido-, PN^*P -Imin- und PNP^H -Aminkomplexe.



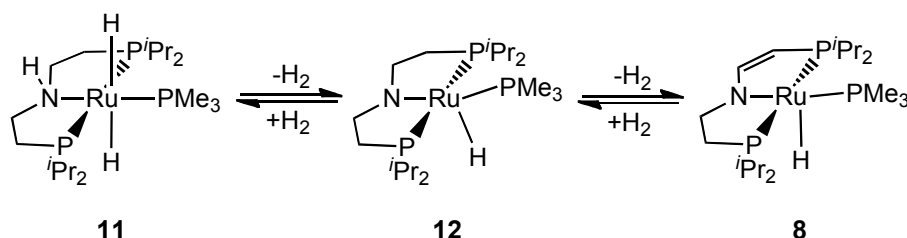
Das synthetische Potential der aliphatischen $\text{Ru}(\text{PNP})$ -Plattform für *kooperative* Reaktivität wird durch vollständig reversible Addition/Eliminierung von zwei Äquivalenten H_2 in der Reihe $\mathbf{11} \rightleftharpoons \mathbf{12} \rightleftharpoons \mathbf{8}$ beispielhaft erläutert (Schema D-5).^[5] Der Pinzettenligand vereint auf einzigartige Art und Weise M-N *Bifunktionalität* mit *Ligandrückgrat-Kooperativität*, die

⁵ M. Käß, A. Friedrich, M. Drees, S. Schneider, *Angew. Chem.* **2009**, *121*, 922; *Angew. Chem. Int. Ed.* **2009**, *48*, 905.

⁶ A. Friedrich, M. Drees, M. Käß, E. Herdtweck, S. Schneider, *Inorg. Chem.* **2010**, *49*, 5482.

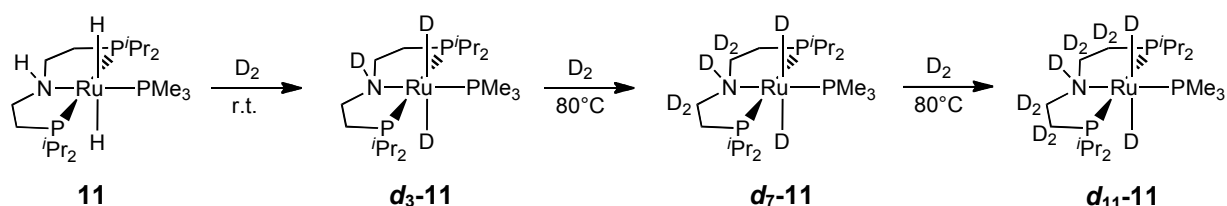
ähnlich zu Milsteins Pyridin-basiertem PNP Ligand ist.^[7] Vor allem ermöglicht die Dehydrierung des Ligandrückgrates die elektronische Feineinstellung der π -Donoreigenschaften des Liganden und ermöglicht so die Steuerung von wichtigen Eigenschaften, wie Struktur und Reaktivität der fünffach koordinierten d^6 Rutheniumkomplexe **8** und **12** (siehe unten). Im Unterschied zu Milsteins Pyridin-basiertem System besitzt **11** zwei kooperative funktionelle Gruppen im Pinzettenrückgrat – die Amingruppe und die Ethylenbrücke – die geeignet sind, um bifunktionelle Wasserstoffaktivierung zu begünstigen und somit die reversible Addition von 2 Äquivalenten H_2 an **8** ermöglichen.

Schema D-5. Reversibles doppeltes H_2 Additions/Eliminierungs Gleichgewicht der Komplexe **11**, **12** und **8**.



Der Mechanismus für dieses Gleichgewicht wurde durch H/D-Isotopenmarkierungsexperimente untersucht.^[6] Die Deuterierung von Ru–H, N–H und den Ligandrückgratprotonen von Komplex **11** erfolgt in 3 Schritten mit deutlich höheren Raten für Ru–H und N–H Deuterierung verglichen mit dem H/D-Austausch im Rückgrat (Schema D-6).

Schema D-6. Beobachtete Isotopomere von **11** bei H/D-Austauschexperimenten.



Der Vergleich der experimentellen Ergebnisse mit DFT Rechnungen zeigten in der beobachteten Regioselektivität des H/D-Austauschs eine Übereinstimmung mit den berechneten relativen Barrieren für die Ru–H, N–H und C–H Aktivierungsprozesse (Abbildung D-1). Der linke Ast der Reaktionssequenz (**11** \rightleftharpoons **12**) ist von besonderem Interesse,

⁷ (a) J. Zhang, G. Leitus, Y. Ben-David, D. Milstein, *J. Am. Chem. Soc.* **2005**, *127*, 10840. (b) J. Zhang, G. Leitus, Y. Ben-David, D. Milstein, *Angew. Chem.* **2006**, *118*, 1131; *Angew. Chem. Int. Ed.* **2006**, *45*, 1113.

da dieser Typ von heterolytischer H_2 Spaltung üblicherweise den ratenbestimmenden Schritt des allgemein anerkannten Mechanismus für bifunktionelle Noyori-artige Hydrierung darstellt. Unsere Rechnungen deuten jedoch darauf hin, dass die H_2 Aktivierung durch direkten intramolekularen Protonentransfer von einem $\eta^2\text{-H}_2$ Ligand zu einem basischen Amidoligand eine relativ hohe Barriere im Vergleich zu experimentellen Ergebnissen besitzt. Darüber hinaus weist die Erhöhung von katalytischen Hydrierungsraten durch Alkali-Alkoxid-Cokatalysatoren, protische Lösungsmittel und Hydrierungsprodukte auf die Beteiligung von Wasserstoffbrücken in der bifunktionellen H_2 Aktivierung hin. Quantitative experimentelle Studien, die diese Beobachtung erklären, waren jedoch vor dieser Arbeit nicht verfügbar.

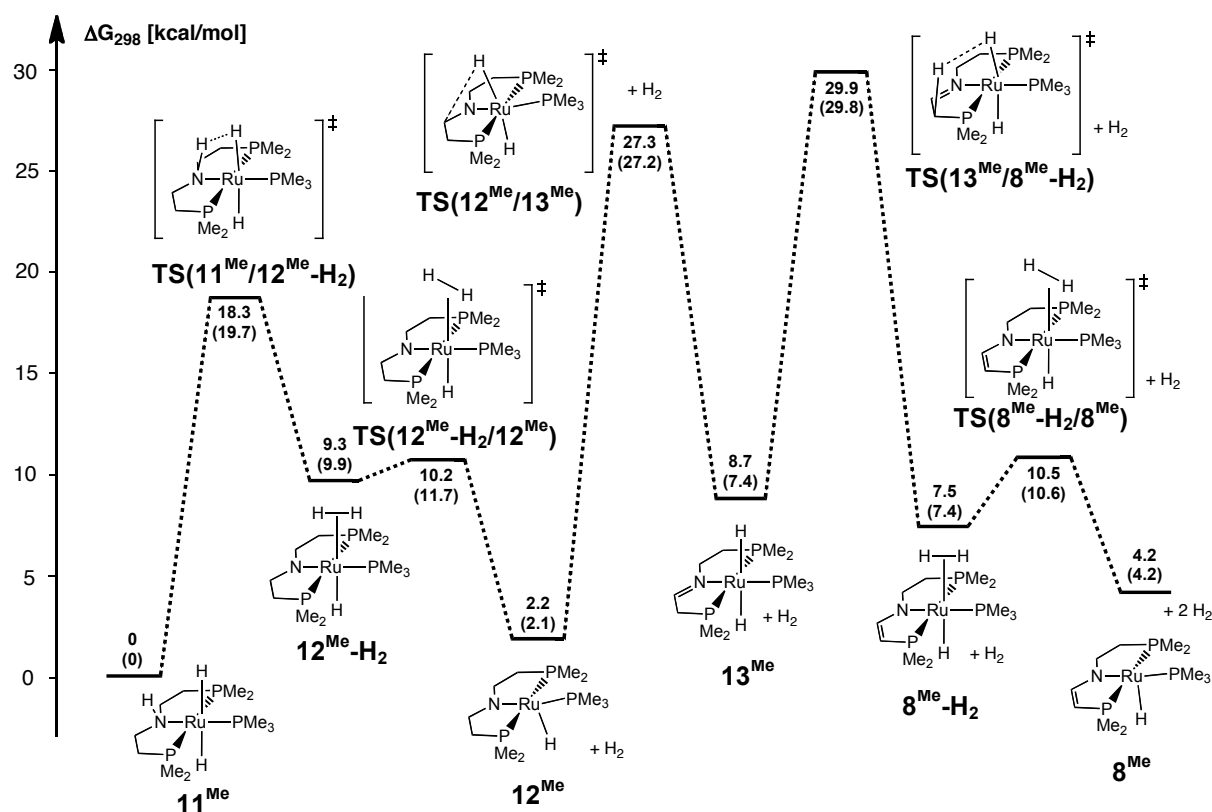


Abbildung D-1. DFT Rechnungen (B3LYP/6-31+G**) für den Mechanismus der H_2 Eliminierung von 11^{Me} in der Gasphase (THF). Die freien Energien in THF (PCM) sind in Klammern angegeben.

Eine schmale ^1H NMR Linienform und 2D ^1H NOESY NMR Spektren weisen auf einen, auf der experimentellen Zeitskala langsamen chemischen Austausch der N-H und Ru-H

Funktionalitäten von Komplex **11** hin.^[8] Die Addition von Wasser zu einer Probe von **11** in d^8 -THF führt jedoch zu einer selektiven Verbreiterung eines der beiden Hydridsignale und dem Zusammenbruch der beiderseitigen Hydrid *trans*-*J*-Kupplung. Variable Temperatur T_1 Messungen weisen auf einen stereoselektiven Protonenaustausch von H₂O mit dem Hydridliganden hin, der sich in Nachbarschaft des Aminprotons befindet. Diese Interpretation konnte durch 2D ¹H EXSY NMR Spektroskopie bestätigt und mit hohen Austauschraten zweiter Ordnung von H₂O mit H^{RuA} und H^{NH} in d^8 -THF erstmals auch quantifiziert werden (Abbildung D-2). Überraschenderweise wurde kein Austausch von H₂O with H^{RuB} beobachtet. Die zwei Hydridliganden befinden sich in sehr ähnlicher sterischer Umgebungen und die *trans*-Dihydridkonfiguration lässt vergleichbare Basizitäten der Hydridliganden vermuten. Aus diesem Grund ist die hohe Stereoselektivität des Hydrid/H₂O Austauschs am Besten durch eine lenkende H^{NH}/H₂O Wasserstoffbrückenbindung erklärbar.

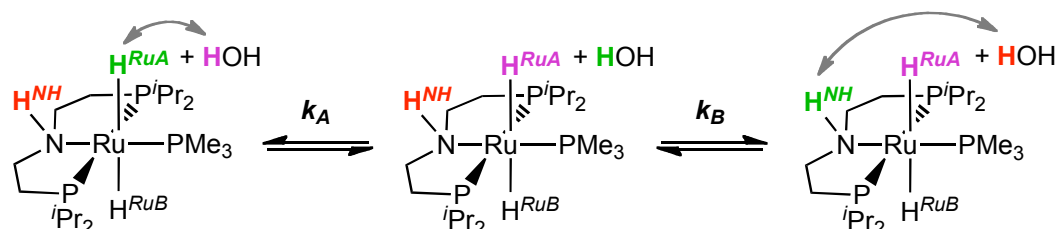


Abbildung D-2. Austausch von H₂O mit H^{RuA} und H^{NH} im Amin-Dihydridokomplex **11**.

Für die weitere Untersuchung des N-H Einflusses wurde das Stickstoffatom durch Methylierung blockiert. Die H₂O Zugabe zu einer Lösung von [Ru(*trans*-H)₂(PMe₃)(PNP^{Me})] (**14**; PNP^{Me} = MeN(CH₂CH₂P^{*i*}Pr₂)₂) in d^8 -THF resultiert in einem sehr langsamen, nicht selektiven Ru–H/H₂O Austausch und bestätigt somit unser mechanistisches Model. Der Proton/Hydrid Austausch sollte über die gleiche Diwasserstoffkomplex-Zwischenstufe (**12-H₂**) verlaufen, wie für die Wasserstoffaddition an Amidokomplex **12**. Diese Ergebnisse lassen somit darauf schließen, dass Wasser die Barriere für die heterolytische Wasserstoffspaltung senkt. DFT Rechnungen ergeben eine um $\Delta\Delta G^\ddagger = 8.2$ kcal/mol niedrigere Barriere für die wasserkatalysierte Wasserstoffspaltung und bestätigen somit diese Annahme. Diese mechanistische Untersuchung unterstreicht die wichtige Rolle von Brønsted-Säuren wie Wasser oder Alkohole für die bifunktionelle Noyori-artige Hydrierungskatalyse.

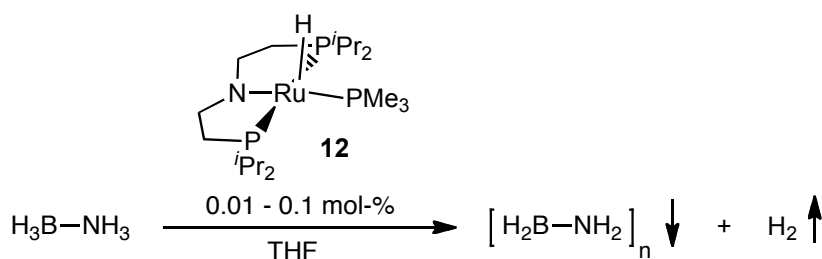
⁸ A. Friedrich, M. Drees, J. Schmedt auf der Günne, S. Schneider, *J. Am. Chem. Soc.* **2009**, *131*, 17552.

Den rechten Ast der Wasserstoff-Aktivierungssequenz betreffend (Abbildung D-1, **12**⇌**8**), ist der Vergleich der ähnlichen Liganden PNP and PN=P besonders interessant, da der Enamido-Pinzettenligand vor dieser Arbeit nicht bekannt war. Während die Molekülstruktur des Amidokomplexes **12** am Besten durch eine Y-förmige verzerrte trigonale Bipyramide beschrieben werden kann, weist die Struktur des analogen Enamidokomplex **8** eher eine quadratisch pyramidale Koordinationsgeometrie auf. Die unterschiedlichen Molekülstrukturen von **12** and **8** können einer deutlich verminderten N→Ru π -Donation in **8** zugeschrieben werden, die einer Delokalisierung des freien Elektronenpaares am Stickstoff durch Konjugation mit der C=C Doppelbindung im Enamidoligand geschuldet ist. Die schwächere π -Donation des dehydrierten Pinzettenligands kann für die Steuerung der Reaktivität der fünffach koordinierten d^6 Komplexe genutzt werden. Das tief liegende LUMO im quadratisch pyramidalen Komplex **8** wird durch die unterschiedlichen Farben rot (**12**) und grün (**8**) zum Ausdruck gebracht und erklärt das Lewis-azide Verhalten von **8**, belegt durch die Bildung des oktaedrischen Komplexes [RuH(PMe₃)₂(PN=P)] (**15**) nach Addition von PMe₃. Im Gegensatz dazu, führt die Reaktion von **12** mit PMe₃ über einen basenassistierten Wasserstoffeliminierungspfad zu einer Mischung von **11** und **15**.^[6] Mit Elektrophilen, wie MeOTf, ist hingegen für **12** und **8** eine vorwiegende N-Methylierung zu RuH(OTf)PMe₃(PNP^{Me}) (**16**) und [RuH(OTf)PMe₃(PN=P^{Me})] (**17**) zu beobachten. Eine C-Methylierung von **8** erfolgt nur in 25% spektroskopischer Ausbeute (³¹P NMR). Diese Reaktivität von **8** steht im Gegensatz zu Pyridin-basierten kooperativen Pinzettenanaloga, die einer bevorzugten C-Methylierung unterliegen und kann der hohen Flexibilität des aliphatischen PN=P Pinzettenligands zugeschrieben werden. Das Struktur- und Reaktivitätsmuster platzieren diesen neuartigen Enamidoligand PN=P zwischen den stark π -donierenden Alkylamido PNP-Liganden und akzeptor-N-substituierte, mäßig π -donierende Amidopinzettenliganden, wie Silylamide N(SiMe₂CH₂PR₂)₂ oder Arylamide N(C₆H₄-2-PR₂)₂. Die Thermodynamik der β -Hydrid-Migrationsreaktionen ist stark von anderen Liganden abhängig, die an das Metall gebunden sind. Dies wird durch die Synthese von Komplex **10** im Vergleich zur Instabilität des flüchtigen Komplexes **13** deutlich. Die *trans*-Dihydride Konfiguration ist somit möglicherweise ein wichtiges Strukturmerkmal zur Stabilisierung von Noyori-artigen Hydrierungskatalysatoren gegen die Deaktivierung zu Iminkomplexen.

2. Kooperative Katalyse

Der Ruthenium PNP Komplex **12** zeigt bisher unerreichte Aktivitäten und Wechselzahlen bei der Dehydrierung von Amminboran ($\text{H}_3\text{N}-\text{BH}_3 = \text{AB}$) bei Raumtemperatur mit niedrigen Katalysatorbeladungen von 0.01 mol% und erweist sich damit als bisher aktivster bekannter homogener Katalysator für die AB-Dehydrierung (Schema D-7).^[5] Starke H_2 Entwicklung von AB findet gemeinsam mit der Bildung eines weißen Polymers $[\text{H}_2\text{NBH}_2]_n$ statt, das unlöslich in allen herkömmlichen organischen Lösungsmitteln ist. Bei Katalysatorbeladungen von 0.1 mol% **12** wird etwas mehr als 1 Äquivalent H_2 freigesetzt, was auf eine quantitative Polyaminoboranbildung mit kleinen Mengen von Borazin zurückzuführen ist.

Schema D-7. Dehydrokupplung von AB mit Katalysator **12**.



In Zusammenarbeit mit den Arbeitsgruppen von Ian Manners (University of Bristol) und Jörn Schmedt auf der Güne (Ludwig-Maximilians-Universität München) wurde das polymere Produkt der AB Dehydrierung näher untersucht.^[9] Dazu wurden Festkörper-¹¹B-MQ-MAS NMR Spektren zur Unterdrückung von Quadrupol-Effekten zweiter Ordnung aufgenommen. Diese zeigen zwei Signale, die BH_2 -Gruppen und BH_3 -Endgruppen im Polymer zugeordnet werden können. Keine Anzeichen für BH - oder quartäre B-Gruppen wurden gefunden, was auf eine Abwesenheit von Quervernetzung im Polymer schließen lässt und in Übereinstimmung mit der Reaktionsstöchiometrie ist. Auf Grund der Unlöslichkeit des Polymers kann dieses Ergebnis nicht mit Informationen zum Molekulargewicht aus der Gelpermeationschromatographie (GPC) verglichen werden. Jedoch führt die Polymerisierung von $\text{MeH}_2\text{N}-\text{BH}_3$ (MAB) und die Copolymerisierung von AB und MAB mit **12** zu linearen Polymeren mit hohem Molekulargewicht, wie mit Hilfe von ¹¹B-MQ-MAS NMR, GPC und

⁹ (a) A. Staubitz, M. E. Sloan, A. P. M. Robertson, A. Friedrich, S. Schneider, P. J. Gates, J. Schmedt auf der Güne, I. Manners, *J. Am. Chem. Soc.* **2010**, *132*, 13332. (b) A. Friedrich, S. Schneider, *unpublished*.

Elektronenspray-Massenspektrometrie gezeigt werden konnte. Dieses Ergebnis ist besonders hinsichtlich des Reaktionsmechanismus von Interesse. Mechanistische Informationen über metallkatalysierte Boranamin-Dehydrierungen sind rar und alle experimentellen und rechnerischen Untersuchungen weisen auf die Bildung von zyklischen Oligoboranaminen oder Borazindervitaten hin, die nur BH₂- und BH-Funktionalitäten aufweisen. Aus diesem Grund deutet die Bildung eines linearen Polymers mit BH₃-Endgruppen und keinen BH-Gruppen in der Dehydrokupplung von AB mit Katalysator **12** auf einen anderen Reaktionsmechanismus hin.

Um weitere Informationen zu erhalten, wurde die Dehydrierung von AB with **12** anhand von kinetischen Experimenten durch Volumenmessung von H₂ untersucht. Die Messung von Anfangsgeschwindigkeiten mit unterschiedlichen Katalysatorbeladungen ergaben eine Abhängigkeit erster Ordnung in **12**. Darüber hinaus wurde für einen großen Bereich an Katalysator- und Substratanfangskonzentration eine Abhängigkeit erster Ordnung in AB über mehr als eine Halbwertszeit gefunden. Ein kinetischer Isotopeneffekt (KIE) von 1.8 für die Dehydrierung von B-deuteriertem Isotopomer H₃N-BD₃ wurde durch die Auftragung von ln[AB] über die Zeit erhalten. Der beobachtete normale Isotopeneffekt ist in qualitativer Übereinstimmung mit den Erwartungen für einen Reaktionsschritt mit symmetrisch verbrücktem μ -Hydridligand im Übergangszustand.^[10] Die Situation für die N-deuterierten Substrate D₃N-BH₃ und D₃N-BD₃ ist allerdings eine andere. In beiden Fällen wurde eine wesentlich kleinere Reaktionsrate mit einer Abhängigkeit nullter Ordnung in Substratkonzentration beobachtet. Daher können die KIEs für diese Isotopomere nicht direkt durch Referenzierung auf unmarkiertes AB erhalten werden. Dieses Ergebnis deutet auf einen Wechsel in der Reaktionsordnung mit einem anderen umsatzlimitierenden Schritt für N-deuterierte Substrate hin. Der bifunktionelle Effekt von **12** wurde durch kinetische Kontrollexperimente mit dem tertiären Aminkomplex [Ru(*trans*-H)₂(PMe₃)(PNP^{Me})] (**14**) als Katalysator gezeigt, der um zwei Größenordnungen kleinere Raten in der Dehydrierung von AB zeigt.^[9b] Diese Messungen ergaben einige wichtige mechanistische Informationen:

¹⁰ Basierend auf einer B-H Streckschwingung von 2350 cm⁻¹ wird ein maximaler H/D Isotopeneffekt für einen vollständigen B-H Bindungsbruch in AB von 4.9 erwartet.

- 1) Die Reaktionskontrolle der AB Dehydrierung mit **12** mittels ^{31}P and ^1H NMR Spektroskopie zeigt zu Beginn der Reaktion ausschließlich Aminkomplex **11**, was auf **11** als katalytischen Ruhezustand hinweist.
- 2) Die geringe Rate der H_2 Abspaltung von Komplex **11**, die ähnlich auch in DFT Rechnungen von Fagnou gefunden wurde,^[11] weist darauf hin, dass ein Mechanismus mit spontanem H_2 Verlust vom entsprechenden Aminkomplex nicht den ratenbestimmenden Schritt darstellt. Darüber hinaus deutet die beobachtete Abhängigkeit der Rate in Substrat auf einen anderen ratenbestimmenden Schritt hin.
- 3) Die Wechselzahl (TON) ist stark abhängig von der Anfangskonzentration des Substrates $[\text{AB}]_0$. Maximale TON's wurden für hohe $[\text{AB}]_0$ Konzentrationen und niedrige Katalysatorbeladungen erhalten, was vom Standpunkt der Wasserstoffspeicherung erstrebenswert ist, um eine hohe gravimetrische H_2 Dichte zu erhalten.
- 4) Katalysatordeaktivierung ist auf die Bildung von $[\text{Ru}(\text{H})(\text{PMe}_3)(\text{H}_2\text{NBH}_2\text{PNP}^{iPr})]$ (**18a**) zurückzuführen.^[12] Dieser Komplex, der einen viergliedrigen M–N–B–H Borametallring besitzt, ist nicht vollständig inaktiv in der AB-Dehydrierung, jedoch sind die katalytischen Raten um einige Größenordnungen kleiner verglichen mit **12**. Die Bildung von **18a** kann der Addition von kurzlebigen Aminoboran $\text{H}_2\text{N}-\text{BH}_2$ entlang der N–Ru Bindung von **12** zugeschrieben werden. Hohe $[\text{AB}]_0$ Konzentrationen unterstützen somit niedrige stationäre Aminoboran Konzentrationen.

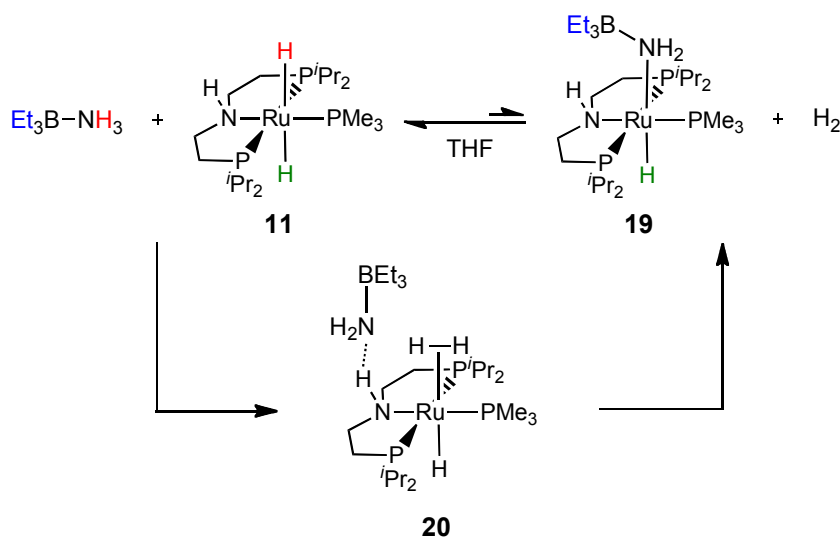
Um die Wechselwirkung der Aminogruppe von Boranaminen mit Komplex **11**, dem postulierten katalytischen Ruhezustand der Boranamin Dehydrokupplung zu untersuchen, wurde B-seitig blockiertes $\text{H}_3\text{N}-\text{BEt}_3$ synthetisiert. Nach dem Mischen der beiden Komponenten wurde mittels NMR Spektroskopie eine geringe Gleichgewichtskonzentration eines neuen Komplexes beobachtet, der dem Boranamidokomplex **19** entspricht (Schema D-8). Das Gleichgewicht wurde mittels 2D ^1H EXSY NMR Spektroskopie, wie für den Austausch von **11** mit anderen Brønsted-Säuren wie Wasser beschrieben, untersucht. Diese Experimente zeigten schnellen chemischen Austausch der Komplexe **11** und **19** und der $\text{H}_3\text{N}-\text{BEt}_3$ N-H Protonen mit dem Ru-H Ligand in *syn*-Stellung zum N-H Proton des Pinzettenliganden. Somit erfolgt ein Austausch über das Diwasserstoffkomplex-Intermediat **20**. Die Zugabe von

¹¹ N. Blaquiere, S. Diallo-Garcia, S. I. Gorelsky, D. A. Black, K. Fagnou, *J. Am. Chem. Soc.* **2008**, *130*, 14034.

¹² A. Friedrich, M. Drees, S. Schneider *Chem. Eur. J.* **2009**, *15*, 10339.

N-seitig blockiertem $\text{Me}_3\text{N}-\text{BH}_3$ zeigte hingegen innerhalb mehrerer Stunden keine Reaktion mit **11**. Die Kooperativität der Aminfunktion für die Bildung einer Diwasserstoffkomplex-Zwischenstufe wurde durch den, auf der NMR-Zeitskala sehr langsamen $\text{Ru}-\text{H}/\text{NH}_3$ Protonenaustausch in einer Reaktionmischung von $\text{H}_3\text{N}-\text{BEt}_3$ und N-methyliertem Katalysator **14** nachgewiesen.

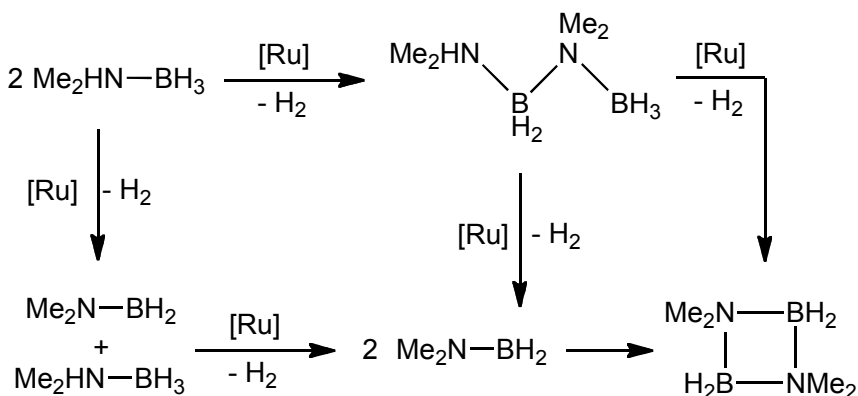
Schema D-8. Reaktion von **11** mit $\text{H}_3\text{N}-\text{BEt}_3$ und vorgeschlagener Mechanismus über den Diwasserstoffkomplex **20**. Die Farben kennzeichnen ausgewählte, im 2D ^1H EXSY NMR Spektrum beobachtete, chemische Austauschsignale.



Weitere mechanistische Informationen wurden durch die Dehydrierung von $\text{Me}_2\text{HN}-\text{BH}_3$ (DMAB) erhalten. Da die Auswertung der Dehydrokupplung von DMAB nicht durch die Bildung von polymeren, unlöslichen B-N Produkten erschwert wird, kann die Reaktion sehr einfach mit Hilfe von ^{11}B Lösungs-NMR Spektroskopie untersucht werden. Die Reaktion verläuft quantitativ mit Katalysator **11** und **12**, wird jedoch nach hohen Anfangsraten deutlich langsamer bevor vollständiger Umsatz erreicht ist. Diese Beobachtung ist auf die schnellere Bildung des Katalysator-Deaktivierungsproduktes $[\text{Ru}(\text{H})(\text{PMe}_3)(\text{Me}_2\text{NBH}_2\text{PNP})]$ (**18b**) im Vergleich zur Bildung von **18a** während der Dehydrokupplung von AB zurückzuführen.^[12] Die Reaktionskontrolle mittels ^{11}B NMR Spektroskopie zeigt die Bildung von kurzlebigen Aminoboran $\text{Me}_2\text{N}-\text{BH}_2$, das rasch dimerisiert. Darüber hinaus wurde lineares Diborazan $\text{Me}_2\text{HN}-\text{H}_2\text{B}-\text{Me}_2\text{N}-\text{BH}_3$ als Zwischenprodukt beobachtet. Die Dehydrozyklisierung von $\text{Me}_2\text{HN}-\text{H}_2\text{B}-\text{Me}_2\text{N}-\text{BH}_3$ mit **12** führte dementsprechend quantitativ zum Endprodukt $(\text{Me}_2\text{N}-\text{BH}_2)_2$ and H_2 . Diese Reaktion erfolgt sowohl über die direkte Dehydrozyklisierung zu $(\text{Me}_2\text{N}-\text{BH}_2)_2$, als auch über die Dehydrierung von Diborazan mit der Freisetzung von $\text{Me}_2\text{N}-$

BH₂, wie aus der ¹¹B NMR spektroskopischen Reaktionskontrolle hervorgeht. Spektroskopische Kinetiken und quantenchemische Rechnungen schlagen für die Bildung des Diborazans Me₂HN–H₂B–Me₂N–BH₃ einen metallkatalysierten Prozess vor, da die Bildung nicht auf eine unkatalysierte Reorganisation von Me₂N–BH₂ mit DMAB zurückzuführen ist. Zur weiteren Aufklärung wurde ein Kontrollexperiment mit einer Mischung aus B-seitig blockiertem H₃N–BEt₃ und N-seitig blockiertem Me₃N–BH₃ in Anwesenheit von Katalysator **11** durchgeführt. Hierbei wurde jedoch keine B-N Kupplung beobachtet, was eine intermolekulare Kopf-Schwanz-Dehydrokupplung von Boranaminen als möglichen Reaktionspfad ausschließt.

Schema D-9. Mechanistischer Vorschlag für die Dehydrozyklisierung von DMAB mit Katalysator **11** oder **12**.



Basierend auf diesen Ergebnissen wurde ein Mechanismus für die Dehydrozyklisierung von DMAB vorgeschlagen, der sowohl eine katalytische Dehydrierung von DMAB, als auch eine katalysierte B-N Kupplung zu Grunde legt (Schema D-9): Intramolekulare Dehydrierung von DMAB setzt Aminoboran Me₂N–BH₂ frei, das entweder in einem metallkatalysierten Prozess mit DMAB zum linearen Diborazan reagiert, oder mit einem weiteren Äquivalent Aminoboran zum Endprodukt dimerisiert. Katalytische Dehydrierung des Diborazan-Zwischenproduktes führt zu Zyklisierung oder B-N Bindungsspaltung. Die resultierenden Aminoboran-Monomere dimerisieren rasch. Wenn diese Ergebnisse zur DMAB-Dehydrierung auf andere Boranamine übertragen werden können, stellen sie eine mechanistische Begründung für die Bildung von linearen Aminoboran-Polymeren - wie sie bei der Dehydrokupplung von AB mit Katalysator **12** beobachtet werden - anstelle von Polyborazin dar.

Die derzeitigen kinetischen, spektroskopischen und quantenchemischen Ergebnisse erlauben einen Vorschlag für ein mechanistisches Model der AB-Dehydropolymerisation, das die Bildung von linearen Aminoboranen berücksichtigt. Der Mechanismus kann in zwei miteinander verbundene Katalysezyklen unterteilt werden (Schema D-10): Der obere Zyklus berücksichtigt die Dehydrierung von AB unter Freisetzung von H₂ und Aminoboran. Ausgehend vom Präkatalysator **12** führt die Reaktion mit AB zum Boranamin-Addukt **21**, das nach Verlust von Aminoboran H₂N-BH₂ anschließend den katalytischen Ruhezustand **11** bildet. Diese Schritte sind auch von Fagnou et al. für die bifunktionelle AB-Dehydrierung vorgeschlagen worden.^[11] Der Hauptunterschied zu Fagnous Vorschlag ist der von uns postulierte Protonen-*shuttle*-Mechanismus für die Bildung des Diwasserstoffkomplexes **22**. DFT-Rechnungen für die Sequenz **11** + AB → **22** + AB → **12** + AB + H₂ → **21** + H₂ → **11** + H₂ + H₂N-BH₂ ergeben eine flache Potentialhyperfläche, die im Einklang mit den außerordentlich hohen, experimentell bestimmten katalytischen Raten steht. Eine Abhängigkeit erster Ordnung in [AB], die für eine Reihe verschiedener Substrat-Anfangskonzentrationen und auch für B-deutrieretes AB gefunden wurde, spricht für **12** + AB + H₂ → **21** + H₂ als ratenbestimmenden Schritt.^[13] Bei N-Deuterierung des Substrates tragen andere Schritte im vorgestellten Zyklus zur Gesamtrate bei, die alle nullter Ordnung in [AB] sind. Die Bildung des beobachteten Katalysator-Deaktivierungsproduktes **18** mit hydridverbrücktem Boraruthenaring kann durch eine Reaktion von **12** mit freiem Aminoboran außerhalb des Zyklus erklärt werden.

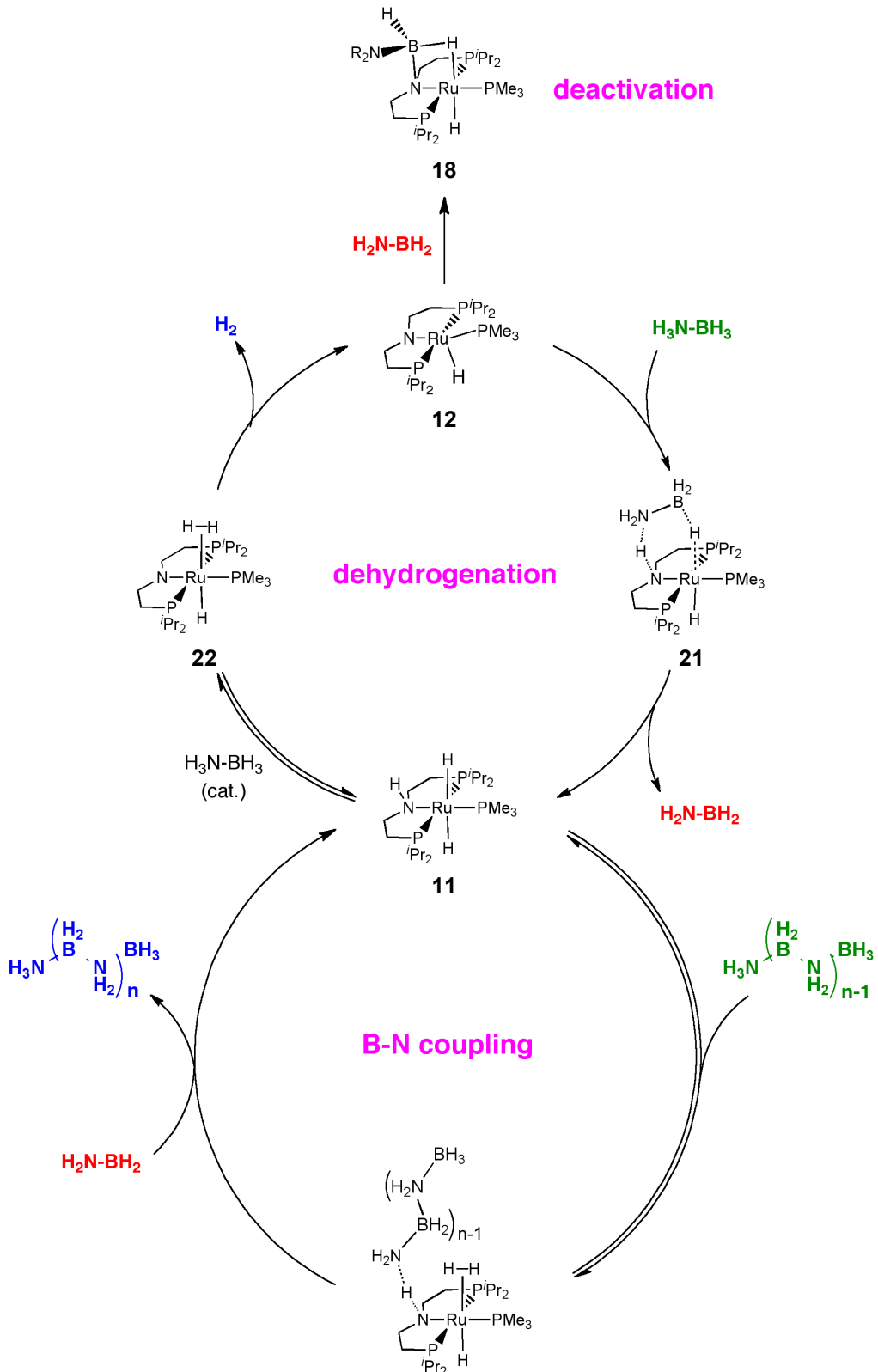
Der untere Zyklus in Schema D-10 berücksichtigt die B-N-Kupplung. Obwohl die Kinetiken zur H₂-Abgabe keine Information über den eigentlichen B-N-Kupplungsschritt liefern, weisen einige qualitative Beobachtungen auf eine metallzentrierte Reaktion hin:

- 1) Die Dehydrierung von Me₂AB zeigt mit höherer Katalysatorbeladung höhere stationäre Konzentrationen des linearen Kupplungsproduktes Me₂HN-BH₂-NMe₂-BH₃.
- 2) Alle experimentellen und quantenchemischen Untersuchungen von anderen Arbeitsgruppen führen die Bildung von zyklischen AB-Dehydrokupplungsprodukten (und letztendlich Borazin und Polyborazin) auf eine unkatalysierte Reorganisation von Aminoboran zurück. Hier werden jedoch nur geringe Mengen an Borazin beobachtet,

¹³ DFT-Rechnungen zum Übergangszustand TS(**12** + AB/**21**) werden aktuell durchgeführt.

die von einer unkatysierten Aminoboran-Kupplung als Nebenreaktion mit höherer Barriere stammen können.

Schema D-10. Vorgeschlagener Katalysezyklus für die Boranamin-Dehydrokupplung mit Katalysator **12**.



Basierend auf DFT-Rechnungen wird ein B-N-Kupplungszyklus mit Ru-katalysierter Aminoboran-Insertion in eine AB N-H-Bindung mit kleinen Barrieren vorgeschlagen. Für die weitere Kettenverlängerung können oligomere und polymere Zwischenprodukte $\text{H}_3\text{N}-(\text{BH}_2-\text{NH}_2)_n-\text{BH}_3$ ($n \geq 1$) anstelle des Ausgangsmoleküls AB in den B-N-Kupplungszyklus eintreten. Schließlich wird die geringe Löslichkeit der Polymere, die eine kritische Kettenlänge überschritten haben, zu einer Ausfällung aus der Lösung führen. In Übereinstimmung mit dem Bericht von Staubitz et al., weisen unsere experimentellen Ergebnisse darauf hin, dass diese Bedingung in THF bei $n \approx 20$ erfüllt ist.^[9a]

Zusammenfassend kann unser Ru(PNP)-Katalysator als *bifunktionell* im wörtlichen und im symbolischen Sinne betrachtet werden. Zum Einen wird ein bifunktionaler Mechanismus angenommen, in dem zwei funktionelle Gruppen des Katalysators an den ratenlimitierenden Schritten beteiligt sind. Zum Anderen übernimmt die Rutheniumverbindung zwei gesonderte Funktionen: als Katalysator für die Dehydrierung und für die B-N-Kupplung. Das mechanistische Modell für außergewöhnlich schnelle Boranamin-Dehydrierung mit Ru(PNP)-Katalysatoren stellt eine ausgezeichnete Grundlage für zukünftiges Katalysatordesign dar und ist eine wichtige Voraussetzung zur Kontrolle der B-N-Polymerstruktur für Materialanwendungen. Die Dehydrierung von anderen polaren anorganischen Substraten, wie Boranphosphan-Addukte oder Aminosilane, können den Zugang zu interessanten neuen anorganischen Polymeren ermöglichen, die z.B. als Ausgangsstoffe für Halbleitermaterialien Anwendung finden.^[14] Im Gegensatz zu den meisten anderen Katalysatoren ist eine Dehydrierung mit Amidohydridkomplex **12** unter basenfreien Bedingungen möglich.

¹⁴ (a) T. J. Clarke, K. Lee, I. Manners, *Chem. Eur. J.* **2006**, *12*, 8634. (b) T. Chievers, I. Manners, in *Inorganic Rings and Polymers of the p-Block Elements*, RSC Publishing, Cambridge, **2009**.

E List of Publications

List of Publications

1 Journal Publications

- (1) "Iridium Olefin Complexes bearing Dialkylamino/amido PNP Pincer Ligands: Synthesis, Reactivity, and Solution Dynamics."
A. Friedrich, R. Ghosh, R. Kolb, E. Herdtweck, S. Schneider* *Organometallics* **2009**, *28*, 708.
- (2) "Ruthenium complexes with cooperative PNP ligands: bifunctional catalysts for the dehydrogenation of ammonia-borane."
M. Käß, A. Friedrich, M. Drees, S. Schneider* *Angew. Chem.* **2009**, *121*, 922; *Angew. Chem. Int. Ed.* **2009**, *48*, 905.
- (3) "Acceptorless dehydrogenation of alcohols: Perspectives for synthesis and H₂ storage."
A. Friedrich, S. Schneider* *ChemCatChem* **2009**, *1*, 72.
- (4) "Ruthenium-Catalyzed Dimethylamineborane Dehydrogenation: Stepwise Metal Centered Dehydrocyclization."
A. Friedrich, M. Drees, S. Schneider* *Chem. Eur. J.* **2009**, *15*, 10339.
- (5) "Facile Double C-H Activation of Tetrahydrofuran by an Iridium PNP Pincer Complex. "
J. Meiners, A. Friedrich, E. Herdtweck, S. Schneider* *Organometallics* **2009**, *28*, 6331.
- (6) "Highly Stereoselective Proton/Hydride-Exchange: Assistance of Hydrogen-Bonding for the Heterolytic Splitting of H₂."
A. Friedrich, M. Drees, J. Schmedt auf der Günne, S. Schneider* *J. Am. Chem. Soc.* **2009**, *131*, 17552.
- (7) "Ruthenium Complexes with Cooperative PNP-pincer Amine, Amido, Imine, and Enamido Ligands: Facile Ligand Backbone Functionalization Processes. "
A. Friedrich, M. Drees, M. Käß, E. Herdtweck, S. Schneider* *Inorg. Chem.* **2010**, *49*, 5482.

- (8) “Hydrogen generation from small molecules using bifunctional Ruthenium complexes.”
A. Friedrich, M. Drees, J. Schmedt auf der Günne, S. Schneider* *Prepr. Pap. - Am. Chem. Soc., Div. Fuel Chem.* **2010**, 55, 287.
- (9) “Catalytic Dehydrocoupling/Dehydrogenation of *N*-Methylamine-Borane and Ammonia-Borane: Synthesis and Characterization of High Molecular Weight Polyaminoboranes.”
A. Staubitz, M. E. Sloan, A. P. M. Robertson, A. Friedrich, S. Schneider, P. Gates, J. auf der Günne, I. Manners* *J. Am. Chem. Soc.* **2010**, 132, 13332.

2 Presentations

Oral Presentations

- (1) "Ruthenium-catalyzed Dehydrogenation of Borane-Amine-Adducts."
5. Koordinationschemietreffen, Erlangen, D, **2009**.
- (2) "Hydrogen generation from small molecules using bifunctional Ruthenium complexes."
239th ACS National Meeting, San Francisco, CA, USA, **2010**.
- (3) "Bifunctional catalysts for the dehydrogenation of amine-boranes."
Anorganisch-Chemisches Kolloquium, TU München, Garching, D, **2010**.

Poster Presentations

- (1) "Complexes of Iridium(I) bearing a PNP Pincer Ligand."
A. Friedrich, E. Herdtweck, S. Schneider, *14. Vortragstagung der Wöhlervereinigung*, Garching, **2008**.
- (2) "Ruthenium Based Efficient Dehydrogenation of Ammonia-Borane."
M. Käß, A. Friedrich, S. Schneider, *14. Vortragstagung der Wöhlervereinigung*, Garching, **2008**.
- (3) "Ruthenium catalyzed Dehydrocoupling of Amine-Borane Adducts."
A. Friedrich, M. Drees, E. Herdtweck, S. Schneider, *XVIII European Conference on Organometallic Chemistry*, Göteborg, S, **2009**.
- (4) "Amine-Borane Dehydrogenation with Bifunctional Ru(PNP)-Pincer Complexes."
A. Friedrich, M. Drees, E. Herdtweck, S. Schneider, *3rd EuCheMS Chemistry Congress*, Nürnberg, D, **2010**.

F Curriculum Vitae

Curriculum Vitae

Personal Information

Name	Anja Friedrich
Date of birth	06. Feb. 1980
Place of birth	Troisdorf, Germany

Education

03/2008 – 12/2010	PhD in organometallic chemistry at the <i>Technical University of Munich</i> , supervised by Prof. Sven Schneider at the chair for inorganic chemistry Prof. W. A. Herrmann (<i>summa cum laude</i>).
10/2002 – 11/2007	Undergraduate studies in chemistry at the <i>Technical University of Munich</i> , degree Dipl.-Chem. Univ. (<i>passed with distinction</i>).
02/2000 – 02/2002	Education to certified Chemical-Technical Assistant at the chemistry school <i>Dr. Erwin Elhardt</i> in Munich (<i>passed with distinction</i>).
10/1999 – 02/2000	Undergraduate studies in geology/paleontology at the <i>Ludwig-Maximilians-Universität</i> in Munich.
09/1995 – 06/1999	Secondary school <i>Luitpold-Gymnasium</i> in Munich, university-entrance diploma (Abitur).
08/1990 – 07/1995	Secondary school <i>Konrad-Adenauer-Gymnasium Westerburg</i> .
08/1986 – 07/1990	Primary school <i>Wolfsteinschule Bad Marienberg</i> .

Work Experience

02/2003 – 03/2007	Student research assistant at the <i>PTS - The Paper Technology Specialists</i> in Munich.
08/2006 – 10/2006	Internship at <i>Süd-Chemie AG</i> in Heufeld.
03/2002 – 09/2002	Employment as Chemical-Technical Assistant at the <i>German Research Center for Food Chemistry</i> in Munich.

Member- and Scholarships

since 05/2010	Member of the <i>TUM graduate school</i> and the <i>GDCh</i> .
since 11/2008	Graduate scholarship of <i>elite network of bavaria</i> and member of the international doctorate program <i>NanoCat</i> .
2004	<i>Oskar-Karl-Forster</i> scholarship.

Skills and expertise

Professional skills	<p>Responsible for a research project in the field of organometallic chemistry.</p> <p>Supervising PhD student for the chair's NMR spectrometers and the glove-boxes.</p> <p>Supervision of a Bachelor thesis and several student research projects.</p> <p>Scientific documentation and presentation on an international level; scientific proposal and paper writing.</p>
Technical skills	<p>Inorganic and organic synthesis – main focus: design of functionalized ligands and metal complexes for catalysis.</p> <p>Deep knowledge of organometallic chemistry and homogeneous catalysis.</p> <p>Characterization of products with spectroscopic methods – main focus: NMR spectroscopy.</p> <p>Kinetic studies with isotopic labeling, FT-IR and NMR.</p> <p>Preparation and characterization of paper coatings.</p>
Interpersonal skills	Enrollment in the transferable skills courses <i>successful communication</i> and <i>self assessment</i> .
Language skills	<p>German - native language.</p> <p>English - fluent.</p> <p>French - basic (A2, European Framework of References).</p> <p>Spanish - basic (A1).</p>